Mendelova univerzita v Brně

VYSOKÉ UČENÍ TECHNICKÉ V BRNĚ

CEITEC

Středoevropský technologický institut

BRNO | ČESKÁ REPUBLIKA

# XIV. Pracovní setkání fyzikálních chemiků a elektrochemiků

**Sborník příspěvků**

**Brno 3.–4. 6. 2014**

XIV. Pracovní setkání

fyzikálních chemiků a elektrochemiků

14th Workshop of Physical Chemists and Electrochemists

# Sborník příspěvků

**3.–4. 6. 2014**

Masarykova univerzita

Brno 2014

INVESTICE DO ROZVOJE VZDĚLÁVÁNÍ

## Organizace pořádající konferenci

Přírodovědecká fakulta Masarykovy univerzity v Brně
Ústav chemie
Kotlářská 2
611 37 Brno
http://www.sci.muni.cz

Agronomická fakulta Mendelovy univerzity v Brně
Ústav chemie a biochemie
Zemědělská 1
613 00 Brno
http://ucb.af.mendelu.cz

Fakulta elektrotechniky a komunikačních technologií Vysokého učení technického v Brně
Ústav mikroelektroniky
Technická 3058/10
616 00 Brno
http://www.umel.feec.vutbr.cz

## Organizační zabezpečení konference

Libuše **Trnková**
libuse@chemi.muni.cz (Ústav chemie, PřF, MU)
René **Kizek**
kizek@sci.muni.cz (Ústav chemie a biochemie, AF, MENDELU)
Jaromír **Hubálek**
hubalek@feec.vutbr.cz (Ústav mikroelektroniky, FEKT, VUT v Brně)

Publikace neprošla jazykovou kontrolou. Jednotlivé příspěvky jsou publikovány tak, jak byly dodány autory. Za věcnou a odbornou správnost jsou plně odpovědni autoři příspěvků. Podrobné informace včetně sborníku příspěvků jsou k dispozici na internetové adrese http://sci.muni.cz/~labifel/


ISBN 978-80-210-6842-1

**Pracovní setkání bylo podpořeno výzkumnými organizacemi a projekty :**








## Sponzoři pracovního setkání

Organizátoři děkují všem letošním sponzorům za podporu, která umožnila pořádat tuto již tradiční akci: Metrohm Česká Republika s.r.o., Eppendorf Czech & Slovakia s.r.o., Sigma - Aldrich spol. s r.o., LABMARK a.s., Chromservis s.r.o., VWR International s.r.o., Biotech a.s., Pragolab s.r.o , Česká společnost chemická, pobočka Brno

Hlavní sponzor

Milí přátelé,

vítáme Vás na dalším, již čtrnáctém ročníku Pracovního setkání fyzikálních chemiků a elektrochemiků (14th Workshop of Physical Chemists and Electrochemists). Letošní konference se koná v nových prostorách Masarykovy univerzity (MU) a my věříme, že se Vám v Univerzitním kampusu Bohunice (UKB) bude líbit. Na organizaci celé akce se podílejí významné brněnské vysoké školy – MU, MENDELU a VUT, které jsou zapojeny do centra vědecké excelence v oblasti věd o živé přírodě, pokročilých materiálů a technologií (CEITEC: Central European Institute of Technology – středoevropský technologický institut). Konáním naší konference bychom chtěli:

a) ukázat, že k rozvoji vědy přispívá zintenzivnění mezioborové spolupráce, tedy úzké propojení vědeckého výzkumu v oblasti živé a neživé přírody,
b) oslavit 95. výročí od založení dvou univerzit – MU a MENDELU,
c) připomenout si 55. výročí udělení Nobelovy ceny za fyzikální chemii prof. Jaroslavu Heyrovskému za objev polarografie a také
d) poskytnout mladým a nadějným vědcům příležitost prezentovat svoje výsledky, diskutovat o nich a získat informace, které jim pomohou se dál vědecky rozvíjet.

Záštitu nad XIV. Pracovním setkáním fyzikálních chemiků a elektrochemiků přijali rektor Masarykovy univerzity doc. PhDr. Mikuláš Bek, Ph.D., rektor Mendelovy univerzity prof. RNDr. Ladislav Havel, CSc., a rektor Vysokého učení technického v Brně prof. RNDr. Ing. Petr Štěpánek, CSc. Na úrovni děkanů se záštity ujali doc. RNDr. Jaromír Leichmann, Dr. (Přírodovědecká fakulta MU), doc. Ing. Pavel Ryant, Ph.D. (Agronomická fakulta MENDELU) a prof. Ing. Jarmila Dědková, CSc. (FEKT VUT). Za technologický institut záštitu převzal i prof. Ing. Radimír Vrba, CSc., vědecký ředitel pro oblast pokročilých materiálů a nanotechnologií CEITEC.

Konference, jako každým rokem, bude jistě plná zajímavých příspěvků ve formě plenárních (6) a zvaných přednášek (7) a také posterových sdělení (38), ale hlavní pozornost bude věnována mladým vědcům a studentům, kteří se zúčastní soutěže v Sekci mladých (SM). Stalo se už zvykem, že studenti magisterského, doktorského, ale i bakalářského studia prezentují v SM v anglickém jazyce své příspěvky a jejich vystoupení je hodnoceno odbornou komisí po stránce obsahové i formální. Nejlepší studenti jsou pak finančně i věcně oceněni. Podobně probíhá soutěž o nejlepší plakátové (posterové) sdělení, které autor uvede s krátkou prezentací. Každý autor má možnost rozhodnout se, zda se této soutěže chce zúčastnit.

Rozšířená abstrakta v anglickém jazyce od všech účastníků konference jsou zpracována do sborníku s přiděleným ISBN, čímž sborník odpovídá kritériím pro hodnocení V a V v kategorii „Článek ve sborníku“.

Děkujeme všem firmám, které podporují Pracovní setkání fyzikálních chemiků a navazující Letní elektrochemickou školu. Děkujeme spolupořadateli

Letní elektrochemické školy, firmě METROHM Česká republika s.r.o. Poděkování patří i České společnosti chemické za příspěvek na knižní ceny vítězným studentům.

Všechny účastníky na půdě Masarykovy univerzity v nových prostorách kampusu vítáme a přejeme jim úspěšnou prezentaci, která spolu s bohatou diskuzí může být další inspirací v jejich krásné činnosti – vědeckém bádání.

"V čem spočívá tvůrčí proces ve vědě? Ve schopnosti poznat, co je důležité a co podružné."

Jaroslav Heyrovský

## Obsah

Investigation of the carbon material based electrodes for supercapacitors 9
The effect of ochratoxin A on DNA adduct formation by the carcinogen aristolochic acid in rats 12
Role of rat cytochromes p450 in oxidation of 17α-ethinylestradiol 15
Structure and spectroscopic characterization of copper(II) complexes with fluoroquinolones 18
NAD(P)H:quinone oxidoreductase 1 is Induced by 3-nitrobenzanthrone, aristolochic acid, ellipticine, Sudan I and dicoumarol in rats - a comparative study 20
Study of structure and chemical composition of soil humic substances isolated from Humic Podzol 23
Effect of bitumen on sorption properties of lignite 28
Piezoelectric biosensors for detection of microorganisms 32
Hight performance sulfur nanocomposites as cathode materials based on conversion reaction 26
Physicochemical methods as a suitable instrument for short DNA fragments study 40
Studium fotochemických chránících skupin pomocí časově rozlišené spektroskopie. Je nano sekunda málo nebo moc pro roztržení vazby? 43
Hyaluronana micro- and nanoparticles 44
Mircorheological characterization of hyaluronic acid gels 47
Development of the cell systém for evaluation of ANTI-PAIIL immmunoglobulin efficacy 51
Cytochrome p450 1A1-catalyzed oxidation of carcinogenic benzo[a]pyrene is modulated by NADH and cytochrome $b_5$ 54
The azobenzene actinometer 57
Deeper Research of Structural Changes of Humic Acids Using Light Scattering Techniques 59
Are flavonoids fenoxide anions better hydrogen atom donors than parent molecules? 64
On the homolytic and heterolytic O–H bond cleavage in vitamin b6 67
Observation of prompt ISC from higher excited states of the anion of p-hydroxyacetophenone 70
Acidity of Frozen Solutions and Its Connection to Degradation of Enzymes upon Freezing 71
Study of nanoparticles formed by negatively charged hyaluroan and cationic surfactant 73
Application of CdTe-Quantum dots nanoparticles for luminiscence determinativ of metal ions 78
Nanosecond laser flash photolysis Study of rose Bengal 81
EPR-UV/Vis/NIR SpectroElectrochemical studies of substituted diarylaminothiophenes 82
EPR-UV/Vis/NIR SpectroElectrochemistry of thienyl derivatives of pyrene 85
How to measure quantitative EPR spectra reproducibly 88
Utilization of fluorescence spectroscopy for studying of the interactions in dried systems of biopolymer and hydrophobic species 91
Determination of organic acids in wine using by biosensors 95
New Kinetic Models in Biopolymer Degradation: Long Term Study of Hyaluronan Samples 99
Oxidation of and DNA adduct formation by benzo[a]pyrene by rat cytochrome p450 1A1 are stimulated by cytochrome $b_5$ and NADH 103

Aryl hydrocarbon receptor ligands benzo[a]pyrene, ellipticine and Sudan I induce expression of cytochrome p450 1A1, NAD(P)H:quinone oxidoreductase 1 and cytochrome $b_5$ 107
Determination of methylxantines on pencil graphite electrodes by cyclic voltammetry 111
Trends in development of functional nanostructured films 114
Biodegradable materials for orthopedic applications 118
An Electrochemical study of d(GCGAAGC) DNA heptamer and its sequential analogues 121
Aromatase (Cytochrome p450 19) is an efficient enzyme activating anticancer drug ellipticine 124
DFT and NMR studies of PPD antioxidants 128
Computational Insight to the Themodynamics of Double H atom abstraction in model phenolics 131
On radical anion generation upon hydrogen atom transfer in dihydroxybenzenes 134
Methylation of Humic acids – the Impact on the Reactivity Studied by Diffusion Techniques 137
Electrochemical sensor for carbonate determination 142
Formation of DNA adducts by ellipticine and its micellar form in Rats – a Comparative Study 145
The site directed mutagenesis of key aminoacids in the heme distal side of an oxygen sensor, YddV, probably converts its character from a $O_2$ sensing protein to a heme oxygenase enzyme 148
Inhibitors of cyclin-dependent kinases as new generation of anticancer drugs 151
Effect of deep freezing to quality of HEK293 Transfected with CaV 3.1 membrane channel 153
Fluorescence study of mixed micelles formation 156
Interaction of heavy metals with graphene and iron based particles 160
FIA-ED: optimization of method for electrochemical study of doxorubicin 163
Flow injection analysis with electrochemical detection for rapid identification of platinum-based cytostatics and platinum chlorides in water 166
Electrophoretic behavior of doxorubicin 169
Utilization of Electrochemistry for detection of bacteria on a 3D printed flow chip 173
Liposomal Transporter with GFP mark for Targeted Binding using a Nucleic Acid Anchor System 176
Interaction study of arsenic(III) ions with metallothionein gene (MT2a) fragment assessed by spectrometry and electrochemistry 179
Automatic Electrochemical determination of heavy metals and application to a remote-controlled robotic platform orpheus-hope 182
Microrna electrochemical detection in connection with specific magnetic separation 185
Interaction of metallothionein with CdTe quantum dots studied by electrochemistry 189
Physical chemistry of inorganic-organic nanostructures 192
Elimination square wave voltammetry 194
Device for dehydration monitoring using potassium concentration in urine measurement 197
Semiconductive $SnO_2$/MWCNTs gas sensor 200
Hight resolution technics for fabrication of special nanoelectrodes 203

# INVESTIGATION OF THE CARBON MATERIAL BASED ELECTRODES FOR SUPERCAPACITORS

Stepan I. YUSIN[1,2], Alexander G. BANNOV[2*], Anastasia A. TIMOFEEVA[2], Maria A. NEMZOROVA[2], Ksenya V. TIKHONINA[2]

[1] *Institute of Solid State Chemistry and Mechanochemistry of the Siberian Branch of the Russian Academy of Sciences, Kutateladze 18, 630098 Novosibirsk, Russian Federation*

[2] *Department of Chemistry and Chemical Technology, Faculty of Mechanics and Technology, K. Marx 20, 630 073 Novosibirsk, Russian Federation*

**bannov.alexander@gmail.com*

**Abstract**

In this work the different types carbon materials, such as carbon fibers, graphite oxide, exfoliated graphite were studied for the using as an electrode materials in supercapacitors. The capacitance of the supercapacitors depends on the surface area of the electrode material, therefore using of the carbon materials with high surface area is more effective.

## 1. INTRODUCTION

Carbon materials find their application as electrode materials or electro-conductive additives in supercapacitors and electrodes of electrochemical power source. In this work carbon fibers, graphite oxide, exfoliated graphite were used as main part of electrodes for supercapacitors [1, 2]. But the capacitance of the supercapacitors based on untreated carbon materials can be very low; therefore, this characteristic can be increased by the using of different treatment techniques. The aim of this work is the investigation of different types of carbon materials for their using as electrode materials in supercapacitors.

## 2. MATERIAL AND METHODS

Graphite oxide was synthesized from high-quality graphite by the different modification of Hummers method [3]. Exfoliated graphite was synthesized from graphite oxide. Also carbon fibers and carbon fiber composite electrodes were investigated. The composite electrodes based on a carbon fibers were prepared by following technique: the particles of metal, oxygen-containing, compounds were deposited from solutions on the Activated Carbon Fiber Material (ACFM) brand “UVIS-AK-V-240” (Russia) by electrophoresis in a controlled conditions [4]. The electrophoresis was carried out in 0,01 M colloidal solution with the particles of metals oxides and metal hydroxides. The colloidal solution passed through ACFM. The electrophoresis was performed in the constant current density of 150 $A/m^2$ by

anodic. After the electrophoresis the ACFM was carefully washed out by distilled water, dried up at 200 $^{o}$C and then electrical capacitance was studied.

The carbon materials were suggested of use as the electrodes, therefore it were investigated by the value of electrical capacitance ($C_{el}$). Voltammetric curves were obtained using Elins P-30SM analyzer (Russia) in accordance with a three electrode scheme. All electrodes were placed into the electrolyte of a 3.5 M $H_2SO_4$ solution.

## 3. RESULTS AND DISCUSSION

The results of the capacitance measurements of electrodes based on carbon fibers, carbon fiber composites, graphite oxide and exfoliated graphite are presented in Table 1. The composite electrodes carbon fiber–$Ni(OH)_2$ and –$Co(OH)_2$ that were prepared by electrophoresis, possessed higher capacitance values: maximum value that were obtained on composite material "ACFM-$Ni(OH)_2$" is 377 F/g – the 7 times higher as compared with initial ACFM fibers. The decreasing of potential scan rate induces the increasing of the capacitance. The electrical capacitance at different scanning rate depends significantly on the formation of electric double layer [5].

**Table 1**: Comparison of the different types of carbon material electrodes.

| Electrode material | $C_{el}$ (F/g) recorded at various of potential scan rate, mV/s | | | Average flow rate, ml/s | Deposition weight, g | Weight gain ω |
|---|---|---|---|---|---|---|
| | 2 | 5 | 10 | | | |
| $ACFM_{initial}$ | 52 | 39 | 30 | - | - | - |
| ACFM -$MnO_2$ | 176 | 100 | 42 | 0,010 | 0,012 | 50% |
| ACFM -$Co(OH)_2$ | 322 | 210 | 120 | 0,012 | 0,010 | 46% |
| ACFM -$Ni(OH)_2$ | 377 | 252 | 123 | 0,017 | 0,007 | 30% |
| Graphite oxide #1 | 21 | 18 | 8 | - | - | - |
| Graphite oxide #2 | 68 | 40 | 19 | - | - | - |
| Exfoliated graphite #1 (obtained from GO) | 101 | 71 | 32 | - | - | - |

Figure 1a shows that the electrophoretic particles precipitate firmly adhered to the fibers or envelops. The exfoliated graphite sample possessed lower surface as compared with carbon fibers, but this material was predominantly mesoporous and obtained 101 F/g capacitance (Figure 1b).

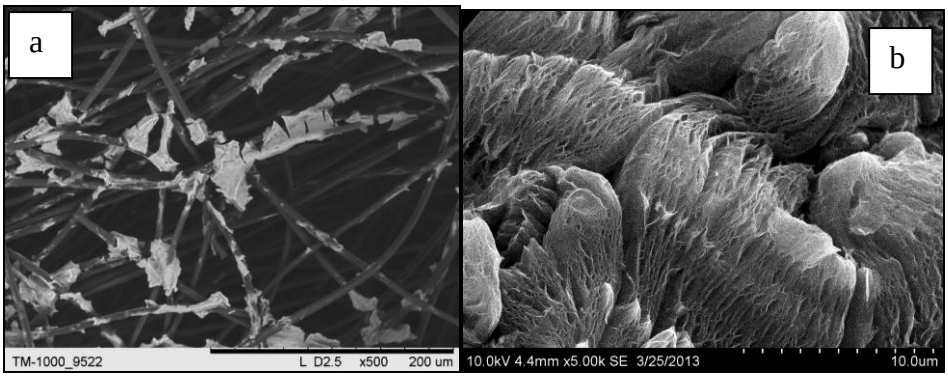


**Figure 1.:** SEM micrographs of "ACFM - $MnO_2$" (a) and exfoliated graphite (b) samples

One of the components for synthesis of graphite oxide – $KMnO_4$, therefore using of certain reagents amounts will provide the formation of $MnO_2$ on the surface of graphite oxide. The exfoliated graphite possessed higher capacitance due to formation of manganese oxide on the porous surface of the material. Therefore the capacitance of the exfoliated graphite was higher than that of for GO. The exfoliation of the graphite oxide tends to the formation of the highly porous material due to the rapid exhausting of the gases produced from surface functional groups.

## 4. CONCLUSION

The results obtained shows that the carbon materials with high surface possess high capacitance and can be used as electrode materials for supercapacitors. The capacitance can be increased by using of different types of modifications which modify the textural properties of the material and amplify the pseudocapacitance effects.

## 5. ACKNOWLEDGEMENT

The work has been supported by the Strategic Development Programme NSTU (project 3.1.2 Implemention of projects by young scientists, the project S-35).

## 6. REFERENCES

[1] Bannov A, Timofeeva A, Shinkarev V, et all.: Protection of Metals and Physical Chemistry of Surfaces, 50 (2014), 2, 183-190

[2] Jung I, Pelton M, Piner R: Nano Lett., 7 (2007), 12, 3569-3575

[3] Hummers W, Offeman R: J. Am. Chem. Soc., 80 (1958), 1339-1339

[4] Uvarov N, Mateyshina Yu, Ulihin A, et all.: ECS Transactions, 25 (2010), 21, 11-16

[5] Artem'yanov A, Sheveleva I: Russian Journal of Applied Chemistry, 7 (2004), 11, 1811-1814

# THE EFFECT OF OCHRATOXIN A ON DNA ADDUCT FORMATION BY THE CARCINOGEN ARISTOLOCHIC ACID IN RATS

Marie STIBOROVA[1*], Frantisek BARTA[1], Katerina LEVOVA[1], Petr HODEK[1], Eva FREI[2], Heinz H. SCHMEISER[3], Volker M. ARLT[4]

[1] *Department of Biochemistry, Faculty of Science, Charles University, Albertov 2030, 128 40 Prague 2, Czech Republic*

[2] *Division of Preventive Oncology, National Center for Tumor Diseases, German Cancer Research Center (DKFZ), In Neuenheimer Feld 280, 69 120 Heidelberg, Germany*

[3] *Division of Radiopharmaceutical Chemistry (E030),, German Cancer Research Center (DKFZ), In Neuenheimer Feld 280, 69120 Heidelberg, Germany*

[4] *Analytical and Environmental Sciences Division, MRC-PHE Centre for Environment and Health, King's College London, London, United Kingdom*

**stiborov@natur.cuni.cz*

**Abstract**

Exposure to the natural plant extract aristolochic acid (AA) leads to the development of aristolochic acid nephropathy (AAN), Balkan endemic nephropathy (BEN) and urothelial cancer in humans. Beside AA, exposure to the mycotoxin ochratoxin A (OTA) potentially contributes to the development of BEN. Therefore, we studied the influence of OTA on the genotoxicity of AA *in vivo*. DNA adduct formation was analyzed in liver and kidney of rats treated with AA, OTA or AA combined with OTA using the $^{32}$P-postlabelling method.

## 1. INTRODUCTION

Balkan Endemic nephropathy (BEN) is a chronic tubulointerstitial nephropathy characterized by an insidious onset and gradual progression to end-stage renal disease, which was first described more than 60 years ago. A charateristic feature of BEN is its close association with upper urothelial carcinomas (UUC) of the renal pelvis and ureter. For the past decades the majority of this research focused on various heavy metals, mycotoxins such as ochratoxin A (OTA) and organic chemicals until recently when the carcinogenic and nephrotoxic plant product aristolochic acid (AA) was identified as the main cause for the development of BEN-associated UUCs [1-5]. Nevertheless a role of the nephrotoxin OTA in the development of BEN cannot be ruled out, even though exposure to OTA was rejected as an important factor for BEN/UUC by the EU Committee on Food Safety [6]. BEN is very similar to another nephropathy, aristolochic acid nephropathy (AAN), which has been unambiguously proven to be caused by AA exposure [2,5,7,8]. In this study we investigated influence of OTA on the

genotoxicity of the plant extract AA, a natural mixture of 8-methoxy-6-nitro-phenanthro-(3,4-d)-1,3-dioxolo-5-carboxylic acid (AAI, Fig. 1) and 6-nitro-phenanthro-(3,4-*d*)-1,3-dioxolo-5-carboxylic acid (AAII) in Wistar rats *in vivo*.

## 2. MATERIAL AND METHODS

Rats were either treated separately with AA and OTA or with AA in combination with OTA, namely, *i.p.* daily for 5 consecutive days with (*i*) a dose of 10 mg/kg body weight (bw) of the natural plant extract AA, (*ii*) a dose of 2 mg/kg bw OTA and with (iii) both AA and OTA at doses mentioned above. DNA of rat liver and kidney were analyzed for the presence of AA-DNA adducts [2,7-9] and OTA-related DNA adducts [10,11] by $^{32}$P-postlabeling. DNA adduct levels (RAL, relative adduct labelling) were calculated as described [9]. AA-DNA adducts were identified using reference standards as described [9]. For OTA-related DNA adducts kidney DNA from OTA-treated Wistar rat [10,11] served as reference.

## 3. RESULTS AND DISCUSSION

Formation of AA-DNA adducts and OTA-related DNA adducts was determined by $^{32}$P-postlabeling in liver and kidney of rats treated with a total *i.p.* dose of 50 mg /kg bw of the plant extract AA (natural mixture of AAI and AAII), with a total *i.p.* dose of 10 mg/kg bw of OTA, and with both these agents together. It is noteworthy that modifications to the nuclease P1 version of $^{32}$P-postlabelling assay were made in order to detect and quantify the AA-DNA adducts [8, 9] and OTA-related DNA adducts [10,11], respectively.

Using the $^{32}$P-postlabeling assay routinely used for the detection of AA-DNA adducts, all liver and kidney samples from Wistar rats treated with AA showed an adduct pattern similar to that found in kidney tissue from BEN and AAN patients [7,8,12]. The adduct pattern consisted of three major adduct spots. Two of them have been identified as 7-(deoxyadenosin-$N^6$-yl)aristolactam I (dA-AAI) and 7-(deoxyadenosin-$N^6$-yl)aristolactam II (dA-AAII). It has been shown previously that the dA-AAII adduct can be generated from AAI and is probably formed via a demethoxylation reaction of AAI or dA-AAI [8]). Another adduct was identified as 7-(deoxyguanosin-$N^2$-yl)aristolactam I (dG-AAI) whereas 7-deoxyguanosin-$N^2$-yl)aristolactam II (dG-AAII) was not detectable. The dG-AAII adduct has been found previously at a low but detectable levels in DNA of rats treated with AAII *in vivo* or in *ex vivo* and *in vitro* experimental systems [8,9]. Therefore, deoxyadenosine is the major target of DNA modification by AA, pointing to the general importance of the dA-AAI and dA-AAII in the carcinogenic process of AA. In contrast, no adducts were found in DNA of control rats treated with vehicle only.

When samples were chromatographed under conditions suitable for the detection of OTA-related adducts [10,11], all three purine AA-DNA adducts were also well separated and none of the AA-DNA adducts migrated in the area of the thin-layer chromatography plate where OTA-related DNA adduct spots would be located. The levels of AA-DNA adducts determined by this method were similar to those found by the $^{32}$P-postlabeling version routinely used for the detection AA-DNA. However, in contrast, no OTA-related DNA adducts were detectable in rats treated with OTA alone. Likewise, no OTA-related DNA adducts were found in liver and kidney of rats treated with AA together with OTA whereas AA-DNA adducts were clearly detectable in these samples and identified as described above.

Generally, in all rats AA-DNA adduct levels were higher in kidney, the target organ of AA genotoxicity, than in liver. In both organs the levels of AA-DNA adducts increased when AA treatment was combined with the OTA exposure. Compared to adduct levels found in rats treated with AA alone, DNA binding was 5.4- and 1.6-fold higher in liver and kidney, respectively, than in rats treated with both AA and OTA. Therefore, OTA, when administered to rats with AA, induces pathways which lead to a higher bioactivation of AA in both organs.

## 4. CONCLUSION

The results are the first findings strongly suggesting a potency of OTA when administrated together with AA during exposure to contribute to the BEN/UUC development.

## 5. ACKNOWLEDGEMENT

The work has been supported by GACR (P303/10/G163) and Charles University (grant 570513).

## 6. REFERENCES

[1] Arlt V.M., Ferluga D., Stiborova, M. et al.: International Journa of Cancer, 101 (2002) 500-502.

[2] Arlt VM, Stiborova M, vom Brocke J, et al.: Carcinogenesis 28 (2007), 2253-2261

[3] Grollman A.P., Shibutani S., Moriya M., et al.: Proceedings of American Chemical Society U.S.A., 104 (2007), 12129-12134

[4] Jelaković B, Karanović S, Vuković-Lela I, et al.: Kidney International, 81 (2012) 559-567.

[5] Gökmen M.R., Cosyns J.P., Arlt, V.M. et al.: *Annals of Internal Medicine*, 158 (2013) 469-477.

[6] EFSA: EFSA Journal, 365 (2006) 1-56.

[7] Nortier J.L., Martinez M.C., Schmeiser H.H., et al.: New England Journal of Medicine, 342, (2000 1686-1692.

[8] Arlt V.M., Stiborova M., Schmeiser, H.H.: Mutagenesis, 17 (2002) 265-277.

[9] Schmeiser HH, Stiborova M, Arlt VM: Current Opinion in Drug Discovery and Development, 12 (2009), 141-148

[10] Pfohl-Leszkowicz A., Grosse Y., Castegnaro M., et al.: IARC Science Publications 124 (1993) 141 -148.

[11] Arlt VM, Pfohl-Leszkowicz A, Cosyns J, et al.: Mutation Research, 494 (2001) 143-150.

[12] Schmeiser HH, Kucab JE, Arlt VM,, et al.: Environmental and Molecular Mutagenenesis, 53 ( 2012) 636-641.

# ROLE OF RAT CYTOCHROMES P450 IN OXIDATION OF 17α-ETHINYLESTRADIOL

Lucie BOREK-DOHALSKA, Petra VALASKOVA, Vera CERNA and Marie STIBOROVA

*Department of Biochemistry, Faculty of Science, Charles University, Albertov 2030, 128 40 Prague 2, Czech Republic*

**Abstract**

17α-ethinylestradiol (EE2) is an endocrine disruptor that is a key active ingredient used in a variety of oral contraceptives. The objective of the present study was to determine a role of individual rat CYP enzymes in EE2 oxidation. The contribution of CYPs in EE2 hydroxylation was investigated using specific inhibitors and/or inducers of individual CYPs. Moreover, the heterologous baculovirus expression systems of rat CYPs (Supersomes™) were used for studying EE2 oxidation. The results found in this work suggest that EE2 is a promiscuous substrate of rat hepatic CYPs, among them the CYP3A and 2C enzymes seem to be most efficient.

## 1. INTRODUCTION

The oxidative metabolism of EE2 has been studied extensively. It undergoes hydroxylation at the 2, 4, 6, and 16 α position of the steroid nucleus [1, 2]. The predominant route of the EE2 oxidative metabolism in both rat and human is its 2-hydroxylation [3]. A 2-hydroxyEE2 derivative can be subsequently methylated to give 2-methoxyethinylestradiol [2]. EE2 oxidation represents only a small portion of the total EE2 metabolism, which can occur by way of glucuronidation, methylation or sulfation [3].

The cytochrome P450 (CYP) enzymes play a major role in hydroxylation of EE2. In early studies with antibody inhibition, CYP3A4 was reported as the major enzyme involved in oxidation of EE2 in human liver [4]. Wang et al. [5] describe the CYP2C9 and 3A4 enzymes predominantly contributing to the 2-hydroxylation of EE2 in human liver microsomes. The authors also showed that recombinant CYP1A1, a predominantly extrahepatic CYP isozyme, exhibited higher intrinsic catalytic activity than recombinant CYP3A4 and/or 2C9. Using immunoinhibitory CYP antibodies, Ball et al. [2] found that CYP2C and 2E could be involved in the 2-hydroxylation of EE2. However, in contrast to the results found by Wang et al. [5], Ball et al. [2] postulated that CYP1A1 does not play an important role in EE2 metabolism.

Since the discrepancies in data identifying CYP enzymes that participate in oxidation of EE2, the aim of the present study was to extend our knowledge on this issue. The rat was used in the study as a suitable model to measure EE2 oxidation in human [6].

## 2. MATERIALS AND METHODS

Incubation mixtures contained in a final volume of 0.5 ml: 0.1 M potassium phosphate buffer, pH 7.4, 50 μM EE2, 50 μl of NADPH-generating system and 0.5 μM microsomal CYP or rat recombinant CYPs (50 pmol). The mixtures were incubated for 15 min at 37$^{o}$ C. The reaction was terminated by addition of 1 ml of ethyl acetate. The metabolites were extracted and the extracts were evaporated to dryness. The residues were dissolved in the mobile phase for HPLC. EE2 and its metabolites were separated on Nucleosil column (C18, 4.6 x 250 mm, 5 μm) with optimalized linear gradient elution. The mobile phase consisted of solvent A (20% acetonitrile) and solvent B (80% acetonitrile). Detection wavelenght and temperature used in a HPLC separation were 280 nm and 35 °C, respectively .

## 3. RESULTS AND DISCUSSION

When 50 μM EE2 was incubated with rat hepatic microsomes in the presence of NADPH, three metabolite products were formed and separated by HPLC, which were characterized to be the X-OH EE2, 2-OH EE2 and a dehydrogenated metabolite of EE2.

To resolve which rat CYP enzymes are responsible for oxidation of EE2, three different approaches were used: (i) the use of CYP inducers, (ii) specific inhibitors of individual CYPs, and (iii) the use of heterologous baculovirus expression systems of rat CYPs (Supersomes$^{TM}$).

Add (i). An increase in formation of X-OH EE2 was formed in microsomes, in which CYP2B/2C and 3A were induced by phenobarbital and PCN, respectively. Other inducers of CYPs were found to decrease formation of this metabolite. Formation of 2-OH EE2 was increased by pretreatment of rats with EtOH and PB indicating that CYP2B/2C and 2E1 might be involved in 2-hydroxylation of EE2.

Add (ii). The inhibition effect was studied using two different protocols. In the first one, the reaction mixtures containing microsomes and a specific inhibitor were incubated 10 min in the presence of NADPH before an addition of EE2. In the other protocol, specific inhibitors were pre-incubated with microsomes for the same time interval, but without NADPH.

All tested inhibitors used in the study decreased oxidation of EE2 to X-OH EE2. Essentially no changes in inhibitory capacity of α-naphtoflavone and ketoconazole were detectable using both experimental protocols. This indicated reversible inhibition of X-OH EE2 formation by these compounds. In contrast to these results, the inhibitory potency of diethyldithiocarbamate (DDTC) and adamantane increased after their preincubation with NADPH and microsomes. These results indicate that during pre-incubation of DDTC and

adamantane with microsomes and NADPH the reactive intermediates modifying CYP2B and 2E1 activities with respect to X-OH formation are formed.

Inhibition of 2-hydroxylation of EE2 was produced by adamantane and ketoconazole using the type of the inhibition protocol, where the reaction mixtures containing microsomes and a specific inhibitor were incubated in the absence of NADPH before an addition of EE2. However, under these conditions almost 1.5- fold increase in amounts of 2-OH EE2 were caused by α-NF, a compound known to stimulate CYP3A activities [7,8], sulphaphenazole and DDTC, respectively. Using the second type of inhibition protocol, EE2 oxidation to 2-OH EE2 was also inhibited by adamantane and ketoconazol. A higher degree of inhibition of 2-OH EE2 formation was mediated by the pre-incubation of these inhibitors in the presence of NADPH. All these results indicated an important role of CYP3A in 2-hydroxylation of EE2, but CYP2B and 2E1 could be also involved.

Add (iii). Using Supersomes$^{TM}$, except of the rat CYP1A1 and 2D2 enzymes, other recombinant CYPs used in the experiments oxidized EE2 to X-OH metabolite. Amounts of X-OH EE2 formed by these CYPs were, however, almost 10-times lower than those generated by hepatic microsomes. In the case of EE2 oxidation to 2-OH EE2, only CYP2A2, 2C6, 2D1 and 3A1/2 catalyzed this reaction. Only a degree of EE2 hydroxylation to this metabolite by CYP2A2 was similar to that found in hepatic microsomes.

## 4. CONCLUSION

The results found in this study indicate that EE2 is a substrate of various rat hepatic CYPs that exhibit different efficiencies in oxidation of this endocrine disruptor.

## 5. ACKNOWLEDGEMENT

The work has been supported by GACR (14-18344S in panel P301) and Charles University in Prague (UNCE 204025/2012).

## 5. REFERENCES

[1] Back D. J., Maggs J. L., Purba H. S., et al.: British Journal of Clinical Pharmacology 18 (1984), 603-607.

[2] Ball S.E., Forrester L.M., Wolf C.R., et al.: Biochemical Journal 267 (1990), 221-226.

[3] Ebner T., Remmel R.P. Burchell, B.: Molecular Pharmacology 43 (1993), 649-654.

[4] Guengerich, F.P., 1988.: Molecular Pharmacology 33 (1988), 500-508.

[5] Wang B., Sanchez R.I., Franklin R.B., et al.: Drug Metabolism and Disposition 32 (2004), 1209-1212.

[6] Laurenzana E.M., Weis C.C., Bryant C.W., et al: Food and Chemical Toxicology 40 (2002), 53-63.

[7] Bořek-Dohalská L., Hodek P., Sulc M., et al.: Chemical and Biological Interaction 138 (2001), 85-106.

[8] Bořek-Dohalská L., Stiborová M.: Collection of Czechoslovak Chemical Communication 75 (2010), 201-220.

# STRUCTURE AND SPECTROSCOPIC CHARACTERIZATION OF COPPER(II) COMPLEXES WITH FLUOROQUINOLONES

Sandra DOROTÍKOVÁ*, Júlia KOŽÍŠKOVÁ, Peter HERICH, Marek FRONC, Lukáš BUČINSKÝ, Dana DVORANOVÁ

*Institute of Physical Chemistry and Chemical Physics, Faculty of Chemical and Food Technology, Slovak University of Technology in Bratislava, Radlinského 9, SK-812 37 Bratislava, Slovak Republic*

**sandra.dorotikova@stuba.sk*

**Abstract**

Copper complexes of fluoroquinolones in the presence and 1,10-phenanthroline have been synthesized and characterized with X-ray, IR and UV-VIS spectroscopy and also by quantum chemical calculations.

## 1. INTRODUCTION

Fluoroquinolones (FQs) possess variety of biological activities including antimicrobial, antiviral (anti-HIV) and antimalarial effects. Moreover, FQs have been demonstrated to possess antitumor activity hand in hand with interesting mechanical effect on the DNA. Nowadays, the attention turns to the synthesis metal complexes with FQs and a nitrogen donor heterocyclic ligand, which increases the biological activity [1]. Thus, this work is focused on the structure, synthesis and spectroscopic characterization of four copper(II) complexes with FQs and 1,10-phenatroline (phen) and compared with theoretical calculations.

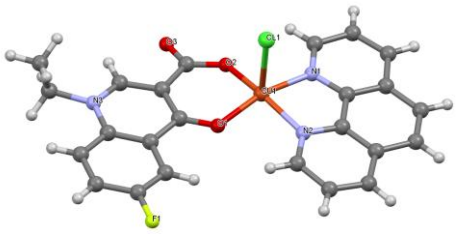

**Figure 1.:** Structure of [Cu(FQ)(phen)Cl]; FQ=6-fluoro-4-oxo-1,4-dihydro-quinolone -3-carboxilate

## 2. MATERIAL AND METHODS

The UV-VIS spectra of the studied complexes were measured in methanol (MeOH) and $H_2O$ by means of UV-3600 UV-VIS-NIR spectrometer (Shimadzu, Japan) in a 1 cm square quartz cell. Infrared spectra in the region 4000-700 $cm^{-1}$ were recorded with the Nicolet model Nexus 470 FT-IR spectrometer at room temperature using reflectance ATR technique. X-ray diffraction data were collected on Oxford Diffraction Gemini R diffractometer equipped with Ruby CCD detector and Mo Kα sealed-tube source at 100K or room temperature. The quantum chemical calculations were performed using Gaussian03 program package [2]. The copper complexes were studied at B3LYP/6-311G* theoretical level. Integral Equation

Formalism Polarizable Continuum Model (IEFPCM) in solvent applied MeOH and $H_2O$ was also taken into account. For all compounds under study the optimal geometries were calculated; including IR line spectra and electron transitions using TD DFT treatment were computed to all studied compounds.

## 3. RESULTS AND DISCUSSION

All complexes exhibit a d–d transition band in the UV–VIS spectra at 640 nm, typical for a distorted square pyramidal geometry. In the IR spectra of the complexes, the replacement of the valence stretching carboxylic vibration $\nu(C{=}O)_{carb}$ of fluoroquinolones at 1672-1720 $cm^{-1}$ by the asymmetric, $\nu(CO_2)_{asym}$, at 1587-1602 $cm^{-1}$ and the symmetric stretching $\nu(CO_2)_{sym}$, in the range 1364-1387 $cm^{-1}$ are indicative that fluoroquinolone ligand is coordinated to the metal via pyridone (O1) and carboxylate oxygen (O2) atoms (see Fig. 1). It was found, that the copper atom is five-coordinated, which confirmed the X-ray and quantum chemical calculations. The slightly distorted square pyramid geometry is built of a bidentate coordination of FQ and phen and a monodentate $Cl^-$ (and/or $H_2O$).

## 4. CONCLUSION

The structure and spectroscopic characterization of four copper complexes with the new FQs in the presence of phenantroline, has been studied experimentally and theoretically. In all complexes was found the formation of the neutral mononuclear complex.

## 5. ACKNOWLEDGEMENT

This work was financially supported by the Research and Development Agency of the Slovak Republic under the contracts No. APVV-0202-10 and APVV-0339-10 and the Scientific Grant Agency (VEGA Project 1/0289/12 and 1/0679/11). The calculations were performed at HPC center, SUT Bratislava (SIVVP project, ITMS code 26230120002, funded by the European region development funds) and Computing Centre SAS, code 26210120002 (Slovak infrastructure for high-performance computing) supported by the Research & Development Operational Programme funded by the ERDF. Kristína Plevová and Viktor Milata are gratefully acknowledged for synthesis of investigated derivatives.

## 6. REFERENCES

[1]Psomas G, Tharusi A, Efthimiadou K. E, et all.: Journal of Inorganic Biochemistry, 100 (2006), 1764-1773

[2]Frisch M.J., et al.: Gaussian 03, Revision C.02; Gaussian, Inc., Wallingford CT, (2004).

# NAD(P)H:QUINONE OXIDOREDUCTASE 1 IS INDUCED BY 3-NITROBENZANTHRONE, ARISTOLOCHIC ACID, ELLIPTICINE, SUDAN I AND DICOUMAROL IN RATS - A COMPARATIVE STUDY

Marie STIBOROVÁ[1*], Helena DRAČÍNSKÁ[1], Michaela MOSEROVÁ[1], Iveta MRÍZOVÁ[1], Věra ČERNÁ[1], Eva FREI[2]

[1] *Department of Biochemistry, Faculty of Science, Charles University in Prague, Albertov 6, 128 43 Prague 2, Czech Republic*

[2] *Division of Preventive Oncology, National Center for Tumor Diseases, German Cancer Research Center (DKFZ), Im Neuenheimer Feld 280, 69 120 Heidelberg, Germany*

**stiborov@natur.cuni.cz*

**Abstract**

Utilizing the Western blotting and the real-time polymerase chain reaction methods, expression of NAD(P)H:quinone oxidoreductase 1 (NQO1) protein and its mRNA, respectively, was found to be induced by treating rats with 3-nitrobenzanthrone (3-NBA), the plant extract aristolochic acid (AA), AAI, ellipticine, Sudan I and dicoumarol. Because these chemicals induced the expression levels of NQO1 essential for metabolism dictating biological activities of a variety of toxic xenobiotics including three of these inducers (3-NBA, AA and AAI), they exert concerted regulatory control on their own genotoxic effects as well as on potential toxic effects of numerous other environmental chemicals.

## 1. INTRODUCTION

Genotoxic effects of most carcinogens and pharmacological efficiencies of many drugs are dependent on their metabolic activation. Although a majority of such xenobiotics is activated by oxidative reactions, participation of reductive metabolism in activation of xenobiotics is unquestionable. Knowledge of enzymes participating in such reductive activations is crucial for many reasons. For example, it is important for elucidation of the fate of protoxicants and procarcinogens, which become toxic after their reductive activation in organisms. Furthermore, it is essential for the development of an ideal cancer chemotherapeutic prodrug, which would be fully inactive until reductively metabolized by tumor-specific enzymes, or by an enzyme that is metabolically competent only for the prodrug under physiological conditions and is unique for the tumor. An enzyme system that fulfils one or both of these criteria might be the cytosolic enzyme, NAD(P)H:quinone oxidoreductase (NQO1; EC

1.6.99.2.). In general, NQO1 activity is higher in tumors than in the surrounding normal tissues [1,2].

The obligatory two-electron reduction of quinones catalyzed by NQO1 circumvents the semiquinone stage and thereby prevents redox cycling and alkylation by these highly reactive compounds [1,2]. Likewise, reductive activation of numerous other compounds such as toxic chemicals (azo dyes and nitroso- or nitroaromatics) or anticancer drugs (e.g. prodrugs mitomycin C and indoloquinone EO9) was discovered as a function of NQO1 [1-3]. Expression and activities of NQO1 and/or other biotransformation enzymes (induction and/or repression) might be essential for their fate in organisms as well as for their toxic or pharmacological efficiencies. The NQO1 enzyme is inducible by a variety of agents [1,2]. Two distinct regulatory elements in the 5'-flanking region of the *NQO1* gene that have been studied extensively are the antioxidant response element (ARE), also called the electrophile response element (EpRE), and the xenobiotic response element (XRE), also called aryl hydrocarbon response element (AhRE). The ARE and the XRE have been shown to mediate NQO1 induction as well as repression, in many cellular systems. Induction through the XRE involves the liganded aromatic hydrocarbon receptor (AhR). ARE-mediated *NQO1* gene expression is increased by a variety of antioxidants, tumor promoters and hydrogen peroxide [1,2]. Nuclear factor-erythroid 2 (NF-E2) related factor 2 (Nrf2) is a basic leucine zipper transcriptional factor that plays a key role in ARE-mediated *NQO1* gene expression [1,2].

The aim of the present study was to compare a potency of several chemicals with different structure to induce NQO1 in liver and kidney of rats.

## 2. MATERIAL AND METHODS

Male Wistar rats were treated intraperitoneally or by a gavage with 3-NBA, the plant extract AA, AAI, ellipticine, Sudan I and dicoumarol as described previously [5-8]. Cytosols were isolated from the livers and kidneys of this animal model [5-8]. The method of Western blot, employing an anti-rat NQO1 antibody, was utilized to evaluate expression of this enzyme. Its mRNA content in rat liver and kidney measured using the real-time polymerase chain reaction (RT-PCR) and measurements of NQO1 enzyme activity were also carried out [5-8].

## 3. RESULTS AND DISCUSSION

Using a method of Western blotting with an antibody raised against rat NQO1 and the RT-PCR, the effects of exposure of rats to 3-NBA, the plant extract AA, AAI, ellipticine, Sudan I and dicoumarol on mRNA and protein expression levels of these proteins were analyzed. We

found that these compounds were inducers of NQO1 in liver and kidney of rats both at the transcriptional and translational levels. Up to more than 20-fold increases in NQO1 protein expression levels were produced by treatment of rats with these compounds. Of them the highest induction effect was caused by AA, followed by 3-NBA > Sudan I > ellipticine > AAI > dicoumarol. The increase in protein levels was paralleled by an increase in mRNA expression in most cases. In addition, an increased NQO1 enzyme activity of this enzyme, measured either with menadione or 3-NBA, AA and AAI as substrates, corresponded to an induction potency of individual tested xenobiotics. Even though the mechanisms of NQO1 induction by these xenobiotics are still not clearly explained, it can be suggested that, depending on the compound, both the ARE and the XRE might be capable of mediating the induction of NQO1 found in this work. Nevertheless, the detailed studies investigating the mechanisms of NQO1 induction by the tested chemical are needed to be performed and are planned to be carried out in our laboratory.

## 4. CONCLUSION

Utilizing the Western blotting method, expression of NQO1 protein was found to be induced by treating rats with 3-NBA, the plant extract AA, AAI, ellipticine, Sudan I and dicoumarol. Since these compounds induced the expression levels of NQO1 that is essential for the metabolism of some of them, dictating their carcinogenic efficienceies (3-NBA, AA, AAI), these compounds exert concerted regulatory control on their own genotoxic and carcinogenic effects.

## ACKNOWLEDGEMENT

The work has been supported by Grant Agency of the Czech Republic (14-18344S in panel P301) and Charles University in Prague (UNCE 204025/2012 and 570513).

## 5. REFERENCES

[1]Ross D., Kepa J.K., Winski S.L., et al.: Chemico-Biological Interactions, 129 (2000), 77-97.

[2]Ross D.: Drug Metabolism Review, 36 (2004) 639-654.

[3]Patterson L.H., McKeown S.R., Robson T., et al.: Anti-cancer Drug Design, 14 (1999), 473-486.

[4]Stiborová M., Dračínská H., Hájková J., et al.: Drug Metabolism and Disposition, 34 (2006), 1398-1405.

[5] Stiborová M., Dračínská H, Aimová D., et al.: Collection of Czechoslovak Chemical Communications, 72 (2007), 1350-1364.

[6]Mizerovská J., Dračínská H., Frei E., et al.: Mutation Research, 720 (2011), 34-41

[7] Stiborová M, Dračínská H, Martínek V, et al.: Chemical Research in Toxicology, 25 (2013), 290-299.

[8]Stiborová M., Levová K., Bárta F., et al.: Mutagenesis, 29 (2014), 189-200.

# STUDY OF STRUCTURE AND CHEMICAL COMPOSITION OF SOIL HUMIC SUBSTANCES ISOLATED FROM HUMIC PODZOL

Vojtěch ENEV[1*], Martina KLUČÁKOVÁ[1], František NOVÁK[2]

[1] *Centre for Materials Research, Faculty of Chemistry, Brno University of Technology, Purkyňova 118, 612 00 Brno, Czech Republic*

[2] *Biology Centre AS CR v.v.i., Institute of soil Biology, Na sádkách 7, 370 05 České Budějovice, Czech Republic*

**xcenev@fch.vutbr.cz*

**Abstract**

The aim of this work was study chemical composition and structure of soil humic substances (HS). Object of our study were three samples HS which were isolated from Humic Podzol (locality Krkonoše, Czech Republic). Isolation of HS was performed according to the procedure recommended by the International Humic Substances Society. All samples of HS were characterized by elemental analysis (EA), ultraviolet-visible spectroscopy (UV/Vis), infrared spectroscopy (FTIR) and steady-state fluorescence spectroscopy. Absorption coefficients ($E_{ET}/E_{Bz}$, $E_2/E_3$ and $E_4/E_6$) of HS were calculated from the absorbance values. Fluorescence coefficients (*Milori index* and *Zsolnay index*) of HS were calculated from the area of the emission spectra.

## 1. INTRODUCTION

Humic substances (HS) are a major component of natural organic matter (NOM) and are the dominant products of plant and animal degradation by microbial activity. HS, the main organic constituents of soil and sediments are widely distributed over the earth's surface, occurring in almost all terrestrial and aquatic environments. Humic substances are complex mixtures of high to low molecular weight species, so they are polydisperse systems with a specific distribution of molecular weights. From a theoretical viewpoint, a better knowledge of the chemical structure of HS is fundamental in order to more fully understand a great number of natural processes occurring in natural ecosystems, such as the dynamics of different elements, principally micronutrients, the transport of xenobiotics or the development of plants and microorganisms; as well as those question related to the chemical features of HS. The following spectroscopic techniques are prominent among those used for characterization of HS: UV/Vis spectroscopy, Fourier-transform infrared spectroscopy (FTIR)

and fluorescence spectroscopy. In addition to those techniques, fluorescence spectroscopy has also been used in the study of HS [1].

## 2. MATERIAL AND METHODS

The objects of our study were three different samples of HS. HAs and FA were isolated from Humic Podzol (locality Krkonoše, Czech Republic). UV-VIS spectra of aqueous solutions were measured by spectrophotometer Hitachi U-3900 in the wavelength range of 200–900 nm. Absorption coefficients ($E_{ET}/E_{Bz}$, $E_2/E_3$ and $E_4/E_6$) of HS were calculated from the absorbance of aqueous solutions HS in UV/Vis spectral range. The Fourier transform infrared spectra (FTIR) of HS were recorded over the range of 4000–400 $cm^{-1}$ on pellets obtained by pressing under reduced pressure a mixture of 1 mg of samples and 400 mg of dried KBr, spectrometry grade. A Nicolet *iS*50 FTIR spectrophotometer operating with a peak resolution of 4 $cm^{-1}$, and 128 scans were performed on each acquisition. Nicolet Omnic software was used to obtain the spectra. For the fluorescence experiments the final concentration of the HAs was adjusted to 10 $mg \cdot dm^{-3}$. The pH-value of the samples was adjusted to seven using a standard phosphate buffer. Total luminescence spectra (TLS) were obtained in the form of excitation/emission matrix (EEM) by scanning the wavelength emission over the range of 300–600 nm, also the excitation wavelength was in 5 nm steps from 240 to 550 nm. The following fluorescence coefficients were obtained: (*i*) *Milori index*: Emission spectra were collected over the range of 460–650 nm using an excitation wavelength of 440 nm, and the total area under these spectra was calculated [2]. (*ii*) *Zsolnay index* (HIX): HIX is calculated from the ratio of two integrated regions of an emission scan (sum from $\lambda_{Em}$ 435–480 nm divided by the sum from $\lambda_{Em}$ 300–345 nm) using a fixed excitation ($\lambda_{Ex}$ 254 nm) [3].

The fluorescence intensity ($I_F$) values (in CPS/MicroAmp.) of samples were corrected using method of Lakowicz [4]. The correction method of Lakowicz uses:

$$F_{corr} = F_{obs} \times 10^{\left[\left(\frac{A_{em}+A_{ex}}{2}\right)\right]}, \quad (1)$$

where $F_{corr}$ and $F_{obs}$ are the corrected and uncorrected fluorescence intensities and $A_{ex}$ and $A_{em}$ are the absorbance values at the current excitation and emission wavelengths. The path of the exciting light is assumed to be equal to the path of the emitted light. Primary inner filter effects are corrected as well as secondary inner filter effects.

## 3. RESULTS AND DISCUSSION

The values of the different indexes calculated from the UV-VIS spectra ($E_{ET}/E_{Bz}$, $E_2/E_3$ and $E_4/E_6$) and elemental composition are presented in Table 1. The higher values of ratio $E_{ET}/E_{Bz}$ of A55 HA (Humic Podzol) may be indicative of the presence of *O*-containing functional

groups (hydroxyl, carbonyl, carboxyl and ester groups). Calculated value of humification index (ratio $E_4/E_6$) was lower for A55 HA isolated from Humic Podzol, which show on "*light brown*" HA with higher molecular mass. The high values of humification index for HS isolated from organic horizon (A15 w HA and A15 w FA) confirmed the presence of HS with lower molecular mass and humification degree. Absorption coefficients $E_2/E_3$ of HS are in good agreement with calculated values of index $E_4/E_6$.

**Table 1:** Elemental composition (weight %) and absorption coefficients ($E_{ET}/E_{Bz}$, $E_2/E_3$ and $E_4/E_6$) of HS

| HS samples | C [%] | H [%] | N [%] | S [%] | O [%] | P [%] | ash [%] | $E_{ET}/E_{Bz}$ | $E_2/E_3$ | $E_4/E_6$ |
|---|---|---|---|---|---|---|---|---|---|---|
| A55 HA | 42.91 | 4.30 | 4.00 | – | 30.52 | 1.08 | 17.19 | 0.76 | 2.82 | 5.62 |
| A15 w HA | 55.80 | 5.36 | 1.93 | – | 35.55 | – | 1.37 | 0.47 | 3.18 | 8.71 |
| A15 w FA | 50.49 | 4.71 | 0.89 | – | 37.96 | – | 5.95 | 0.53 | 3.76 | 11.30 |

All spectra feature common and distinctive absorption bands, with some differences in their relative intensity. The main characteristics of these spectra are the following: about 3400–3300 $cm^{-1}$ (O–H stretching and, secondarily, N–H stretching of various functional groups); about 2935–2925 $cm^{-1}$ (asymmetric C–H stretching or of $CH_2$ groups); about 1720–1710 $cm^{-1}$ (C=O stretching of COOH), whose higher relative intensity was determined for FA; 1620–1600 $cm^{-1}$ (aromatic C=C skeletal vibrations, C=O of strongly H-bonded conjugated ketones, whose higher intensity were determined for HAs; about ≈1510 $cm^{-1}$ (preferentially ascribed to simple aromatic C=C vibrations, N–H deformation and, C=N stretching of amides); about 1420 $cm^{-1}$ (O–H deformation and C–O stretching of phenolic OH); about ≈1380 $cm^{-1}$ (C–H deformation of $CH_2$ and $CH_3$ groups, and/or asymmetric stretching of $COO^-$ groups); about 1270–1260 $cm^{-1}$ (C=O stretching of aryl esters), whose higher intensity were detected for HAs (A15 w HA and A15 w FA); about 1220 $cm^{-1}$ (C–O stretching of aryl ethers and phenols); 1130–1080 $cm^{-1}$ (C–O stretching of secondary alcohols and/or ethers); and, finally, about 1045–1041 $cm^{-1}$ (C–O stretching of polysaccharides or polysaccharide-like substances, and/or Si–O of silicate impurities). The results provided by FTIR spectroscopy are in good agreement with elemental analysis and UV/Vis spectroscopy.

The values of the fluorescence intensity and excitation-emission wavelength pair of the main peaks in the EEM spectra and fluorescence coefficients of HS are presented in Table 2. The fluorescence EEM spectrum of A15 w HA was characterized by two unique fluorophores centered at an excitation/emission wavelength pair (EEWP) of 275/425 nm (*peak A*) and 380/450 nm (*peak C*). The fluorescence EEM spectrum of A55 HA was characterized by three unique fluorophores centered at an excitation/emission wavelength pair (EEWP) of

270/500 nm (*peak A*), 360/500 nm (*peak $C_1$*) and 445/510 nm (*peak $C_2$*). The long wavelength and less fluorescence intensity of the major peaks of HAs may be ascribed to the presence of an extended, linearly-condensed aromatic ring network, and other unsaturated bond systems capable of a great degree of conjugation in large molecular size and extensively humified "macromolecules". The fluorescence EEM spectrum of A15 w FA were located by three fluorescence maxima at an excitation/emission wavelength pair of 250/430 nm (*fulvic-like*), 310/430 nm (*humic-like*) and 270/310 nm (*tyrosine-like*) which are typical for terrestrial origin. On the contrary, the prevalence of fluorescence bands and peaks with high relative intensity at short wavelengths, such as those measured for the peaks of FA, is associated with the presence of simple structural components of wide molecular heterogeneity and small molecular weight, small degree of aromatic condensation, small level of conjugated fluorophores, and small humification degree.

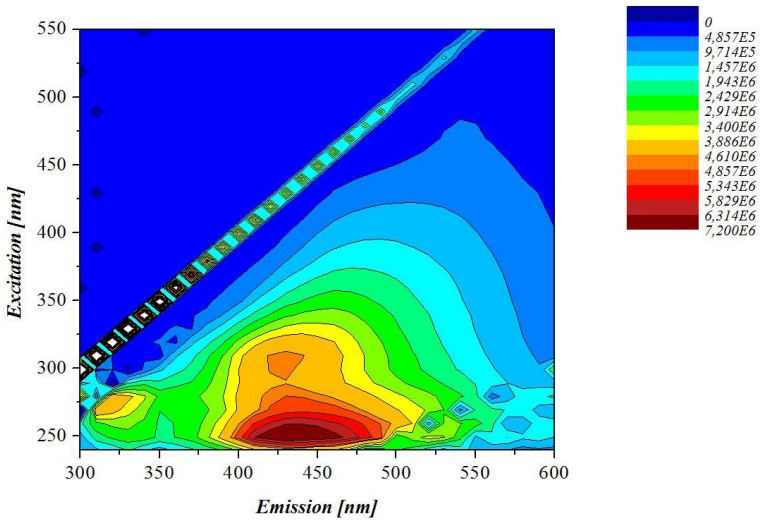


**Figure 1:** Excitation-emission spectrum of fulvic acid isolated from organic horizon of soil Humic Podzol

**Table 2:** Position of excitation-emission wavelength pair of the main peaks in the EEM spectra and values of fluorescence intensity these fluorescence peaks of HS

| sample HS | peak fulvic-like | | peak humic-like | | peak tyrosine-like | |
|---|---|---|---|---|---|---|
| | EEWP [nm] | $I_F$ [CPS] | EEWP [nm] | $I_F$ [CPS] | EEWP [nm] | $I_F$ [CPS] |
| A55 HA | 270/500 | 6408185 | 360/500 | 2153173 | – | – |
| | | | 445/510 | 1611386 | | |
| A15 w HA | 275/425 | 3937767 | 380/450 | 1015414 | – | – |
| A15 w FA | 250/430 | 7039711 | 310/430 | 4764966 | 270/310 | 4606052 |

Also, values of *Zsolnay* and *Milori index* of HS are in agreement with previous results.

## 4. CONCLUSION

Our results showed that the chemical properties of the different HS used in these experiments were well described using five complementary indexes derived from the ultraviolet-visible and fluorescence spectra ($E_{ET}/E_{Bz}$ ratio, $E_2/E_3$ ratio, $E_4/E_6$, *Zsolnay* and *Milori index*). Soil

A55 HA was characterized high molecular weight, low molecular heterogeneity, high degree of aromatic polycondensation, high level of conjugated fluorophores, and high humification degree. HS isolated from organic horizon were characterized lower molecular mass, simple structural components of wide molecular heterogeneity, lower degree of aromatic polycondensation, and lower humification degree.

## 5. ACKNOWLEDGEMENT

This work has been supported by Ministry of Education, Youth and Sports, Project LO1211.

## 6. REFERENCES

[1]Stevenson F. J, Humus Chemistry: Genesis, Composition, Reactions. Wiley-Interscience, New York.

[2]Milori D, Martin-Neto L, et all.: Soil Science, 167 (2002), 739–749

[3]Zsolnay A, Baigar E, et all.: Chemosphere, 38 (1999), 45–50

[4]Lakowicz, J. 2006. Principles of fluorescence spectroscopy. 3rd ed. New York: Springer.

# EFFECT OF BITUMEN ON SORPTION PROPERTIES OF LIGNITE

Leoš DOSKOČIL[1], Vojtěch ENEV[1*], Miloslav Pekař[1]

[1] *Centre for Materials Research, Faculty of Chemistry, Brno University of Technology, Purkyňova 118, 612 00 Brno, Czech Republic.*

**xcenev@fch.vutbr.cz*

**Abstract**

The effect of bitumen on sorption properties of the South Moravian lignite was investigated. Methylene blue and copper ion were selected as sorbates for sorption tests. The absence of bitumen in lignite resulted in a higher sorption efficiency of copper ions and a lower one of methylene blue compared with lignitem before the extraction with chloroform.

## 1. INTRODUCTION

Lignite is young coal with a high content of water, oxygen, humic acids (up to 70 wt%) and with low caloric value. It could not be therefore viewed as a fuel but rather as a valuable natural product and chemical raw material. Hence, lignite can be used as a sorbent of heavy metals, dyes etc. From water [1].

Bitumen represents an extractable non-polar part of lignite which is formed by predominantly aliphatic structures, in smaller degree aromatic molecules and functional groups comprising carboxyl acids, esters, ethers, alcohols and highly conjugated carbonyl groups [2].

Sorption of methylene blue on lignite is explained by ion-exchange interactions through positive charge of nitrogen (alternatively sulphur) of molecule and/or carboxyl, phenol groups [3, 4]. Similarly, mechanism of sorption of heavy metals on lignite is explained by ion-exchange interactions and the formation of metal complexes [5, 6].

The objective of this work is to determine the effect of bitumen on sorption properties of lignite using methylene blue and copper ions as sorbates.

## 2. MATERIAL AND METHODS

Lignite (Mikulčice, Czech Republic) was used in its natural state before and after the extraction with chloroform. By Soxhlet extraction with $CHCl_3$, bitumen was obtained from lignite. The size fraction of samples less than 0.2 mm was used for sorption tests.

Sorption procedure was performed for this study as follows: 0.1 g of samples was weighted and 20 ml of methylene blue solution (1000, 500 and 250 mg $L^{-1}$) or of copper ions solution

(500, 350, 200, 100, 50 and 10 mg $L^{-1}$) was added. Values of pH of prepared solutions were about 5. The suspensions were shaken for 24 h under ambient temperature. After sorption tests, equilibrium concentration of methylene blue or copper ions was determined by UV-Vis spectrometry (ultraviolet-visible spectrophotometry, Hitachi U-3900H) or AAS (atomic absorption spectroscopy, Varian SpectrAA-30), respectively. All experiments were performed in triplicates; the standard deviation did not exceed 5 %.

## 3. RESULTS AND DISCUSSION

Results of sorption tests of methylene blue on lignite and bitumen-free lignite are show in Fig. 1. The adsorption capacity of methylene blue on lignite is higher in compare with bitumen-free lignite. Differences between adsorption capacities are more pronounced with increasing initial concentration of the dye. The extraction of bitumen resulted in pH decrease in aqueous leaching of bitumen-free lignite (pH 5.9) contrary to lignite (pH 6.2). Thus, higher acidity of lignite after the extraction should lead to greater sorption efficiency of methylene blue according to the mechanism of sorption. This fact is not observed probably due to the hydrophobic character of the methylene blue molecule. Methylene blue may thus interact with the bitumen to be stabilized and dispersion forces and hydrophobic interactions. In the absence of bitumen in lignite, methylene blue molecules can not apparently penetrate deeper into the structure and interact with other carboxyl groups due to their hydrophobic nature.

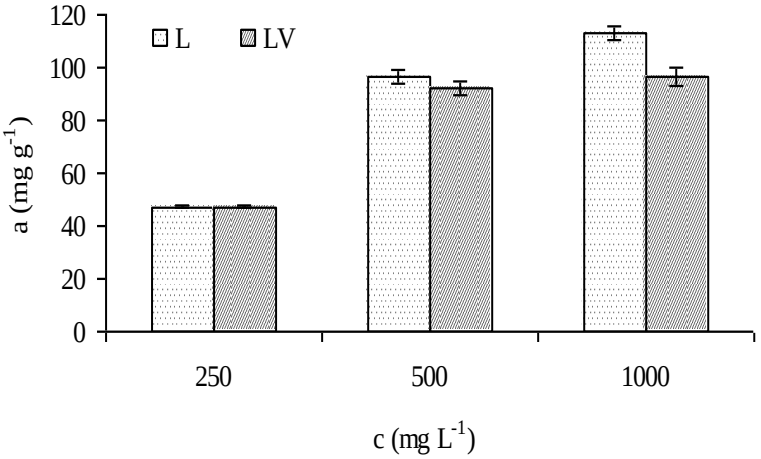


**Figure 1.:** Dependence of adsorption capacity on initial concentration of methylene blue onto lignite (L) and bitumen-free lignite (LV).

Results of sorption tests of copper ions on lignite and bitumen-free lignite are show in Fig. 2. As can be seen, the absorption capacity of lignite for $Cu^{2+}$ is smaller compared to the sorption capacity of lignite extracted with chloroform. Lower sorption efficiency of lignite in

compared to bitumen-free lignite is in contrast to the observation of the methylene blue adsorption. This fact can be explained similarly as in the previous case. By removal of bitumen from lignite, acidic functional groups become accessible to the dissociation of hydrogen and the space around them is accessible to hydrophilic molecules. The water-solvated copper ions can gradually adsorb on sites that were previously inaccessible due to bitumen molecules.

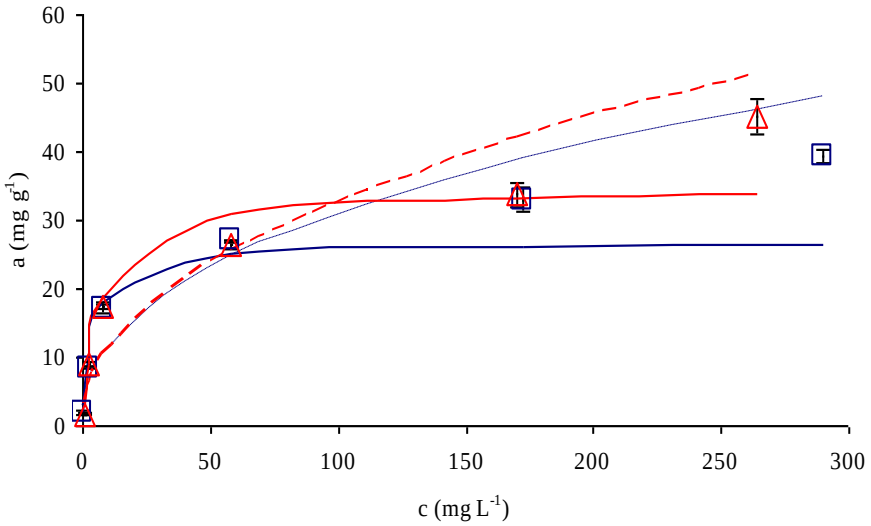


**Figure 2.:** Dependence of adsorption capacity on equilibrium concentration of copper ions onto lignite (blue) and bitumen-free ignite red). Experimental points are fitted to the Freundlich equation (dashed line) and Langmuir equation (continuous line).

MATLAB software was used to fit experimental data to Freundlich and Langmuir equations. The data were better fitted to the Langmuir equation (paramters not shown). The maximum adsorption capacities calculated from Langmuir isotherms were for lignite 26.74 mg $g^{-1}$ and for lignite withaout bitumen 34.60 mg $g^{-1}$.

## 4. CONCLUSION

Bitumen in lignite has the positive effect on the sorption of methylene blue probably due to dispersion forces and hydrophobic interactions. Vice versa, bitumen has the negative effect on the sorption of copper ions because the adsorption capacity of lignite was lower than the capacity of bitumen-free lignite. The maximum adsorption capacities calculated from Langmuir isotherms were for lignite 26.74 mg $g^{-1}$ and for lignite withaout bitumen 34.60 mg $g^{-1}$.

## 5. ACKNOWLEDGEMENT

This work has been supported by Ministry of Education, Youth and Sports,Project LO1211.

## 6. REFERENCES

[1]Doskocil L, Pekar M: Fuel Processing Technology, 101 (2012), 29-34

[2]Stefanova M, Ivanov D, Yavena N, et all.: Organic Geochemistry, 39 (2008), 11, 1589-1605

[3]Rafatullah M, Sulaiman O, Hashim R, et all.: Journal of Hazardous Materials, 177 (2010), 1-3, 70-80

[4]Qi Y, Andrew F, Hoadley A, et all.: Fuel, 90 (2011), 4, 1567-1574

[5]Pehlivan E, Gode A: Fuel Processing Technology, 88 (2007), 1, 99-106

[6]Jochova M, Puncochar M, Horacek J, et al.: Fuel, 83 (2004), 9, 1197-1203

# PIEZOELECTRIC BIOSENSORS FOR DETECTION OF MICROORGANISMS

Zdeněk FARKA[1,*], David KOVÁŘ[1,2], Petr SKLÁDAL[1,2]

[1] *Department of Biochemistry, Faculty of Science, Masaryk University, Kotlářská 2, 611 37 Brno, Czech Republic*

[2] *CEITEC MU, Masaryk University, Kamenice 5, 625 00 Brno, Czech Republic*

**farka@mail.muni.cz*

**Abstract**

Piezoelectric biosensors provide fast, specific and economic way of detection for a wide range of analytes ranging from metabolites to microorganisms. Specific antibodies were immobilised on gold electrodes of piezoelectric crystal and the biosensor was applied for real-time detection of model microorganisms. Three nonpathogenic strains of *Escherichia coli* (BL21, DH5α and K-12) were used because of easy cultivation and availability of antibodies. Several methods of antibody immobilisation were compared. The immobilisation of reduced antibody using Sulfo-SMCC was the most effective achieving the limit of detection (LOD) $10^5$ CFU·mL$^{-1}$. Active and passive operation modes of quartz crystal microbalance were compared concluding that for detection of microorganisms, both approaches are practically identical. The developed biosensor was connected to the cyclone air sampler allowing detection of microorganisms disseminated in the form of aerosol inside bioaerosol chamber. The achieved LOD was $1.45 \cdot 10^4$ CFU·L$^{-1}$ of air and the time from sample collection to detection was 16 min.

## 1. INTRODUCTION

Monitoring of microorganisms has a crucial role in many fields. The traditional microbiological methods are reliable but not suitable for fast detection. The need of rapid detection is met by piezoelectric biosensors that are also sensitive, specific and cheap [1]. There are two possible operational modes of measurements with piezoelectric biosensors – active one, where crystal oscillates and its resonance frequency is measured using frequency counter [2], and passive one, where detailed impedance characteristics of the resonator are measured [3]. The passive mode requires more expensive equipment but can differentiate changes of mass and viscosity [4].

## 2. MATERIAL AND METHODS

### Microorganisms and antibodies

Three strains of *E. coli* (BL21, DH5α and K-12) were cultivated aerobically in LB Broth (Duchefa Biochemie, Netherlands) at 37 °C overnight. The obtained suspension was centrifuged thrice at 4500 RCF for 10 min and resuspended in 50 mM PBS (pH 7.4). Two antibodies were used, Abcam ab25823 for detection of strains BL21 and DH5α and Serotec 4329-4906 for detection of K-12.

### Piezoelectric immunoassay

The antibodies were immobilised to gold electrodes of 10 MHz quartz crystals (ICM, USA) using three different approaches. In the first one, the sensor surface was activated using cysteamine (20 $mg \cdot mL^{-1}$, 2 h), glutaraldehyde (5 %, 1 h) and staphylococcal protein A (SpA, 1 $mg \cdot mL^{-1}$, 20 h) that specifically binds Fc fragments of antibodies. In the next step, the antibody was bound (100 $\mu g \cdot mL^{-1}$, 20 h) and free reactive groups were deactivated using ethanolamine (50 mM, 30 min). The second approach was based on the same procedure but the antibody was bound directly to glutaraldehyde omitting the SpA. The last method was based on binding of reduced antibody (100 $\mu g \cdot mL^{-1}$) to cysteamine-modified sensor surface using Sulfo-SMCC (3 $mg \cdot mL^{-1}$) [5].

The prepared sensor was placed in a flow-through cell and affinity interactions were measured in real-time using either active (QCM Analyzer, KEVA, Czech Rep.) or passive mode (Agilent 4294A, Agilent, USA), in both cases PBS was used as a running buffer. The microbes were disseminated inside an in-house made bioaerosol chamber and captured by cyclone SASS 2300 (Research International, USA). The piezoelectric biosensor was on-line coupled with the cyclone allowing remote control.

## 3. RESULTS AND DISCUSSION

Interactions of *E. coli* with antibodies were studied using piezoelectric biosensor. Fig. 1 shows calibration curves for combinations of *E. coli* strain and antibody immobilisation method measured using the active method. The dependence of signal on concentration exhibits saturation character and therefore linearisation by transforming *x* axis to log-scale is typically done. The highest sensitivity was achieved using the sensor with antibody immobilised using protein A, but surprisingly this sensor provided the worst LOD ($5 \cdot 10^6$ $CFU \cdot mL^{-1}$). The sensor with antibody immobilised directly had LOD $10^6$ $CFU \cdot mL^{-1}$

for all tested *E. coli* strains. The best results (LOD $10^5$ CFU·mL$^{-1}$) were achieved using the sensor with reduced antibody linked using Sulfo-SMCC. Measurements in the passive mode were done too, but no improvement of LOD was achieved with the impedance analyser.

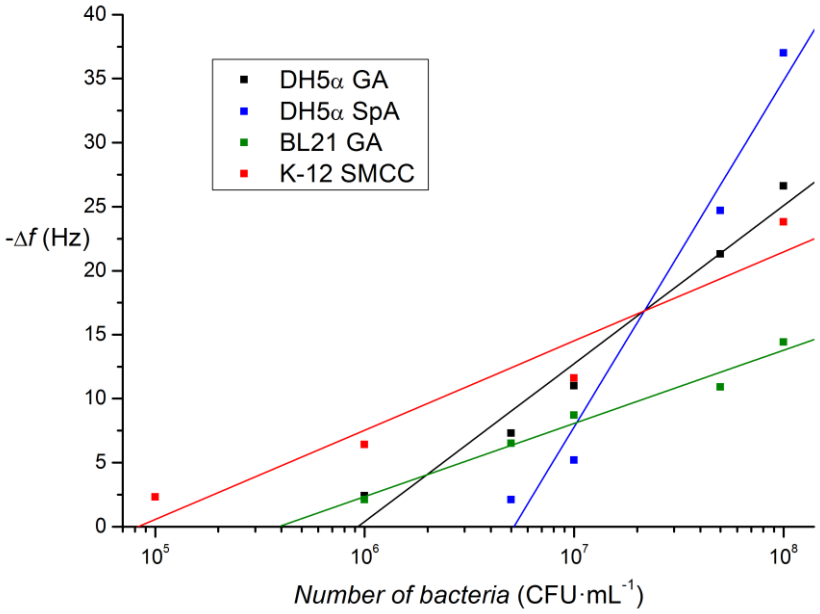


**Figure 1:** Calibration curves for QCM biosensors with antibodies immobilised using various procedures. GA – antibody linked directly using glutaraldehyde, SpA – antibody immobilised using staphylococcal protein A, SMCC – reduced antibody immobilised using Sulfo-SMCC.

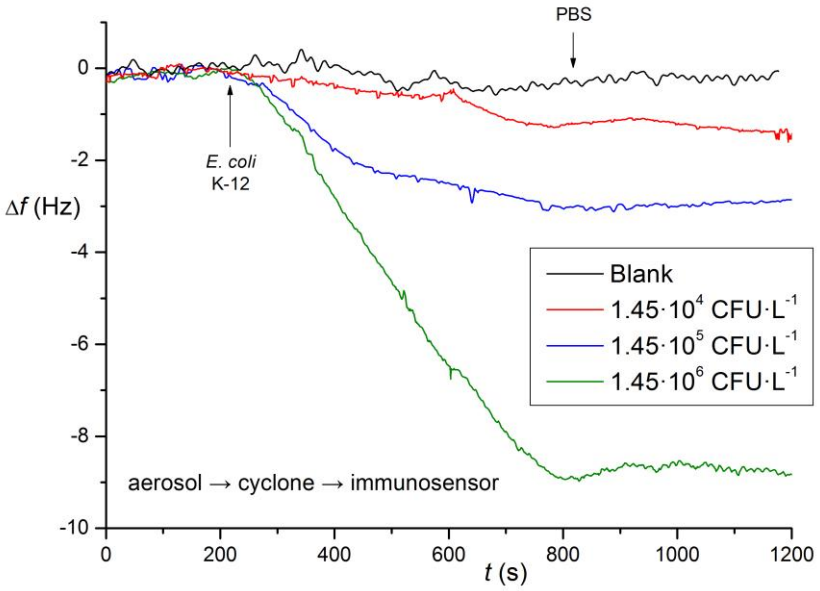


**Figure 2:** The interactions of *E. coli* K-12 captured from aerosol with reduced antibody Serotec 4329-4906 immobilised using Suflo-SMCC. Change of resonant frequency ($\Delta f$) in time is shown.

Using the developed biosensors, measurements of bioaerosols were done. Fig. 2 shows interactions between *E. coli* K-12 and antibody immobilised using Sulfo-SMCC. Measurements with this sensor were done with LOD $1.45 \cdot 10^4$ CFU·L$^{-1}$ of air based on the levels expected from the disseminated amounts of microbes. Time from sample collection to detection was 16 min. LODs for bioaerosol detection that are comparable to infection doses of various pathogens [6] were allowed by preconcentration effect of the cyclone air sampler.

## 4. CONCLUSION

Piezoelectric biosensor for rapid detection of microorganisms was developed and tested with three strains of *E. coli* (BL21, DH5α and K-12). For liquid samples, LOD $10^5$ CFU·mL$^{-1}$ was achieved using sensor with reduced antibody immobilised by Sulfo-SMCC, detection time was 10 min. Active and passive modes of QCM were compared but no major differences were observed in case of microorganism detection. The developed immunosensor was finally connected to cyclone air sampler which allowed detection of microorganisms in form of aerosol. The achieved LOD was $1.45 \cdot 10^4$ CFU·L$^{-1}$ of air with the time from sample collection to detection 16 min. The obtained data demonstrate that piezoelectric biosensors have great potential for fast and reliable detection of microorganisms.

## 5. ACKNOWLEDGEMENT

The work has been supported by the Ministry of Defence of Czech Republic (projects no. OVVTUO2008001 and OSVTUO2006003) and by CEITEC – Central European Institute of Technology (CZ.1.05/1.1.00/02.0068) from European Regional Development Fund.

## 6. REFERENCES

[1]Farka Z, Kovář D, Přibyl J, Skládal P: Int. J. Electrochem. Sci. 8 (2013), 1, 100-112

[2]Arnau A: Sensors. 8 (2008), 1, 370-411

[3]Zhang J, Su X D, O'Shea S J: Biophys. Chem. 99 (2002), 1, 31-41

[4]Itoh A, Ichihashi M: Meas. Sci. Technol. 19 (2008), 7

[5]Hermanson G T: Bioconjugate Techniques, Academic Press, London, 2008

[6]Sabelnikov A, Zhukov V, Kempf R: Biosens. Bioelectron. 21 (2006), 11, 2070-2077

# HIGH PERFORMANCE SULFUR NANOCOMPOSITES AS CATHODE MATERIALS BASED ON CONVERSION REACTION

Andrea STRAKOVÁ FEDORKOVÁ[1,2*], Ondrej ČECH[1], Tomáš KAZDA[1], Renáta ORIŇÁKOVÁ[2], Marie SEDLAŘÍKOVÁ[1]

[1] *Department of Electrical and Electronic Technology, Faculty of Electrical Engineering and Communication, Brno University of Technology, Technicka 10, 616 00 Brno, Czech Republic*

[2] *Institute of Chemistry, Faculty of Science, P.J. Šafárik University, Moyzesova 11, SK-041 54 Košice, Slovakia*

** andrea.fedorkova@upjs.sk*

**Abstract**

Li/S batteries are potentially viable ultrahigh energy density chemical power sources, which could potentially offer specific energies up to 2600 $Whkg^{-1}$ being rechargeable. It possesses the advantages of low cost, environmentally benign and high safety characteristics. Sulfur-carbon (S-C) composites and sulfur-$LiFePO_4$ (S-LFP) composites were prepared with MWCNTs additive by evaporation and solid state reaction. It is found that the S-LFP cathode with MWCNTs shows improvement of not only discharge capacity but also cycling stability. It exhibits an initial discharge capacity of 1167 mAh/g sulfur, or 70% of theoretical capacity. The capacity of S-LFP-MWCNTs composite after 20 cycles was 80% of the initial value and remained stable.

## 1. INTRODUCTION

The lithium-sulfur battery is a "conversion" type battery, because the electrochemical reactions which take place during charging and discharging of the battery result in new chemical compounds [1-3]. By contrast, lithium-ion batteries operate in accordance with the "insertion" principle. This means that lithium ions occupy spaces in the crystal structure of the cathode, without substantially changing the structure of the cathode material (Fig 1). Sulfur as the active cathode material has a theoretical specific capacity of 1672 $mAhg^{-1}$ and an average discharge potential of 2.2 V versus lithium. While for lithium ion batteries using intercalation cathodes a limit in energy density of about 200 $Whkg^{-1}$ is expected, for the lithium sulfur battery energy densities of up to 600 Wh $kg^{-1}$ might be achievable. Furthermore cost reduction and safety increase are attractive features since sulfur is widely available, less expensive and less toxic when compared to conventional cathodes. However, various challenges are

connected to the lithium sulfur cell chemistry, which need to be solved within systematic studies and by the development of new material concepts. In the present work, we report a simple method to synthesize S-C and S-LFP cathode material with MWCNTs as additional electronic conductor. SEM studies of morphological changes of the cathodes, thermogravimetry and charge–discharge performance of the S-C and S-LFP composites with MWCNTs were used to investigate and characterize the sulfur electrodes.

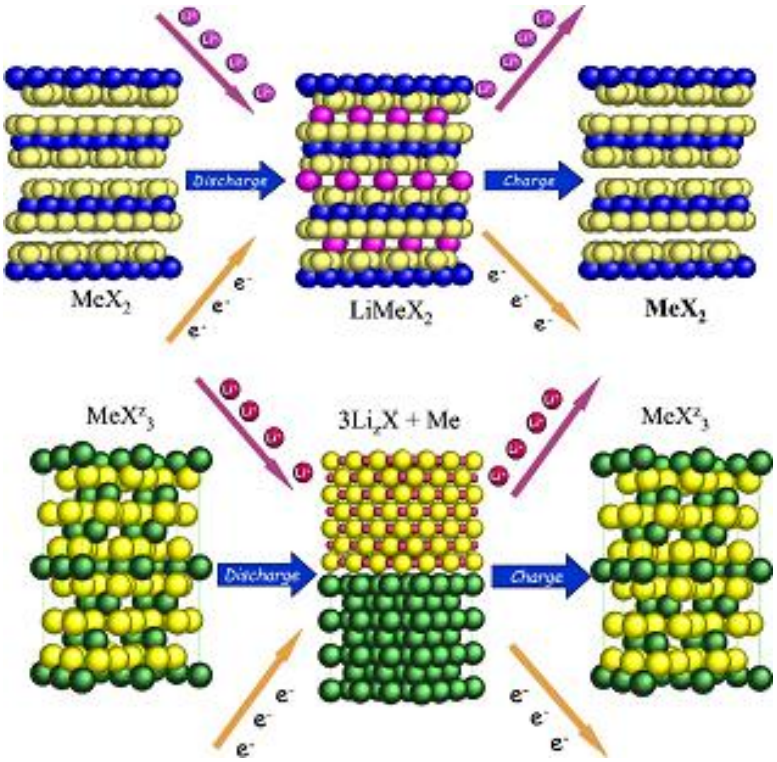


**Figure 1**.: Comparison of Intercalation and conversion reaction for energy storage [4].

## 2. RESULTS AND DISCUSSION

The morphologies of the S-based composite electrodes were investigated by SEM. Two different structures were observed for S-C composite. The surface of the Sulfur-Carbon sample is compact without cracks or holes but the structure is porous enough to enable $Li^+$ ion transport and electrolyte penetration. The porous and homogeneous basis of sample with MWCNTs is retained but addition of MWCNTs caused the formation of larger pores and holes. The MWCNTs are also clearly visible and provide the connections between S and C. In the case of S-LFP a coarser granularity is observed as compared with S-C. Yet, the corresponding S-LFP-MWCNTs composite presents a more homogeneous structure with oriented fibres of MWCNTs on the surface. Thus, the presence of MWCNTs in both samples was found to cause a significant change in porosity and homogeneity.

Figure 2a shows a moderate capacity loss from the initial high values of ca. 1160 mAh/g-sulfur down to values of specific capacities still larger than 800 mAh/g-sulfur after 10 cycles. It should be underscored that these values, still remarkably large, remain stable in subsequent cycles. It can also be noted that the S-LFP-MWCNT cathode presents a stabilized specific capacity of 980 mAh/g-sulfur a 20 % higher than that of S-C-MWCNT (780 mAh/g-sulfur). The discharge capacity gradually decreases as the current rate is raised from 0.1 C to 0.5 C for both of the cells (Fig. 2b). The higher discharge capacities of 1170, 855 and 750 mAh/g-sulfur were achieved at a current density of 0.1, 0.2, and 0.5 C, respectively for S-LFP composite material. The excellent rate performance can be ascribed to the high effective electron pathways provided by the MWCNTs and an optimal distribution of pores as electrolyte channels in the cathode.

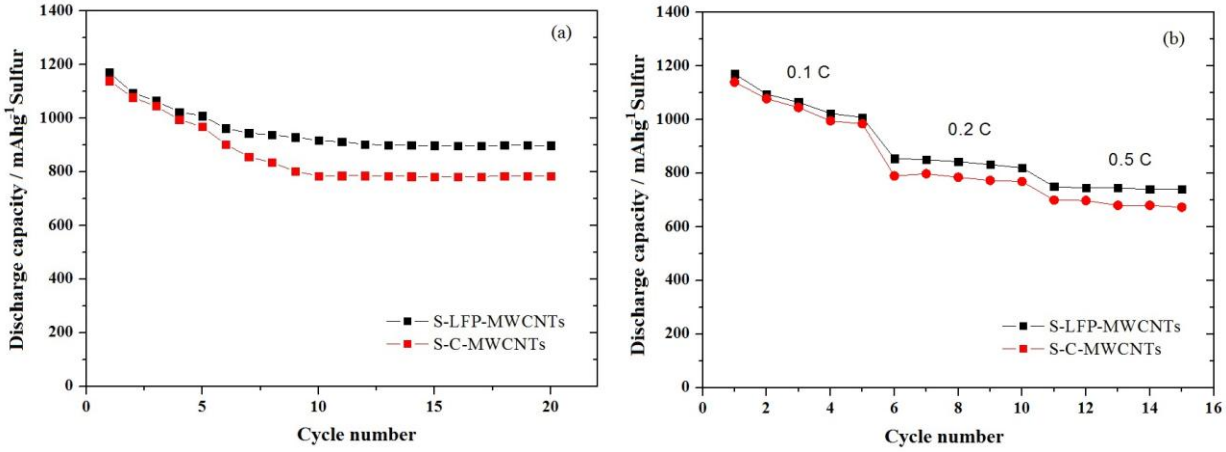


**Figure 2.:** Discharge capacity vs. cycle number measured on S-C-MWCNTs and S-LFP-MWCNTs cathodes at C-rate C/10 (a), cycling performance of S-C-MWCNTs and S-LFP-MWCNTs cathodes at various C-rates (b).

## 3. CONCLUSION

Sulfur-carbon composite was synthesized by thermal heating of sulfur onto conductive carbon black (Super P). Sulfur-LFP composite was prepared by simple solid-state reaction in a ball mill. These simple methods have been shown here to produce very porous sulfur cathode composites. A high initial discharge capacity of 1167 mAh/g-sulfur at 0.1 C was achieved with the S-LFP-MWCNTs composite. The excellent electrochemical performance can be attributed to the homogeneous dispersion of MWCNTs in the composites, which not only accommodate the volume change during charge/discharge processes, and absorb the polysulfides byproducts but also provide stable electrical and ionic transfer channels. All results described in this publication indicate that the combination of sulphur, $LiFePO_4$ and

MWCNTs is a promising candidate cathode material for high-performance lithium/sulfur batteries.

## 4. ACKNOWLEDGEMENT

Authors gratefully acknowledge financial support from the Ministry of Education, Youth and Sports under projects No. LO1210 - "Energy for Sustainable Development (EN-PUR)" and CZ.1.07/2.3.00/30.0039 solved in the Centre for Research and Utilization of Renewable Energy and bilateral project No. 7AMB13AR008 between Czech Republic and Argentina.

## 5. REFERENCES

[1] P.G. Bruce, S.A. Freunberger, L.J. Hardwick, J.M. Tarascon, Nat. Mater., 11 (2012), p. 19

[2] X. Ji, L.F. Nazar, J. Mater. Chem., 20 (2010), p. 9821

[3] D. Aurbach, E. Pollak, R. Elazari, G. Salitra, J. Electrochem. Soc., 156 (2009), p. A694

[4] http://www.physics.rutgers.edu/Bartgroup/EnergyStorage.htm

# PHYSICOCHEMICAL METHODS AS A SUITABLE INSTRUMENT FOR SHORT DNA FRAGMENTS STUDY

Libor GURECKÝ[1], and Libuše TRNKOVÁ[1,2,*]

[1]*Department of Chemistry, Faculty of Science, Masaryk University, Kamenice 5, CZ – 625 00 Brno, Czech Republic, gurinabox@gmail.com*

[2]*Central European Institute of Technology – CEITEC, University of Technology, Technicka 10, CZ – 616 00 Brno, Czech Republic, *libuse@chemi.muni.cz*

**Abstract**

Oligodeoxynucleotides (ODNs) are observed in the promoter region of the oncogens and of human telomeric DNA as a multiple repetitive C- or G- sequences. These sequences form tetraplex structures. C- rich ODNs form the so called i-motif, a hemiprotonated C-$C^+$ base pairing structures, at slightly acidic pH. G- rich ODNs form a G-quartet, made from four guanines and stabilized by a metal kation and can be folded into a G-tetraplex. We used electrochemical methods to study the behaviour of these compounds in buffered solutions with different pH, so we can comparatively evaluate the structure and fiction of each homo-ODN for better understanding their behaviour in solutions and on the charged interface. The study was completed by circular dichroism spektra to confirm the structure. Results should provide better understanding of these compounds, so the suitable biosensor could be designed.

## 1. INTRODUCTION

An electrochemical and spectral study of short cytosine- or guanine-rich oligodeoxynucleotides (ODNs) on a hanging mercury drop electrode (HMDE) in buffered solutions with different pH is presented. We found out that C- or G-rich ODNs form stable structures at a slightly acidic pH. Besides the common electrochemical methods, such as linear sweep voltammetry (LSV) and cyclic voltammetry (CV), in this study was used elimination voltammetry procedure (EVP). Spectral study consists of the absorption spectra and circular dichroism spectra. Comparative evaluation of the structure and function of each homo-ODN (dCx, where x is 3-9, and y is 3, 6, 9) helps to understand the behaviour of the studied homo-ODN in solutions and on charged interface depending on pH, temperature, ionic strength, and chain lenght. It was discovered, that in slightly acidic buffers C-rich ODNs form stable structures, the so-called i-motifs, requiring a partially protonised nucleobase, exept for oligo-deoxynucleotide dC3, which i stoo short to forma n i-motif structure. Guanine

ODN structures have recently been paid great interest, and it was discovered, that they can form multiplex (tetraplex) structure via a g-quartet, which was found in DNA telomerase repetitions and in the promoter regions of certain proto-oncogenes. Since more cimplicated structures (multiplexes, hairpins) conditioned by Hoogsteen base pairing in the ODN with multiple repetitive C- or G-sequences are often observed in the promoter region of the oncogenes and of human telomeric DNA, such a study is significant [1-3].

## 2. MATERIAL AND METHODS

ODNs, $dC_3$ and $dC_4$ were purchased from Thermo Fisher Scientific, Ulm, Germany; $dC_5$, $dC_6$, $dC_9$, $dG_3$, $dG_6$ and $dG_9$ from Integrated DNA Technologies, Inc., USA.

The voltammetric experiment was performed using the electrochemical analyzer AUTOLAB PGSTAT 20 (Ecochemie, Utrecht, The Netherlands) in connection with GPES software. The experimental conditions were as follows: potential range from -1 V to -1.7 V, time of adsorption 0 s or 60 s, and scan rate from 50 mV/s to 800 mV/s.

## 3. RESULTS AND DISCUSSION

From our results we figured out, that all dCx form the i-motif exept the dC3 and the stability of ordered structure is conditioned by pH. With rising pH we observed transition of ordered structures to unordered structures (confirmed by CD spectroscopy) depending on chain length. This attribute also correlate when we calculate the diffusion coefficient from Randles-Ševčík equation.

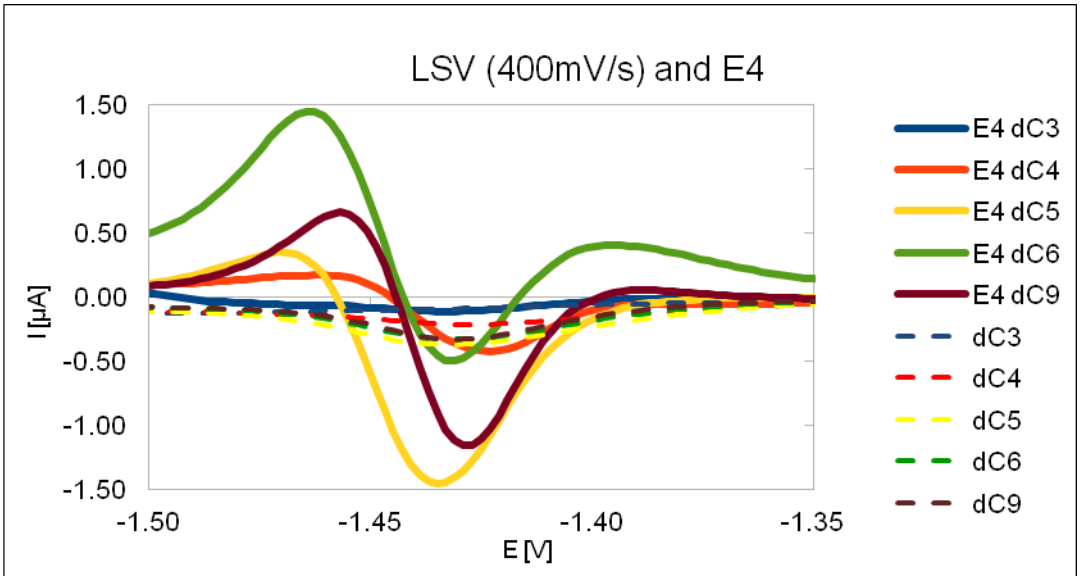


**Figure 1.:** LSV and the elimination voltammetric procedure of $dC_x$ at pH 6,8 (without adsorption)

In G-rich ODNs we didn't manage to find the transition midpoints due to the better stability of ordered structures. We assume that these structures are more resistant to pH changes and so the further investigation in alkaline pH is needed to prove it and for helping us to find out better conditions for developing the biosensor.

At this point there is better chance to develop the biosensor to C-rich ODNs because of their large differences in behavior in buffered solutions.

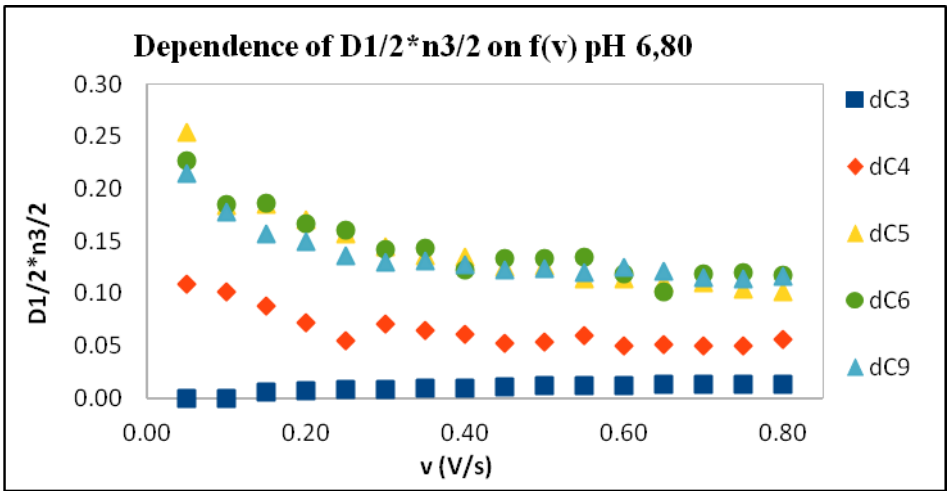


**Figure 2.:** Dependence of D1/2*n3/2 on f(v) at pH 6,8

## 4. CONCLUSION

Study helps to deeply understand the different behavior of C- and G-rich ODNs in buffered solutions and on the charged interface electrode/electrolyte and gives us useful incentives for next ODN investigation and provide helps for suitable biosensor designing.

## 5. ACKNOWLEDGEMENT

CEITEC – Central European Institute of Technology Project CZ.1.05/1.1.00/02.0068

NanoBiometalNet (Partnerská síť centra ecxelentního bionanotechnologického výzkumu) CZ.1.07/2.4.00/31.0023, MUNI/A/0992/2009 od MŠMT České Republiky

## 6. REFERENCES

[1] Dryhurst G.: Electrochemistry of Biological Molecules, Academic Press, New York (1977).

[2] Trnkova L., Friml J., Dracka O.: Bioelectrochemistry, 54 (2001) 131.

[3] Trnkova L.: Jelen F., Postbieglova I.: Electroanalysis, 15 (2003) 1529-1535.

# STUDIUM FOTOCHEMICKÝCH CHRÁNÍCÍCH SKUPIN POMOCÍ ČASOVĚ ROZLIŠENÉ SPEKTROSKOPIE. JE NANO SEKUNDA MÁLO NEBO MOC PRO ROZTRŽENÍ VAZBY?

Dominik HEGER[1,2*]

[1]*Department of Chemistry, Faculty of Science, Masaryk University, Kamenice 5/A8, Brno 602 00, Czech Republic*

[2] *Research Centre for Toxic Compounds in the Environment, Faculty of Science, Masaryk University, Kamenice 3, 625 00 Brno, Czech Republic*

**hegerd@chemi.muni.cz*

Přednáška bude zaměřena na principiální popis fotochemických chránících skupin z perspektivy vědeckého přínosu našeho pracovního týmu. Fotochemické chránící skupiny jsou stále častěji používané pro mnohé technické a biochemické aplikace jako je například litografie či metody sledujících velmi rychlé děje (přenos nervového vzruchu).[1, 2] Tyto aplikace budou ukázány s konkrétními chránícími skupinami, jejichž návrhy a zkoumání mechanismů odstoupení je naší vědeckou náplní. Rychlostní konstanta odstoupení chránící skupiny může být limitujícím parametrem pro použití pro časově rozlišené studie. Proto budou představeny principy časově rozlišených spektroskopických metod na sub nano sekundové škále a ukázána jejich použití při řešení mechanismů odchránění některých biochemicky aktivních látek. [3-5]

## REFERENCES

1. Givens, R. S.; Rubina, M.; Wirz, J., Applications of p-hydroxyphenacyl (pHP) and coumarin-4-ylmethyl photoremovable protecting groups. *Photochemical & Photobiological Sciences* **2012,** 11, 472-488.

2. Klan, P.; Solomek, T.; Bochet, C. G.; Blanc, A.; Givens, R.; Rubina, M.; Popik, V.; Kostikov, A.; Wirz, J., Photoremovable Protecting Groups in Chemistry and Biology: Reaction Mechanisms and Efficacy. *Chemical Reviews* **2013,** 113, 119-191.

3. Givens, R. S.; Heger, D.; Hellrung, B.; Kamdzhilov, Y.; Mac, M.; Conrad, P. G., II; Cope, E.; Lee, J. I.; Mata-Segreda, J. F.; Schowen, R. L.; Wirz, J., The photo-Favorskii reaction of p-hydroxyphenacyl compounds is initiated by water-assisted, adiabatic extrusion of a triplet biradical. *Journal of the American Chemical Society* **2008,** 130, 3307-+.

4. Klicova, L.; Sebej, P.; Solomek, T.; Hellrung, B.; Slavicek, P.; Klan, P.; Heger, D.; Wirz, J., Adiabatic Triplet State Tautomerization of p-Hydroxyacetophenone in Aqueous Solution. *Journal of Physical Chemistry A* **2012,** 116, 2935-2944.

5. Solomek, T.; Heger, D.; Ngoy, B. P.; Givens, R. S.; Klan, P., The Pivotal Role of Oxyallyl Diradicals in Photo-Favorskii Rearrangements: Transient Spectroscopic and Computational Studies. *Journal of the American Chemical Society* **2013,** 135, 15209-15215.

# HYALURONAN MICRO- AND NANOPARTICLES

Jana HEJNÁ[1,2*], Miloslav PEKAŘ[1,2], Filip MRAVEC[1,2], Tereza Halasová[1,2]

[1]*Institute of Physical and Applied chemistry, Faculty of Chemistry, Brno University of Technology, Purkyňova 118, 612 00 Brno*

[2]*Materials Research Center, Faculty of chemistry, Brno University of Technology, Purkyňova 118, 621 00 Brno, Czech Republic*

**xchejnaj@fch.vutbr.cz*

**Abstract**

A rheological properties and particle size for two different molecular weights of hyaluronic acid have been studied. We measured these properties depending on time, on concentration of hyaluronic acid and on liquid that hyaluronic acid was dissolved in. Rheological properties and particle size independent on time. Particle size was smaller for hyaluronic acid dissolved in physiological solution than for hyaluronic acid dissolved in aqueous solution. Particle size grows depending on grows concentration of hyaluronic acid.

## 1. INTRODUCTION

Sodium (potassium) salt of hyaluronic acid (HyA) is material which occurs in human body (e. g. extracellular matrix, synovial fluid, vitreous humour) [1]. HyA is obtained by isolation from natural resources (cockscomb, beef blood solution) or by isolation from *Streptococcus* bacteria. We do research on HyA as on a material suitable for drug delivery on our faculty [2, 3]. It was decided to research properties of HyA. We measured its rheological properties in water solution and particle size in aqueous solution and in 0.15 M sodium chloride solution (physiological solution). HyA occurs in wide range of molecular weight, therefore we chose two different molecular weights (106 kDa and 1.36 MDa).

## 2. MATERIAL AND METHODS

***Material:***

Sodium hyaluronan of molecular weight 106 kDa and 1.36 MDa (CPN, Lt. Dolní Dobrouč), sodium chloride (Lach Ner s.r.o.) and deionized water.

***Methods:***

*Sample preparation:* Solution of HyA was prepared in concentration 0.01; 0.1 and 1 $g \cdot dm^{-3}$ in aqueous solution and in physiological solution (0.15 M NaCl).

Viscosity of samples was measured by instrument Rheometer ARG2 (TA Instruments). Viscosity was measured for two different molecular weights of HyA depending on time (solution was measured during one week).

Particle size of sample was measured by instrument Zetasizer Nano ZS (Malvern Instrument) by dynamic light scattering techniques. Particle size was observed for two different molecular weight of HyA depending on concentration of HyA, on liquid that HyA was dissolved in and on time (solution was measured during one week).

## 3. RESULTS AND DISCUSSION

We observed rheological properties of high and low molecular weight HyA depending on time. We detected from results that high molecular weight of HyA behaves as non-Newtonian fluid and low molecular weight of HyA behaves as Newtonian fluid. We also detected that rheological properties of HyA didn´t change in our timescale.

In our work we measured particle size for two different molecular weight of HyA depending on time, on liquid that HyA was dissolved in and on concentration of HyA. We detected from results that particle size didn´t change in our timescale. Samples in physiological solution had smaller particle size compared to samples of same concentration in aqueous solution. The samples with the lowest concentration weren´t suitable for measuring by dynamic light scattering (see picture 1). Autocorrelation function doesn´t have ideal shape. Autocorrelation function doesn´t have high value and lower part of function doesn´t decline zero. Farther you can see in figure 1 that particle size grows with higher concentration of HyA.

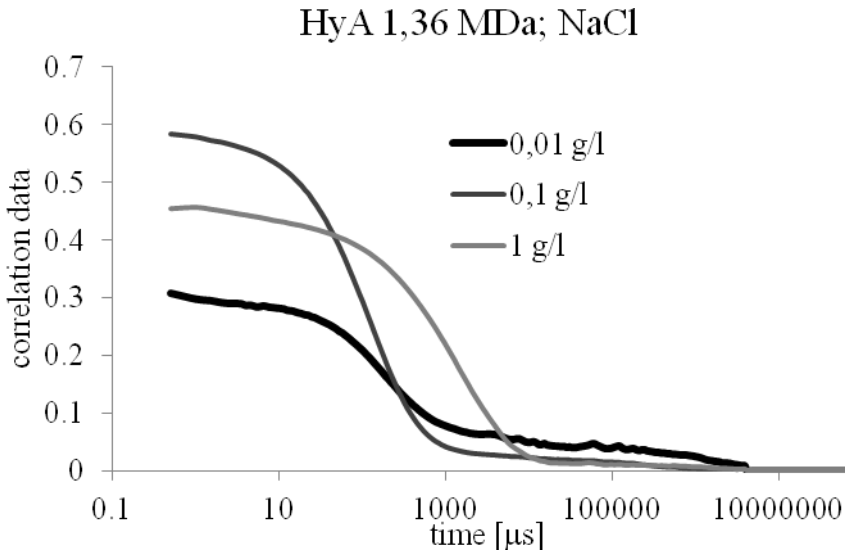


**Figure 1.:** Autocorrelation function for different concentration of HyA molecular weights of HyA are 1.36 MDa in physiological solution.

**Table 1.:** Particle size for HyA 1 g·dm$^{-3}$

| molecular weight of HyA | solution | particle size [d. nm] | | |
|---|---|---|---|---|
| 106 kDa | aqueous | 328±103 | 813±129 | 1259±169 |
| | 0.15 M NaCl | 30±5 | 397±46 | 763±123 |
| 1,36 MDa | aqueous | 185±82 | 858±105 | 1387±288 |
| | 0.15 M NaCl | 52±15 | 240±87 | 655±101 |

## 4. CONCLUSION

We measured rheological properties and particle size in HyA solution. We found out from rheological measure that low molecular weight HyA behaves as Newtonian fluid, however high molecular weight HyA behaves as non-Newtonian fluid. During our timescale, neither rheological properties nor particle size didn´t change in HyA solutions. Farther we found out, that when we used physiological solution as solvent we detected better autocorrelation function while HyA formed smaller particles independent on molecular weight HyA.

## 5. ACKNOWLEDGEMENT

This work was supported by the project “Centres for materials research at FCH BUT” No. CZ.1.05/2.1.00/01.0012 from ERDF.

## 6. REFERENCES

[1] C. V., Hascall, C.T. Laurent, Dr.: Hyaluronan: Structure and Phyaical Properties. *Glycoforum* [online], 1997.

[2]T. Halasová, J. Kroutská, F. Mravec, M. Pekař, Colloid Surface A, 391(2011), pp.25-31.

[3]T. Halasová, F. Mravec, M. Pekař, Carbohyd. Polym., 14(2013), pp. 34-37.

# MIRCORHEOLOGICAL CHARACTERIZATION OF HYALURONIC ACID GELS

Zuzana HNYLUCHOVÁ[1*], Tereza HALASOVÁ[1], Miloslav PEKAŘ[1]

[1]*Department of Physical Chemistry, Faculty of Chemistry, Brno University of Technology, Purkyňova 118, 612 00 Brno, Czech Republic*

**xchnyluchova@fch.vutbr.cz*

**Abstract**

Particle tracking microrheology as one of the passive microrheology methods is a novel approach for determining viscoelastic properties of soft materials. Passive microrehology method is based on thermal motion of particles inserted into the investigated sample. Four different hyaluronic acid gels formed by mixing diverse concentrations of hyaluronic acid and cethyltrimethylammonium bromide (CTAB) and three different sizes of probes were used to characterize viscoelastic response of gel microstructure characterizing by elastic G´(ω) and viscous G´´(ω) moduli. Our measured data show significant dependence of viscoelastic properties on used particle size, which point out the diversity of hyaluronic acid gel microstructure.

## 1. INTRODUCTION

Hyaluronic acid is a substance that is naturally present in the human body. It plays important role in human tissues (main artery, tendon, valve, synovial fluid) where it serves as a connective tissue organizer and water holding substance. Because of its versatility, it is widely used in the pharmaceutical and cosmetic industries as well as hyaluronic acid gels could be used for medical and cosmetic use. The more precise we know properties and characteristic of the substance, the better and easier its following utilization in industry.

Viscoelastic properties are very important material parameters affecting their industrial applicability. The most useful method for determining such properties is classical rheology. Nevertheless, classical rheology is not utilizable for every material considering relatively huge amount of sample (around 10 ml) needed for one measurement. New fast emerging method called microrheology has been developed for determining viscoelastic properties of material. As the name already suggest, the sufficient amount of sample for one measurement several microliters.

## 2. MATERIALS AND METHODS

Particle tracking microrheology method is based on the small well defined particles embedded into the investigated material. Size of the particles allows subjecting of the Brownian motion, which depends on the viscosity of surrounding material and the temperature [1,2]. Mean squared displacement (MSD or $\Delta x^2(t)$) relates to diffusion coefficient by equation $(\Delta x^2(t)) = 2dD\tau^{\alpha}$ where $d$ is dimension, $\tau$ is time and $\alpha$ is time exponent. According to the Stokes - Einsten equation we can calculate viscosity of material if the size of the particle and temperature is known.

$$D = \frac{k_B T}{6\pi\eta a},$$

Value of time exponent α varies from 0 (newtonian fluid) to 1 (elastic material). Very important step is transferring MSD(t) into frequency dependent elastic and viscous moduli characterizing contribution of viscosity and elasticity in the sample [3,4]. Generalized Stokes-Einstain equation is used involving Laplace-transformed quantities:

$$\tilde{D}(s) = \frac{kT}{6\pi a s\tilde{\eta}_s},$$

where $a$ is the radius of the probe sphere, $\eta_s$ is the Laplace transformed frequency dependent viscosity, $D(s)$ is the Laplace transformed frequency dependent diffusion coefficient and $s$ is the Laplace frequency, from which frequency dependent shear modulus can be determined. Samples for measurement were place into the "glass pocket" to avoid its drying or flowing [5].

## 3. RESULTS AND DISCUSSION

Four hyaluronic acid gels were prepared mixing different stock solutions of cethyltrimethylammonim bromide and hyaluronic acid in the 1:1 ratio (Table 1)

Table 1:

| Sample | Hyaluronic acid c (w%) of stock solution | CTAB c (mM) of stock. solution |
|---|---|---|
| 1 | 0,5 | 50 |
| 2 | 0,5 | 200 |
| 3 | 2 | 50 |
| 4 | 2 | 200 |

From particle trajectories mean-squared displacements (MSD) as a function of time were calculated for three different sizes of particles. Functions MSD were converted into frequency dependent elastic and viscous moduli as you can see in Figure 1. From the graph it is obvious, that moduli are size particle dependent. Each particle size reflects structure of local microenvironment based on the mesh size of the gel. The point, where elastic modulus of the sample cross the viscous modulus (G´ = G´´) is called cross-over point and characterizes moment where the elastic modulus becomes larger than the viscous modulus. With the increasing size of particle, the cross point appears at lower value of frequency as you can see in the picture. Small particles detected cross-over point at the highest frequency, because in the same sample probably they do not interact so much with the polymer structure and can reflect their microenvironment containing mainly solvent. This phenomenon was observed for every hyaluronic acid gel.

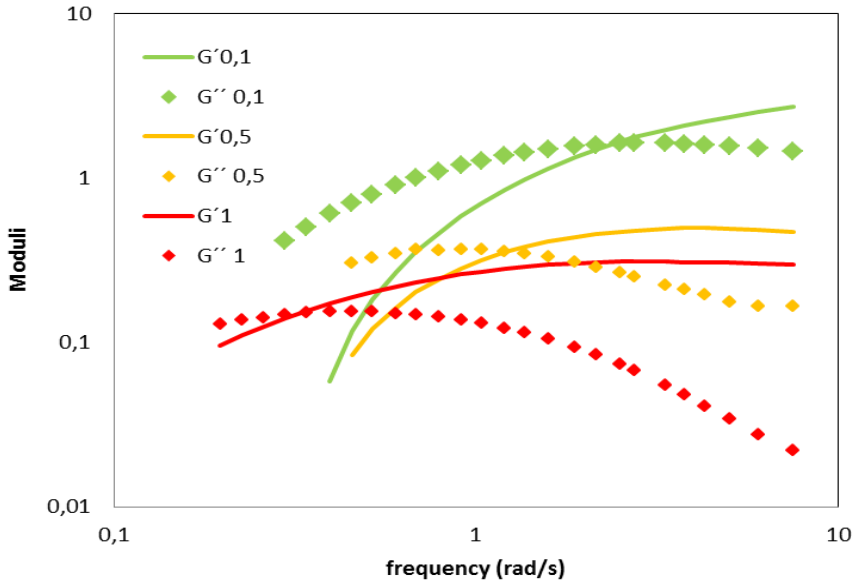


**Figure 1**.: Elastic and viscous moduli for hyaluronic acid gel 2 for trhee different sizes of particles

## 4. CONCLUSION

Microrheology measurements were performed on the four different hyaluronic acid gel with the molecular weight 90 - 130 kDa. It was observed that characterization of rheological properties of these gels is strongly dependent on the selected particle size, which reflects its microenvironment.

**5. ACKNOWLEDGEMENT**

The work has been supported by Material Research Centre, Faculty of Chemistry, Brno University of Technology.

**6. REFERENCES**

[1]Bekah D.: Disertation. Ryerson University ( 2010)

[2]Cicuta P, Donald, A. M: Soft Matter. 3 (2007), 12, 1449-1455

[3]Levine A, Lubensky T. C.: Phys. Rev. Let,( 2000), 85**,** 1774–1777

[4]Wirtz, D: Annual Review of Biophysics 38 ( 2009), 1, 301-326

[5]Mason, T. G. et all.: Physical Review Letters, 79, 1997,17, 3282-3285

# DEVELOPMENT OF THE CELL SYSTEM FOR EVALUATION OF ANTI-PAIIL IMMUNOGLOBULIN EFFICACY

Lucie VAŠKOVÁ[1], Libuše NOSKOVÁ[1], Barbora BLÁHOVÁ[1], Michaela WIMMEROVÁ[2], Marie STIBOROVÁ[1], Petr HODEK[1*]

[1]*Department of Biochemistry, Faculty of Science, Charles University in Prague, Hlavova 8, 128 40 Prague 2, Czech Republic*
[2]*Department of Biochemistry, Faculty of Science, Masaryk University, Kamenice 753/5, 625 00 Brno, Czech Republic*
** hodek@natur.cuni.cz*

**Abstract**

Using fluorescently labeled immortalized epithelium cell lines derived from normal or cystic fibrosis (CF) human lungs the well plate assay was set upped. This assay was used for sensoring chicken yolk antibody prophylaxis against adhesion of *Pseudomonas aeruginosa* (PA) at a molecular level. Antibodies against PA lectin, PAIIL, significantly prevented bacteria adhesion in both cell lines. In agreement with *in vivo* data our plate assay showed higher susceptibility of CF cells to PA compared to normal epithelium.

## 1. INTRODUCTION

Cystic fibrosis (CF) is an autosomal recessive disorder caused by mutations in a single gene coding for the CF transmembrane conductance regulator (CFTR) protein. Resulting pathophysiology changes of lungs are associated with increased susceptibility of CF patients towards microbial infections. Frequent airway bacterial infections with pathogens such as *Pseudomonas aeruginosa* (PA) lead to a progressive lung disease resulting in chronic endobronchial colonization, which is connected with an intense neutrophilic inflammatory response. These conditions make cystic fibrosis to be one of the most common life-shortening genetic disorders. While the antibiotics are administered to slow decline in pulmonary function and reduce frequency and morbidity of pulmonary exacerbations, there is an urgent need to develop novel and effective therapies. In addition to efforts in CF gene therapy and corrections of CFTR function, the antimicrobial management, such as CF patient immunization against invading pathogens is being extensively studied. The concept of immunization of CF patients with vaccines derived from a PA virulence factor, however, suffers from impaired secretion of immunoglobulins at mucosal membranes of CF airways. Thus, the passive immunization via anti-pseudomonal immunoglobulins seems to be only a feasible prevention of lung PA infection. In this respect chicken yolk antibodies (IgY) provide

great potential to become an efficient tool of passive immunization. The most significant advantage of IgY, in contrast to mammalian IgG, consists in their inability to induce inflammatory reaction when antigen is bound. Moreover, the large production of IgY (100 mg/yolk) makes these antibodies well suited for prophylaxis of bacterial infections.

## 2. MATERIAL AND METHODS

### Antibody preparation

Antibodies were prepared from egg yolks laid by chickens immunized with recombinant PA lectin, PAIIL, as described elsewhere [1]. Pre-immune IgY sample (control) was purified from eggs collected a week prior to the immunization. The presence of anti-PAIIL IgY was determined on ELISA and Western blots using PAIIL and PA lysate as antigens, respectively.

### Bacterial adhesion assay

NuLi or CuFi cells (immortalized epithelium cell lines derived from normal or CF human lungs, respectively, ATCC) were stained with a fluorescent dye PKH67, seeded onto well plates (24 wells) and incubated for 24 h at 37°C, 5% $CO_2$ to form a confluent layer. *Ps. aeruginosa* PAO1 was labeled with a fluorescent dye PKH26, pre-treated for 10 min with anti-PAIIL or control IgYs (1 mg/ml), or L-fucose, D-galactose (1% solution) or PBS, and finally applied onto well plates. After incubation (2 hrs) non-adhered bacteria were removed by extensive washing with PBS. Using spectrofluorometer (Tecan Infinite M200 Pro) the adhered PA on epithelial cells were quantified (Ex 522 nm, Em 569 nm for PA; Ex 470 nm, Em 505 nm for NuLi/CuFi). Results were expressed as a relative fluorescence ratio PA/NuLi or PA/CuFi.

## 3. RESULTS AND DISCUSSION

Bacterial adherence to epithelial is an important initial step in the pathogenesis of PA. It is thought that airway surfaces of CF patients are lacking the sialylation of glycoconjugates such as GM1, which enables the binding of PA [2]. As the PA lectin, PAIIL, is considered to be involved in bacteria adhesion on host cells, we expressed the recombinant PAIIL and prepared chicken yolk antibodies against it. To examine the prophylactic properties of anti-PAIIL IgY against the colonization of lung epithelial cells with PA the bacterial adhesion assay was developed. The experimental setup is based on the dual fluorescence determination of PA (labeled with a dye PKH26) on epithelial cells stained with a fluorescence dye PKH67. The efficacy of anti-PAIIL IgY in prevention of adherence to epithelial cells was tested in conditions *ex vivo* with two cell lines derived from normal (NuLi) and CF-patient (CuFi) lung

tissues. The bacteria adherence is dependent on the incubation time – 2 hrs is sufficient to determine number of adhered PA. Figure 1 shows the prophylactic effect of anti-PAIIL IgY (S-IgY) against the adherence of PA on CuFi/NuLi cells. While saccharide ligands D-galactose of PAIL and L-fucose of PAIIL failed in the protection of epithelial cells against PA adhesion, control IgY (C-IgY) seems even to stimulate the PA binding. This unexpected effect might be attributed to agglutination of PA *via* PAIIL, which binds to highly mannosylated glycoconjugates present on each heavy chain of IgY. In the case of specific anti-PAIIL IgY, the saccharide binding site of lectin is blocked by immunoglobulin and thus excluded from the interaction with the IgY heavy chain. Prophylactic properties of anti-PAIIL IgY will be examined further with experimental animals infected with PA.

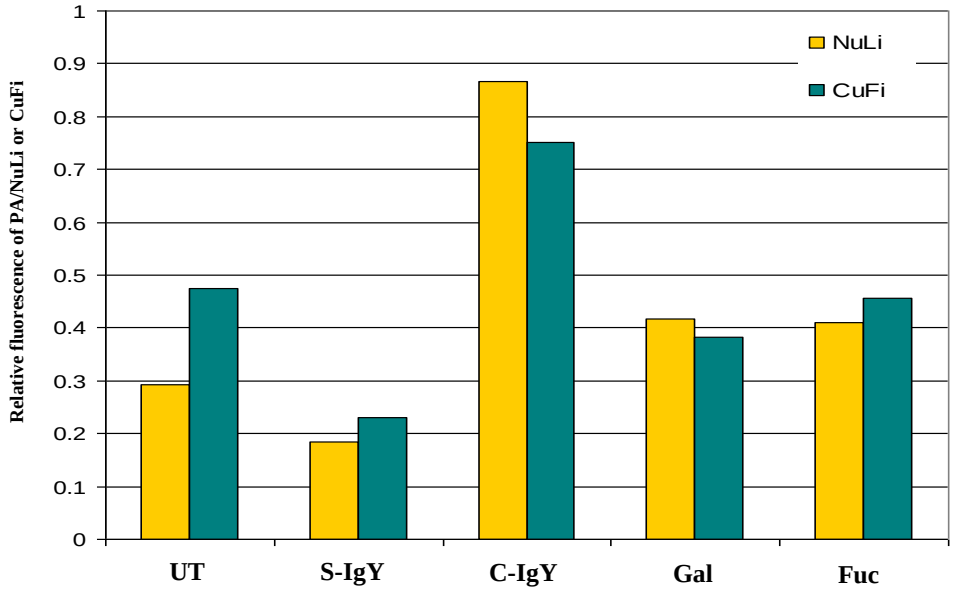


**Figure 1.:** Effect of IgYs and saccharides on PA adhesion on epithelial cells. Cells (**CuFi**, **NuLi**) were treated with anti-PAIIL IgY (**S-IgY**), control IgY (**C-IgY**), D-galactose (**Gal**), L-fucose (**Fuc**), or with PBS only (**UT**). PA adherence is expressed as a ratio of relative fluorescences of PA vs. NuLi/CuFi.

## 4. CONCLUSION

Specific chicken yolk antibodies against *Ps. aeruginosa* lectin PAIIL proved to be effective in reducing bacteria adhesion on human airway epithelia cells under experimental condition used.

## 5. ACKNOWLEDGEMENT

The work has been supported by GAUK 1584814 and UNCE 204025/2012.

## 6. REFERENCES

[1]Hodek P, Trefil P, Simunek J, et al.: International Journal of Electrochemical Science, 5 (2013), 113-124

[2]Bryan R, Kube D, Perez A, et al.: American Journal of Respiratory Cell and Molecular Biology, 19 (1998), 269-277

# CYTOCHROME P450 1A1-CATALYZED OXIDATION OF CARCINOGENIC BENZO[*A*]PYRENE IS MODULATED BY NADH AND CYTOCHROME $B_5$

Radek INDRA[1], Michaela MOSEROVÁ[1], Volker M. ARLT[2], Marie STIBOROVÁ[1*]

[1] *Department of Biochemistry, Faculty of Science, Charles University, Albertov 2030, 128 40 Prague 2, Czech Republic*

[2] *Analytical and Environmental Sciences Division, MRC-PHE Centre for Environment and Health, King's College London, United Kingdom*

**stiborov@natur.cuni.cz*

**Abstract**

Oxidation of benzo[a]pyrene (BaP) by cytochrome P450 (CYP) 1A1 expressed in a eukaryotic systems (microsomes, Supersomes$^{TM}$) is stimulated by cytochrome $b_5$ and NADH. In contrast, no such effects were produced by this CYP expressed in a prokaryotic system (in a membrane fraction of *Escherichia coli* cells).

## 1. INTRODUCTION

Benzo[*a*]pyrene (BaP) has been classified as human carcinogen (Group 1) by the International Agency for Research on Cancer [1]. This is genotoxic carcinogen that covalently binds to DNA after metabolic activation by cytochrome P450 (CYP) [2]. CYP1A1 is the most important enzyme in BaP bioactivation [2,3], in combination with microsomal epoxide hydrolase (mEH). First, CYP1A1 oxidizes BaP to an epoxide that is then converted to a dihydrodiol by mEH (*i.e.* BaP-7,8-dihydrodiol); then further bio-activation by CYP1A1 leads to the ultimately reactive species, BaP-7,8-dihydrodiol-9,10-epoxide (BPDE) that can react with DNA, forming adducts preferentially the 10-(deoxyguanosin-$N^2$-yl)-7,8,9-trihydroxy-7,8,9,10-tetrahydrobenzo[*a*]pyrene adduct *in vitro* and *in vivo* [4]. BaP is, however, oxidized also to other metabolites, such as the other dihydrodiols, BaP-diones and hydroxylated metabolites that are mainly the detoxification products.

The CYP enzyme, including CYP1A1, is a component of mixed function oxidase system located in the membrane of endoplasmic reticulum that contains beside the CYPs also another enzyme, NADPH:cytochrome P450 reductase (POR), and cytochrome $b_5$ accompanied with its NADH:cytochrome $b_5$ reductase. *Via* the activation of molecular oxygen, this multienzyme system catalyzes the monooxygenation of a variety of xenobiotics, including BaP [5]. The oxygen is activated in the active center of CYPs by two electrons transferred from NADPH

and/or NADH by means of POR and cytochrome $b_5$, respectively. Whereas POR is an essential constituent of the electron transport chain towards CYP, the role of cytochrome $b_5$ is still quite enigmatic. Likewise, a potential of NADH as a donor of electrons to the CYP-mediated reaction cycle is still not exactly known. Even though the second electron in the CYP reaction cycle might also be provided by the system of NADH:cytochrome $b_5$ reductase, cytochrome $b_5$ and NADH, there is still rather enigmatic whether this system might participate in donation of the first electron to CYP. Therefore, here we investigated the effect of cytochrome $b_5$ and NADH on a potency of CYP1A1 to oxidize BaP.

## 2. MATERIAL AND METHODS

Liver microsomes of rats, in which CYP1A1 was induced with Sudan I, Supersomes™ isolated from insect cells transfected with baculovirus constructs containing cDNA of human CYP1A1 and expressing POR, and human recombinant CYP1A1 expressed with its reductase in a membrane fraction of *Escherichia coli* cells transfected with *cDNA* of human CYP1A1 were used as model enzyme systems.

## 3. RESULTS AND DISCUSSION

Rat hepatic microsomes, in which CYP1A1 was induced with Sudan I, oxidized BaP to eight metabolites separated by HPLC. They were identified to be BaP-9,10-dihydrodiol, a metabolite Mx, the structure of which has not been identified as yet, BaP-4,5-dihydrodiol, BaP-7,8-dihydrodiol, BaP-1,6-dione, BaP-3,6-dione, BaP-9-ol and BaP-3-ol. These results correspond to those found in earlier studies reporting that these metabolites were formed by CYP1A1 in combination with mEH [2]. Interestingly, the used rat hepatic microsomes formed in the presence of NADH the same BaP metabolites as microsomes with NADPH. The amounts of metabolites were also comparable.

Human CYP1A1 expressed with POR in Supersomes™ oxidized BaP to seven metabolites, namely BaP-9,10-dihydrodiol, the unknown metabolite Mx, BaP-7,8-dihydrodiol, BaP-1,6-dione, BaP-3,6-dione, BaP-9-ol and BaP-3-ol. This finding indicates that BaP is metabolized not only by CYP1A1 present in this enzyme system, but also by mEH, which is important for the hydration of BaP epoxides to produce dihydrodiols. Therefore, this enzyme has to be present in the Supersomal system. Similar to hepatic microsomes human recombinant CYP1A1 expressed with POR in Supersomes™ oxidized BaP to the above mentioned metabolites even when NADH was present instead of NADPH. Addition of cytochrome $b_5$ to the CYP1A1 system led to a more than 2-fold increase in BaP oxidation to its metabolites. Because only the levels of individual BaP metabolites, but not of their pattern, were changed

by cytochrome $b_5$, the effect of this protein on an electron transfer to CYP1A1 seems to be the predominant mechanism responsible for the observed increase in oxidation of BaP.

In contrast to supersomal CYP1A1, only five metabolites were formed by human CYP1A1 expressed with POR in *E. coli* (Bactosomes); the metabolite Mx, BaP-1,6-dione, BaP-3,6-dione, BaP-9-ol and BaP-3-ol. The BaP-9-ol metabolite was formed in more than the 3.5-fold higher amounts in this CYP1A1 system than by CYP1A1 in Supersomes™. The results found in experiments using a membrane of *E. coli* containing CYP1A1 and POR indicated that mEH seems to be present in very low concentrations that are not sufficient for catalysis of these reactions. Addition of cytochrome $b_5$ to the system of CYP1A1 expressed in *E. coli* led to essentially no stimulation effect in BaP oxidation. Furthermore, in contrast to CYP1A1 expressed in Supersomes™, no BaP metabolites were formed by CYP1A1 expressed with POR in *E. coli* when NADH was added instead of NADPH. However, BaP incubated *ex-vivo* with the bactosomal CYP1A1, NADH:cytochrome $b_5$ reductase, cytochrome $b_5$ and NADH without NADPH was oxidized. The same metabolites as those formed by CYP1A1, POR and NADPH were formed in this system.

## 4. CONCLUSION

The results found indicate that the POR-mediated electron transfer from NADPH to CYP1A1 in the membrane of endoplasmic reticulum is stimulated by cytochrome $b_5$. Because of this effect, cytochrome $b_5$ is a biologically important factor influencing BaP-mediated carcinogenesis. The results also suggest that NADH can, to some extent, substitute NADPH as an electron donor for the CYP1A1 reaction cycle of BaP oxidation

## 5. ACKNOWLEDGEMENT

The work has been supported by GACR (P301/10/0356) and Charles University in Prague (GAUK 640712 and UNCE 204025/2012).

## 6. REFERENCES

[1]IARC: IARC Monographs of Evaluation of Carcinogens. Risk of Chemicals for Human, 92 (2010), 1-853

[2]Baird WM, Hooven LA, Mahadevan B: Environmental and Molecular Mutagenesis, 45 (2005), 106–114

[3]Hamouchene H, Arlt VM, Giddings I, et al.: BMC Genomics 12 (2011), 333

[4]Phillips DH, Venitt S: International Journal of Cancer, 131 (2012), 2733-2753

[5]Coon MJ: Nutrition Review, 36 (1978), 319-328

# THE AZOBENZENE ACTINOMETER

Jamaludin AL ANSHORI,[1,*] Pavel DVOŘÁK,[3] Roman BERÁNEK,[1] Jakob WIRZ,[4]
Petr KLÁN,[1,2] and Dominik HEGER[1,2,*]

1. *Department of Chemistry, Faculty of Science, Masaryk University, Kamenice 5/A8, 625 00, Brno, Czech Republic.*
2. *RECETOX, Faculty of Science, Masaryk University, Kamenice 126/3, 625 00 Brno, Czech Republic.*
3. *Department of Physical Electronics - Physics Section, Faculty of Science, Masaryk University, Kotlářská 267/2, 611 37 Brno, Czech Republic.*
4. *Department of Chemistry, University of Basel, Klingelbergstrasse 80, CH-4056 Basel, Switzerland.*

* *jamaludinalanshori@gmail.com*; *hegerd@chemi.muni.cz*

**Abstract**

Azobenzene has already been reported to be a very useful and readily available actinometer in the spectral range of 254–436 nm.[1-4] It undergoes the *E*-*Z* photoisomerization which is a simple reaction, both azobenzene isomers have unique physical properties, and moreover, the *E*-azobenzene is a cheap, thermally stable, and recyclable starting material.[4] The photoisomerization of azobenzene has not only been utilized in actinometry but also in biology to drive the functional changes in peptides, proteins, nucleic acids, lipids, and carbohydrates.[5] To revise the standard protocol of the azobenzene's quantum yield ($\Phi$) determination and find inconsistencies of the reported molar absorption coefficients of *Z*-azobenzene, we determined the molar absorption coefficients of azobenzene isomers and the quantum yields of the *E*-*Z* isomerization with a higher accuracy. The molar absorption coefficients of *E*-azobenzene in MeOH was calculated from the UV/Vis absorption spectra of various concentrations of the samples, while those of the *Z*-isomer were obtained using an algebraic minimization approach from the measured UV/Vis absorption spectra of irradiated *E*-azobenzene along with the corresponding concentration ratio of the isomers obtained from the $^1$H-NMR measurements and known molar absorption coefficients of *E*-azobenzene. The quantum yield ($\Phi$) of the *Z*-*E* isomerization in MeOH at 313 nm was found to be 0.20 ± 0.01 which was almost two times lower than the reported one (0.30[4] or 0.37[6]), while the quantum yield of *E*-*Z* isomerization was 0.14 ± 0.004 which is in agreement with that reported by Gauglitz and Ronayette (0.13[4] or 0.14[7]). In addition, the pseudo quantum yield of *Z*-*E* isomerization in MeOH at 313 nm was calculated to be 3588 ± 27.

**REFERENCES**

(1) Zimmerman, G.; Chow, L. Y.; Paik, U. J. *J. Am. Chem. Soc.* 1958, *80*, 3528.

(2) Marco Montalti, A. C., Luca Prodi, M. Teresa Gandolfi *Handbook of Photochemistry*; 3rd ed.; CRC Press Taylor & Francis Group: Boca Raton, 2006.

(3) Leighton, W. G.; Forbes, G. S. *J. Am. Chem. Soc.* 1930, *52*, 3139.

(4) Gauglitz, G.; Hubig, S. *J. Photochemistry* 1985, *30*, 121.

(5) Beharry, A. A.; Woolley, G. A. *Chem. Soc. Rev.* 2011, *40*, 4422.

(6) Siampiringue, N.; Guyot, G.; Monti, S.; Bortolus, P. *J. Photochem.* 1987, *37*, 185.

(7) Ronayette, J.; Arnaud, R.; Lebourgeois, P.; Lemaire, J. *Can. J. Chem.* 1974, *52*, 1848.

# DEEPER RESEARCH OF STRUCTURAL CHANGES OF HUMIC ACIDS USING LIGHT SCATTERING TECHNIQUES

Michal KALINA*, Aneta CHYTILOVÁ, Martina KLUČÁKOVÁ

*Materials Research Center, Faculty of Chemistry, Brno University of Technology, Purkyňova1464/118, 612 00 Brno, Czech Republic*

**xckalina@fch.vutbr.cz*

**Abstract**

Humic acids are remarkable substance, which significantly participate in natural processes. For structural modelling and also for their possible future application parameters as particle size and conformation seem to be essential. This contribution is dealing with study of both these parameters measured by means of dynamic light scattering method. The main aim of the work was the study of behavior of lignite humic acids in their aqueous dispersions. The effect of pH, purification and selective modification is during the work discussed. All these parameters significantly influence behavior of humic acids in aqueous solutions by impacting on their supramolecular stabilization and their aggregation processes.

## 1. INTRODUCTION

Humic acids are remarkable natural compounds, which play a significant role in binding, transport and biological uptake of different nutrients and contaminants in soils and aquatic environments. The main function of humic acids (HA) in soils and sediments is to impact the porosity and to act as a sorbent and reservoir of water and different kind of chemicals. Well–known and described is high affinity of HA toward different species such as metals, surfactants, dyes and hydrophobic species [1, 2, 3, 4]. These facts hand by hand with humic acids colloidal size, rich natural availability and relatively low–cost extraction techniques create from them extremely important material for practical applications. For basic structural modelling, study of reactivity and possible future applications of humic acids basic parameters such as particle size and shape as well as molecular weight must be taken into account. Light scattering techniques can provide easy methods, which can be applied for such characterization [5]. Application of light scattering methods in the area of humic particle characterization upraises recent years as novel techniques. This area of research is still encountered by few experimental difficulties mainly caused because of the heterogenic and polydisperse character of humic materials.

## 2. MATERIAL AND METHODS

Humic acids, studied in this work, were obtained in the process of alkaline extraction from South Moravian lignite. More details on the method of isolation of humic acids as well on the characterization can be found in [2, 4, 6]. Obtained humic acids were repeatedly washed in water and freeze dried to decrease the content of inorganic salts.

For study of the aggregation processes of humic acids in aqueous solutions two different groups of humic sols were prepared. The first group (SOL A and B) was represented by samples prepared by direct dissolving of solid humic acids in 0.1 M NaOH (SOL A). SOL B contained of solid humic acids dispersed in water (followed by adjusting of pH to value 12 using 5 M NaOH). The second group can be described as neutral sols of HA. SOL C was prepared by neutralization of solution of HA in 0.1 M NaOH using 0.1 M HCl (volume ration of 0.1 M NaOH to 0.1 M HCl was 1:1). The second type of neutral humic sol was prepared by diluting of most concentrated SOL A using 0.1 M NaCl. Final concentrations of HA in all utilized sols were following: 0.01; 0.02; 0.1; 0.2; 0.5; 1; 1.5; 2; 4; 5; 6 and 10 $g \cdot dm^{-3}$.

To study the influence of often utilized selective blocking (methylation) of functional groups (mainly carboxylic and phenolic) of HA washed samples were treated with methylation agent. For these purposes TMS-N2 (trimethylsilyl diazomethane) was used. More details about this process can be found in [4]. Success of the methylation process was verified using FTIR spectroscopy. FTIR spectra of solid humic powders in KBr pellets were measured using spectrometer Nicolet iS50.

Particle size distribution for all studied humic acids dispersion were obtained using Zetasizer Nano ZS system from Malvern Instrument by means of the method of dynamic light scattering. Obtained size distributions represent valuable tool for characterization of the aggregation processes in humic acids solutions and for comparison of different sources of humic acids, different humic conditions of preparation of humic sols and also pre–treatment. All presented size distribution represent average values from five repeated measurements. The measurements were carried out at temperature (25.0±0.1) °C.

## 3. RESULTS AND DISCUSSION

The main part of this work was dealing with the utilization of dynamic light scattering for basic particle characterization of different humic dispersions. The basic output from dynamic light scattering method is intensity size distribution, which shows dependence of relative intensity of scattered light on distribution of particle size classes. Intensity size distribution can be converted, using mathematical algorithm called Mie theory, to a volume distribution.

The volume distribution describes more clearly the distribution of mass in the sample. First part of the work was investigating the effect of purification of HA on obtained particle size distributions. Figure 1A describes the volume particle distribution of SOL A after different purification steps. This pre–treatment of HA significantly decreased their content of ash from 30.5 weight % to 26.6 weight % after repeated washing respectively to 2 weight % after applying of freeze–drying. From Figure 1A is obvious that decreased level of ash in the sample decrease also the process of aggregation of HA. By these reasons the freeze-dried HA were used as source material for preparation of all the humic dispersions in this work.

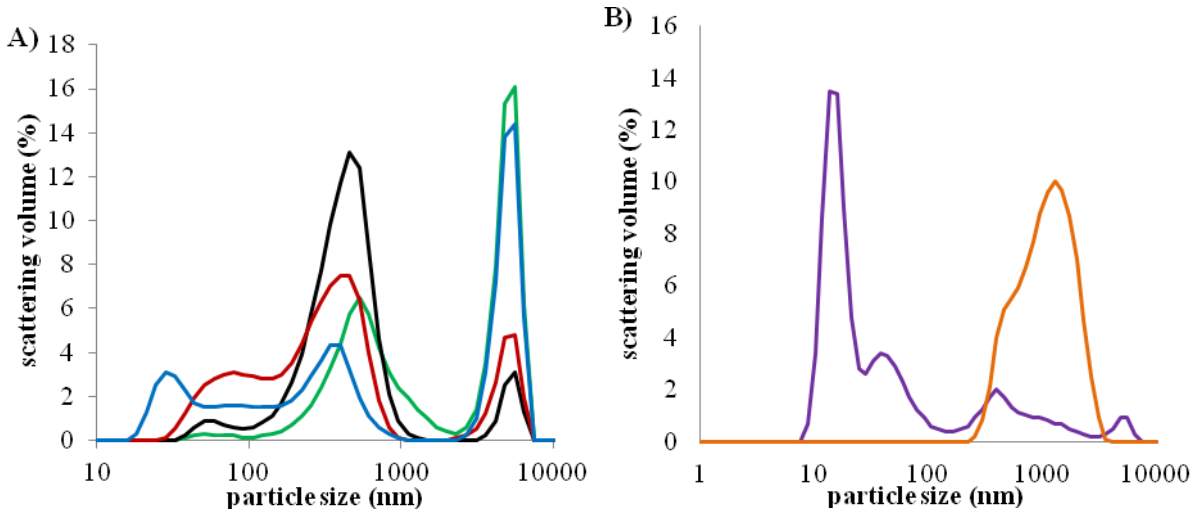


**Figure 1.:** A) Volume particle size distributions of lignite HA after different pre-treating steps – lignite HA in 0.1 M NaOH (SOL A - green line), washed HA in 0.1 M NaOH (blue line) and freeze-dried HA in 0.1 M NaOH (red line) and lignite HA dissolved in water (SOL B – black line); B) Volume particle size distributions of lignite HA in mixture of 0.1 M NaOH + 0.1 M HCl (SOL C – purple line) and lignite HA in 0.1 M NaCl (SOL D – orange line).

Figure 1A illustrates the comparison of HA dissolved in 0.1M NaOH (SOL A) and in water (SOL B). Both these alkali groups of dispersions show three different parts in their distributions. First region is up to 100 nm, which can be defined as single humic particles. The peaks round 400 nm can be assigned to supramolecular assemblies of humic particles stabilized by non-covalent interactions. The last part of the distributions above 2000 nm can be described as aggregates of molecules. These findings are consistent with new supramolecular models of HA structure [7]. Figure 1B describe the volume particle size distributions of neutral HA dispersions (SOL C and SOL D). The different way of preparation and mainly the different pH of the dispersions significantly influenced the particle distributions. The particle distribution of SOL C shows that decrease of pH of the solutions

caused by its neutralization destroyed the non–covalent stabilization of humic supramolecular assemblies. On the other side SOL D contained high level of low–molecular ions ($Na^+$, $Cl^-$), which significantly decreased stability of these HA dispersions and aggregation of HA particles occurred.

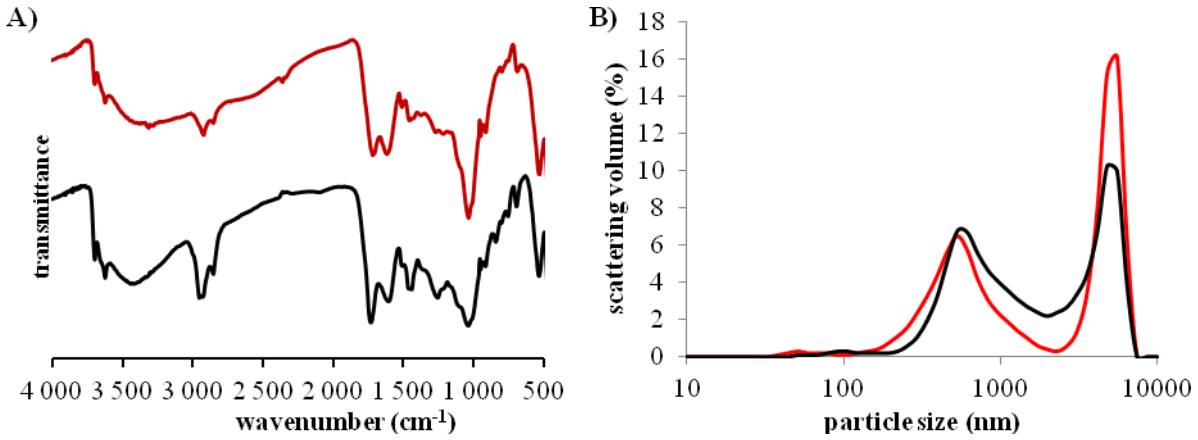


**Figure 2.:** A) Infrared spectra of lignite humic acids (red) and their methylated forms (black) B) Volume particle size distribution of lignite humic acids (red) and their methylated equivalent (black)

The last part of the work was investigating the effect of selective modification of reactive functional groups of HA in the process of selective methylation using TMS-N2 [4]. The FT-IR spectra of HA and MHA (Figure 2A) confirmed the modification of humic acids after methylation. On the other side Figure 2B displayed that the methylation process of HA did not increase significantly their aggregation. The only difference in obtained particle size distributions can be found in the area round 1000 nm, which can be connected to change of the conformation of HA in the solutions.

## 4. CONCLUSION

The results of this study shed new light on behavior of humic acids in aqueous solutions. The work emphasized the purification as important pre–treatment step for humic acids to decrease their aggregation. Obtained data confirmed the supramolecular model of humic acids structure. On the other side the effect of pH and content of low molecular ions has to be also taken into mind. Both these parameters significantly influence humic acids behavior in aqueous solutions.

**5. ACKNOWLEDGEMENT**

This work has been supported by Materials Research Centre at FCH BUT- Sustainability and Development, REG LO1211, with financial support from National Program for Sustainability I (Ministry of Education, Youth and Sports)

**6. REFERENCES**

[1]Tipping E: Cation Binding by Humic Substances, (2002), 434 p.

[2]Sedlaček P, Smilek J, Klučáková M: Reactive and Functional Polymers, 7, (2013), 1500-1509.

[3]Ishiguro M, Tan W, Koopa, L K: Colloids and Surface A: Physicoch,. and Eng. Aspects, 306 (2007), 29-39.

[4]Klučáková M, Kalina M, Sedláček P: Journal of Soils and Sediments, 14 (2014), 368-376.

[5]Brown W: Dynamic light scattering: The Method and Some Applications, (2011), 752 p.

[6]Peuravuori J, Žbanková P, Pihlaja K: Fuel Processing Technology, 87 (2006), 9, 829-839.

[7]Piccolo A, Nardi S, Concheri G: Chemosphere, 4 (1996), 33, 595-602.

# ARE FLAVONOIDS FENOXIDE ANIONS BETTER HYDROGEN ATOM DONORS THAN PARENT MOLECULES?

Ján RIMARČÍK, Erika SENAJOVÁ, Adam VAGÁNEK, Erik KLEIN*

*Institute of Physical Chemistry and Chemical Physics, Faculty of Chemical and Food Technology, Slovak University of Technology in Bratislava, Radlinského 9, SK-812 37 Bratislava, Slovakia*

**erik.klein@stuba.sk*

**Abstract**

In this work, we have theoretically studied the thermodynamics of the O–H bonds homolytic cleavage in various fenoxide anions formed from quercetin and kaempferol in the terms of corresponding BDEs.

## 1. INTRODUCTION

Flavonoids represent a large class of naturally occurring polyphenols, mainly found in fruits, vegetables and cereals. Growing interest in flavonoids research can be attributed mainly to the antioxidant and free radical scavenging activities related to their OH groups [1], Fig. 1.

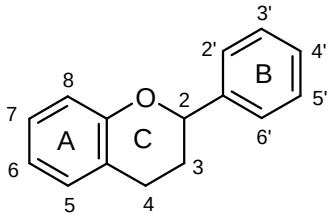


**Figure 1:** Atom numbering and ring denotation in flavonoids.

Experimental works indicate that phenoxide anions, $ArO^-$, formed from flavonoids can be better radical scavengers than neutral molecules, ArOH [2–4]. Therefore, in this work we decided to study the thermodynamics of the hydrogen atom transfer (HAT) from the fenoxide anions of quercetin and kaempferol (Fig. 2) in three environments: gas-phase, benzene, and water. Homolytic OH group splitting-off leading to the formation of the radical anion $ArO^{\bullet -}$ is driven by O–H bond dissociation enthalpy, BDE.

## 2. COMPUTATIONAL DETAILS

All calculations were performed using Gaussian 09 program package [5]. The geometries of all species were optimized using DFT method with B3LYP [6] functional without any

constraints (energy cut-off of $10^{-5}$ kJ mol$^{-1}$, final RMS energy gradient under 0.01 kJ mol$^{-1}$ Å$^{-1}$). Calculations were performed in 6-311++G** basis set [7]. Solvent contribution to the total enthalpies was computed using integral equation formalism IEF-PCM method [8, 9].

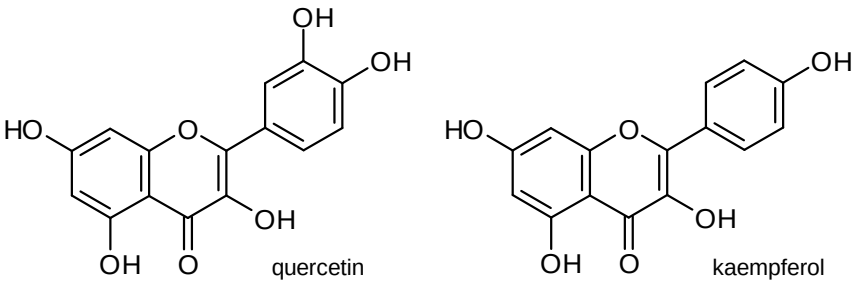


**Figure 2:** Parent molecules ArOH.

## 3. RESULTS AND DISCUSSION

For chosen anions, BDE values calculated for $T$ = 298 K are compiled in the Table 1. The first column shows splitted-off OH group, second column presents the reacting anion. First row of each table section shows BDEs for the neutral parent molecule.

**Table 1**: B3LYP/6-311++G** BDE values in kJ mol$^{-1}$.

| ArO$^{\bullet-}$ | ArO$^-$ | quercetin | | | kaempferol | | |
|---|---|---|---|---|---|---|---|
| | | gas | benzene | water | gas | benzene | water |
| 3'-OH | — | 316 | 324 | 316 | | | |
| | 4'-O$^-$ | 326 | 324 | 302 | | | |
| | 3-O$^-$ | 257 | 272 | 279 | | | |
| | 5-O$^-$ | 281 | 301 | 306 | | | |
| | 7-O$^-$ | 286 | 306 | 308 | | | |
| 4'-OH | — | 305 | 313 | 305 | 338 | 343 | 331 |
| | 3'-O$^-$ | 299 | 303 | 287 | | | |
| | 3-O$^-$ | 224 | 242 | 251 | 249 | 265 | 271 |
| | 5-O$^-$ | 257 | 279 | 288 | 282 | 303 | 311 |
| | 7-O$^-$ | 260 | 283 | 290 | 284 | 306 | 313 |
| 3-OH | — | 339 | 338 | 317 | 340 | 340 | 318 |
| | 3'-O$^-$ | 295 | 304 | 296 | | | |
| | 4'-O$^-$ | 290 | 295 | 283 | 290 | 295 | 284 |
| | 5-O$^-$ | 328 | 328 | 307 | 334 | 323 | 308 |
| | 7-O$^-$ | 311 | 315 | 300 | 310 | 315 | 300 |
| 7-OH | — | 362 | 366 | 351 | 360 | 365 | 352 |
| | 3'-O$^-$ | 284 | 303 | 304 | | | |
| | 4'-O$^-$ | 285 | 300 | 300 | 285 | 302 | 304 |
| | 3-O$^-$ | 271 | 280 | 278 | 271 | 280 | 279 |
| | 5-O$^-$ | 315 | 327 | 326 | 309 | 323 | 324 |

For all anions (with the exception of 3',4'- radical anion of quercetin in gas-phase and benzene), HAT from $ArO^-$ shows lower BDE in the comparison to the parent molecules. Differences are often in order of tens of kJ $mol^{-1}$. For both flavonols, the lowest BDEs are attributed to 4'-OH group splitting-off in 3-$O^-$ fenoxide anions. For the majority of formed radical anions, lowest BDEs are related to 3-$O^-$ fenoxide anions. For HAT running at 3-OH group, the lowest BDE was obtained for 4'-$O^-$ fenoxide anion. However, we should note that reaction enthalpies of the deprotonation of individual OH groups in parent molecules are different and dramatically depend on the environment [10]. Thus, to find the lowest overall reaction enthalpy for the formation of radical anion $ArO^{\bullet -}$ from the parent ArOH molecule the sum of the reaction enthalpies of the two steps (deprotonation and HAT) has to be taken into account.

## 4. CONCLUSION

In the gas-phase, benzene and water, we have confirmed that all OH groups present in the fenoxide anions $ArO^-$ formed from quercetin and kaempferol are, from the thermodynamic point of view, actually better hydrogen atom donors than the parent molecules.

## 5. ACKNOWLEDGEMENT

This work has been supported by the Slovak Grant Agency (VEGA 1/0735/13 and 1/0307/14).

## 6. REFERENCES

[1] Procházková D, Boušová I, Wilhelmová N: Fitoterapia 82 (2011), 513–523
[2] Musialik M, Kuzmicz R, Pawlowski TS, Litwinienko G: J. Org. Chem. 74 (2009), 2699–2709
[3] Jovanovic SV, Steenken S, Tosic M, Marjanovic M, Simic MG: J. Am. Chem. Soc. 116 (1994), 4846–4851
[4] Lemanska K, et al.: Free Radic. Biol. Med. 31 (2001), 869–881
[5] Frisch MJ, et al. Gaussian 09, Revision C.01, Gaussian, Inc., Wallingford, CT, 2010
[6] Becke A: J. Chem. Phys. 98 (1993), 5648–5652
[7] Binkley JS, Pople JA, Hehre WJ: J. Am. Chem. Soc. 102 (1980), 939–947
[8] Cances E, Mennucci B, Tomasi J: J. Chem. Phys. 107 (1997), 3032–3041
[9] Cances E, Mennucci B: J. Math. Chem. 23 (1998), 309–326
[10] Vagánek A, Rimarčík J, Lukeš V, Klein E: Comput. Theor. Chem. 991 (2012), 192–200

# ON THE HOMOLYTIC AND HETEROLYTIC O–H BOND CLEAVAGE IN VITAMIN B6

Peter ŠKORŇA, Ján RIMARČÍK, Michaela KLENOVIČOVÁ, Erik KLEIN*

*Institute of Physical Chemistry and Chemical Physics, Faculty of Chemical and Food Technology, Slovak University of Technology in Bratislava, Radlinského 9, SK-812 37 Bratislava, Slovakia*

**erik.klein@stuba.sk*

**Abstract**

This work is focused on the thermodynamic study of the reaction enthalpies related to the three mechanisms of primary antioxidants action of the three vitamin B6 components, as well as 4-pyridoxic acid that represents their metabolite.

## 1. INTRODUCTION

Current experimental research results indicate that vitamin B6, Fig. 1, shows an antioxidant activity in plants [1]. It is more powerful singlet oxygen, $^1O_2$, scavenger than vitamins C and E [2]. In blood, it shows higher antioxidant activity than vitamin C [3], too.

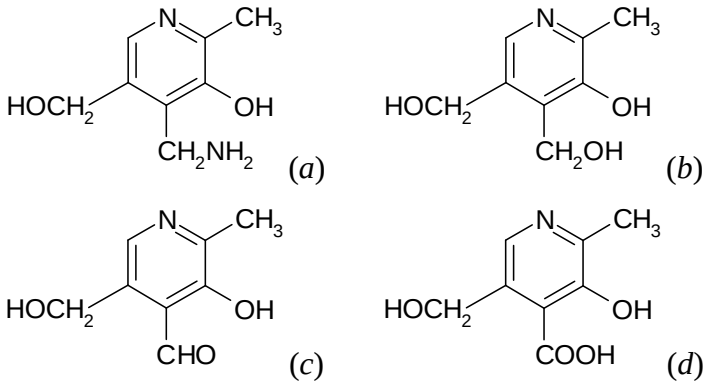


**Figure 1:** Vitamin B6: pyridoxamine (a), pyridoxine (b), pyridoxal (c); 4-pyridoxic acid (d).

In this work we decided to study the reaction enthalpies related to the three mechanisms of primary antioxidants action for pyridoxamine, pyridoxine, pyridoxal, and 4-pyridoxic acid in three environments: gas-phase, benzene, and water. Antioxidant action of investigated compounds can be ascribed to the OH group attached directly to the aromatic ring, placed in the *meta* position to nitrogen. One of the aims of the work is to compare calculated reaction

enthalpies with data available for typical primary phenolic antioxidants, such as tocopherols or flavonoids.

## 2. COMPUTATIONAL DETAILS

All calculations were performed using Gaussian 09 program package [4]. The geometries of all studied species were optimized using DFT method with B3LYP [5] functional without any constraints (energy cut-off of $10^{-5}$ kJ mol$^{-1}$, final RMS energy gradient under 0.01 kJ mol$^{-1}$ Å$^{-1}$). Calculations were performed in 6-311++G** basis set [6]. Solvent contribution to the total enthalpies was computed using integral equation formalism IEF-PCM method [7, 8]. From the total enthalpies, following reaction enthalpies were calculated for the above mentioned reaction centre: (*i*) O–H bond dissociation enthalpies; (*ii*) ionization potentials and (*iii*) proton dissociation enthalpies; (*iv*) proton affinities of anions formed by OH group deprotonation and (*v*) electron transfer enthalpies (for the definitions, see ref. [9]) at $T$ = 298 K.

## 3. RESULTS AND DISCUSSION

In all environments, bond dissociation enthalpies, BDE, reached similar values. In the gas-phase, they lie in the 346–400 kJ mol$^{-1}$ range. The lowest value was found for pyridoxamine and pyridoxine (difference between the corresponding values only 1 kJ mol$^{-1}$). The highest BDEs were found for 4-pyridoxic acid (390 kJ mol$^{-1}$) and pyridoxal (400 kJ mol$^{-1}$), because CHO and COOH groups form strong intramolecular hydrogen bonds with the OH group representing the reaction center. The lowest ionization potential and electron transfer enthalpy values were found for pyridoxamine. On the contrary, lowest proton dissociation enthalpies in all studied environments were obtained for 4-pyridoxic acid. Lowest proton affinities were found for pyridoxine. In solution-phase, reaction enthalpies for processes including charged species are significantly lower than corresponding gas-phase values. In general, found reaction enthalpies are similar to those found for phenolic antioxidants – tocopherols or flavonoids [9].

Currently, obtained results are analyzed in order to (*i*) identify the effect of –$CH_2NH_2$, – $CH_2OH$, –CHO, and –COOH groups in the *para* position to nitrogen atom (Fig. 1) on the studied reaction enthalpies, and (*ii*) to assess the role of the environment.

## 4. CONCLUSION

In this ongoing theoretical work, we study pyridoxamine, pyridoxine, pyridoxal, and 4-pyridoxic acid in the various environments with the focus on the thermodynamics of aromatic OH group homolytic and heterolytic splitting-off. Calculated reaction enthalpies are analyzed to shed light on the effect of the substituent located in the *para* position to nitrogen atom.

## 5. ACKNOWLEDGEMENT

This work has been supported by the Slovak Grant Agency (VEGA 1/0735/13 and 1/0307/14).

## 6. REFERENCES

[1] Denslow A S, Walls AA, Daub, EM: Physiol. Mol. Plant. P. 66 (2005), 248–249

[2] Bilski P, Li YM, Ehrenshaft M, Daub EM, Chignell FC: Photochem. Photobiol. 71 (2000), 129–134

[3] Stocker P, Lesgards J-F, Vidal N, Chalier F, Prost M: Biochim. Biophys. Acta 1621 (2003), 1–8

[4] Frisch MJ, et al. Gaussian 09, Revision C.01, Gaussian, Inc., Wallingford, CT, 2010

[5] Becke A: J. Chem. Phys. 98 (1993), 5648–5652

[6] Binkley JS, Pople JA, Hehre WJ: J. Am. Chem. Soc. 102 (1980), 939–947

[7] Cances E, Mennucci B, Tomasi J: J. Chem. Phys. 107 (1997), 3032–3041

[8] Cances E, Mennucci B: J. Math. Chem. 23 (1998), 309–326

[9] Vagánek A, Rimarčík J, Lukeš V, Klein E: Comput. Theor. Chem. 991 (2012), 192–200

# Observation of prompt ISC from higher excited states of the anion of *p*-hydroxyacetophenone

J. Krausko [1*)], J. A. Anshori [1)], M. Chrástková [1)], D. Nachtigallová [2)], D. Heger [1)]

[1]*Department of Chemistry, Faculty of Science, Masaryk University, Kamenice 5/A8, Brno 602 00, Czech Republic; Research Centre for Toxic Compounds in the Environment, Faculty of Science, Masaryk University, Kamenice 3, 625 00 Brno, Czech Republi*

[2]*Institute of Organic Chemistry and Biochemistry, Flemingovo nam. 2, 166 10 Prague, Czech Republic.*

**krausko@mail.muni.cz*

Phenacyl compounds are promising candidates for use as photoremovable protecting groups (PPGs) enabling spatial and temporal control over the release of various molecules of interest (neurotransmitters, drugs, etc.) [1]. However, detailed knowledge of their photophysics is needed.

The anion of *p*-hydroxyacetophenone ($pHA^-$) was reported by us and others not to give a triplet state upon the excitation at the red edge of its absorption spectrum (355 nm) whereas excitation at lower wavelengths produced triplet effectively[2,3,4]. This observation is thoroughly demonstrated by luminescence and LFP experiments which bring us to the explanation that is underlined by quantum chemical calculations. The S1 state is giving only the fluorescence, while the S2 is more effectively ISC to the T2 than IC to S1.

[1] P. Klán, T.Šolomek, et al., *Chem. Rev.* **2013**, *113 (1)*, 119–191.

[2] Ľ. Klíčová, P. Šebej, et al., *The Journal of Physical Chemistry A* **2012**, *116*, 2935-2944.

[3] P. Zuo, C. S. Ma, et al., *J. Org. Chem.* **2005**, *70*, 8661-8675.

[4] V. B. Kammath, T. Šolomek, B. P. Ngoy, D. Heger, P. Klán, M. Rubina, R. S. Givens, *Journal of Organic Chemistry* **2013**, *78*, 1718

# ACIDITY OF FROZEN SOLUTIONS AND ITS CONNECTION TO DEGRADATION OF ENZYMES UPON FREEZING

Ľubica Krausková[1], Jitka Procházková[1], Martina Klašková[1], Václav Hutník[1], Petr Klán[1,2], Dominik Heger[1,2]

[1] *Department of Chemistry, Faculty of Science, Masaryk University, Kamenice 5/A8, Brno 602 00, Czech Republic*

[2] *Research Centre for Toxic Compounds in the Environment, Faculty of Science, Masaryk University, Kamenice 3, 625 00 Brno, Czech Republic*

When a buffered solution is frozen, its acidity may change considerably due to sequential crystallization of individual buffer components, as was shown for sodium phosphate and succinate buffer systems [1, 2]. For example, when sodium phosphate buffer is frozen, $Na_2HPO_4$ starts to precipitate, leaving only $NaH_2PO_4$ in the remaining solution and a pH decreases as much as 3 pH units [3]. Such an abrupt pH change can affect stability of proteins and other biomolecules during the process of freezing.

Addition of neutral salts to a solution prior to freezing also affects pH of the frozen solution. Cations and anions are not incorporated into the ice lattice equally; it leads to charge imbalance between the ice and the unfrozen solution and Workman-Reynolds freezing potential is generated. The excess charges are eventually neutralized via interfacial transport of $H^+$ / $OH^-$ ions and the acidity of the remaining solution can change significantly and permanently [4, 5].

We applied UV-Vis absorption and diffuse reflectance spectroscopy to measure acidities of frozen aqueous solutions of common buffers and salts under various conditions. A low amount of acid-base indicator cresol red was used as an internal probe [6]. The observed pH changes and their consequences for enzymes freezing and thawing will be discussed in the presentation.

## REFERENCES

1. Murase, N. and F. Franks, *Salt Precipitation During the Freeze-Concentration of Phosphate Buffer Solutions.* Biophysical Chemistry, 1989. **34**(3): p. 293-300.

2. Sundaramurthi, P., E. Shalaev, and R. Suryanarayanan, *Calorimetric and Diffractometric Evidence for the Sequential Crystallization of Buffer Components and the Consequential pH Swing in Frozen Solutions.* Journal of Physical Chemistry B, 2010. **114**(14): p. 4915-4923.

3. Gomez, G., M.J. Pikal, and N. Rodriguez-Hornedo, *Effect of initial buffer composition on pH changes during far-from-equilibrium freezing of sodium phosphate buffer solutions.* Pharmaceutical Research, 2001. **18**(1): p. 90-97.

4. Workman, E.J. and S.E. Reynolds, *Electrical Phenomena Occurring during the Freezing of Dilute Aqueous Solutions and Their Possible Relationship to Thunderstorm Electricity.* Physical Review, 1950. **78**(3): p. 254.

5. Bronshteyn, V.L. and A.A. Chernov, *Freezing Potentials Arising on Solidification of Dilute Aqueous-Solutions of Electrolytes.* Journal of Crystal Growth, 1991. **112**(1): p. 129-145.

6. Heger, D., J. Klanova, and P. Klan, *Enhanced protonation of cresol red in acidic aqueous solutions caused by freezing.* Journal of Physical Chemistry B, 2006. **110**(3): p. 1277-1287.

# STUDY OF NANOPARTICLES FORMED BY NEGATIVELY CHARGED HYALUROAN AND CATIONIC SURFACTANT

Tereza KRUTIŠOVÁ[1*], Miloslav PEKAŘ[1]

[1]*Brno University of Technology, Faculty of Chemistry, Institute of Physical and Applied Chemistry, Purkyňova 464/118, 612 00 Brno, Czech Republic*

**xckrutisova@fch.vutbr.cz*

**Abstract**

Negatively charged hyaluronan binds to cationic surfactant via electrostatic interactions which result in self-assembly nanoparticles formation. These particles have a core-shell like structure and can be used in targeted drug delivery of hydrophobic active substances. A hydrophobic inner core contains aggregated surfactant molecules and hyaluronan creates a hydrophilic shell layers.

The aim of our study was to prepare and study hyaluronic acid nanoparticles based on electrostatic interactions with oppositely charged surfactant molecules.

Interactions of hyaluronan and surfactants were investigated using dynamic light scattering and Laser Doppler Velocimetry methods. Titration experiments (size distribution and zeta potential measurements and isoelectric point) were utilized to explore the formation of aggregates. Hyaluronan or surfactant was used as titrant for comparison of two preparation methods of these systems. Effect of molecular weight and concentration of hyaluronan were investigated.

Aggregates formation is influenced by preparation of systems. Different types of particles are formed if hyaluronan is added to surfactant solution or vice versa. If hyaluronan have a role of titrant, final particles are smaller than in the case of surfactant as titrant and can be more suitable for drug delivery applications.

Assuming in the isoelectric point is reached compensation of charges of hyaluronan and surfactant, real degrees of hyaluronan dissociation were determined. Concentration of hyaluronan and conformation of hyaluronan in the system have a significant effect on established degree of dissociation.

## 1. INTRODUCTION

Hyaluronan is a naturally occurring linear polysaccharide. It is a negatively charged biopolymer possessing one carboxylate group per disaccharide repeating unit (D-glucuronic acid and N-acetyl-D-glucosamine residues linked by β(1-4) and β(1-3) bonds). Hyaluronan can be found primarily in the extracellular matrix of all higher organisms, and is therefore an attractive building block for new biocompatible and biodegradable materials that could have applications in drug delivery, tissue engineering, wound healing or surgery [1].

Hyaluronan cannot be directly used to carry nonpolar substances (hydrophobic drugs e.g. for fighting cancer) due to its highly hydrophilic character and large hydration shell. A combination of hyaluronan with surfactant may lead to formation of associates in which the surfactant hydrophobic domains solubilize hydrophobic substances and hyaluronan plays a role of biocompatible carrier and targeting agent [2].

Complex formation is influenced by preparation of systems. Different types of particles are formed if hyaluronan is added to surfactant solution or vice versa. In the case of surfactant as titrant as the ratio of surfactant molecules to charged sites on the polyelectrolyte approaches unity, precipitation of the complex occurs due to charge neutralization of the polyelectrolyte and to the hydrophobic nature of the bound surfactants, which adopt a conformation in which their ionic headgroups are effectively removed from the solution. On addition of further surfactant, the insoluble polymer-surfactant complex redissolves. This is due to cooperative binding of surfactant molecules on the polymer chains, whereby hydrophilic micelles are formed [3]. Formation of hyaluronan-surfactant complex nanoparticles can be done by addition of hyaluronan to surfactant solution. It is necessary use surfactant concentration under a critical micelle concentration to presence of micelles aggregates in solution.

Dynamic light scattering method and zeta potential measuremtns is one of many techniques for study of polyelectrolyte-surfactant interaction [4]. Results confirmed that these systems are formed due to electrostatic interactions and it depends on molar ratio of components.

## 2. MATERIAL AND METHODS

Hyaluronan (as sodium salt of hyaluronic acid; HyA) was purchased from CPN, Ltd., Czech Republic. Cationic surfactant cetyltrimethylammonium bromide (CTAB) of the best available purity was purchased from Sigma-Aldrich, Czech Republic.

Stock solutions of hyaluronan and CTAB were prepared in aqueous solution. All stock solution were prepared by slow dissolution of powdered substances upon stirring and left stirred for 24 hours to ensure complete dissolution.

Titrations of substances were performed for investigation of interactions between hyaluronan and surfactant. Surfactant or hyaluronan was used as titrant. Isoelectric points (point of zero charge) were determined and compared. In the case of surfactant as titrant, concentration of surfactant titrant was 5 mM or 50 mM and hyaluronan concentration was 15 $mg \cdot l^{-1}$, 1 $g \cdot l^{-1}$, respectively. In the case of hyaluronan as titrant, concentration of hyaluronan titrant was 1 $g \cdot l^{-1}$ and surfactant concentration was 1 mM. Hyaluronan was used at two molecular weights, 116 kDa and 1669 kDa.

Finally colloids were characterized by dynamic light scattering and laser Doppler Velocimetry methods. Size distribution (correlation function) and zeta potential measurements were utilized to explore the formation of complex micelles. All measurements were performed using Zetasizer Nano ZS (Malvern Instruments). All Zetasizer units provide a z-average figure which is the intensity weighted mean hydrodynamic size of the ensemble collection of particles measured by dynamic light scattering. Z-averages of size distribution were compared and plotted.

## 3. RESULTS AND DISCUSSION

Titration experiments were performed using hyaluronan or surfactant as titrant. In the case of surfactant as titrant, surfactant concentration linearly increased during the experiments and zeta potential increased mostly linearly during the titration, too. Initial zeta potential values of hyaluronan were about −30 mV. These values generally indicate high stability of the colloid system.

Size distribution of particles in the systems indicate that hyaluronan oneself without surfactant creates a wide-ranging domains in the solution. A small addition of the surfactant to hyaluronan solution decreases size distribution of particles in the system. With the increasing zeta potential of the system, close to isoelectric point, particles size distribution increases due to precipitation of the complex occurs owing to charge neutralization. The colloidal system exhibits in this point zero zeta potential and minimum stability. When surfactant concentration in the system dominates, size distribution stabilizes about 200-500 nm.

In the case of hyaluronan as titrant, situation of size distribution is analogous to previously case. Size distribution of stabilized nanoparticles when hyaluronan is in the system dominate, is about 200 nm. This may be more suitable method to formation drug delivery nanoparticles, which sizes should be in the range of 6 and 200 nm [5].

In case that surfactant was used as titrant isoelectric point or more precisely point of zero charge shows concentration of surfactant when positive charge of surfactant equals to

negative charge carrying on hyaluronan chain. It was found that measured isoelectric point does not correspond to theoretical isoelectric point supposing 100% dissociation of carboxylate groups of hyaluronan chain. Isoelectric point occurred at much lower surfactant concentration. It means that less than 100 % of hyaluronan carboxylate groups dissociate, practically about 50 %.

When hyaluronan was used as titrant, zeta potential decreases linearly during the titration. Point of zero charge was found at lower hyaluronan concentration than theoretical value if 100% dissociation is assumed. It was found that only 20 % carboxylate group was dissociated. Increase of size distribution of aggregates before isoelectric point was observed, too.

Concentration of hyaluronan and conformation of hyaluronan in the system have a significant effect on established degree of dissociation.

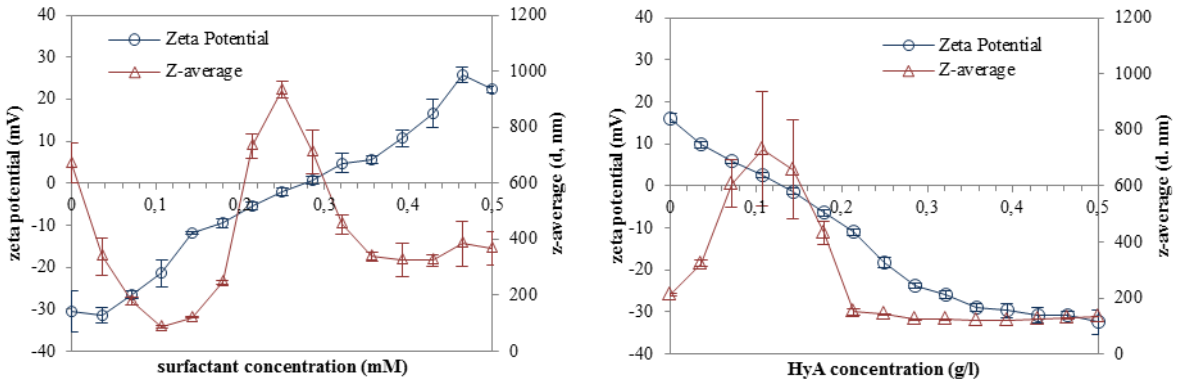


**Figure 1.:** Left – Zeta potential and z-average in depending of surfactant concentration ($M_w$ HyA = 116 kDa), Right - Zeta potential and z-average in depending of hyaluronan concentration ($M_w$ HyA = 116 kDa).

## 4. CONCLUSION

Titration experiments were performed to investigation of interaction between hyaluronan and opposite charged surfactant and to study differences between two methods of preparation of this system. Increase of aggregates size was observed near point of zero charge. The hyaluronan-surfactant system exhibits in this point zero zeta potential and minimum stability result in phase separation. It was found that in the case of hyaluronan as titrant, final aggregates are smaller and more stable than when we used surfactant as titrant and therefore are more suitable for drug delivery applications.

## 5. ACKNOWLEDGEMENT

The work has been supported by Materials Research Centre at FCH BUT- Sustainability and Development, REG LO1211, with financial support from National Programme for Sustainability I (Ministry of Education, Youth and Sports) and COST action CM1101, project No. LD12068.

## 6. REFERENCES

[1] Girish, K.S. a K. Kemparaju. The magic glue hyaluronan and its eraser hyaluronidase: A biological overview. Life Sciences. 2007, vol. 80, issue 21, s. 1921-1943. DOI: 10.1016/j.lfs.2007.02.037.

[2] Balazs, Endre A. Therapeutic use of hyaluronan. Structural Chemistry. 2009, vol. 20, issue 2, s. 341-349. DOI: 10.1007/s11224-009-9435-y.

[3] WESLEY, Robin D., Terence COSGROVE, Laurie THOMPSON, Steven P. ARMES a Fiona L. BAINES. Structure of Polymer/Surfactant Complexes Formed by Poly(2-(dimethylamino)ethyl methacrylate) and Sodium Dodecyl Sulfate. Langmuir. 2002, vol. 18, issue 15, s. 5704-5707.

[4] RAO, J. Prasad a Kurt E. GECKELER. Polymer nanoparticles: Preparation techniques and size-control parameters. Progress in Polymer Science. 2011, vol. 36, issue 7, s. 887-913. DOI: 10.1016/j.progpolymsci.2011.01.001.

[5] GAUCHER, Geneviève, Marie-Hélène DUFRESNE, Vinayak P. SANT, Ning KANG, Dusica MAYSINGER a Jean-Christophe LEROUX. Block copolymer micelles: preparation, characterization and application in drug delivery. Journal of Controlled Release. 2005, roč. 109, č. 1–3, s. 169–188. DOI: 10.1016/j.jconrel.2005.09.034.

# APPLICATION OF CdTe-QUANTUM DOTS NANOPARTICLES FOR LUMINISCENCE DETERMINATION OF METAL IONS

Lenka ŘEZÁČOVÁ[1], Romana ŠEVČÍKOVÁ[1], Jakub VANĚK[1,2], Přemysl LUBAL[1,2*]

[1]*Department of Chemistry, Faculty of Science, Masaryk University, Kotlářská 2, 611 37 Brno, Czech Republic*

[2]*Central European Institute of Technology, Masaryk University, Kamenice 5, 625 00 Brno, Czech Republic*

**lubal@sci.muni.cz*

**Abstract**

The contribution deals with synthesis and characterization of CdTe-QD nanoparticles covered by mercaptopropionic acid (MPA). The luminescence of particles (diameter 3-5 nm, zeta-potential -40 mV, pH ~ 6.5) is quenched in presence of metal ions ($Cu^{2+}$, $Pb^{2+}$) which can be utilized for their fast, simple and sensitive determination (LOD ~ 0.5 μM).

## 1. INTRODUCTION

Quantum Dots (QD´s) semiconductor particles of 1-10 nm diameter are mostly sparingly soluble cadmium compounds CdX (X = S, Se, Te). Covering mercaptopropionic acid (MPA), glutathione, cystein[2-7] (see Fig. 1) the colloid solubility is increased while the ionization of their functional groups placed on particle surface ensures their solubility. Their unique physico-chemical as well as optical luminescence properties can be employed for detection and determination of ions, biologically important molecules and many other analytes[1-5] since they do have broad excitation and narrow emission bands which can be tuned by their size, morphology and kind of nanoparticles[1-5]. This contribution presents optimization of synthesis of CdTe-QD nanoparticles, their characterization and their potential application for determination of metal ions by means of luminescence spectroscopy.

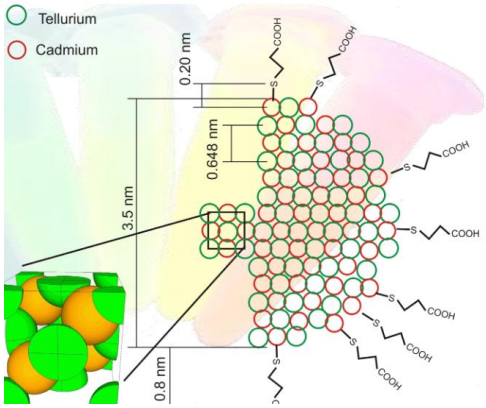


**Figure:** *Structure of CdTe-QD nanoparticels (adapted according to ref. [6])*

## 2. MATERIAL AND METHODS

The CdTe-QD nanoparticles covered by MPA were synthesized according to literature procedure[7] and they were characterized on Zetasizer Nano ZS equipment (Malvern, UK) in order to determine diameter and zeta potential. Luminescence measurements were carried out on spectrofluorimeter AvaSpec 2048 (AVANTES, Netherland) in wavelength region 350-1100 nm using violet laser (wavelength 405 nm, power 200 mW) for excitation.

## 3. RESULTS AND DISCUSSION

Several procedures found in literature[1-7] were utilized for synthesis of CdTe-QD nanoparticles. No differences in physico-chemical properties were observed for samples prepared in the time course 3-4 hours. The bright-orange colloid solution (pH ~ 6.5) emits greenish radiation (maximum of emission band about 544 nm) after laser excitation and thus the size 3.2 nm was estimated for nanoparticles. In addition, the measurement of nanoparticles size by means of laser scattering ($\lambda$ = 633 nm) shows that their size is about 5 nm and zeta-potential is -40 mV. The decrease of solution pH of prepared of CdTe-QD's leads to increase of zeta-potential and size of nanoparticles (>10 nm) since the carboxylic functional groups located on surface are gradually protonated. Zeta-potential value is then approaching to zero at pH<3 as consequence of fully neutralization of negatively-charged carboxylic groups by protons leading to agglomeration of nanoparticles to highly organized structures (up to 1500 nm at pH < 3) and then to precipitation of nanoparticles in form of less soluble compound.

The self-quenching of CdTe-QD nanoparticles in concentration region 0 – 1.6 $\mu g \cdot ml^{-1}$ was not observed when diluting stock solution (c ~ 4 $\mu g \cdot ml^{-1}$, pH ~ 6.5). On contrary, this effect was observed for higher concentration of CdTe-QD nanoparticles therefore all other experiments have to be done with solution of lower concentration and all other experiments were carried out at concentration level 1.6 $\mu g \cdot ml^{-1}$ (pH ~ 6.5). Adding $CuCl_2$ stock solution ($c$ = 1 $mmol.l^{-1}$), the shape of luminescence spectra of CdTe-QD's was not changed, only the intensity is decreased. This effect can be described as

$$\frac{I_0 - I}{I} = K_{SV}[\mathrm{M}]$$

where $I_0$ and $I$ are intensities without and in presence of metal ion, $K_{SV}$ is Stern-Volmer constant derived for static character of quenching[5]. The following parameters ($K_{SV}$ ~ 3200, limit of detection 0.64 $\mu$M) were calculated.

Adding $Pb^{2+}$ ions to solution of CdTe-QD nanoparticles, the analogous effect of quenching is observed. Limit of detection is comparable as found for $Cu^{2+}$ ions, however Stern-Volmer constant $K_{SV}$ is one order of magnitude higher ($K_{SV}$ ~ 21500), thus the determination of larger Pb(II) ion is more sensitive than for smaller $Cu^{2+}$ ion. The results can be slightly improved for the purified CdTe-QD-nanoparticles.

## 4. CONCLUSION

The CdTe-QD nanoparticles covered by MPA were synthesized and characterized (size, zeta-potential). The presence of some heavy metal ions ($Cu^{2+}$, $Pb^{2+}$) led to luminescence quenching of nanoparticles in solution and this effect was utilized to their sensitive determination which is comparable with results obtained by other analytical methods (*e.g.* ISE potentiometry, differential pulse polarography, molecule absorption spectroscopy, *etc.*).

## 5. ACKNOWLEDGEMENT

This work was supported by Ministry of Education of the Czech Republic (ME09065), Grant Agency of Czech Republic (grants 13-08336S, 14-12653S) and EU (CEITEC CZ.1.05/1.1.0/02.0068) program.

## 6. REFERENCES

[1] Hlaváček A., Skládal P., Chem. Listy, 105 (2011), 611-615.

[2] Zhang H., Wang D., Yang B., J. Am. Chem. Soc., 128 (2006), 10171-10180.

[3] Zhang L., Xu Ch., Li B. Microchim Acta, 166 (2009), 61-68.

[4] Murphy CJ, Anal Chem, 74 (2002), 520A-526A.

[5] Ali E. M., Zheng Y., Yu H., Y.Ying J., Anal Chem., 79 (2007), 9452-9458.

[6] Hezinová V., Ph.D. Thesis, VUT Brno 2011.

[7] Duan J. L., Song L. X., Zhan J. H., Nano Res., 2 (2009), 61-68.

# NANOSECOND LASER FLASH PHOTOLYSIS STUDY OF ROSE BENGAL

Lucie Ludvíková[1], Peter Šebej[1], Dominik Heger[1] and Petr Klán[1]*

[1] *Department of Chemistry, Faculty of Science, Masaryk University, Kamenice 5, 625 00, Brno, Czech Republic and RECETOX, Faculty of Science, Masaryk University, Kamenice 5, 625 00 Brno, Czech Republic.*

**lucielud@email.cz, klan@sci.muni.cz*

**Abstract**

Rose bengal (RB) is a well-known xanthene dye used in photodynamic therapy, textile industry and cosmetics.[1] Here we report a detailed and complete mechanistic study of the triplet excited state and of oxidized and reduced forms of RB. The kinetics of these reactive species were studied by steady–state spectroscopic and kinetic nanosecond laser flash photolysis using a 532 nm laser as a source of excitation. Scheme 1 summarizes the processes that can be involved upon RB excitation (a): The RB triplet ($^3RB^{2-}$)disproportionates to give the oxidized ($RB^{\bullet -}$) and reduced ($RB^{\bullet 3-}$) forms of RB (b, c) or undergoes a triplet–triplet annihilation (c). This detailed study is an essential step towards understanding of its role in the photochemical tissue bonding.[2]

(a) $RB^{2-} \xrightarrow[2.\ ISC]{1.\ h\nu} {}^3RB^{2-} \xrightarrow{k_d} RB^{2-}$

(b) $^3RB^{2-} + RB^{2-} \xrightarrow{k_{gs}} RB^{\bullet -} + RB^{\bullet 3-}$ or $2\ RB^{2-}$

(c) $^3RB^{2-} + {}^3RB^{2-} \xrightarrow{k_{T\text{-}T}} RB^{\bullet -} + RB^{\bullet 3-}$ or $2\ RB^{2-}$

**Scheme 1**: Photochemistry of the triplet excited state of RB

## REFERENCES

1 I. E. Kochevar and R. W. Redmond, *Singlet Oxygen, Uv-a, and Ozone*, 2000, **319**, 20-28.

2 T. S. Johnson, A. C. O'Neill, P. M. Motarjem, C. Amann, T. Nguyen, M. A. Randolph, J. M. Winograd, I. E. Kochevar and R. W. Redmond, *J. Surg. Res.*, 2007, **143**, 224-229.

# EPR-UV/VIS/NIR SPECTROELECTROCHEMICAL STUDIES OF SUBSTITUTED DIARYLAMINOTHIOPHENES

Peter MACHATA*, Peter RAPTA, Vladimír LUKEŠ

*Department of Physical Chemistry, Slovak University of Technology, Radlinského 9, SK-812 37 Bratislava, Slovak Republic*

**peter.machata@stuba.sk*

**Abstract**

In this contribution, 1,4-bis-(2-diphenylamino-thiophen-5-yl)-benzene (**A**) and (1,4-bis-[2-(phenothiazin-10-yl)-thiophen-5-yl]-benzene (**B**) consisting of three different groups, namely the diphenylamino-, bithiophene- and central phenylene moiety, respectively, were studied in detail to get insights to their oxidation mechanism. Different voltammetric techniques, in situ EPR-UV/Vis/NIR and NMR spectroelectrochemistry as well as a theoretical study based on DFT calculations were used to achieve this goal.

## 1. INTRODUCTION

In the last decades functionalized oligothiophenes found applications in organic field-effect transistors, organic light emitting diodes and solar cells due to their easy structure variation and large variety of electronic properties [1-4]. The combination of thiophene derivatives with diphenylamino-groups made these structures useful as hole-transporting materials for optical and microelectronic devices [5]. Based on this finding different diarylamino substituted oligothiophenes were synthesized and their redox reactions have been studied by in situ spectroelectrochemistry [5-7].

In this contribution,1,4-bis-(2-diphenylamino-thiophen-5-yl)-benzene (**A**) and (1,4-bis-[2-(phenothiazin-10-yl)-thiophen-5-yl]-benzene (**B**) consisting of three different groups, namely the diphenylamino-, bithiophene- and central phenylene moiety, respectively, were studied in detail [8]. The only difference between **A** and **B** is that in **B** the diphenylamino moiety of **A** is replaced by a phenothiazinyl unit.

## 2. MATERIAL AND METHODS

A standard three electrode arrangement of a platinum wire as working electrode, a platinum wire as counter electrode, and silver wire pseudoreference electrode was used in cyclic voltammetric experiments with a PAR Potentiostat-Galvanostat Model 273A in glove box.

Decamethylferrocene (DmFc) was used as internal potential standard. Sample solutions with approximate concentration of 0.5 mM, prepared with 0.2 M $TBAPF_6$ supporting electrolyte in $CH_2Cl_2$. Spectroelectrochemical experiments were carried out in flat spectroelectrochemical cell (Pt mesh working electrode) in the optical EPR cavity (ER4104OR, Bruker, Germany). The EPR spectra were recorded on an X-band EMX EPR spectrometer (Bruker, Germany). For in situ EPR-UV/Vis/NIR spectroelectrochemical studies, diode-array Avantes UV/Vis/NIR spectrometer and potentiostat Heka PG 284 (HEKA Elektronik, Germany) were used. All spectroelectrochemical studies were performed in the Centre of Spectroelectrochemistry at IFW Dresden (Germany).

## 3. RESULTS AND DISCUSSION

Cyclic voltammetry of **A** and **B** was performed in $CH_2Cl_2$ containing $TBAPF_6$ as supporting electrolyte. Both investigated compounds give cyclic voltammograms at low oxidation potentials (0.69 V vs. $DmFc^+$/DmFc for **A** and 0.81 V vs. $DmFc^+$/DmFc for **B** – Fig. 1). At cyclic voltammograms, ratio of current between **A**, repectively **B** and internal standard DmFc at the first CV peak was estimated to 2 indicating two electron process. The peak-to-peak separation corrected for *iR* drop was estimated to be 60 mV for DmFc, 45 mV for **A** and 39 mV for **B**. If the second oxidation potential is lower as the first one ( $E_1^{\circ'} > E_2^{\circ'}$ ), and the second oxidation potential doesn't exceeds 180 mV comparing to the first one, the CV peak exhibits two electron transfer characteristics.

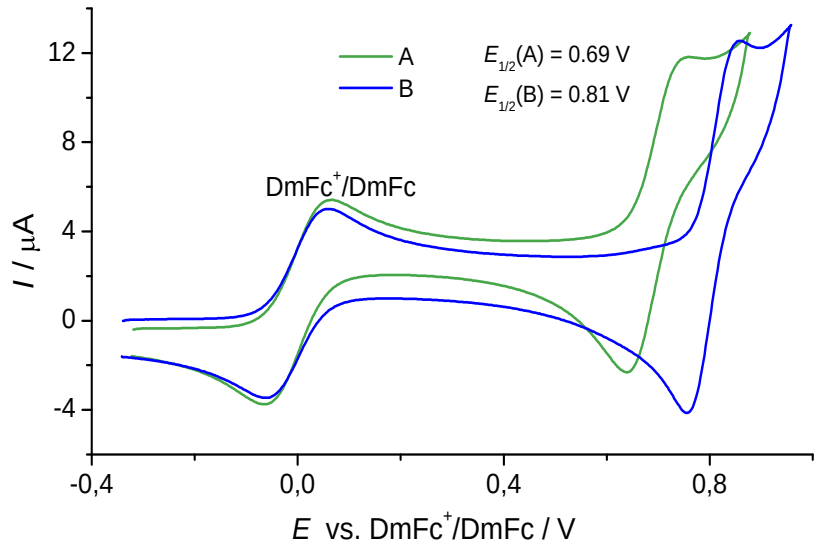


**Figure 1.:** Cyclic voltammograms of 0.5 mM **A** (green line) and **B** (blue line) in $CH_2Cl_2$/$TBAPF_6$ in the presence of 0.5 mM DmFc (scan rate 50 mV $s^{-1}$).

Upon electrochemical oxidation of **A** two optical transitions arise at 662 nm and 1510 nm at the potential of the first oxidation peak. Simultaneously broad unresolved EPR spectra with a relatively low *g*-factor value of 2.0015 was observed, indicating the presence of a large set of splittings. For $\mathbf{A}^{\bullet+}$, spin density is suggested to be delocalized over a large part of the molecule (corresponding with shape of HOMO orbital. **B** gives upon electrochemical oxidation similar optical transitions at 700 nm and 1475 nm appear Simultaneously a line-broadened EPR spectrum with a shifted *g*-factor value ($g$ = 2.0047) was observed. An EPR splitting constant is caused just by one nitrogen atom with $a_N$ = 0.65 mT. The high *g*-factor value and the shape of the EPR signal point to the localization of the additional charge and spin at the phenothiazinyl moiety. This result is in agreement with shape of HOMO orbital. Applying Marcus theory of mixed valence (MV) systems approach the cation $\mathbf{A}^{\cdot+}$ can be assigned to delocalized class III Robin-Day MV system. On the other hand the cation $\mathbf{B}^{\cdot+}$ exhibits characteristics of a localized (class II) MV system.

## 4. CONCLUSION

Anodic oxidation of **1** leads to the unstable initially generated radical cation which rapidly dimerizes to the corresponding EPR-silent protonated dimer. The radical cation $\mathbf{4}^{\cdot+}$ formed by electrooxidation **4** is rather stable. For monomers **2a**, **2b** and **3**, the oxidation leads immediately to the electrodeposition of an polymer film on the electrode surface. The electrochemical stability of these polymers and reversible changes of their UV/Vis/NIR spectra in the broad wavelength range upon redox cycling indicate their promising application as stable electrochromic materials.

## 5. ACKNOWLEDGEMENT

The financial support of the Slovak Grant Agency VEGA (contract No. 1/0307/14 and No. 1/0289/12) and APVV-0202-10 and IFW Dresden is gratefully acknowledged.

## 6. REFERENCES

[1] Facchetti, A.: Mater. Today 10 (2007) 28-37.

[2] Li, Z.H., Wong, M.S., Fukutani, H., Tao, Y.: Chem. Mater 17 (2005) 5032-5040.

[3] Shirota, Y., Kageyama, H.: Chem. Rev. 107 (2007) 953-1010.

[4] Mishra, A., Ma, C.-Q., Bäuerle, P.: Chem. Rev. 109 (2009) 1141-1278.

[5] Schumann, J., Kanitz, A., Hartmann, H.: Synthesis 9 (2002) 1268-1277.

[6] Gerstner, P., Rohde, D., Hartmann, H.: Synthesis 17 (2002) 2487-2489.

[7] Tabet, A., Schroder, A., Hartmann et al.: L., Org. Lett. 5 (2003) 1817-1820.

[8] Rapta, P., Haubner, K., Machata, P. et al.: Electrochim. Acta, 110 (2013) 670–680

# EPR-UV/VIS/NIR SPECTROELECTROCHEMISTRY OF THIENYL DERIVATIVES OF PYRENE

Peter MACHATA*, Peter RAPTA, Vladimír LUKEŠ

[1] *Department of Physical Chemistry, Slovak University of Technology, Radlinského 9, SK-812 37 Bratislava, Slovak Republic*

**peter.machata@stuba.sk*

**Abstract**

A detailed spectroelectrochemical and theoretical study of thienyl derivatives based on pyrene, namely 1-(2-thienyl)-pyrene (**1**), 1,6-bis(2-thienyl)-pyrene (**2a**), 1,4-bis(2-thienyl)-pyrene (**2b**), 1,3,6-tris(2-thienyl)-pyrene (**3**) and 1,3,6,8-tetra(2-thienyl)-pyrene (**4**), and their oxidation products with focus on the formation of their corresponding cationic states are presented. Regioregular polymeric systems were prepared by means of electrochemical polymerization from monomers **2a**, **2b** and **3**. The redox behavior of the corresponding polymers was studied by cyclic voltammetry and *in situ* EPR-UV/Vis/NIR spectroelectrochemistry with the aim of obtaining details on the type of charge carriers within the polymer film.

## 1. INTRODUCTION

Fluorescence probes based on pyrene moieties have attracted considerable attention over the last decades [1, 2]. The pyrene moiety represents a unique fluorescent probe and its derivatives have found brought applications in sensors [3, 4], liquid crystals [5], organic light-emitting diodes [6], as electrochromic applications [7], transistors [8], photoactive polypeptides [9] and genetic probes [10]. Pyrene units can serve as components for various types of fluorescent polymers and dendrimers [11].

In this work, we performed a detailed spectroelectrochemical and theoretical study on the electron transfer in new thienyl derivatives of pyrene and their oxidation products with focus on the formation of their corresponding cationic states [12].

## 2. MATERIAL AND METHODS

A standard three electrode arrangement of a platinum wire as working electrode, a platinum wire as counter electrode, and silver wire pseudoreference electrode was used in cyclic voltammetric experiments with a PAR Potentiostat-Galvanostat Model 273A in glove box.

Decamethylferrocene (DmFc) was used as internal potential standard. Sample solutions with approximate concentration of 0.5 mM, prepared with 0.2 M $TBAPF_6$ supporting electrolyte in $CH_2Cl_2$. Spectroelectrochemical experiments were carried out in flat spectroelectrochemical cell (Pt mesh working electrode) in the optical EPR cavity (ER4104OR, Bruker, Germany). The EPR spectra were recorded on an X-band EMX EPR spectrometer (Bruker, Germany). For in situ EPR-UV/Vis/NIR spectroelectrochemical studies, diode-array Avantes UV/Vis/NIR spectrometer and potentiostat Heka PG 284 (HEKA Elektronik, Germany) were used. All spectroelectrochemical studies were performed in the Centre of Spectroelectrochemistry at IFW Dresden (Germany).

## 3. RESULTS AND DISCUSSION

Anodic cyclic voltammetry of investigated thienyl derivatives of pyrene **1**–**4** differs substantially and depends on the number of thienyl rings present on the pyrene molecule. A dominant dimerization reaction was proposed for oxidation of **1** (Fig. 1-a). The lifetime of the radical cation $\mathbf{1}^{\cdot+}$ was estimated to be approximately $10^{-5}$ s using fast scan voltammetry. After proton release, a new π-conjugated dimer **D1** is formed irreversibly with a lower oxidation peak potential as for the monomer confirming an elongation of the π-conjugation in the dimer. For electrochemical oxidation of **4**, a reversible first anodic peak is found using a scan rate of 0.1 V $s^{-1}$. Even the second oxidation step was found ant it exhibits nearly reversible behavior (Fig. 1-b). Therefore, the radical cation $\mathbf{4}^{\cdot+}$ formed by electrooxidation is rather stable. However, at low scan rates (e.g. 0.005 V $s^{-1}$) a new cathodic peak at lower oxidation potential is already observed indicating dimerization or oligomerization reactions.

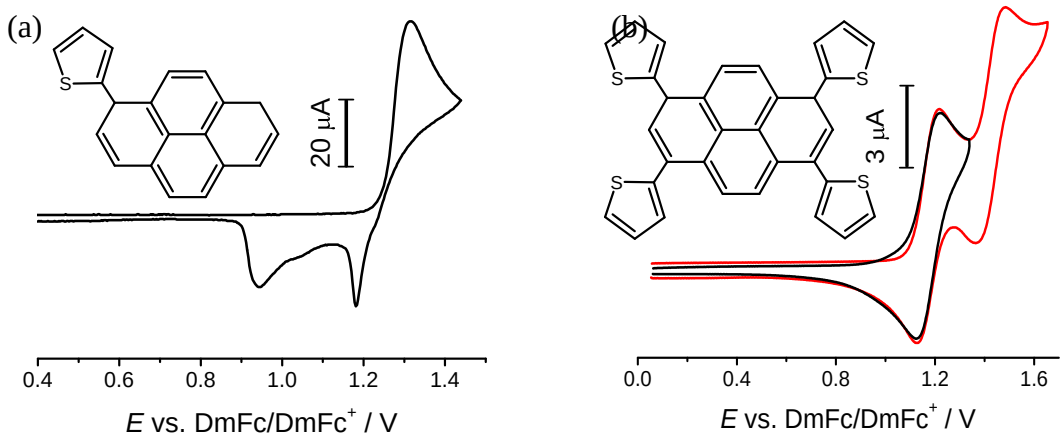


**Figure 1.:** Cyclic voltammetry at 0.1 V $s^{-1}$ in 0.2 M $TBAPF_6/CH_2Cl_2$ solution of (a) **1** and (b) **4** – one oxidation step (black line) and two oxidation steps (red line).

For monomers **2a**, **2b** and **3**, the anodic oxidation leads immediately to the electrodeposition of an electroactive material on the electrode surface. After the first scan new redox couples started to appear and the corresponding current increased after each cycle step. After washing with free monomer electrolyte, the film was redox cycled in 0.2 M $TBAPF_6$ in $CH_2Cl_2$ a well defined an reversible redox behavior of such a prepared polymer $(\mathbf{2a})_n$, $(\mathbf{2b})_n$ and $(\mathbf{3})_n$ was confirmed. The simultaneously measured narrow EPR singlet is similar to that of other conducting polymers indicating a delocalized spin.

## 4. CONCLUSION

Anodic oxidation of **1** leads to the unstable initially generated radical cation which rapidly dimerizes to the corresponding EPR-silent protonated dimer. The radical cation $\mathbf{4}^{\cdot+}$ formed by electrooxidation **4** is rather stable. For monomers **2a**, **2b** and **3**, the oxidation leads immediately to the electrodeposition of an polymer film on the electrode surface. The electrochemical stability of these polymers and reversible changes of their UV/Vis/NIR spectra in the broad wavelength range upon redox cycling indicate their promising application as stable electrochromic materials.

## 5. ACKNOWLEDGEMENT

The financial support of the Slovak Grant Agency VEGA (contract No. 1/0307/14 and No. 1/0289/12) and APVV-0202-10 and IFW Dresden is gratefully acknowledged.

## 6. REFERENCES

[1] Benniston, A. C., Fortage, J.: Tetrahedron Lett. 49 (2008) 4292-4295.

[2] Čapek, I.: Adv. Colloid Interface Sci. 97 (2002) 91-149.

[3] Martínez-Máñez, R., Sancenón, F.: Chem. Rev. 103 (2003) 4419-4476.

[4] Yuasa, H., Miyagawa, N., Nakatani, M., et al.: Org. Biomol. Chem. 2 (2004) 3548-3556.

[5] De Halleux, V. Calbert, J.-P., Brocorens, et al.: Adv. Funct. Mater. 14 (2004) 649-659.

[6] Daub, J., Engl, R., Kurzawa, J. et al.: J. Phys. Chem. A 105 (2001) 5655-5665.

[7] Kung, Y. C., Hsiao, S. H., J.: Mater. Chem. 21 (2011) 1746-1754.

[8] Anant, P., T. Lucas, N., Ball, J. M. et al.: Synth. Met. 160 (2010) 1987-1993.

[9] Jones II, G., Vullev, V. I.: Org. Lett. 4 (2002) 4001-4004.

[10] Hwang, G. T., Seo, Y. J., Kim, B. H.: J. Am. Chem. Soc. 126 (2004) 6528-6529.

[11] Baker, L. A., Crooks, R. M.: Int. J. Biol. Macromol. 33 (2000) 9034-9039.

[12] Machata, P., Rapta, P., Lukeš, V. et al.: Electrochim. Acta 122 (2014) 57-65.

# HOW TO MEASURE QUANTITATIVE EPR SPECTRA REPRODUCIBLY

Milan MAZÚR*, Marián VALKO

*Department of Physical Chemistry, Institute of Physical Chemistry and Chemical Physics, Faculty of Chemical and Food Technology, Slovak Technical University in Bratislava, Radlinského 9, SK-812 37 Bratislava, Slovakia*

**milan.mazur@stuba.sk*

**Abstract**

The objective of this contribution is to provide useful suggestions, recommendations and simple procedures to minimise the influence of primary error sources in quantitative EPR measurements. When the below presented recommendations and procedures were used in our quantitative EPR experiments (with a Bruker EPR spectrometer using a Bruker double $TE_{104}$ rectangular cavity and air conditioning) the EPR signal intensity of a wide range of samples could be obtained with experimental errors between 3-5%. We believe that these tips can be helpful in quantitative EPR practice.

## 1. INTRODUCTION

A multitude of error sources influence the data accuracy of quantitative EPR spectroscopy. The serious problems associated with reproducibility in quantitative EPR measurements were clearly demonstrated in the comparison of the results obtained from international experiments in 1962 (coordinated by prof. Kohnlein [1]) and 1992-92 (coordinated by prof. Yordanov [2]). In principle, experimental errors in quantitative EPR measurements for a given laboratory and a given EPR spectrometer, may be reduced in carefully performed experiments to 2-5% [1, 2]. However, in practice, quantitative analysis of the same sample in different laboratories produced results, which in the worst cases were incompatible and in others gave an uncertainty between ca 100-200% [1, 2]. No satisfactory explanation for this discrepancy has been found at present. The main objective of this contribution is to provide useful suggestions, recommendations and simple procedures to minimise the influence of the selected primary error sources in quantitative EPR measurements.

## 2. MATERIAL AND METHODS

The pairs of the cylindrical samples of various internal diameter (i.d.) and length (L) were prepared. Quantitative EPR spectra were recorded and evaluated according to the same procedures as described in our previous papers. For further details see elsewhere [3, 4].

## 3. RESULTS AND DISCUSSION

As a representative example, the comparison of cylindrical samples with identical volumes but different shapes is illustrated. The experimental arrangement is outlined in the Figure 1.

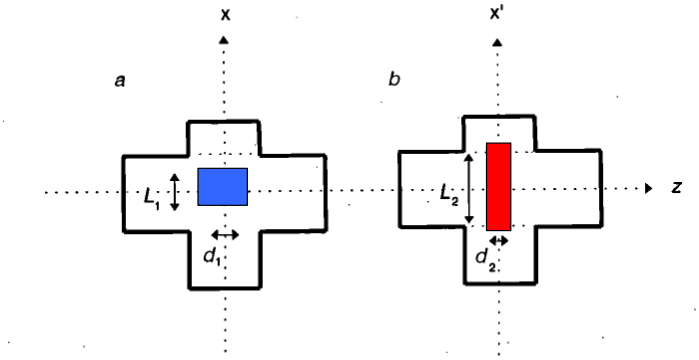


**Figure 1.:** Schematic diagram of the cross section of the microwave rectangular cavity, in the centre of which cylindrical samples with identical volume, but different shape (a) and (b) are inserted.

The material, volume and mass of the pairs of the compared samples was identical. The experimentally observed difference in the EPR signal intensity, Ipp(1)−Ipp(2), between the given samples with shape (a) and (b) are summarised in the Table 1.

**Table 1.:** Pairs of cylindrical samples with identical sample volume (V) but with different sample shape indicated by corresponding sample internal diameter (i.d.) and length (L). The experimentally obtained Ipp(1)−Ipp(2)} difference is given as a percentage of the smaller Ipp value.

| V [mm$^3$] | i. d. [mm] | L [mm] | Ipp(1)/Ipp(2) [a.u.] | Ipp(1) - Ipp(2) [%] |
|---|---|---|---|---|
| 62.83 | 4 | 5 | 2.98 | 198 % |
| 62.83 | 2 | 20 | | |
| 125,66 | 4 | 10 | 3.78 | 278 % |
| 125.66 | 2 | 40 | | |
| 15,71 | 2 | 5 | 4.13 | 313 % |
| 15.71 | 1 | 20 | | |
| 31,42 | 2 | 10 | 5.32 | 432 % |
| 31.42 | 1 | 40 | | |

It is clear from Table 1 that the comparison of the pairs of the samples with identical volumes but different sample shapes show signal intensity differencies between ca 200-400 %. However, when the sample shapes were identical the differencies were found between 3-5%. It is obvious that the different sample shape (in the spite of identical sample volume, material and also sample mass) could be responsible for the essential difficulties in the quantitative EPR measurements. For more information see Ref. [3].

## 4. CONCLUSION

For the samples which are to be compared in quantitative EPR measurements, the following recommendations were selected: a) The shape of all samples should be identical. b) The position of the sample/reference in the cavity should be identical. c) The wall thickness of sample tubes should be identical. d) The shape and wall thickness of quartz Dewars (if used) should be identical. d) A double $TE_{104}$ rectangular cavity should be used in quantitative EPR spectroscopy. e) The dielectric properties of unknown and standard samples should be as close as possible. f) The use of commercially distributed software for postrecording spectra evaluation is a basic necessity. g) The sample and laboratory temperature should be kept constant during all measurements. See Ref. [5] for further detailed information. When the above mentioned recommendations and procedures were used in our quantitative EPR experiments (with a field modulated CW Bruker EPR spectrometer using an original Bruker double $TE_{104}$ rectangular microwave cavity and air conditioning) the EPR signal intensity of a wide range of samples could be obtained with experimental error between 3-5%.

## 5. ACKNOWLEDGEMENT

This work was supported by the Slovak Research and Development Agency under the contract Nos. (APVV-0202-10 and APVV-0339-10) and Scientific Grant Agency of the Slovak Republic (Projects VEGA 1/0765/14 and VEGA 1/0289/12).

## 6. REFERENCES

[1] Kohnlein W.: In Ebert M., Howard A. (Eds.), Radiation Effects in Physics, Chemistry and Biology, Nord-Holland, Amsterdam, 1963, p.206.

[2] Yordanov N.D., Ivanova M.: Appl. Magn. Reson. 6 (1994) 333.

[3] Mazur M., Morris H., Valko M.: J. Magn. Reson. 129 (1997) 188–200.

[4] Mazur M., Valko M., Morris H.: Appl. Magn. Reson. 20 (2001) 317–344.

[5] Mazur M.: Anal. Chim. Acta 561 (2006) 1–15.

# UTILIZATION OF FLUORESCENCE SPECTROSCOPY FOR STUDYING OF THE INTERACTIONS IN DRIED SYSTEMS OF BIOPOLYMER AND HYDROPHOBIC SPECIES

Petra MICHALICOVÁ*, Miloslav PEKAŘ, Filip MRAVEC

*Centre for Material Research, Faculty of Chemistry, Brno University of Technology, Purkynova 118, 612 00 Brno, Czech Republic*

**xcmichalicovap@fch.vutbr.cz*

**Abstract**

Molecules of biopolymers such as hyaluronan or carboxymethylcellulose have hydrophilic character. On the other side the chains of these natural compounds contain also hydrophobic areas. These parts are often protected by water molecules that are probably highly organized. The interactions between native hydrophilic biopolymers and hydrophobic solutes were studied using the method of fluorescence spectroscopy. It was observed, that drying of the systems open up the binding sites for hydrophobic compounds. After system rehydration the hydrophobic solutes are locked up the hydrophobic solutes are locked up on the chain of biopolymer by the molecules of water.

## 1. INTRODUCTION

Hyaluronan is a biopolymer, which can be qualified as essential for vertebrates. It is a major component of most of tissues. Besides of the mechanical functions this compound is important for many biological processes 0, 00. The molecule of hyaluronan has hydrophilic character. The chain of biopolymer contains also the hydrophobic parts, but they are not accessible and the hydrophilic character of molecule prevails. 0. On the other side, many of drugs or vitamins are hydrophobic 0. The aim of this work was the study of systems biopolymer-fluorescence probe. The drug in our studied system is substituted by the hydrophobic fluorescence probe which allows the monitoring of the interaction between components using fluorescence spectroscopy. Besides the hyaluronan another model biopolymers were used too.

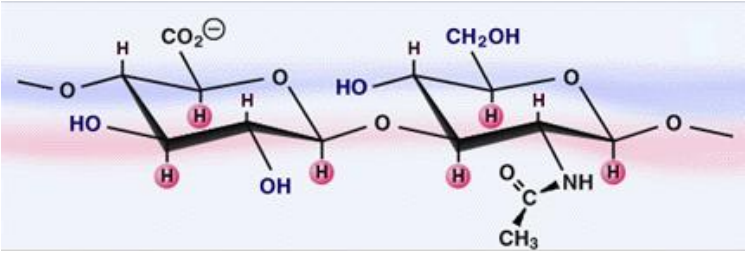


**Figure 1.:** Hydrophilic (blue) and hydrophobic (red) parts on the chain of hyaluronan 0

## 2. MATERIAL AND METHODS

In the first part of the work the samples for drying were prepared. Three different molecule masses of hyaluronan (CPN spol. s r.o.) were used (100 kDa; 420 kDa; 1,46 MDa) and the concentration of the biopolymer was 1 g·dm$^{-3}$. As the fluorescence probe, perylene (Sigma Aldrich) was chosen for his significant hydrophobic character. Concentration of perylene was $5 \cdot 10^{-6}$ mol·dm$^{-3}$. All components were prepared in water solution and dried by low pressure. After complete drying the samples, the product was rehydrated by water.

These samples were measured on spectrofluorimeter Fluorolog Horiba Jobin Yvon at the temperature 25 ºC. For comparison the blank samples were prepared from the biopolymer and fluorescence probe in the water without drying step.

The same approach was used with other biopolymers such as carboxymethylcellulose (Sigma Aldrich) or sodium alginate (Sigma Aldrich), but in this paper we selected just the results with hyaluronan.

## 3. RESULTS AND DISCUSSION

The molecule of perylene, which was for purposes of this work used as replacement for drug molecule, has high hydrophobic character. By this reason perylene is non-soluble in water and therefore it does not provide fluorescence signal. After dissolving in more hydrophobic environment, the fluorescence response is more significant. This fact is basic for discussion of supporting of interactions by drying of our systems 0.

Figure 2 shows, that undried sample with 100 kDa hyaluronan and perylene dissolved in water has almost zero intensity of fluorescence (orange line). This tells us that without supporting of the interactions with drying the perylene dissolved in water does not interact with hyaluronan chain. The hydrophobic parts on the chain of biopolymer were not accessible for molecules of hydrophobe. Organized water creates the barrier and molecules of fluorescence probe stay undissolved in the water. After drying of the system enough, the desired areas on the chain are locked up and the molecules of perylene can interact with

biopolymer. Perylene surrounded by hydrophobic environment of the chain provided strong fluorescence signal. The intensity of the fluorescence is related to the polarity index of sample. The green line in the Figure 2 shows significant increase of the fluorescence signal, so we can suppose that the components interact. Similar results we observed from all measurements, even with different biopolymers (CMC, sodium alginate).

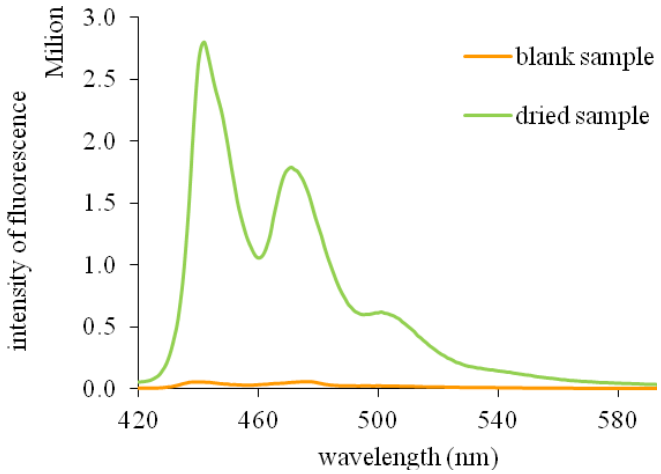


**Figure 2.:** Emission scan of dried and undried system containing hyaluronan with molecular mass 100 kDa and concentration 1 g·dm$^{-3}$ and perylene with concentration 5·10$^{-6}$ mol·dm$^{-3}$

On Figure 3 is displayed the influence of drying on supporting of the interactions in studied systems for three different molecular mass of hyaluronan. With increasing molecular mass of biopolymer the fluorescence signal decreases. This trend is contrary to the expected results. Longer chain of biopolymer should provide more binding places for hydrophobic probe. This can be caused by conditions or duration of drying. Other experiments with different concentration or biopolymer do not show such a trend. The most important fact is that the interactions between the components of system were confirmed for all measurements.

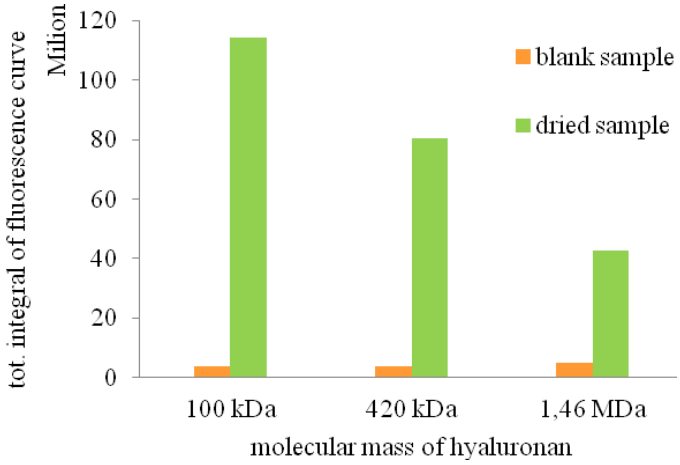


**Figure 3.:** Influence of drying on increasing of fluorescence signal of three different molecular mass of hyaluronan in the system with perylene

## 4. CONCLUSION

The method of fluorescence spectroscopy was used as main measuring method for investigation of the interactions between hydrophilic native biopolymers and hydrophobic fluorescence probe. As studied biopolymers hyaluronan, carboxymethylcellulose and sodium alginate were chosen. Perylene was used as the fluorescence probe. The results show that the perylene has no fluorescence response if we just mixed up the components in water solution. On the other side dried and rehydrated system provided significant fluorescence signal. Therefore we consider the drying of the studied system as a useful tool for supporting of the interactions between biopolymers and hydrophobic species.

## 5. ACKNOWLEDGEMENT

Materials Research Centre at FCH BUT- Sustainability and Development, REG LO1211, with financial support from National Programme for Sustainability I (Ministry of Education, Youth and Sports).

## 6. REFERENCES

[1]Vandamme E, De Baets S, Steinbüchel A.: Biopolymers – Polysaccharides 1. Wiley, (2002), 379–406

[2]Scott J: Glycoforum [online], (1998)

[3]Hascall V, Laurent T: Glycoforum [online], (1997)

[4]Brown T: Current pharmaceutical biotechnology, 4 (2008), 253–260

[5]Valeur, B.: Molecular Fluorescence: Principles and Applications. Wiley, (2001), 34–70

# DETERMINATION OF ORGANIC ACIDS IN WINE USING BY BIOSENSORS

Miodrag MILOVANOVIC[1], Jiri ZERAVIK[2], Petr SKLADAL[1,2]

*[1]Department of Biochemistry, Faculty of Science, and [2]CEITEC – Central European Institute of Technology Masaryk University, Kamenice 5, 625 00 Brno, Czech Republic*

*e-mail: mikimilovanovic@gmail.com*

**Abstract**

The flow-through one-channel amperometric biosensor is presented for determination of organic (carboxylic) acids. It is based on two sensor layers that are deposited on a platinum elctrode. The inner layer eliminates interferences by limiting diffusion of electrochemically active substances such as ascorbic acid, polyphenol compounds. This layer is electro-polymerized using the equimolar mixture of *o*-phenylenediamine and resorcinol. The outer layer is prepared by cross-linking the enzyme sarcosine oxidase and bovine serum albumin using glutaraldehyde. The formation of enzymatically produced hydrogen peroxide is monitored at 650 mV vs. an Ag/AgCl reference electrode. The addition of carboxylic acids causes competitive inhibition of the enzyme and a decrease in signal. The assay was optimized for determination of carboxylic acids in wine samples. Following 10-fold dilution, most samples contain 1–10 mM individual carboxylic acids and thus a 5 mM concentration of sarcosine was chosen as being optimal for competition. In case of real samples, the biosensor measured the sum of all carboxylic acids, which serves as a parameter describing the quality of wines. Results from testing of 31 wines are reported.

## 1. INTRODUCTION

Organic acids are one of the most important components which are especially responsible for its acidity and tartness. The content of carboxylic acids in wine is dependent on the region of grapes growing and the associated climatic conditions. Wines originating in the northern regions typically contain a greater proportion of acids, particularly malic acid, while the wines from the Mediterranean area exhibit lower acidity. The predominant representants found in wines are tartaric, malic, citric, succinic, lactic and acetic acids. Tartaric, malic and citric acid originate in grapes while succinic and acetic acid are produced during the fermentation process. The wines from northern regions typically contain higher amounts of malic acid; the

level of malic acid is decreased by the malolactic fermentation, resulting in reduction of acidity and tartness [1].

This fermentation is rather difficult to control, hence monitoring of ratio of malic and lactic acids in treated wine is require. In our case, sarcosine oxidase (SOD) was used for monitoring of this process using an electrochemical biosensor. The decrease of malic acid was monitored through decreasing inhibition of SOD.

The widely employed analytical methods for the determination of organic acids in wine are based on determination of the total quantity of acids in wine. Capillary electrophoresis with direct and undirect detection (CE) was performed [2]. As another alternative, various types of biosensors for determination of individual organic acids were introduced. Biosensor for the determination of malate employs enzyme malate dehydrogenase (MDH) [3]. Another way to monitor the acids content is the use of enzyme inhibition by organic acids. Developed biosensor was based on competitive reversibile inhibition of sarcosine oxidase (SOD) by organic acids in the presence of sarcosine. SOD was inhibited by malate, citrate, succinate, acetate, formate and partially tartrate while lactate provided very small inhibition effect. The goal of this work was comparison of the SOD biosensors with capillary electrophoresis (CE) as standard method. In this case, 31 wine samples from companies Znovín (Znojmo) and winery Jaroslav Tichý (Rybníky,) were analysed.

## 2. MATERIAL AND METHODS

Sarcosine oxidase (SOD, EC 1.5.3.1, from *Bacillus* sp., 25–50 units·mg-1), sarcosine, bovine serum albumin, o-phenylenediamine, resorcinol, glutaraldehyde (GA), L-lactic acid, L-malic acid, succinic acid, phthalic acid and cetyltrimethylammonium bromide (CTAS) were purchased from Sigma. Acetic acid, citric acid, formic acid, tartaric acid, glycine, sodium hydrogenphosphate, sodium dihydrogenphosphate, potassium chloride, hydrogen peroxide and L-ascorbate were purchased from Penta.

*Polymerization proces*

The working electrode was coated with a thin layer of the selective noncondutive copolymer (2mM *o*-phenylenediamine and 2mM resorcinol) which grows until its maximum thickness. As the surface becomes isolated, electric current decreases in relation with increasing polymer thickness.

*Biosensors*

Enzyme layer was prepared by cross-linking of SOD (5 $U.cm^{-2}$) with 2% GA in 50 mM phosphate (pH 7.4). The mixture was supplemented with 100 $mg.ml^{-1}$ BSA in order to reach

the density of 2 mg.cm$^{-2}$. The immobilization mixture was deposited on the copolymer-coated working electrode and stored at 4°C.

*Capillary electrophoresis*

An Agilent 7100 CE System (Waldbronn, Germany) equipped with a diode-array UV–Vis detector was used to perform all analyses.

## 3. RESULTS AND DISCUSSION

*Copolymer permeability*

Permeability was monitored with 10 mM hydrogen peroxide (analyte) and 1 mM ascorbic acids (interfering compound) before and after deposition of the copolymer; measurements were performed on gold working electrode at +650 mV vs. Ag/AgCl in 100 mM KCl and 10 mM potassium phosphate pH 7.4.

| **Table 1**: Permeability of copolymer | | Spontaneus deposition |
|---|---|---|
| | Before [%] | After [%]* |
| $H_2O_2$ | 100 | 117 |
| Ascorbate | 100 | 0.001 |

*The percentage values were calculated using following formula: $\%_{(after)} = i_{after} / i_{befor} \times 100$

*Principle of competitive reversible inhibition*

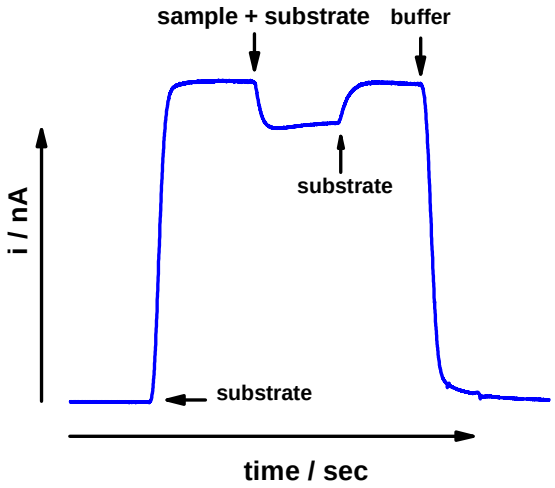


**Figure 1:** Amperometric signal during competitive reversible inhibition of immobilized sarcosine oxidase

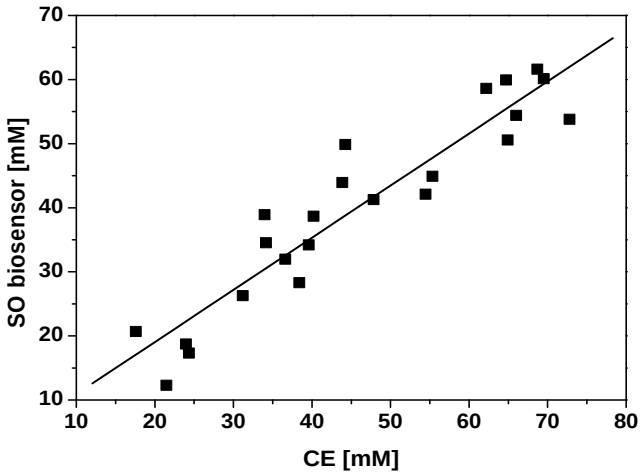


**Figure 2:** Comparison of SOD biosensor responses vs. CE analysis

| **Table 2**: The effect of carboxylic acids on the activity of immobilized sarcosine oxidase in the presence of 5 mM sarcosine | Inibitor | Slope of inhibition x $10^{-6}$ [$L.mol^{-1}$] | Linear range[$mol.L^{-1}$] |
|---|---|---|---|
| | Citric acid | 98.9 | 0.5-5 |
| | Succinic acid | 59.7 | 0.5-8 |
| | Malic acid | 56.6 | 0.5-8 |
| | Acetic acid | 35.5 | 0.5-10 |
| | Formic acid | 32.2 | 0.5-10 |
| | Lactic acid | 2.8 | - |

## 4. CONCLUSION

Analysis of wine samples using biosensors and CE showed correlation between the results obtained by both methods. From that is evident the biosensors can not fully replace the standardized method, but on the other hand, its mobility and simplicity of determination allow their use in the field during on-line monitoring of fermentation processes in comparison to CE. In this case, their function is not to determine the absolute values of the analytes, but continuous monitoring of increase or decrease of the signal in the time frame which can be a major shift in the production of quality wines.

## 5. ACKNOWLEDGEMENT

This work was supported by the Ministry of Education, Youth and Sports of Czech Republic, programme NPV II (2B08035).

## 6. REFERENCES

[1] Casey JA (1990) Oenology: Acidity, pH and sourness in wine.The Aust Grapegrower and Winemaker 313:15

[2] Compendium of International Methods of Wine and Must Analysis, Volume 1, OIV, Paris, Edition 2013.

[3]R. Monosik, M. Strednansky, G. Greif, E. Sturdik, Cent. Eur. J. Chem., 10 (2012) 157.

# NEW KINETIC MODELS IN BIOPOLYMER DEGRADATION: LONG TERM STUDY OF HYALURONAN SAMPLES

Jakub Mondek*, Vasile Simulescu, Miloslav Pekař

*Materials Research Centre, Faculty of Chemistry, Brno University of Technology, Purkyňova 118, 612 00 Brno, Czech Republic*

**xcmondek@fch.vutbr.cz*

**Abstract**

Degradation of hyaluronan samples was studied by size exclusion chromatography - multi angle laser light scattering (SEC-MALLS). The degradation was observed in powder as well as in solution. Rate of degradation increased at room temperature as expected according to Arrhenius law. It was not possible to use first order kinetics for description of the degradation. We used zero order kinetic model and empiric model, but similar to first order kinetics.

## 1. INTRODUCTION

Hyaluronan is a linear natural polysaccharide of the glycosaminoglycans family. Its chemical structure comprises disaccharide units composed of D-glucuronic acid and N-acetyl-D-glucosamine, which are alternatively linked through 1,3 and 1,4 glycosidic bonds 0.

All the authors deal with degradation dependent on pH 0,0, temperature 0,0 or they deal with addition of other compound (hydrogen peroxide 0 for instance). But no one deals with stability of hyaluronan powder or hyaluronan solutions after hyaluronan powder is dissolved in water. What is the time stability of hyaluronan after mixing the solution? We report about the time stability of hyaluronan solution and kinetics of time degradation.

## 2. MATERIALS AND METHODS

In our work we studied the hyaluronan degradation in aqueous solutions of two different molecular weight hyaluronic acid samples by using SEC-MALLS, in order to observe the modification of molar mass, polydispersity and polymer conformation in time.

SEC-MALLS technique allows:

the separation of different polymeric compounds function of molecular weight

the determination of absolute molar mass averages (eqs. 1-3) from $10^2$ Da to $10^9$ Da

$$M_n = \frac{\sum n_i M_i}{\sum n_i} \quad (1) \; ; \quad M_w = \frac{\sum n_i M_i^2}{\sum n_i M_i} \quad (2) \; ; \quad M_z = \frac{\sum n_i M_i^3}{\sum n_i M_i^2} \quad (3)$$

$M_n$ - number average molar mass; $M_w$ - weight average molar mass; $M_z$ - z average molar mass; $n_i$ - number of molecules with molar mass $M_i$.

The mobile phase used was 0.1 M $NaNO_3$ aqueous solution, containing 3 mM $NaN_3$ to prevent microorganism growing. For the same reason an UV lamp was also used.

All hyaluronic acid samples used in this study were obtained from Contipro (Czech Republic) where are produced by fermentation (Streptococcus equi., subsp. Zooepidemicus bacterial strain). The analyzed samples were of different molar masses, as follows (HA - hyaluronic acid or hyaluronan):

HA 1MDa: Mw = 1 MDa

HA 0.75MDa: Mw = 752 kDa

## 3. RESULTS AND DISCUSSION

According to Tokita and Okamoto 0, degradation of hyaluronan obeys first order kinetics. Dependencies of molecular weights on time, determined in samples kept at room temperature, suggest exponential decay. By linearizing first order kinetic equation we found out that dependencies are not linear.

Explanation is found in comparison of linear dependencies of the same hyaluronan samples kept in the fridge and non-linear dependencies of samples kept at room temperature and in behaviour of low molecular weight hyaluronan. Degradation of hyaluronan kept in the fridge should be slower than in samples at room temperature according to Arrhenius law. The experimental data depicted in Figure 1 support this prediction.

Also the probability of degradation of low molar mass hyaluronan is lower, because there are less glycosidic bonds to break. We suggest two degradation models for the rate of hyaluronan degradation. First is zero order kinetics. We suggest that degradation rate changes when certain level of degradation is reached (12.5 % for HA 1 MDa, 6.8 % for HA 0.75MDa). This means that every dependence looks as exponential decay, but mathematically is not possible to fit dependencies with first order kinetic exponential function and linearizing of the equation ($\ln M_w = -kt + \ln M_0$), and the data, gives us non-linear dependence as in case of non-linearized data. In fact, there are two separate kinetic units in each sample kept at room temperature. Samples kept in the fridge probably have linear dependence because they did not reach the second degradation level to date. Thus, kinetic model suggested by Tokita and Okamoto is not useful in our study. We suggest that time degradation of hyaluronan obeys zero order kinetics according to approximated equation for zero order kinetics:

$$M_w = M_0 + kt\,, (4)$$

where $M_w$ represents molecular weight of degraded hyaluronan, $M_0$ initial molecular weight of hyaluronan, $k$ the rate constant of degradation and $t$ is time. Time derivative of Equation 4 gives us rate constant as a slope of linear dependence:

$$\frac{dM_w}{dt} = k\,. (5)$$

By fitting Equation 4 in molar mass decrease from Figure 1, the final values found for the degradation rates in solution at room temperature after 30 days are obtained: $9.43\cdot10^{-2}$ kDa$\cdot$hour$^{-1}$ for HA 1MDa and $6.84\cdot10^{-2}$ kDa$\cdot$hour$^{-1}$ in the case of HA 0.75 MDa, respectively. After 30 days, rate constants decreased to $2.56\cdot10^{-3}$ kDa$\cdot$hour$^{-1}$ and $1.02\cdot10^{-2}$ kDa$\cdot$hour$^{-1}$ for HA 1 MDa and HA 0.75 MDa hyaluronan, respectively. The dependences of $M_w$ on time of samples kept in the fridge are strictly linear for both 1 MDa and 0.75 MDa hyaluronan solutions. Again from the fit of $M_w = f($ we obtained rate constants of degradation of $1.05\cdot10^{-2}$ kDa$\cdot$hour$^{-1}$ and $1.11\cdot10^{-2}$ kDa$\cdot$hour$^{-1}$ for HA 1 MDa and HA 0.75 MDa hyaluronan, respectively. We cannot compare individual values of rate constants of different molecular weights, because we have different range of *y* axis. But when we compare rate constants of each hyaluronan sample, we can see slower degradation in second decrease region as mentioned above. It is actually expected, because hyaluronan has lower molecular weight and probability of degradation of lower molecular weight should decrease, which is shown by fitting Equation 4 in experimental data. Kinetic calculations also confirm behaviour of degradation at different temperature in according to Arrhenius law.

The second degradation model for samples at room temperature was derived empirically:

$$Mw = M_\infty + M_{diff}\, e^{-kt}\,, (6)$$

where $M_{diff}$ represents difference between molecular weight of fresh hyaluronan sample and last determined value of measured molecular weight. $M_\infty$ represents asymptotic value at $t = \infty \Rightarrow e^{-\infty} = 0$. At these conditions, Equation 6 changes to:

$$M_w = M_\infty\,. (7)$$

Fit of $M_w = f($ with Equation 6 yields overall rate constants for all hyaluronan samples. Comparison of adjusted R-square determined by Origin shows, that statistically is better to use exponential dependence derived empirically but in first phase of degradation, zero order kinetics fits as well. But in case of hyaluronan samples kept in the fridge it was not possible to

fit the data with Equation 6 so in that case we used only zero order kinetics to extract rate constants of degradation.

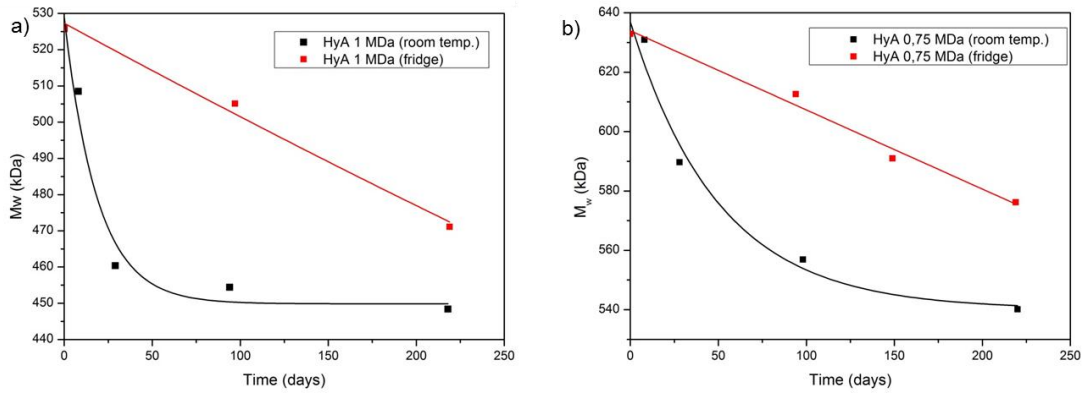


**Figure 1**: The degradation of HA 0.75 MDa (a) and HA 1MDa (b) in time at room temperature and in the fridge

## 4. CONCLUSION

We suggest two kinetic models for hyaluronan degradation. Zero order kinetic model fits the data for samples at room temperature and for samples kept in the fridge. Equation 6 fits well data for samples kept at room temperature. Therefore we show that degradation of hyaluronan at room temperature is possible to describe by two models as described above. For samples kept in the fridge we cannot use Equation 6 to fit the data, because these dependencies are linear.

## 5. ACKNOWLEDGEMENT

The authors acknowledge the financial support of project Excellent Teams - CZ.1.07/2.3.00/30.0005 and the project LO 1211 Ministry of Education, Youth and Sports of Czech Republic

## 6. REFERENCES

[1]Lapcík L; De Smedt S; Demeester J; et all., Chemical Reviews, 8 (1998), 2663-2684

[2]Tokita Y; Okamoto A, Polymer Degradation and Stability, 2 (1995), 269-273

[3]Bothner H; Waaler T; Wik O, International Journal of Biological Macromolecules, 5 (1988), 287-291

[4]Reháková M;Bakoš D; Soldán M;et all., International Journal of Biological Macromolecules, (1994),121-124

[5]Šoltés L; Brezová V; Stankovská M; et all., Carbohydrate Research, 5 (2006), 639-644

# OXIDATION OF AND DNA ADDUCT FORMATION BY BENZO[A]PYRENE BY RAT CYTOCHROME P450 1A1 ARE STIMULATED BY CYTOCHROME $B_5$ AND NADH

Marie STIBOROVÁ[1*], Michaela MOSEROVÁ[1], Radek INDRA[1], Petr HODEK[1], Eva FREI[2], Volker M. ARLT[3]

[1] *Department of Biochemistry, Faculty of Science, Charles University in Prague, Albertov 6, 128 43 Prague 2, Czech Republic*

[2] *Division of Preventive Oncology, National Center for Tumor Diseases, German Cancer Research Center (DKFZ), Im Neuenheimer Feld 280, 69 120 Heidelberg, Germany*

[3] *Analytical and Environmental Sciences Division, MRC-PHE Centre for Environment and Health, King's College London, London, United Kingdom*

**stiborov@natur.cuni.cz*

**Abstract**

Oxidation of and DNA adduct formation by benzo[a]pyrene (BaP) by rat cytochrome P450 (CYP) 1A1 enzyme systems is stimulated by cytochrome $b_5$ and NADH.

## 1. INTRODUCTION

Benzo[*a*]pyrene (BaP) is a genotoxic carcinogen that covalently binds to DNA after metabolic activation by cytochrome P450 (CYP) [1,2]. CYP1A1 is the most important enzyme in BaP bioactivation [2,3], in combination with microsomal epoxide hydrolase (mEH). First, CYP1A1 oxidizes BaP to an epoxide that is then converted to a dihydrodiol by mEH (*i.e.* BaP-7,8-dihydrodiol); then further bio-activation by CYP1A1 leads to the ultimately reactive species, BaP-7,8-dihydrodiol-9,10-epoxide (BPDE) that can react with DNA, forming preferentially the 10-(deoxyguanosin-$N^2$-yl)-7,8,9-trihydroxy-7,8,9,10-tetrahydrobenzo[*a*]pyrene adduct [4]. BaP is, however, oxidized also to other metabolites such as the other dihydrodiols, BaP-diones and hydroxylated metabolites. Even though most of these metabolites are the detoxification products, BaP-9-ol is a precursor of 9-hydroxy-BaP-4,5-epoxide, which can form another adduct with deoxyguanosine in DNA [5,6]. Therefore, regulation of CYP1A1-mediated oxidation of BaP leading to either metabolites forming BPDE, 9-hydroxy-BaP-4,5-epoxide or the BaP metabolites that are the detoxification products is of major importance. In order to modulate CYP1A1-catalyzed oxidation of BaP in human,

knowledge on such modulation of the CYP1A1 enzyme from suitable animal models that might mimic oxidation of BaP in human should be investigated and the results found applied to regulation of BaP oxidation by human CYP1A1. In fact, the first step of such investigations is to find which of the animal model CYP1A1 enzyme oxidizes BaP similarly to human CYP1A1. Recently, similarities between human and rat CYP1A1 in BaP oxidation indicating that rats are a suitable model mimicking BaP oxidation in human were demonstrated [7].

However, there are still not clearly explained how an electron transfer mediated by NADPH:CYP reductase (POR) on CYP1A1 during BaP oxidation in the microsomal enzymatic system occurs, and whether cytochrome $b_5$ might influence this electron transfer. Namely, the oxygen needed for BaP oxidation is activated in the active center of CYPs by two electrons transferred from NADPH and/or NADH by means of POR and cytochrome $b_5$, respectively [8]. Whereas POR is an essential constituent of the electron transport chain towards CYP, the role of cytochrome $b_5$ is still quite enigmatic. Likewise, a potential of NADH as a donor of electrons to the CYP-mediated reaction cycle is still not exactly known. Even though the second electron in the CYP reaction cycle might also be provided by the system of NADH:cytochrome $b_5$ reductase, cytochrome $b_5$ and NADH, there is still rather enigmatic whether this system might participate in donation of the first electron to CYP. Therefore, here we investigated the effect of cytochrome $b_5$ and NADH on a potency of CYP1A1 to oxidize BaP to its metabolites and on formation of BaP-DNA adducts *in vitro*.

## 2. MATERIAL AND METHODS

Liver microsomes of uninduced rats and/or those in which CYP1A1 was induced with Sudan I, and Supersomes™ isolated from insect cells transfected with baculovirus constructs containing cDNA of rat CYP1A1 and expressing POR were used as model enzyme systems.

## 3. RESULTS AND DISCUSSION

Rat hepatic microsomes are natural systems containing all components of a monooxygenase system located in a membrane of endoplasmic reticulum, CYPs, POR, cytochrome $b_5$, and NADH:cytochrome $b_5$ reductase, in addition to mEH. Rat hepatic microsomes oxidized BaP to BaP-9,10-dihydrodiol, the unknown metabolite Mx, BaP-7,8-dihydrodiol, BaP-4,5-dihydrodiol, BaP-1,6-dione, BaP-3,6-dione, BaP-9-ol and BaP-3-ol. These results indicate that BaP is metabolized not only by CYP1A1 present in this enzyme system, but also by mEH, which is important for the hydration of BaP epoxides to produce dihydrodiols. An up to more than 3.5-fold increase in amounts of BaP metabolites were generated in microsomes, in

which CYP1A1 was induced. Interestingly, the used rat hepatic microsomes formed in the presence of NADH the same BaP metabolites as microsomes with NADPH. The amounts of metabolites were also comparable. Rat recombinant CYP1A1 expressed with POR in Supersomes$^{TM}$ oxidized BaP to the analogous spectrum of metabolites as rat hepatic microsomes. These results indicate that BaP is metabolized in this system not only by CYP1A1, but also by mEH. Similar to hepatic microsomes the supersomal CYP1A1 oxidized BaP to the above mentioned metabolites even when NADH was present instead of NADPH. Addition of cytochrome $b_5$ to the supersomal CYP1A1 system led to a more than 2-fold increase in BaP oxidation to its metabolites; the highest increase in formation of BaP-7,8,dihydrodiol, BaP-9,10-dihydrodiol and BaP-3-ol was found.

In further experiments, the formation of BaP-derived DNA adducts was investigated in the same enzymatic systems. In *ex-vivo* incubations containing hepatic microsomes of control and Sudan I-pretreated rats, DNA, BaP and NADPH generated two major DNA adducts detectable by $^{32}$P-postlabeling [6]. Induction of CYP1A1 by Sudan I resulted in a more than 25-fold increase in total DNA adduct levels. Similar to formation of BaP-metabolites, also the BaP-DNA adducts were generated in the microsomal system containing NADH instead of NADPH. Activation of BaP by rat CYP1A1 reconstituted with POR in the presence of DNA and NADPH resulted in formation of only one BaP-DNA. Therefore, this adduct is formed by CYP1A1-catalyzed oxidation of BaP alone, without the contribution of mEH. This adduct was tentatively identified as the adduct derived from a reaction of deoxyguanosine in DNA with 9-hydroxy-BaP-4,5-epoxide [5,6]. Addition of mEH to the *ex-vivo* incubation containing BaP, CYP1A1 reconstituted with POR and NADPH resulted in formation also another adducts, which was identified as dG-$N^2$-BPDE [6]. The question whether the substitution of NADPH by NADH influences BaP-DNA adducts formation by the CYP1A1-reconstituted system is planned to be answered. Addition of cytochrome $b_5$ to the CYP1A1-reconstitution system stimulated the formation of both BaP-DNA adducts, but their levels depended on ratios of CYP1A1:POR:mEH:cytochrome $b_5$.

## 4. CONCLUSION

The results demonstrate that the POR-mediated electron transfer from NADPH to CYP1A1 is stimulated by cytochrome $b_5$ and suggest that NADH can, to some extent, substitute NADPH as an electron donor for the CYP1A1-reaction cycle catalyzing oxidative activation of BaP.

## 5. ACKNOWLEDGEMENT

The work has been supported by GACR (P303/10/G163).

## 6. REFERENCES

[1]IARC: IARC Monographs of Evaluation of Carcinogens. Risk of Chemicals for Human, 92 (2010), 1-853

[2]Baird WM, Hooven LA, Mahadevan B: Environmental and Molecular Mutagenesis, 45 (2005), 106–114

[3]Hamouchene H, Arlt VM, Giddings I, et al.: BMC Genomics, 12 (2011), 333

[4]Phillips DH, Venitt S: International Journal of Cancer, 131 (2012), 2733-2753

[5]Fang A.H., Smith W.A., Vouros P., et al.: Biochemical and Biophysical Research Communication, 281 (2001) 383-389

[6]Stiborová M., Moserová M., Cerná V., et al.: Toxicology, 318 (2014) 1-12

[7]Indra R., Moserova M., Sulc M., et al.: Neuro Endocrinology Letters, 34 Suppl. 2 (2013) 55-63

[8]Coon MJ: Nutrition Review, 36 (1978), 319-328

# ARYL HYDROCARBON RECEPTOR LIGANDS BENZO[*A*]PYRENE, ELLIPTICINE AND SUDAN I INDUCE EXPRESSION OF CYTOCHROME P450 1A1, NAD(P)H:QUINONE OXIDOREDUCTASE 1 AND CYTOCHROME $B_5$

Marie STIBOROVÁ[1*], Iveta MRÍZOVÁ[1], Michaela MOSEROVÁ[1], Helena DRAČÍNSKÁ[1], Věra ČERNÁ[1], Eva FREI[2], Volker M. ARLT[3]

[1] *Department of Biochemistry, Faculty of Science, Charles University in Prague, Albertov 2030, 128 43 Prague 2, Czech Republic*

[2] *Division of Preventive Oncology, National Center for Tumor Diseases, German Cancer Research Center (DKFZ), Im Neuenheimer Feld 280, 69 120 Heidelberg, Germany*

[3] *Analytical and Environmental Sciences Division, MRC-PHE Centre for Environment and Health, King's College London, London, United Kingdom*

**stiborov@natur.cuni.cz*

**Abstract**

Utilizing the Western blotting and the real-time polymerase chain reaction (RT-PCR) methods, expression of cytochrome P450 1A1 (CYP1A1), NAD(P)H:quinone oxidoreductase 1 (NQO1) and cytochrome $b_5$ proteins and mRNAs, respectively, was found to be induced by treating rats with three aryl hydrocarbon receptor ligands, benzo[*a*]pyrene (BaP), ellipticine and Sudan I. Because these chemicals induced the expression levels of the enzymes essential for their oxidation dictating their biological activities (CYP1A1 and cytochrome $b_5$), they exert concerted regulatory control on their own genotoxic and/or pharmacological effects.

## 1. INTRODUCTION

Cytochromes $b_5$ are heme proteins, which are capable of accepting and transferring a single electron [1]. One of cytochromes $b_5$, which is located in the membrane of endoplasmic reticulum (microsomal cytochrome $b_5$), is involved in fatty acid desaturation, cholesterol and plasmalogen biosyntheses as well as in various hydroxylation reactions catalyzed by mixed function oxidase system [2,3]. It can accept an electron from either NADH:cytochrome $b_5$ reductase or NADPH:cytochrome P450 (CYP) reductase [3,4] and then reduced cytochrome $b_5$ transfers this electron to CYPs and other enzymes. The role of microsomal cytochrome $b_5$ in catalytic function of CYPs has not been fully understood yet. Cytochrome $b_5$ has been

shown to be able to stimulate, inhibit or have no effect on CYP mediated reactions (for a review, see [2-4]). One of hypotheses trying to explain the influence of cytochrome $b_5$ on CYP reactions suggests a role of cytochrome $b_5$ in a direct transfer of the second electron to the CYP enzyme, which is considered to be the rate limiting step in the catalytic cycle of the CYP monooxygenase reaction [4]. The electron transfer from reduced cytochrome $b_5$ to CYP is faster than the input of electron from NADPH:CYP reductase [5]. Another possible mechanism of the cytochrome $b_5$ action is the formation of a complex between cytochrome $b_5$ and CYP, which can receive two electrons from NADPH:CYP reductase in a single step, one for reduction of CYP and another for that of cytochrome $b_5$ [3]. While CYP without cytochrome $b_5$ has to undergo two separate interactions with NADPH:CYP reductase to complete one catalytic cycle, in the case of the presence of cytochrome $b_5$, only one single interaction of complex of CYP and cytochrome $b_5$ with NADPH:CYP reductase is sufficient; cytochrome $b_5$ provides the second electron to CYP promptly after oxygen binding. Interaction of cytochrome $b_5$ with CYP may also induce conformational changes in CYP proteins leading to breakdown of oxygenated hemoprotein complex with substrates to products. This hypothesis is based on findings showing that not only holoprotein of cytochrome $b_5$, but also its apo-form (devoid of heme), which is not capable of electron transfer, can contribute to stimulation effects [3-5].

It is clear from such investigations that expression levels of cytochrome $b_5$ in a cell are crucial for efficiencies of several CYPs to oxidize xenobiotics. This is also true for the oxidation of the anticancer drug ellipticine and the carcinogens benzo[*a*]pyrene (BaP) and Sudan I (1-phenylazo-2-hydroxynaphtalene); their oxidation by CYP1A1, dictating their biological effects, is strongly influenced by cytochrome $b_5$ [6-10]. Therefore, here the effect of BaP, ellipticine and Sudan I on expression of cytochrome $b_5$ protein in rats *in vivo* was investigated. Their potency to induce the CYP1A1 and NQO1 enzymes was also investigated.

## 2. MATERIAL AND METHODS

Male Wistar rats were treated intraperitoneally with BaP, ellipticine and Sudan I as described previously [7-10]. Microsomes were isolated from the livers and kidneys of this animal model [9]. The method of Western blot, employing anti-rat CYP1A1, NAD(P)H:quinone oxidoreductase 1 (NQO1) and cytochrome $b_5$ antibodies, was utilized to evaluate expression of these proteins. Their mRNA contents in rat liver and kidney measured using the real-time polymerase chain reaction (RT-PCR) were also carried out [7-10].

## 3. RESULTS AND DISCUSSION

Using a method of Western blotting with antibodies raised against rat CYP1A1, NQO1 and cytochrome $b_5$ and a RT-PCR method, the effects of exposure of rats to BaP, ellipticine and Sudan I on expression levels of mRNA and proteins of these enzymes were analyzed. We found that these compounds act as inducers of cytochrome $b_5$ in liver and kidney of rats. Here, the mechanism of such induction was investigated. Beside a potency of BaP, ellipticine and Sudan I to induce cytochrome $b_5$, they also induced enzymes that are regulated by activation of the aryl hydrocarbon receptor (AHR), CYP1A1 and NQO1, both at mRNA and protein levels. This finding corresponds to their ability to act as AHR ligands.

Up to 5-, 10- and 100-fold increases in NQO1, cytochrome $b_5$ and CYP1A1 protein expression levels, respectively, were caused by treatment of rats with these compounds. The increase in protein levels was paralleled by an increase in mRNA expression in most cases. Because of the induction of cytochrome $b_5$ by the tested xenobiotics in parallel to that of CYP1A1 and NQO1, an analogous induction mechanism *via* the activation of AHR might be suggested. Nevertheless, further studies investigating the effects of AHR expression on induction of these proteins are needed to be performed to support this suggestion.

## 4. CONCLUSION

Utilizing the Western blotting method, expression of CYP1A1, NQO1 and cytochrome $b_5$ protein was found to be induced by treating rats with BaP, ellipticine and Sudan I. Since these compounds induced the expression levels of the enzymes essential for their oxidation dictating their biological activities (CYP1A1 and cytochrome $b_5$), they exert concerted regulatory control on their own genotoxic and/or pharmacological effects.

## 5. ACKNOWLEDGEMENT

The work has been supported by Grant Agency of the Czech Republic (P301/10/0356) and Charles University in Prague (UNCE 204025/2012 and 640712).

## 6. REFERENCES

[1]Velick SF, Strittmatter P: Journal Biological Chemismy, 221 (1956), 265-275.

[2]Vergeres G, Waskell L.: Biochemie, 77 (1995), 604-620.

[3]Schenkman JB, Jansson I: Pharmacology and Therapy, 97 (2003), 139-152.

[4]Guengerich FP:, Archives of Biochemistry and Biophysics, 440 (2005,) 204-211.

[5]Schenkman JB, Jansson I: Drug. Metabolism Review, 31 (1999), 351-364.

[6]Aimová D., Svobodová L., Kotrbová V., et al.: Drug Metabolism and Disposition. 35 (2007), 1926-1934.

[7]Arlt VM, Stiborová M, Henderson CJ, et al.: Carcinogenesis, 29 (2008), 656-665.

[8]Kotrbová V., Mrázová B., Moserová M., et al.: Biochemical Pharmacology, 82 (2011), 669-680.

[9]Vranová I, Moserová M, Hodek P, et al.: International Journal of Electrochemical Science, 8 (2013), 1586-1597.

[10]Stiborová M, Dračínská H, Martínek V, et al.: Chemical Research in Toxicology, 25 (2013) 290-299.

# DETERMINATION OF METHYLXANTHINES ON PENCIL GRAPHITE ELECTRODES BY CYCLIC VOLTAMMETRY (CV)

Dominika MOTLOVÁ[1], Rudolf NAVRÁTIL[1], Libuše TRNKOVÁ[1,2*]

[1] *Department of Chemistry, Faculty of Science, Masaryk University, Kamenice 5, CZ-625 00 Brno, Czech Republic*

[2] *Central European Institute of Technology, Brno University of Technology, Technická 3058/10, CZ-616 00 Brno, Czech Republic*

**libuse@chemi.muni.cz*

**Abstract**

This work deals with voltammetric determination of xanthine (Xan) and its methylated derivatives (1-, 3-, 7-, and 9-mXan) in the presence of copper ions, which form *in situ* complexes with corresponding xanthines and enable more sensitive detection of these substances by voltammetric methods on pencil graphite electrodes (PeGE). To enhance the sensitivity of detection we used the elimination voltammetric procedure (EVP), which is able to increase oxidation signals and to uncover the minor processes of the reaction.

## 1. INTRODUCTION

Xanthine and its methyl derivatives are biologically important substances and their concentration, particularly in urine, can be a suitable indicator of various types of diseases [1-2]. Monovalent copper allows the formation of the Cu(I)-purine complex, which provides in voltammetric measurements (LSV - Linear Sweep Voltammetry) anodic response at a potential of around 0.4 V, while there is a simultaneous increase in the oxidative signal of the corresponding purine during detection [3,4]. For a simple, sensitive and fast electrochemical detection of methylxanthines on pencil graphite electrodes (PeGE) in the presence of copper, we used adsorptive stripping techniques in connection with the elimination voltammetric procedure (EVP) [5]. The entire elimination procedure was described in several earlier works [6-8] and enables us to eliminate some current components while others are maintained. These techniques were proven to be a useful tool in the study of the oxidation process because of their easy instrumentation and very small consumption of controlled substances [9].

In this work we studied the redox behavior of the methyl derivatives of xanthine; the formation of complexes of Cu(I)-methylxanthine and the influence of the methyl group on the redox behavior was also investigated at different pH and solution composition. The acquired knowledge was used to design a procedure that combines in situ formation of the purine complex with monovalent copper ions on the surface of PeGE and the adsorptive stripping

technique coupled with the elimination procedure for qualitative and quantitative analysis of these substances and subsequently for its use in medicine and pharmacy.

## 2. MATERIAL AND METHODS

All measurements were performed on an Autolab PGSTAT30 potentiostat (Metrohm, Czech Republic) using a three-electrode system with an auxiliary platinum electrode, the reference Ag/AgCl/KCl (3M) electrode and a pencil graphite electrode (PeGE, diameter 0.5 mm, surface area 16 $mm^2$) from Tombow (Japan) as the working electrode. The chemicals including xanthine (Xan) and its methyl derivative (1-, 3-, 7- and 9-mXan) were purchased from Sigma-Aldrich. Before the measurements, all graphite electrodes were activated in 0.1 M acetate buffer, pH 5.1, using a 30-second pulse insertion at a potential of 1.4 V. For CV measurements we used a potential between -0.1 V and 1.4 V with 120 s adsorption at a potential of -0.15 V. To calculate the elimination E4 functions (f(I), equation 1) we used the average values of the currents of three independent CV measurements (scan rates 200, 400 and 800 mV/s). More information can be found in a previous publication [6].

$$f(I) = -11.657 I_{vref/2} + 17.485 I_{vref} - 5.8284 I_{2vref} \qquad (1)$$

where $I_{vref}$ is an LSV curve scanned at the reference scan rate, $I_{vref/2}$ and $I_{2vref}$ are scan rates of the half and twice the value of the scan rate.

## 3. RESULTS AND DISCUSSION

A typical record of the elimination procedure has the form of *f(I)* vs. the E and elimination function is shown in Fig. 1. The elimination function E4 (Equation 1) is the eliminating kinetic and capacitycurrent component and conserves the diffusion current component [6-8].

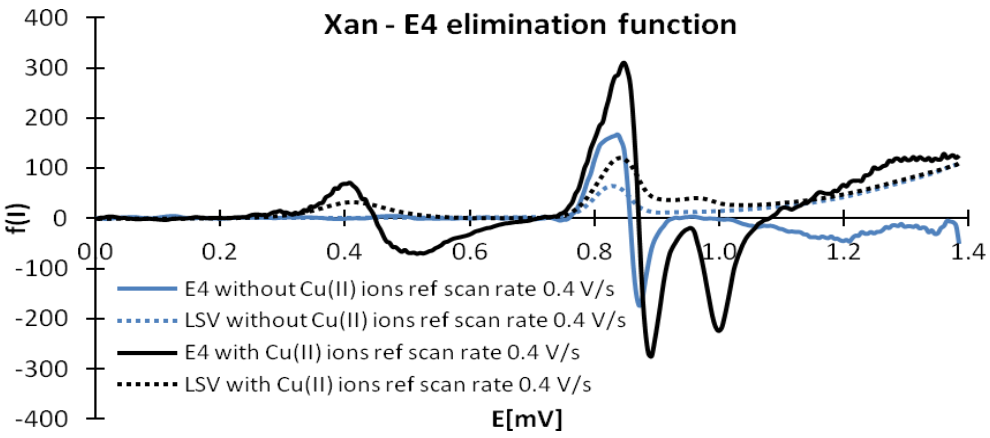


**Fig. 1.** Elimination (EVP E4) curves of 20 µM Xan without 20 µM Cu(II) and with 20 µM Cu(II) ions; reference scan rate 0.4 V/s, acetate buffer pH 5.1.

The electroactive substance in the adsorbed state provides or accepts an electron, and we can observe a specific signal in the form of peak-counterpeak. Compared with LSV the elimination procedure provides a significantly increased signal in the absence or presence of Cu (II).

## 4. CONCLUSION

The electrochemical analysis of xanthine (Xan) and its methyl derivatives (mXan) was performed on pencil graphite electrodes (PeGE) in the presence of copper ions using linear sweep voltammetry (LSV) in combination with the adsorptive stripping voltammetric technique and the elimination procedure (EVP) to increase the sensitivity of detection. The analysis of mXan is based on the electrochemical surface modification of PeGE by monovalent copper and formation of complex Cu(I)-mXan, which is formed by in situ reduction of the copper ions Cu(II) by anodic polarization of PeGE and allows determination of methylxanthines with the use of EVP. In accordance with the theory the peak-counterpeak signals arising after the use of elimination procedures reveal that the charge transfer process is mediated by particles in the adsorbed state and in addition an EVP significantly increasing the detection sensitivity and reducing the detection limits (nanomolar concentrations).

## 5. ACKNOWLEDGEMENT

The work has been supported by projects: (a) MUNI/A/0972/2013 and (b) KONTAKT II (LH 13050) of the Ministry of Education, Youth and Sports of the Czech Republic, (c) CEITEC – Central European Institute of Technology Project CZ.1.05/1.1.00/02.0068.

## 6. REFERENCES

[1] Scheindlin S.: Mol. Intervent. 7, (2007) 236-242.

[2] Goyal R.N., Thankachan P.P., Kumar N., Sangal A.: Indian J. Chem. 39, (2000) 953-963.

[3] Ibrahim M.S., Temerk Y.M., Kamal M.M., Ahmed G.A.W., Ibrahim H.S.M.: Microchim. Acta. 144, (2004) 249-256.

[4] Aladag N., Trnkova L., Kourilova A., Ozsoz M., Jelen F.: Electroanalysis. 22, (2010) 1675-1681.

[5] Jelen F., Hason S., Trnkova L., in: Utilizing of Bio-Electrochemical and Mathematical Methods in Biological Research (Adam V., Kizek R., eds.), chap. 8. Research Signpost, Kerala, India, 2007.

[6] Trnkova L., Kizek R., Dracka O.: Electroanalysis. 12, (2000) 905-911.

[7] Trnkova L.: J. Electroanal. Chem. 582, (2005) 258-266.

[8] Trnkova L., in: Utilizing of Bio-Electrochemical and Mathematical Methods in Biological Research (Adam V., Kizek R., eds.), chap. 4. Research Signpost, Kerala, India, 2007.

[9] Navratil R., Pilarova I., Jelen F., Trnkova L.: Int. J. Electrochem. Sci. 7, (2013) 4397-4408.

# TRENDS IN DEVELOPMENT OF FUNCTIONAL NANOSTRUCTURED FILMS

Andrej ORIŇÁK[1*], Renáta ORIŇÁKOVÁ[1], Ondrej PETRUŠ[1], Ján MACKO[2], Branislav ERDELYI[3], Patrik STRAŇÁK[1]

[1] *Department of Physical Chemistry, Faculty of Natural Sciences, P.J.Šafárik University in Košice, Moyzesova 11,041 54Košice, Slovak Republic*

[2] *Department of Physical Chemistry, Faculty of Sciences, Komensky University Bratislava, Mylnská dolina II, Bratislava, Slovak Republic*

[3] *Deapartment of Physics, Faculty of Natural Sciences, P.J.Šafárik University in Košice, Moyzesova 11,041 54Košice, Slovak Republic*

**andrej.orinak@upjs.sk*

**Abstract**

Nanostructured surfaces pose, in many cases like functional layers – they feature with specific fiction/s. It is due to nanospecific phenomenons resulting in analytical signal enhancement, specific optical properties, separation abilities or capturing of analytes, leading an electric current or catalyse specific reactions. The use of these metallic nano/microstructures in many applications (surface enhanced Raman spectroscopy (SERS) and separation ability) has been studied. Free-template electrodeposition is used for the synthesis of metallic nano/microstructures on solid substrates in order to facilitate their practical applications as nanobuilding blocks for plasmonic films, nanoseparation/filtration or capturing media followed with an integration of functional films into nanodevices. This contribution reviews a recent trends in this field of science.

## 1. INTRODUCTION

Electrochemical deposition of nanostructured functional films means to create well-ordered nanostructured surfaces , compact layers and microdevices, featuring exquisitely defined geometry and morfology, controlled surface chemistry, and tunable physical properties. Research teams are interested in materials and structures whose properties can be tuned or optimized by variations in size, geometry, crystallinity, composition of surface. This strategy is applied primarily to problems related to sensing films, cell capturing media, mechanical devices, biomedical materials, culture heritage surfaces, renewable energies and magnetism.

There are a lot of results with producing metallic (Co, Ni, Co, Pt, Au, etc.) nanowires and nanotubes with various functionalities (e.g. fer-romagnetic, Tip Enhanced Raman Scattering,

etc.) where authors use electrochemical deposition process inside high as-pect ratio membrane templates (Anodic Alumina Oxide or polycarbonate). Controled was the main growth parameters during the deposition in order to tailor crystal structure and morphology of the metallic nanostructured films. Structural, electrical and mechanical properties were studied in correlation with the synthesis conditions employed. The most electroformed components are nanocrystalline and the use of templates to produce homogenous nanostructured film is recommended.

With new advances in material science, newer strategies arise that result in sophisticated architecture for chemical separations based on molecular self-assembly. These processes result from spontaneous molecular interactions to control the size, shape, or surface characteristics of the assembly, often resulting in what is a highly ordered and unique structure. These molecular assemblies may possess nanoscale features as well as unique properties that macroscale materials often lack. Among those structures are nanotubes, nanocavities, nanowires, nanoposts, nanocones, nanospheres, molecular imprints, nanoparachutes (conical monodendrons), and general nanoparticles with random structures [1]. The integration of porous structures into microchannels is known to enable unique and useful separations both in electrophoresis and chromatography. Etched pillars and other nanostructures have received considerable interest in recent years as a platform for creating microchannels with pores tailored to specific applications. Demonstrated was application of chiral and chevron nanostructures. This versatility in structural design could facilitate new developments in on-chip separations [2]. In this contribution we documment a recent status in development of plasmonic films as well surface with separation ability as well integration of multifunctional elements into a microfluidic devices and chips.

## 2. MATERIAL AND METHODS

The silver nanostructured films were prepared by electrochemical deposition of silver at polystyrene nanosphere template to prepare nanocavity film. Different cavities were applied and spectral signal enhancement in SERS as well cells encapturing have been studied. Second film has been made by silver electrodeposition to AAO membráně to get nanowires nanostructured surface. The thin gold layer prepared by evaporation on AAO membrane was used as cathode and the platinum electrode as anode. The alumina template was dissolved in 1 M NaOH for 1 hour after filling the membrane pores by the deposited silver. Nanosized structure consists of nanowires 25 nm in diameter and 3000 nm long. The mixture of rhodamine 6G and 4- aminothiophenol was analysed by SERS and secondary ion mass

spectrometry (SIMS) to clarify mechanism of spectral signal enhancement or separation ability of nanostructured films.

## 3. RESULTS AND DISCUSSION

General equation (1) defines parameters of nanostructured surface with plasmonic, SERS signal enhancement function.

$$E_{out}(x,y,z) = E_0\hat{\boldsymbol{z}} - \alpha E_0\left[\frac{\hat{\boldsymbol{z}}}{r^3} - \frac{3z}{r^5}(x\hat{\boldsymbol{x}} + y\hat{\boldsymbol{y}} + z\hat{\boldsymbol{z}})\right] \qquad (1)$$

Final energy of surface plasmon polariton formed at nanostructured film is given in a equation (2).

$$E_{SP} = \frac{\varepsilon - \varepsilon_0}{\varepsilon + 2\varepsilon_0}\left(\frac{r}{r+d}\right)^3 E_0 \qquad (2)$$

Intenzity of a surface plasmon is well defined for spheric nanoparticles and requires corrections for a shape different to a sphere. At Fig. 1 is a micrograph of ~ 500nm silver nanocavity nanostructured film that allows entrapping of colon cancer cells and enhances spectral signal in SERS 10 times.

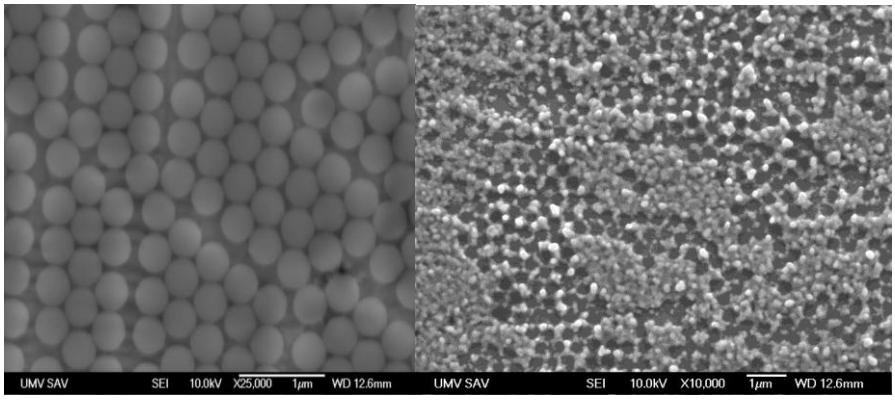


**Figure 1.:** Polystyrene nanospheres litography of silver nanocavity film.

Stronger SERS signal enhancement has been obtained with other silver nanostructured films prepared by template-free electrodeposition method. Nanospecific phenomenon attaches 4-minothiophenol self-assembled (SAM) formation to make signal enhancement extremely intensit, founded at value $10^{12}$ (see Table1 to copare with another films). Separation ability of silver nanowires nanostructured films were confirmed by SIMS.

**Table 1**: Comparison of various characterictic values in course of one year.

| **Type of Nanostructured Film** | **Spectral Signal Enhancement SERS** | **LOD** [mol/dm$^3$] | **Spectral Signal Enhancement SIMS** |
|---|---|---|---|
| nanoAg-PIGE | $10^5$ | R6G $10^{-8}$ | 10 |
| Au/Si nanovlákna | $10^8$ | R6G $10^{-12}$ | 100 |
| nanoAg | $10^{12}$ | R6G $5.10^{-16}$ | -- |
| nanoAg/SAM | $10^{12}$ | 4-ATF $10^{-16}$ | -- |

4-aminothiophenol separates from rhodamine 6G in mixture by forming 4-aminothiophenol SAM while rhodamine 6G migrates alone along the silver nanostructured film. Spectral separation has been calculated directly from SIMS spectra .

## 4. CONCLUSION

Nanostructured thin films feature with nanospecific functionality that can be applied in different areas of research. Nanoscopic phenomenon allows to introduce novel micro/nanosensors with detection of one molecule. Nanocavities with different diameter can capture migrating tumor cells and separate mixtures. Moreover, cavity down 40 nm diameter looks to be sensitive for microscopic RNA (miRNA) induced at cancer. When present, it switches signal at cavity. Integration of functional nanostructures to micro/nanofluidic systems and chips couples benefits of both.

## 5. ACKNOWLEDGEMENT

This research has been financialy supported by grant MŠ SR VEGA 1/0211/12 and APVV – 0280-11.

## 6. REFERENCES

[1] S.A.Archer-Hartmann, L.A.Holland, R.E.Majors: Self-Assembled Nanomaterials for Enhanced Chemical Separation, LC-GC International, May 1(2011) 1-7.

[2] L.W. Bezuidenhout, N. Nazemifard, A.B.Jemer, D.J.Harrison and M.J.Brett: Lab on a chip. 11(2011)1671-1678.

# BIODEGRADABLE MATERIALS FOR ORTHOPEDIC APPLICATIONS

Renáta ORIŇÁKOVÁ[1*], Andrej ORIŇÁK[1], Miriam KUPKOVÁ[2],
Monika HRUBOVČÁKOVÁ[2], Ján MACKO[3]

[1]*Department of Physical Chemistry, Faculty of Science, P.J. Šafárik University, Moyzesova 11, SK–04154 Košice, Slovak Republic*

[2]*Institute of Materials Research, Slovak Academy of Sciences, Watsonova 47, SK-040 01 Košice, Slovak Republic*

[3]*Department of Physical and Theoretical Chemistry, Faculty of Natural Sciences, Comenius University, Mlynská dolina, SK-84215 Bratislava 4, Slovak Republic*

**Renata.Orinakova@upjs.sk*

**Abstract**

Ironphosphate coated carbonyl iron powder (Fe/P) was prepared by phosphating method. Moreover, the Fe/P-Mn alloy was produced by sintering of Fe/P powder mixed with manganese powder. Bare carbonyl iron samples, Fe/P and Fe/P-Mn sintered samples have been tested with respect to their microstructure, and hemocompatibility. Addition of P and Mn resulted in higher surface inhomogeneity, porosity and roughness. All the samples were found to be hemocompatible.

## 1. INTRODUCTION

The degradable biomaterials have been proposed as a novel class of highly bioactive biomaterials which are expected to disappear via corrosion after providing structural support for a certain period of time depending on the application site [1]. Metals, ceramics and polymers are the most commonly used materials in the biomedical field [2]. Metals are more mechanically interesting compared to polymers for load-bearing implants. Two classes of metals have been mainly used: iron based [3, 4] and magnesium based alloys [5, 6].

The aim of the present work was to investigate the usability of iron based sintered materials as a potential degradable biomaterial. The effect of iron phosphate coating of carbonyl iron powder and manganese addition on the microstructure and in vitro biocompatibilities of sintered materials has been evaluated in this study.

## 2. MATERIAL AND METHODS

### Materials preparation and characterisation

The carbonyl iron powder (type CC, d50 value 3.8 – 5.3 μm) was used for the experiments as a starting material. Carbonyl iron powders were coated in phosphating solution using the

modified precipitating method. Phosphated iron powders were dried and calcined in air. Content of phosphorus in resulted sintered samples was ~ 0.5 wt.%.

The samples with addition of Mn were prepared from the mixtures of 30 wt.% of Mn powder (APS <10 μm, 99,6%) and carbonyl iron powder.

The powder mixtures were cold pressed at 600 MPa into cylinders (Ø 10 mm, h 2 mm) and sintered for 1 hour at 1120 °C in reductive H2. The samples Fe/P were sintered at 1050°C to avoid the liquid-phase sintering.

The microstructure of the experimental samples was observed by a scanning electron microscope (JOEL JSM-7001F, Japan).

**Biocompatibility studies**

For this purpose, 1 ml of healthy sheep blood containing sodium citrate (3.8 wt %) in the ratio of 9:1was taken and diluted to 10 ml with normal saline. The haemolysis test, thrombus formation test and platelet adhesion test described in details in [11] were conducted.

## 3. RESULTS AND DISCUSSION

Figure 1 shows the micrographs of Fe, Fe/P and Fe/P-Mn samples. Sintering of powder compacts resulted in some differences in microstructures. Small isolated pores with size up to 1 μm are visible in microstrucure of Fe and Fe/P compacts. Approximately ten times larger pores occur in Fe/P-Mn samples.

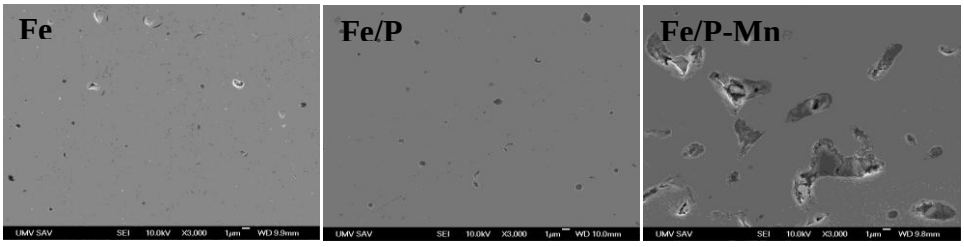


**Figure 1.:** Carbonyl iron based sintered material prepared by powder metallurgy: Fe, Fe/P, Fe/P-Mn.

The calculated values of hemolysis percentage were 7.00%, 5.33% and 3.96% for Fe, Fe/P and Fe/P-Mn samples, respectively. Addition of P and Mn to the iron powder resulted in lowering of hemolytic activity compared to pure iron sample. All the experimental samples can all be categorized as hemocompatible and Fe/P-Mn sample can be categorized as highly hemocompatible.

The slight decrease in thrombus formation was observed for the sintered material prepared from phosphated iron powder as compared with bare iron sample. Addition of Mn resulted in significant decrease of thrombus weight.

Fig. 2 shows representative SEM images of platelets adhering to the experimental samples. It is clearly visible that more platelets were present on the bare iron surface as compared with the Fe/P and Fe/P-Mn materials. Platelets adhering to the iron surface have more afinity to the metal surface and form pseudopodia-like structures whereas those present on the surface of Fe/P and Fe/P-Mn samples maintained their integrity, as shown by arrows.

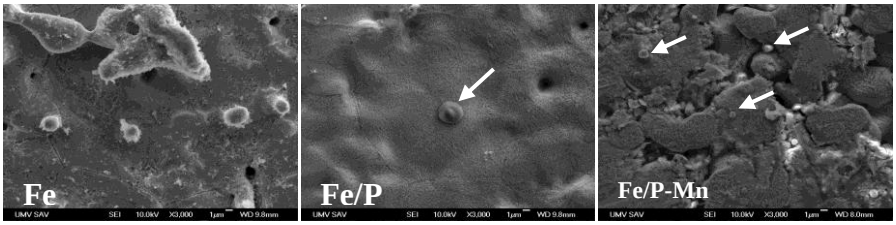


**Figure 2.:** SEM images of platelets adhering to the different carbonyl iron based sintered material prepared by powder metallurgical method: Fe, Fe/P, and Fe/P-Mn.

## 4. CONCLUSION

Iron based sintered material was fabricated via powder sintering method. The samples with addition of phosphorus and Mn were manufactured to increase the hemocompatibility.

## 5. ACKNOWLEDGEMENT

The authors wish to acknowledge financial support from the Slovak Research and Development Agency, Project APVV-0677-11 and Grant Agency of the Ministry of Education of the Slovak Republic, Grant No. 1/0211/12 and grant VVGS-2013-114.

## 6. REFERENCES

[1]Wegener B, Sievers B, Utzschneider S, et all.: Materials Science and Engineering B. 176 (2011) 1789-1796

[2]Wang YB, Xie XH, Li HF, et all.: Acta Biomaterialia 7 (2011) 3196-3208

[3]Schinhammer M, Hanzi AC, Loffler JF, et all.: Acta Biomaterialia 6 (2010) 1705-1713

[4]Hermawan H, Alamdari H, Mantovani D, et all.: Powder Metallurgy 51 (2008) 38–45

[5]Levesque J, Hermawan H, Dube D, et all.: Acta Biomaterialia 4 (2008) 284–295

[6]Xin Y, Liu C, Zhang X, et all.: Journal of Materials Research 22 (2007) 2004–2011

# AN ELECTROCHEMICAL STUDY OF d(GCGAAGC) DNA HEPTAMER AND ITS SEQUENTIAL ANALOGUES

Iveta PILAŘOVÁ[1], Michaela VORLÍČKOVÁ[2,3], Iva KEJNOVSKÁ[2,3], Libuše TRNKOVÁ[1,3*]

[1] *Department of Chemistry, Faculty of Science, Masaryk University, Kamenice 5, CZ-625 00 Brno, Czech Republic*

[2] *Institute of Biophysics of the AS CR, v.v.i., Královopolská 135, CZ–612 65 Brno, Czech Republic*

[3] *Central European Institute of Technology, Brno University of Technology, Technická 3058/10, CZ-616 00 Brno, Czech Republic*

**libuse@chemi.muni.cz*

**Abstract**

DNA molecules can adopt many unusual structures (hairpins, i-motifs, G – quadruplexes and others), linked with many neurodegenerative diseases (X syndrome, Friedreich's ataxia, Huntington's disease). The aim of our contribution is the electrochemical investigation of different structures of DNA heptamers with AAA, CCC, GAA, GGG and TTT sequence in the molecule center as the effect of adsorption on the electrode surface (mercury electrode, pencil graphite electrode).

## 1. INTRODUCTION

DNA molecules can adopt many unusual and less well characterized structures, different from the classical Watson–Crick arrangement (B–DNA, known since 1953), such as hairpin structures, i–motifs, G – quadruplexes, left–handed Z–DNA and other structures, playing an important role in DNA functions and pathology [1, 2]. It is known that i–motifs and hairpin structures are linked with expansion events of triplet repeat expansions, associated with many neurodegenerative diseases (X syndrome, Huntington's disease, Friedreich's ataxia or myoclonic epilepsy) [3-5]. From this point of view, the knowledge of DNA fragment structure and its function *in vivo* is very important. For the investigation of conformational properties of DNA molecules, the circular dichroic spectroscopy combined with native polyacrylamide gel electrophoresis (PAGE) is a very suitable tool [2]. Nowadays, great attention has also been paid to the electrochemical study of DNA fragments and it was found that electrochemical methods can also help in studying the primary and secondary structure of DNA fragments [5]. The aim of our contribution is the electrochemical study of DNA fragments with different sequences in the molecule center (AAA, CCC, GAA, GGG and TTT). The different structural arrangement of DNA heptamers studied, revealed by circular dichroic spectroscopy and

absorption spectroscopy and verified by PAGE, was investigated by cyclic voltammetry in the dependence of the time of adsorption on the negatively charged electrode surface, and the ability of the different structural arrangement reflection was monitored.

## 2. MATERIAL AND METHODS

All electrochemical experiments were performed using the electrochemical analyzer μAUTOLAB TYPE III (Metrohm, Switzerland), connected with VA Stand 663 and controlled by GPES Manager software. The samples of DNA heptamers (Integrated DNA Technologies, Inc., USA) were dosed into the electrochemical cell, consisting of three electrodes: a hanging mercury drop electrode (HMDE) with an effective area of 0.3 $mm^2$ or a pencil graphite electrode (PeGE) with an effective area of 15.9 $mm^2$ as the working electrodes, and Ag/AgCl/3M KCl and Pt wire as the reference and auxiliary electrodes, respectively. The experimental conditions for the reduction on the mercury electrode were as follows: $c_{DNA\ heptamers} = 2 \cdot 10^{-6}$ $mol \cdot L^{-1}$, potential range: from 0 to -1.7 V, scan rate: 200, 400 and 800 mV/s, accumulation time $t_a$ = 0 – 300 s, t = 25 °C, phosphate–acetate buffer (pH 5.8). For oxidation on PeGE the following parameters were set: $c_{DNA\ heptamers} = 1 \cdot 10^{-5}$ $mol \cdot L^{-1}$, potential range: from -0.15 to 1.6 V, scan rate: 200, 400 and 800 mV/s, accumulation time $t_a$ = 0 – 300 s, t = 25 °C, phosphate–acetate buffer (pH 5.8).

The voltammetric curves obtained were smoothed by using the Savitzky–Golay filter, level 2, and the elimination voltammetric procedure EVP E4 was used and the elimination function E4 according to the equation $f(I) = 17.485I - 11.657I_{1/2} - 5.8584I_2$ was calculated.

## 3. RESULTS AND DISCUSSION

At the beginning of our research we supposed that all DNA heptamers studied adopted the hairpin structure. However, later it was found, based on PAGE results, that only DNA heptamers with GAA and AAA sequence in the molecule center adopt the hairpin structure. In the case of DNA heptamers with CCC and TTT sequence in the molecule center the duplex structure was observed; in the case of DNA heptamer with GGG sequence in the molecule center, we observed supramolecular G–quadruplex structure formation. And there was a very important question for us: Is electrochemistry able to reflect these DNA heptamer structures on the negatively charged electrode surface? Based on the electrochemical results, it was found that the negatively charged surface of the mercury electrode is able to reflect the structural changes of DNA heptamers studied. As follows from Figure 1A presenting the dependence of peak current $I_p$ on the time of adsorption, the DNA heptamers with GAA and AAA sequence in the molecule center (hairpin structures) provided the characteristic isothermal dependence, but in the case of DNA heptamers with CCC (duplex) and GGG

(tetramolecular G–quadruplex) sequence in the molecule center, a different behavior was observed.

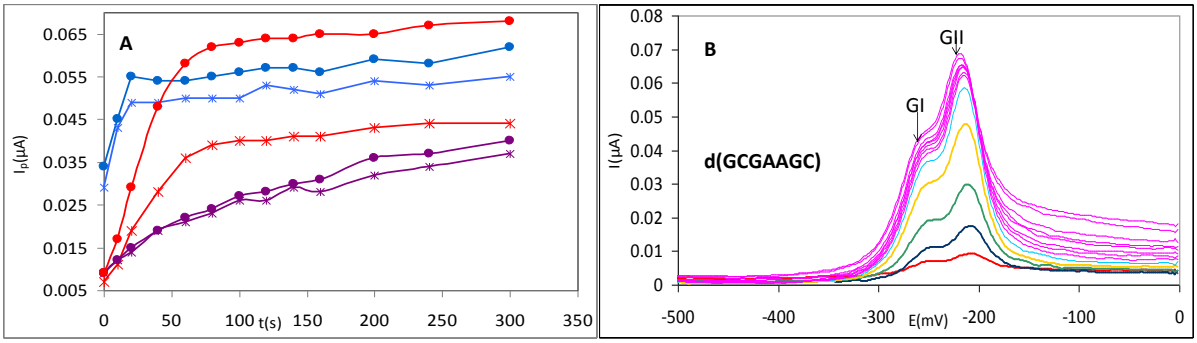


**Figure 1:** (A)The dependence of peak height $I_{pI}$ (asterisks) and $I_{pII}$ (balls) of GI and GII oxidation signals on the time of adsorption for DNA heptamers with GAA (red), CCC (blue) and GGG (violet) sequence in the molecule center. The GI and GII oxidation signals are presented on the Figure 1B.

Compared to the mercury electrode, no effect of the adsorption time was observed on the PeGE electrode.

## 4. CONCLUSION

It was found that the negative surface of the mercury electrode is able to reflect structural differences of DNA heptamers as the effect of adsorption time, but in the case of PeGE we were unable to detect any structural changes.

## 5. ACKNOWLEDGMENTS

The work has been supported by projects: (a) MUNI/A/0972/2013 and (b) KONTAKT II (LH 13050) of the Ministry of Education, Youth and Sports of the Czech Republic, (c) CEITEC – Central European Institute of Technology Project CZ.1.05/1.1.00/02.0068, and (d) P205/12/0466 of the GACR.

## 6. REFERENCES

[1] M. Vorlickova, I. Kejnovska, K. Bednarova, D. Renciuk, J. Kypr: Chirality, 24 (2012), 691-698.
[2] J. Kypr, I. Kejnovská, D. Renčiuk, M. Vorlíčková: Nucleic Acids Research, 37 (2009) 1713-1725.
[3] P. Padrta, R. Stefl, L. Kralik, L. Zidek, V. Sklenar: Journal of Biomolecular NMR, 24 (2002) 1-14.
[4] C.T. Ashley, S.T. Warren: Annual Review of Genetics, 29 (1995) 703-728.
[5] L. Trnkova, I. Postbieglova, M. Holik: Bioelectrochemistry, 63 (2004) 25-30.

# AROMATASE (CYTOCHROME P450 19) IS AN EFFICIENT ENZYME ACTIVATING ANTICANCER DRUG ELLIPTICINE

Jitka POLJAKOVA[1], Lucie BOREK-DOHALSKA[1], Rene KIZEK[2], Eva FREI[3], Marie STIBOROVA[1*]

[1] *Department of Biochemistry, Faculty of Science, Charles University, Albertov 2030, 128 40 Prague 2, Czech Republic*

[2] *Department of Chemistry and Biochemistry, Faculty of Agronomy, Mendel University in Brno, Zemedelska 1, 613 00 Brno, Czech Republic*

[3] *Division of Preventive Oncology, National Center for Tumor Diseases, German Cancer Research Center (DKFZ), In Neuenheimer Feld 280, 69 120 Heidelberg, Germany*

**stiborov@natur.cuni.cz*

**Abstract**

Aromatase (CYP19) activates ellipticine to form covalent DNA adducts identical to those formed in breast adenocarcinoma MCF-7 cells. The formation of CYP19-mediated-ellipticine-DNA adducts is modulated by cytochrome $b_5$.

## 1. INTRODUCTION

Ellipticine is an efficient anticancer compound that functions through multiple mechanisms (for a summary see [1-6]). The predominant mechanisms of ellipticine's biological effects is its efficacy to cause DNA damage. Among them, the formation of covalent DNA adducts after its enzymatic activation with cytochromes P450 (CYPs) and peroxidases seems to be most important [1-4,6]. Ellipticine oxidation to 12-hydroxy- and 13-hydroxyellipticine dissociating to ellipticine-12-ylium and ellipticine-13-ylium lead to formation of two major covalent DNA adducts determined by the $^{32}$P-postlabeling method (see Fig. 1) [3,4,6]. The same adducts are also formed, in rats and mice, in several cancer cell lines and in DNA of mammary adenocarcinoma of rats treated with this drug [3,4,6] (Fig. 1).

Aromatase (CYP19) is the CYP enzyme catalyzing the conversion of the androgenic substrates androstenedione, testosterone and 16-hydroxytestosterone with high specificity, and converts them to their respective oestrogens: oestrone, oestradiol and oestriol [7]. As in adipose tissue, stromal cells of disease-free breast express low levels of aromatase. However, malignant breast cancers produce large amounts of oestrogens due to high levels of aromatase [8]. Aromatase has been clearly localised to both the malignant epithelial cells and surrounding fibroblasts in breast tumour tissues. Independently of the source, oestrogen production in malignant epithelial cells contributes significantly to tumour growth in the

breast. The clinical relevance of these findings is exemplified by the successful use of aromatase inhibitors to treat breast cancer [9]. CYP19 is also highly expressed in human breast adenocarcinoma MCF-7 cells, which we found to be sensitive to ellipticine [3,4,6,10]. Here, we investigated the efficiency of human CYP19 to activate this drug to species forming covalent DNA adducts that are responsible for its cytotoxicity to MCF-7 cells.

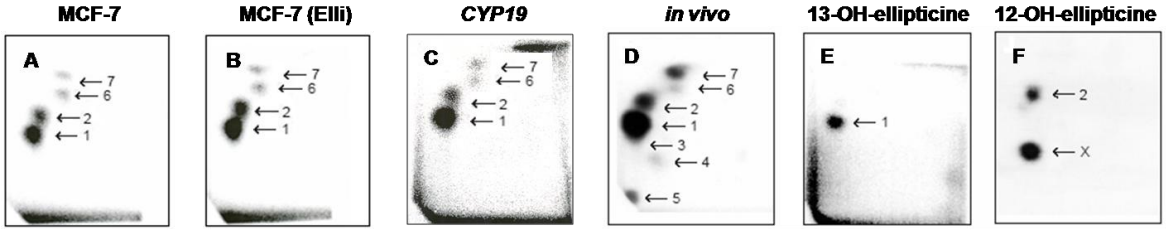


**Figure 1.:** Autoradiographic profiles of ellipticine-derived DNA adducts analyzed with the $^{32}$P-postlabeling assay. Adduct profiles obtained from DNA of from MCF-7 cells (A), from MCF-7 (Elli) cells, the cells pre-treated with 0.1 μM ellipticine for 72 h (B), exposed to 5 μM ellipticine for 24 h, from DNA incubated *in vitro* with CYP19 (C), from liver of rats treated with 40 mg ellipticine/kg body weight (D), from calf thymus DNA reacted with 13-hydroxyellipticine (E) and 12-hydroxyelipticine (F). Analyses were performed by the nuclease P1 version of the $^{32}$P-postlabeling assay. Adduct spots 1-7 correspond to the ellipticine-derived DNA adducts. Besides adduct 2 formed by 12-hydroxyellipticine, another strong adduct (spot X in panel F), which was not found in any other activation systems or *in vivo* was generated.

## 2. MATERIAL AND METHODS

MCF-7 cells were cultivated as described previously [10]. DNA was incubated with ellipticine, CYP19, NADPH and with or without cytochrome $b_5$ as shown in [4,6]. The formation of ellipticine-derived DNA adduct was measured with $^{32}$P-postlabeling [1-4,6].

## 3. RESULTS AND DISCUSSION

Two major ellipticine-DNA adducts (spots 1 and 2 in Fig. 1), generated by 13-hydroxy- and 12-hydroxyellipticine, are formed in breast adenocarcinoma MCF-7 cells exposed to ellipticine. Moreover, two additional minor adducts (adducts spots 6 and 7 in Fig. 1), the structure of them is not known, are formed in MCF-7 cells. In these cells, their pre-treatment with 0.1 μM ellipticine for 72 h resulted in an increase in formation of ellipticine-derived DNA adducts exposed thereafter to 2.5 and 5 μM ellipticine for 24 h. In addition, the $IC_{50}$ values for ellipticine in MCF-7 cells indicate that their pre-treatment with 0.1 μM ellipticine led to an increase in toxicity of ellipticine to these cells. The $IC_{50}$ value of ellipticine for the control (untreated) and the pre-treated cells are 1.25 and 0.7 μM, respectively (Table 1).

CYP19 activates ellipticine to form two major ellipticine-DNA adducts, identical to those derived from 13-hydroxy- or 12-hydroxyellipticine to levels similar to those formed by CYP1A1 and 3A4 (Fig. 2) [1-4,6].

**Table 1.** DNA adduct formation by ellipticine and cytotoxicity of this agent in human MCF-7 cells

| Cells | Levels of DNA adducts (RAL x $10^{-7}$)[a] | | | | | $IC_{50}$ (μM) |
|---|---|---|---|---|---|---|
| | Adduct 1 | Adduct 2 | Adduct 6 | Adduct 7 | Total | |
| **MCF-7** | | | | | | |
| + 2.5 μM ellipticine | 2.12 ± 0.21 | 1.38 ± 0.14 | 0.38 ± 0.04 | 0.23 ± 0.02 | 4.11 ± 0.41 | **1.25 ± 0.13** |
| + 5 μM ellipticine | 3.45 ± 0.35 | 1.59 ± 0.16 | 0.56 ± 0.06. | 0.45 ± 0.05 | 6.05 ± 0.61 | |
| **MCF -7 (Elli)** | | | | | | |
| + 2.5 μM ellipticine | 2.95 ± 0.30 | 1.43 ± 0.14 | 0.43 ± 0.04 | 0.23 ± 0.02 | 5.04 ± 0.50** | **0.70 ± 0.07*** ** |
| + 5 μM ellipticine | 6.37 ± 0.64 | 2.55 ± 0.26 | 0.76 ± 0.08 | 0.64 ± 0.06 | 10.30 ± 1.10*** | |

MCF-7 cells and MCF-7 (Elli), the cells pre-treated with 0.1 μM ellipticine for 72 h, were exposed to 2.5 or 5 μM ellipticine for 24 h. DNA adducts were analyzed by $^{32}$P-postlabeling. [a]RAL, relative adduct labeling; averages and S.D. of three experiments. $IC_{50}$ values were calculated from the linear regression of the dose-log response curves. Values are mean ± S.D. of 3 experiments. Comparison was performed by *t*-test analysis; $^{**}P < 0.01$, $^{***}P < 0.001$, different from cells that were not pre-treated with ellipticine.

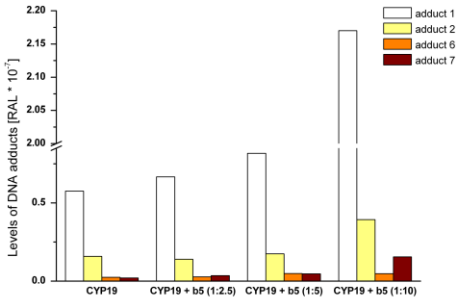


**Figure 2.:** Ellipticine-DNA adducts formed by CYP19-mediated ellipticine activation in the absence and presence of cytochrome $b_5$.

The formation of these adducts is dependent on concentrations of ellipticine and CYP19. Cytochrome $b_5$ modulates CYP19-mediated activation of ellipticine, increasing its activation to reactive species forming DNA adducts.

## 4. CONCLUSION

The $^{32}$P-postlabeling method is a suitable tool to determine the CYP19-mediated ellipticine-DNA adducts formed in breast adenocarcinoma MCF-7 cells.

## 5. ACKNOWLEDGEMENT

The work has been supported by GACR (P301/10/0356) and Charles University in Prague (UNCE 204025/2012).

## 3. REFERENCES

[1]Stiborová M., Bieler C.A., Wiessler M., et al.: Biochemical Pharmacology, 62 (2001), 1675-1684.
[2]Stiborová M., Rupertová M., Schmeiser H.H., et al.: Biomedical Papers, 150 (2006), 13-23.
[3]Stiborová M., Rupertová M., Frei E.: Biochimica et Biophysica Acta, 1814 (2011), 175-185.
[4]Kizek R., Adam V., Hrabeta J., et al.: Pharmacology & Therapeutics, 133 (2012), 26-39.
[5]Garbett N.C., Graves D.E.: Current Medicinal Chemistry. Anti-Cancer Agents, 4 (2004), 149-172.
[6]Stiborová M., Frei E.: Current Medicinal Chemistry, 21 (2014), 575-591.
[7]Stocco C.: Steroids, 77 (2012) 27-35.
[8]Bulun S.E., Lin Z., G. Imir G., et al. Pharmacological Reviews, 57 (2005), 359–383.
[9]Lonning P.E.: Annul Oncology, 22 (2011), 503-514.
[10]Borek-Dohalska L., Frei E., Stiborová M.: Collection of Czechoslovak Chemical Communication, 69 (2004) 603-615.

# DFT AND NMR STUDIES OF PPD ANTIOXIDANTS

Ingrid PUŠKÁROVÁ[1*], Michal ŠTUJBER[1], Martin BREZA[1]

[1] *Faculty of Chemical and Food Technology, Slovak Technical University in Bratislava, Radlinskeho 9, SK-81237 Bratislava, Slovak Republic*

**ingrid.puskarova@stuba.sk*

**Abstract**

NMR shifts of a series of *N*-phenyl-*N*'-alkyl-p-phenylenediamines in DMSO have been measured as well as evaluated by quantum-chemical calculations. Very good correlation of NMR shifts of hydrogen atoms bonded to amine nitrogens with the antioxidant activity of the studied compounds can be concluded.

## 1. INTRODUCTION

Aromatic secondary amines, particularly *N*-phenyl-*N*'-alkyl-p-phenylenediamines (PPD) represent the most important group of antioxidants used in rubber industry. The antioxidant effectiveness of a series of *p*-phenylenediamines in polyisoprene rubber has been studied by non-isothermal DSC measurements [1,2] and their molar antioxidant effectiveness (AEM) has been determined (Table 1).

**Table 1**. Studied antioxidants notation and their Molar Antioxidant Effectiveness (AEM) [1,2].

| Acronym | Compound name | AEM/kg.mol$^{-1}$ |
|---|---|---|
| DPPD | N,N'-diphenyl-p-phenylenediamine | 738 |
| SPPD | N-phenyl-N´-(1'-methylbenzyl)-p-phenylenediamine | 351 |
| 6PPD | N-phenyl-N'-(1,3-dimethyl-butyl)-p-phenylenediamine | 277 |
| IPPD | N-phenyl-N´-isopropyl-p-phenylenediamine | 177 |
| CPPD | N-(1-methyl-1-phenylethyl)-N'-phenyl-p-phenylenediamine | 0 |

It is supposed that the antioxidant effectiveness depends on the bond strength of hydrogens to amine nitrogens between aromatic rings (N1) and at the side aliphatic chain (N2) as well as at its neighboring tertiary carbon. The aim of our study is to correlate the AEM values of the above PPD antioxidants with NMR data obtained experimentally as well as by Density Functional Theory (DFT) calculations.

## 2. MATERIAL AND METHODS

### NMR analysis

All NMR spectra were measured on an Agilent 600 MHz VNMRS spectrometer equipped with an inverse "triple resonance" probe. Physically available samples of DPPD, SPPD, 6PPD and IPPD were readily soluble in $d_6$-DMSO. Series of standard homonuclear and heteronuclear 2D NMR spectra were measured (including COSY, HSQC, HMBC and $^{15}$N-HSQC) from each of the mentioned samples in order to obtain the complete assignment of signals. The chemical shift scale was calculated using tetramethylsilane (TMS) as an internal standard and correctly referenced using the $^{2}$H signal of the deuterated solvent.

### Calculations

Standard B3LYP/6-311G* geometry optimizations of DPPD, SPPD, CPPD, 6PPD and IPPD neutral molecules in DMSO solutions in the singlet spin states have been performed using Gaussian03 program package [6]. Solvent effects have been accounted within Integral Equation Formalism Polarizable Continuum Model (IEFPCM) [7]. The stability of the resulting structures has been confirmed by vibrational analysis (no imaginary vibrations). Absolute shieldings of individual atoms have been calculated by the Gauge-Independent Atomic Orbital (GIAO) method [6] at B3LYP/6-311++G** level of theory. NMR shifts relative to TMS were evaluated according to [4,5].

## 3. RESULTS AND DISCUSSION

The measured and calculated NMR shifts δ of hydrogen atoms bonded to N1 and N2 atoms are presented in Table 2. Our results indicate that they very well correlate with the PPD antioxidant activity evaluated as AEM values. The parameters of linear equation

$$AEM = A + B\,\delta(X) \qquad (1)$$

where δ(X) are chemical shifts of hydrogens bonded to N1 or N2 atoms are presented in Table 2. As DPPD does not contain the N2 atom, $H_{N1}$ NMR shifts have been assigned to the $H_{N2}$ ones as well. As expected, the influence of the side aliphatic chain variations on NMR shifts of $H_{N2}$ atoms is significantly higher than on the $H_{N1}$ ones due to shielding by the aromatic ring. The correlation of the antioxidant activity with NMR shifts of other atoms in the compounds under study is significantly worse.

**Table 2**. Experimental and calculated NMR shifts δ(X) (in ppm) of atoms X in the systems under study (see Tab. 1) and the parameters of AEM=f(δ(X)) linear function (1).

| | Experimental | | Calculated | |
|---|---|---|---|---|
| | $\delta(^1H_{N2})$ | $\delta(^1H_{N1})$ | $\delta(^1H_{N2})$ | $\delta(^1H_{N1})$ |
| DPPD | 7,880 | 7,880 | 6,309 | 6,309 |
| SPPD | 5,891 | 7,437 | 4,888 | 5,938 |
| 6PPD | 4,939 | 7,458 | 4,472 | 5,939 |
| IPPD | 5,020 | 7,446 | 3,643 | 5,998 |
| A /kg.mol$^{-1}$ | -660 ± 160 | -7800 ± 1900 | -670 ± 150 | -7100 ± 2600 |
| B/kg.mol$^{-1}$ | 176 ± 26 | 1080 ± 250 | 220 ± 30 | 1250 ± 420 |
| Correlation coefficient | 0,937 | 0,860 | 0.945 | 0,721 |

## 4. CONCLUSION

We have shown that NMR shifts of hydrogen atoms bonded to amine nitrogens in PPD antioxidants might be used for predicting their antioxidant activity. NMR shifts can be fairly well evaluated by DFT calculations and so our results can be used the target synthesis of new, more effective antioxidants. Further theoretical and experimental studies in this field are desirable.

## 5. ACKNOWLEDGEMENT

The work has been supported by Slovak grant agency VEGA (Project No. 1/0327/12).

## 6. REFERENCES

[1]Cibulková Z, Šimon P, Lehocký P, Balko J, Polymer. Degradation and Stability, 87, (2005), 479

[2]Cibulková Z, Šimon P, Lehocký P, Balko J, Journal of Thermal Analysis and Calorimetry, 80, (2005), 357

[3]Frisch M.J., et al.: Gaussian 03, Revision C.02; Gaussian, Inc., Wallingford CT, (2004)

[4]Blanco F, Alkorta I, Elguero J, Magnetic Resonance in Chemistry, 45, (2007), 797

[5]Silva A.M.S, Sousa R.M.S, Jimeno M.L, Blanco F, Alkorta I, Elguero J, Magnetic Resonance in Chemistry, 46, (2008), 859

[6]Wolinski K, Hilton J.F, Pulay P, Journal of the. American. Chemical. Society. 112, (1990), 8251

[7]Tomasi J, Mennucci B, Cancès E, Journal of. Molecular. Structure. (Theochem) 464, (1999), 211

# COMPUTATIONAL INSIGHT TO THE THEMODYNAMICS OF DOUBLE H ATOM ABSTRACTION IN MODEL PHENOLICS

Ján RIMARČÍK*, Erika SENAJOVÁ, Erik KLEIN

*Institute of Physical Chemistry and Chemical Physics, Faculty of Chemical and Food Technology, Slovak University of Technology in Bratislava, Radlinského 9, SK-812 37 Bratislava, Slovak Republic*

**jan.rimarcik@stuba.sk*

**Abstract**

Theoretical DFT calculations of model aromatics possessing two OH groups reveal their thermodynamic behavior by double H atom abstractions in gas-phase, benzene and water.

## 1. INTRODUCTION

Phenolic compounds represent important group of natural/synthetic free radical scavengers [1,2]. They can act via three different mechanism; (*i*) H atom transfer, governed by O–H Bond Dissociation Enthalpy (BDE), (*ii*) electron transfer followed by proton transfer – described by Ionization Potential (IP) and Proton Dissociation Enthalpy (PDE), (*iii*) sequential proton loss – electron transfer characterized by Proton Affinity (PA) and Electron Transfer Enthalpy (ETE) [3,4]. Their antioxidant potential is determined by the molecular structure; compounds with two OH groups should be more potent scavengers than phenol. Therefore, we decided to calculate reaction enthalpies for homolytic and heterolytic hydrogen atom abstractions from the two OH groups in simple models of polyphenols (Fig. 1).

## 2. COMPUTATIONAL DETAILS

All calculations were performed in Gaussian 09 program package [5] using B3LYP/6-311++G** approach. For all studied particles, solvent contribution to their enthalpies was estimated with integral equation formalism polarizable continuum model (IEF-PCM). Further details and solvation enthalpies of proton and electron can be found in [6,7].

## 3. RESULTS AND DISCUSSION

Reaction enthalpies of first OH group splitting-off (BDE1, IP1, PDE1, PA1, ETE1) for the studied phenolics (Fig. 1*a*) are relatively well explored theoretically, as well as

experimentally (BDEs) [1,3,4]. Therefore, chosen computational DFT approach should be considered appropriate.

Consecutive second OH group splitting-off provides the second set of reaction enthalpies (BDE2, IP2, PDE2, PA2, ETE2). Except proton affinities, PA2 values, reaction enthalpies of second H (homolytic or two-step heterolytic) abstraction are higher than those for the first OH group.

a)

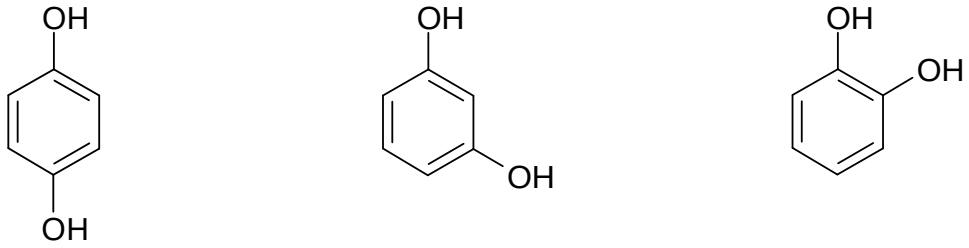


(**I**) (**II**) (**III**)

b)

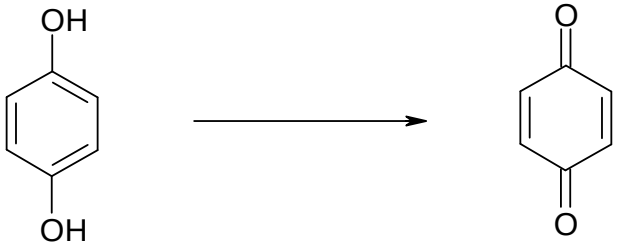


**Figure 1.:** *a*) Structures of studied molecules: hydroquinone (I), resorcinol (II) and catechol (III); *b*) scheme of studied process from parent molecule (hydroquinone) to corresponding quinone structure (*para*-quinone).

In the case of hydroquinone (I in Fig. 1*a*), BDE2s are higher by 37 % in gas-phase to 46 % in water. The largest enthalpy rises are found for ETE2s, up to 119 % in gas-phase.

Proton loss from phenoxyl radical is energetically more favorable than from the parent molecule. PA2 values reached 93 % (gas-phase), 79 % (benzene) and 66 % (water) of PA1s. Two OH groups in each studied molecule allow scavenging of two free radicals. The reaction enthalpies of two H atom abstractions should be interpreted from the macroscopic point of view as the average of the two steps. Table 1 present these average values for the BDE, IP and PA values.

Generated biradical structure after double H atom abstractions, is stabilized through the formation of its quinone structure (hydroquinone and catechol). This rearrangement is

exothermic, for hydrochinone this enthalpy is ca –200 kJ $mol^{-1}$ in all environments. If this value is added to the BDE2, the drop in average BDE will be evident (Tab. 1)

**Table 1**: Average values of reaction enthalpies for the three studied mechanism of double H atom abstraction in hydroquinone in kJ $mol^{-1}$. Data in parenthesis incorporate *para*-quinone formalism.

| | Gas-phase | Benzene | Water |
|---|---|---|---|
| $BDE_{AVE}$ | 386 (172) | 394 (180) | 386 (175) |
| $IP_{AVE}$ | 809 | 694 | 516 |
| $PA_{AVE}$ | 1403 | 397 | 179 |

## 4. CONCLUSION

Reaction enthalpies for three possible mechanisms in gas-phase, benzene and water were calculated for simple phenolics bearing two hydroxyl groups. Novel data for H atom abstraction from phenoxyl radical are presented. Solvent has strong influence on individual enthalpies, especially in the case of charged species. If the molecule is able to form quinone structure after double H atom abstraction, further stabilization and decrease in respective reaction enthalpy occurs.

## 5. ACKNOWLEDGEMENT

This work has been supported by the Slovak Grant Agency (VEGA 1/0735/13 and 1/0307/14).

## 6. REFERENCES

[1]Vagánek A, Rimarčík J, Lukeš V, Klein E: Comput. Theor. Chem., 991 (2012), 192-200

[2]Lengyel J, Rimarčík J, Vagánek A, Klein E: Phys. Chem. Chem. Phys., 15 (2013), 26, 10895-10903

[3]Klein E, Rimarčík J, Lukeš, V: Acta Chimica Slovaca, 2, (2009), 2, 37-51

[4]Amić A, Marković Z, et al.: Food Chem., 152 (2014), 578-585

[5]Frisch MJ, et al.: Gaussian 09, Revision C.01, Gaussian, Inc., Wallingford, CT, 2010

[6]Rimarčík J, Lukeš V, Klein E, Griesser M, Kelterer A-M: Chem. Phys., 353 (2008), 1-3, 177-184

[7]Rottmanová L, Škorňa P, Rimarčík J, Lukeš V, Klein E: Acta Chimica Slovaca, 6 (2013), 1, 60-63

# ON RADICAL ANION GENERATION UPON HYDROGEN ATOM TRANSFER IN DIHYDROXYBENZENES

Ján RIMARČÍK*, Erika SENAJOVÁ, Erik KLEIN

*Institute of Physical Chemistry and Chemical Physics, Faculty of Chemical and Food Technology, Slovak University of Technology in Bratislava, Radlinského 9, SK-812 37 Bratislava, Slovak Republic*

**jan.rimarcik@stuba.sk*

**Abstract**

Dihydroxybenzenes represent model phenolics for the study of H atom transfer from their phenoxide anions. This process was quantified by theoretical DFT approach in terms of reaction enthalpies in gas-phase, benzene and water.

## 1. INTRODUCTION

Phenolic antioxidants, both natural and synthetic, play important role in our live, mainly as health protective agents or industrially used substances preventing oxidation of various materials [1-3]. Dihydroxybenzenes, such a hydroquinone, resorcinol and catechol (Fig. 1), can be considered as models of phenolics or they can also represent functional moieties of naturally occurring antioxidants. They react by dissociation of phenolic O–H group, which can take place *via* different pathways – homolytic or heterolytic. After homolytic H atom transfer, phenoxyl radical is formed and its reaction enthalpy is known as O–H Bond Dissociation Enthalpy (BDE).

Hydroxy group can also be broken in heterolytic way – releasing proton and generating phenoxide anion. Corresponding reaction enthalpy is Proton Affinity, PA. Consecutive electron transfer from this anion leads again to the phenoxyl radical. This process is governed by Electron Transfer Enthalpy, ETE. Phenols are considered to be weak acids, therefore phenoxide anions can be expected in the reaction system, too. Concentration of anions is strongly dependent on the environment.

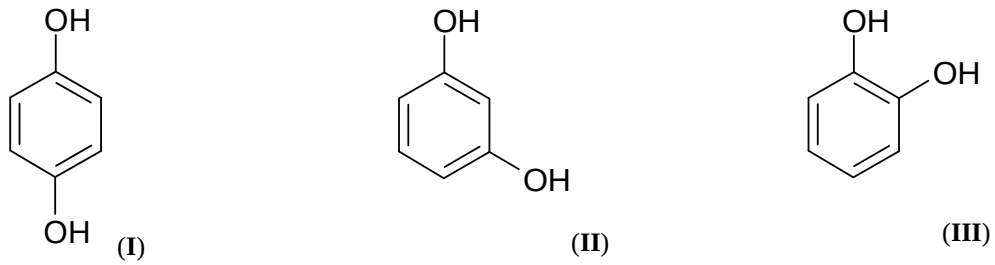


**Figure 1.:** Structures of studied molecules: hydroquinone (I), resorcinol (II) and catechol (III).

Indeed, if formed phenoxide anion contains another OH group (dihydroxybenzenes), its homolytic dissociation is possible. To distinguish this reaction enthalpy from BDE, we denoted it as $BDE_m$. This pathway may be important in free radical scavenging. Because experimental works indicate that phenoxide anions can abstract H atoms more easily than neutral parent molecules [4-6], the goal of this work is to calculate $BDE_m$ values for dihydroxybenzenes in the gas-phase, benzene and water.

## 2. COMPUTATIONAL DETAILS

All calculations were performed in Gaussian 09 program package [5] using B3LYP/6-311++G** approach. For all studied particles, solvent contribution to their enthalpies was estimated with integral equation formalism polarizable continuum model (IEF-PCM). Further details and solvation enthalpies of proton and electron can be found in [6,7].

## 3. RESULTS AND DISCUSSION

Studied reaction enthalpies, $BDE_m$, PA, ETE and BDE, are listed in Table 1. Corresponding reaction scheme can be found in Fig. 2. Data in Table 1 show that $BDE_m$ values are lower than BDEs for all three studied systems regardless on the environment (gas-phase, benzene, water).

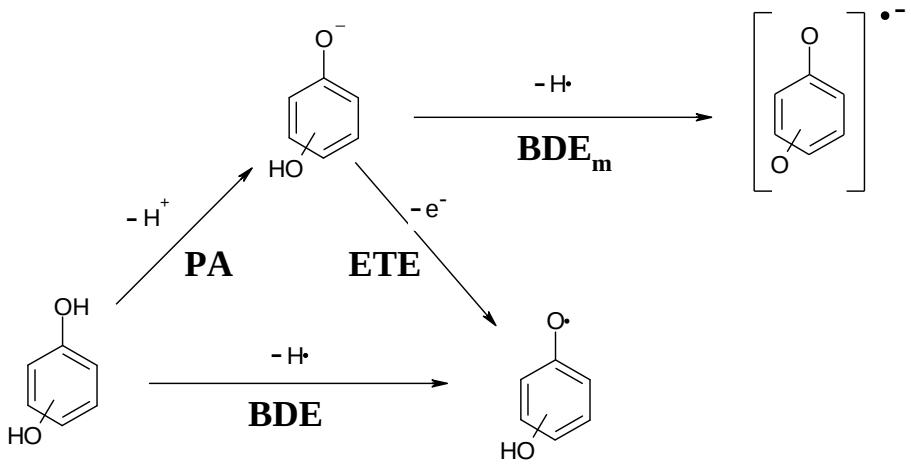


**Figure 2.:** Scheme of possible dissociations of two O–H groups in dihydroxybenzenes.

Here, we should note that the formation of anion is energetically demanding especially in the hypothetical gas-phase (PAs are higher than a thousand of kJ $mol^{-1}$). On the other hand, in polar solvent (water) releasing of proton is more favorable than H atom transfer from the neutral molecule, i.e. all PA(water) values are lower than corresponding BDEs. The presence of anionic forms in the system is thus plausible.

**Table 1**: Reaction enthalpies for dihydroxybenzenes in kJ $mol^{-1}$.

| | | hydroquinone | resorcinol | catechol |
|---|---|---|---|---|
| $BDE_m$ | gas-phase | 219 | 299 | 301 |
| | benzene | 234 | 309 | 302 |
| | water | 241 | 304 | 284 |
| PA | gas-phase | 1456 | 1442 | 1410 |
| | benzene | 444 | 429 | 403 |
| | water | 216 | 204 | 185 |
| BDE | gas-phase | 326 | 345 | 310 |
| | benzene | 329 | 350 | 317 |
| | water | 315 | 338 | 309 |
| ETE | gas-phase | 191 | 226 | 221 |
| | benzene | 299 | 335 | 328 |
| | water | 298 | 333 | 323 |

The inspection of Table 1 also reveals that in the gas-phase phenoxide anions prefer to release electron to create the phenoxyl radical than to abstract the hydrogen atom from the second OH group to form the radical anion. However, in the solution phase, even in non-polar benzene, it is *vice versa*, all $BDE_m$(solv) values are lower in comparison to respective ETEs.

## 4. CONCLUSION

Theoretical calculations suggest that from the thermodynamic point of view dihydroxybenzenes release H atom more easily from their anionic form than from the neutral molecule regardless on the studied environment.

## 5. ACKNOWLEDGEMENT

This work has been supported by the Slovak Grant Agency (VEGA 1/0735/13 and 1/0307/14).

## 6. REFERENCES

[1]Vagánek A, Rimarčík J, Lukeš V, Klein E: Comput. Theor. Chem., 991 (2012), 192-200

[2]Lengyel J, Rimarčík J, Vagánek A, Klein E: Phys. Chem. Chem. Phys., 15 (2013), 26, 10895-10903

[3]Amić A, Marković Z, et al.: Food Chem., 152 (2014), 578-585

[4]Musialik M, Kuzmicz R, Pawlowski TS, Litwinienko G: J. Org. Chem. 74 (2009), 2699-2709

[5]Jovanovic SV, Steenken S, Tosic M, Marjanovic M, Simic MG: J. Am. Chem. Soc. 116 (1994), 4846-4851

[6]Lemanska K, Szymusiak H, Tyrakowska B, Zielinski R, et al.: Free Radic. Biol. Med. 31 (2001), 869-881

[7]Frisch MJ, et al.: Gaussian 09, Revision C.01, Gaussian, Inc., Wallingford, CT, 2010

[8]Rimarčík J, Lukeš V, Klein E, Griesser M, Kelterer A-M: Chem. Phys., 353 (2008), 1-3, 177-184

# METHYLATION OF HUMIC ACIDS – THE IMPACT ON THE REACTIVITY STUDIED BY DIFFUSION TECHNIQUES

Jiří SMILEK[1*], Petr SEDLÁČEK[1], Martina KLUČÁKOVÁ[1], Michal KALINA[1], Vojtěch ENEV[1]

[1]*Brno University of Technology, Faculty of Chemistry, Materials Research Centre, Purkyňova 464/118, 612 00 Brno, Czech Republic*

**xcsmilek@fch.vutbr.cz*

**Abstract**

The diffusion cell technique processes of chosen ionic compounds (basic organic dyes – Rhodamine 6G) was studied in supported hydrogel matrix for the study on reactivity of humic acids (standard samples of humic acids – International Humic Substances Society – Leonardite). The reactivity of humic acids was studied by interactions with basic organic dyes by the simple diffusion techniques realized in the diffusion cell. The rate of interactions of humic acids with chosen organic dye was compared by fundamental diffusion parameters such as the lag time (time needed for penetration of organic dye through hydrogel sample), the sorption capacity of humic acids and the effective diffusion coefficients. The reactivity of humic acids especially sorption capacity is strongly dependent on the amount of carboxylic groups. The influence of carboxylic groups was modified by methylation. Carboxylic groups became occupied by methyl groups during methylation, so the sorption capacity and the total reactivity of these humic acids should be lower.

## 1. INTRODUCTION

Humic acids (HA), form the key constituent of natural organic matter in numerous natural environments (soil, sediments). HA are one of the most important part of soil organic matter and they are responsible for crucial ecological effects such as self-detoxification of soils, transport of water and nutrients etc. The interesting nature of HA stands behind the positive affinity to pollutants such as heavy metal ions. HA are able to form the stable complexes with heavy metal ions and because of this fact; they are able to immobilize these pollutants. The function of HA in their natural environment is known very well, but the objective reactive-mapping tool at laboratory conditions is still missing.

The reactivity of HA is mostly studied by classical sorption experiments. Valuable parameters such as binding capacity and partition coefficients can be determined by these types of experiments. Klucakova et al. (1) realized the classical sorption experiments on HA isolated

from lignite. But these experiments have a few insufficiencies. The reactivity or binding capacity is studied in powder form, but HA can be found in their natural environment mostly in colloidal or hydrogel form. This paper brings the new view on the study on reactivity of HA. The reactivity is studied by simple diffusion techniques in supported hydrogel matrix. The diffusion cell technique is based on the penetration of basic cationic organic dyes (Rhodamine 6G) through the hydrogel matrix with incorporated HA. The interactions between anionic HA and cationic organic dye are expected. The rate of interactions depends on the nature of HA (content of acidic groups) and modification.

The main aim of this paper is study on reactivity of standard HA samples (IHSS). The impact of methylation (the most important functional groups are occupied by the methylene) is studied as well.

## 2. MATERIAL AND METHODS

### Modification (methylation) of HA

The main objective of presented paper is the study on the impact of methylation on the reacitivty of standard samples of HA. Humic acids were isolated from Leonardite by alkali extraction according IHSS procedure. Standard samples of HA were modified by methylation. Preparation of methylated HAs was following: 1 g of HA was mixed with 4 $cm^3$ of chloroform, 2 $cm^3$ methanol and 4 $cm^3$ of trimethylsilyl diazomethane. The reaction was carried by 2 hours on vortex. Obtained product was dried at 40 °C for 2 hours under nitrogen atmosphere.

### Preparation of IPN hydrogel

The diffusion experiments mentioned in this paper were realized in supported hydrogel matrix based on agarose (purchased from Sigma-Aldrich, routine class use, moisture content < 10 wt. %). The preparation of interpenetrating polymer network (IPN) from HA in a supporting hydrogel-forming polymer based on agarose was prepared via thermoreversible processes. The network of agarose chains is interpenetrated by molecules of HA at higher temperature – both compounds were dissolved at 85 °C and the mixture was then filled up in pre-heated mold. Accurately weighted amount of agarose powder was dissolved in deionized water (preparation of pure agarose hydrogels) or in aqueous solutions of HA of the corresponding concentration (preparation of agarose/HA hydrogels). The mixture was slowly heated and stirred continuously to 85 °C. The solution of agarose with/without HA was poured into the pre-heated PTFE mold and the glass slides (also pre-heated) were placed on the opposite sides

of mold. The mixture of agarose with HA gradually solidified into the cylindrical hydrogel plate sample (40 mm in diameter and 5 mm thick).

**Infrared spectroscopy of HA**

The effect of methylation was studied by infrared spectroscopy with Fourrier transformation (Nicolet iS 50 with ATR). The infrared spectra for powder humic acids and powder modified humic acids were collected in tablet from potassium bromide.

**Preparation of diffusion experiments**

Presented diffusion techniques are based on the assumption that HAs are homogenously distributed in the hydrogel matrix (non-reactive linear polysaccharide agarose hydrogel is used). The hydrogel in PTFE mold was placed between two chambers of diffusion cell. One chamber of diffusion cell was filled by 0.01 $g \cdot dm^{-3}$ Rhodamine 6G and the second chamber was filled by deionized water. Both chambers of diffusion cell were filled by 60 $cm^3$ of solutions simultaneously. Rhodamine 6G was purchased from Sigma-Aldrich (dye content > 95 wt. %) and were used without further purification. The change of concentration of diffusion probe is determined by ultraviolet-visible fiber spectrometer USB 2000+ (Ocean Optics, Inc.) in the receiving part of diffusion cell as the time function. The ultraviolet-visible spectra were collected continuously in given time intervals. After the termination of the diffusion experiments, the absorbance in source part of diffusion cell was measured. The water-jacketed side-by-side diffusion cell purchased from Permegear Inc.

**Determination of the fundamental diffusion parameters**

The reactivity of humic studied by simple laboratory diffusion techniques was compared by fundamental diffusion parameters (steady-state diffusion flux, effective diffusion coefficients and the lag time). The values of steady-state diffusion flux and the lag time were determined from linear region of the break through curve according equation 1.

$$ln\frac{(c_D - c_A)_t}{(c_D - c_A)_0} = -\beta Dt \qquad (1)$$

## 3. RESULTS AND DISCUSSION

**Infrared spectroscopy of HA**

From infrared spectra was obvious the effect of methylation. Carboxylic groups were occupied by methylene groups. The slower rate of interaction for methylated IHSS humic acids was expected; because the positive affinity to cationic compounds (the immobilization of cationic pollutants) according literature is given mainly by carboxylic acidity.

**Diffusion experiments**

Our previous publications (2,3) clearly illustrate the effect of interactions between HAs isolated from lignite according IHSS procedure and Methylene Blue on the transport of this ionic dye in model aqueous environments provided by agarose hydrogel. The data presented in this paper continues with the same experimental approach.

It is obvious that the small increase of concentration of HAs in 1 wt. % agarose hydrogel slows down the rate of diffusion processes. Figure 2 summarized the effective diffusion coefficients for IHSS HA (Leonardite) samples in comparison with methylated IHSS HA for Rhodamine 6G. The diffusion processes of chosen organic dye is faster in agarose hydrogels with modified HA (effective diffusion coefficients have higher values), because of methylation. Carboxylic groups are mainly responsible for sorption of heavy metal ions or simple organic dyes but carboxylic groups in modified samples of HA are occupied by methyl groups and because of this fact the binding capacity is lower in comparison with standard sample of IHSS HA (Leonardite).

Increasing content of HA in the hydrogel samples led to a considerable increase in absorbed amount of chosen dye in the hydrogel and to the decrease in steady-state diffusion flux. The total content of HA (also modified) significantly affected also the value of lag time (see Figure 2) which indicates extensive physic-chemical interactions between diffusing organic dyes and HAs contained in the hydrogel. When the binding capacity is depleted all of binding sites are occupied by molecules of diffusion probe. Lag time is indirectly connected with ability of samples to retain active compounds. The influence of concentration of HAs and the impact of modification is proofed by different rate of interactions of HAs with Rhodamine 6G.

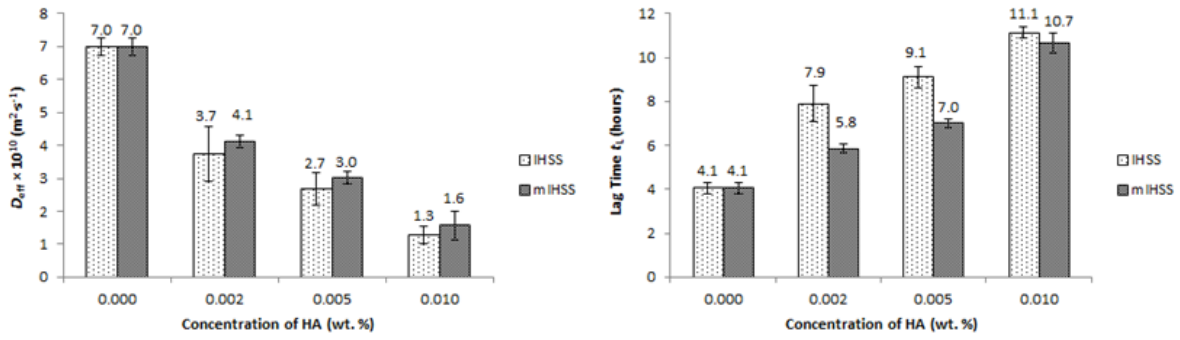


**Figure 1.:** Effective diffusion coefficients for agarose hydrogels with different content of humic acids (left) and the lag time of chosen diffusion probe needed for penetration through the hydrogel for the same samples (right).

## 4. CONCLUSION

Diffusion cell techniques presented in this paper represent an interesting alternative approach for the traditional reactivity mapping studies in the systems containing humic substances and similar reactive compounds. The presented experiments provided comprehensive illustration of the influence of interaction between anionic HA and cationic active compounds (organic dyes) on barrier properties of HAs and represent valuable approach in order to better understanding the behavior of humic substances in their natural environments.

## 5. ACKNOWLEDGEMENT

This work has been supported by Materials Research Centre at FCH BUT- Sustainability and Development, REG LO1211, with financial support from National Program for Sustainability I (Ministry of Education, Youth and Sports).

## 6. REFERENCES

[1]Klučáková M, Pekař M: Colloids and Surfaces A: Physicochemical and Engineering Aspects, 286 (2006), 1-3, 126-133.

[2]Sedláček P, Smilek J, Klučáková M: Reactive and Functional Polymers, 73 (2013), 11, 1500-1509.

[3]Sedláček P, Smilek J, Klučáková M: Reactive and Functional Polymers, 78 (2014), 1-6.

# ELECTROCHEMICAL SENSOR FOR CARBONATE DETERMINATION

Filip SMRČKA[1*], Jakub VANĚK[1,2], Přemysl LUBAL[1,2]

[1] *Department of Chemistry, Faculty of Science, Masaryk University, Kotlářská 2, 611 37 Brno, Czech Republic*

[2] *Central European Institute of Technology, Masaryk University, Kamenice 5, 625 00 Brno, Czech Republic*

**filip.smrcka@gmail.com*

**Abstract**

Specific electrochemical, spectroscopic and magnetic properties of Ln(III) ions make them perfect candidates for use in many chemical, biological and environmental systems. $H_2$DO2A and $H_3$DO3A are hexa- and heptadentate ligands forming very stable complexes with europium(III) ion, where three, resp. two coordination places are occupied by water molecules. These complexes form ternary complexes with small mono- and bidentate ligands (e.g. fluoride, acetate, phosphate, oxalate, carbonate etc.). Different stability of these ternary complex systems can be used as a sensor for selective determination of different anions. Dual electrochemical-luminescent sensor based on [Eu(DO3A)(L)] and [Eu(DO2A)(L)] (L = picolinate, dipicolinate, isoquinoline-3-carboxylate) ternary complexes was developed for simple and rapid determination of carbonate and other relevant anions in potential biological samples and complicated matrixes under aerobic conditions.

## 1. INTRODUCTION

Ln(III) complexes with macrocyclic ligands (mainly DOTA derivatives) are commonly used as radiopharmaceuticals ($^{90}$Y, $^{153}$Sm, $^{166}$Ho, $^{177}$Lu) or MRI contrast agents (Gd) in medicine or as luminescent probes (Eu, Tb in VIS and Yb, Nd in NIR regions). The 1,4,7,10-tetraazacyclododecane-1,7-diacetic acid ($H_2$DO2A) and 1,4,7,10-tetraazacyclododecane-1,4,7-triacetic acid ($H_3$DO3A) are hexa- and heptadentate macrocyclic ligands that yield very stable complexes with europium(III) ion. Both complexes also form ternary lanthanide(III)-containing species with both mono- and bidentate ligands. The binary complexes of the Ln(III)-$H_2$DO2A and Ln(III)-$H_3$DO3A may be employed for determination of anions known to form the ternary complexes [1]. In this contribution, we demonstrate selective anionic sensors suitable for carbonate anion determination based on the [Ln$(H_2O)_2$(DO2A)] and

[Ln($H_2O$)$_2$(DO3A)] complexes. The results shown here suggest a potential utility of this sensor for a construction of sensor arrays.

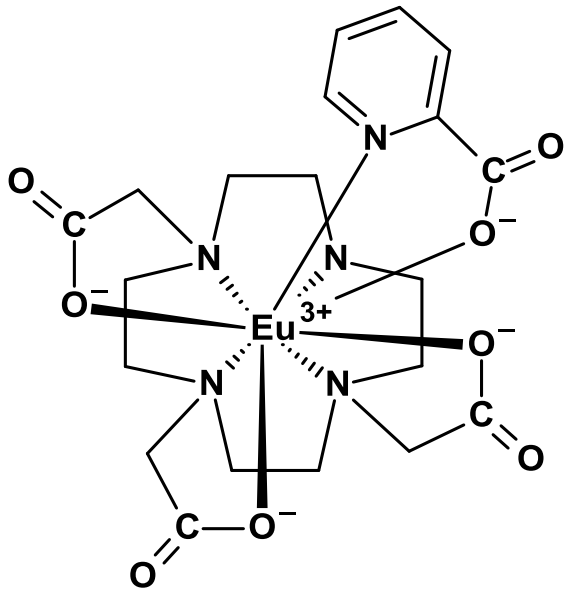


**Figure 1.:** Scheme of [Eu(DO3A)(picolinate)]$^-$ ternary complex.

## 2. MATERIAL AND METHODS

Cyclic voltammetry measurements were performed on Metrohm 910 PSTAT mini (Switzerland) using Screen Printed Electrodes (SPEs). Luminescent data were recorded on luminescence spectrometer Aminco-Bowman Series 2 (Thermo-Spectronic, USA).

## 3. RESULTS AND DISCUSSION

We have focused on study of formation of ternary species with bidentate ligands (picolinate, dipicolinate, isoquinoline-3-carboxylate) having potential analytical application. The thermodynamic study of formation of ternary Eu(III) species was followed by cyclic voltammetry and luminescence spectroscopy. As it can be seen on example of [Eu(DO3A)(picolinate)]$^-$ (Figure 1), the formation of ternary Eu(III) complex is accompanied by increase of fluorescence intensity and also by significant change of electrochemical signal (Figure 2). Adding hydrogencarbonate in solution, the new, more stable, ternary [Eu(DO3A)(Carb)]$^{2-}$ complex is formed.

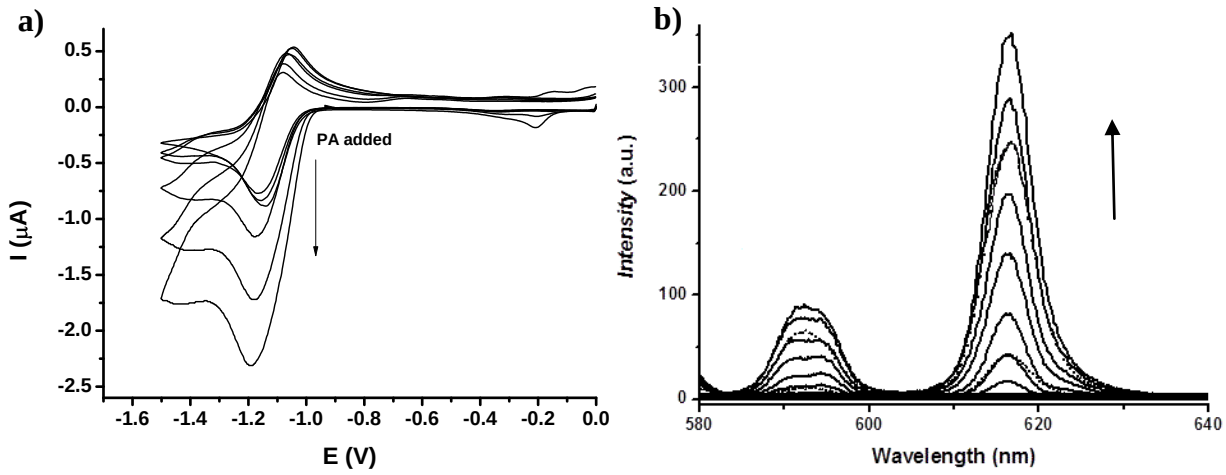


**Figure 2.:** Formation of $[Eu(DO3A)(picolinate)]^-$ ternary complex followed by a) cyclic voltammetry, b) luminescence spectroscopy.

## 4. CONCLUSION

The bound water molecules in the $[Eu(H_2O)_2(DO3A)]$ complex undergoes substitution with various anions to form stable ternary adducts. The stability constants values of the ternary Eu(III)-$H_3$DO3A-ligand complexes with bidentate ligands follow the order $CO_3^{2-}$ > oxalate$^{2-}$ > picolinate$^-$ > phthalate$^{2-}$ ≈ citrate$^{3-}$. The proposed analytical procedure using the ternary complexes $[Eu(DO3A)(L)]^-$ (L = picolinate, dipicolinate, isoquinoline-3-carboxylate) can be used for a fast, selective and sensitive determination of carbonate/bicarbonate in the milimolar concentration range in biological and water samples.

## 5. ACKNOWLEDGEMENT

This work was supported by Ministry of Education of the Czech Republic (ME09065), Grant Agency of Czech Republic (grants 13-08336S) and EU (CEITEC CZ.1.05/1.1.0/02.0068) program.

## 6. REFERENCES

[1] J. Vaněk, P. Lubal, P. Hermann, P. Anzenbacher Jr., J. Fluorescence 23 (2013) 57-69.

# FORMATION OF DNA ADDUCTS BY ELLIPTICINE AND ITS MICELLAR FORM IN RATS – A COMPARATIVE STUDY

Marie STIBOROVA[1*], Zuzana MANHARTOVA[1], Petr HODEK[1], Vojtech ADAM[2], Rene KIZEK[2], Eva FREI[3]

[1] *Department of Biochemistry, Faculty of Science, Charles University, Albertov 2030, 128 40 Prague 2, Czech Republic*

[2] *Department of Chemistry and Biochemistry, Faculty of Agronomy, Mendel University in Brno, Zemedelska 1, 613 00 Brno, and Central European Institute of Technology, Brno University of Technology, Technicka 3058/10, 616 00 Brno, Czech Republic*

[3] *Division of Preventive Oncology, National Center for Tumor Diseases, German Cancer Research Center (DKFZ), In Neuenheimer Feld 280, 69 120 Heidelberg, Germany*

**stiborov@natur.cuni.cz*

**Abstract**

Formation of covalent ellipticine-DNA adducts after the ellipticine enzymatic activation is one of the most important mechanisms of pharmacological action of this anticancer drug. Here we investigated whether ellipticine might be released from its micellar (encapsulated) form to be able to form the covalent DNA adducts as free ellipticine. Here, we compared the efficiencies of free ellipticine and its micellar form [the poly(ethylene oxide)-*block*-poly(allyl glycidyl ether) (PAGE-PEO) block copolymer, P 119 nanoparticles] to form ellipticine-DNA adducts in rats *in vivo*. The results demonstrate that treatment of rats with free ellipticine or this anticancer agent in micelles resulted in formation of ellipticine-derived DNA adducts *in vivo* and suggest that a gradual release of ellipticine from its micellar form might produce the enhanced permeation and retention effect of this ellipticine-micellar delivery system

## 1. INTRODUCTION

Ellipticine (5,11-dimethyl-6*H*-pyrido[4,3-*b*]carbazole) and its derivatives are efficient anticancer compounds that function through multiple mechanisms (for a summary see [1-6]). The predominant mechanisms of ellipticine's biological effects is its efficacy to cause DNA damage. Among them, the formation of covalent DNA adducts after ellipticine enzymatic activation with cytochromes P450 (CYP) and peroxidases seems to be most important [1-4,6]. Ellipticine oxidation to 12-hydroxy- and 13-hydroxyellipticine dissociating to ellipticine-12-ylium and ellipticine-13-ylium lead to formation of two major covalent DNA adducts (Fig. 1) [3,4,6]. The same adducts are also formed, in rats and mice, in several cancer cell lines treated with this drug and in DNA of rat mammary adenocarcinoma *in vivo* [3,4,6] (Fig. 1). However,

this antineoplastic agent exhibits also severe adverse toxic effects, including nephrotoxicity, renal toxicity, hemolysis, xerostomia, hypertension, nausea and vomiting [5]. Hence, the studies of our laboratory are targeted on development of efficient and reliable methods for targeted delivery of ellipticine as well as on preparation of this drug in the forms that exhibit lower side effects and leads to an increase in their anticancer effects.

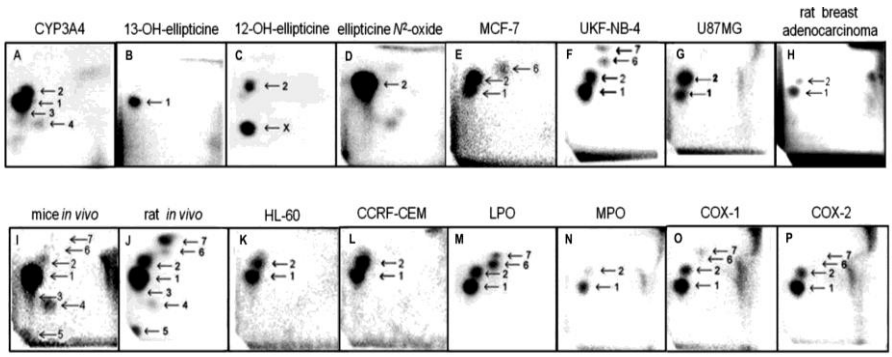


**Figure 1.:** Autoradiographic profiles of ellipticine-derived DNA adducts analyzed with the $^{32}$P-postlabeling assay. Adduct profiles obtained from calf thymus DNA reacted with ellipticine and CYP3A4 (A), from calf thymus DNA reacted with 13-hydroxyellipticine (B), 12-hydroxyelipticine (C), ellipticine $N^2$-oxide (D), from DNA of breast adenocarcinoma MCF-7 cells (E), neuroblastoma UK-NB-4 cells (F) and glioblastoma U87MG cells (G) treated with 10 □M ellipticine, from DNA of breast adenocarcinoma of Wistar rats treated *i.p.* with 4 mg ellipticine per kilogram body weight (H), from liver DNA of C57BL/6 mice treated *i.p.* with 10 mg ellipticine per kilogram body weight (I), from liver DNA of Wistar rats treated *i.p.* with 40 mg ellipticine per kilogram body weight (J), from leukemia HL-60 (K) and CCRF-CEM cells (L) treated with 10 □M ellipticine, from calf thymus DNA reacted with ellipticine and bovine lactoperoxidase (LPO) (M), human myeloperoxidase (MPO) (N), ovine cyclooxygenase (COX)-1 (O) and human COX-2 (P). Adduct spots 1-7 correspond to the ellipticine-derived DNA adducts. Besides adduct 2 formed by 12-hydroxyellipticine, another strong adduct (spot X in panel C), which was not found in any other activation systems or *in vivo* was generated.

Here, we utilized ellipticine encapsulated in micelles to study the biodistribution of ellipticine in this micellar form to reach the tissues in which the formation of covalent ellipticine-derived DNA adducts are generated. Since polymeric micelles improve solubility and bioavailability of hydrophobic drugs [7], they were used for ellipticine as a hydrophobic compound.

## 2. MATERIAL AND METHODS

The poly(ethylene oxide)-*block*-poly(allyl glycidyl ether) (PAGE-PEO) block copolymer (P 191 nanoparticles) [7] that were a gift of Dr. M. Hruby (Institute of Macromolecular Chemistry AS CR, Prague, Czech Republic) were used to prepare a micellar form of ellipticine, in which ellipticine is bound by hydrophobic interactions, and to investigate its biodistribution among the tissues of Wistar rats that are suitable to mimic the fate of ellipticine in humans [3,4,6]. The formation of ellipticine-derived DNA adducts mediated by free ellipticine and its micellar form, measured with the $^{32}$P-postlabeling method [1-4,6], were employed to determine their biodistribution in rats *in vivo*.

## 3. RESULTS AND DISCUSSION

In the present study, polymeric nanoparticles P 119 [7] containing hydrophobically bound ellipticine (0.595 mg ellipticine per ml) under the concentration of polymer of 25.9 mg per ml were prepared and used for further experiments. Utilizing the $^{32}$P-postlabeling assay found previously to be suitable to detect and quantify ellipticine-derived DNA adducts formed *in vitro* and *in vivo* [1-4,6], their formation from free ellipticine and its micellar form (the P 119 nanoparticles) in rats *in vivo* was determined. Our results demonstrate that treatment of rats with free ellipticine or this anticancer agent in micelles resulted in formation of ellipticine-derived DNA adducts in liver, spleen, kidney, heart, lung and brain of rats treated with these forms of ellipticine. Two major ellipticine-DNA adducts (see adducts 1 and 2 in Fig. 1) were formed in most tested organs of rats treated either with free ellipticine or its micellar form. The results of this study indicate that both free ellipticine and ellipticine present in micelles are capable of transferring the biological membrane reaching the target tissues. The levels of ellipticine-DNA adducts formed in rat tissues after their administration with micelles of ellipticine was one order of magnitude lower in most organs than in those of rats with free ellipticine, with an exception of brain. In brain, the levels of ellipticine-DNA adducts formed by ellipticine in micelles were higher than in DNA of brain of rats treated with free ellipticine. This finding emphasizes that a micellar form of ellipticine might be employed to treat the brain tumors, treatment of which by cytostatics is usually limited because of strict selectivity of the hematoencephalic barrier (the blood-brain barrier). The lower levels of ellipticine-DNA adducts in other organs suggest a gradual release of ellipticine that might produce the enhanced permeation and retention effect of the ellipticine-micellar delivery system.

## 4. CONCLUSION

The results suggest a suitability of a micellar form of ellipticine as the drug delivery system.

## 5. ACKNOWLEDGEMENT

We thank Dr. M. Hruby (Institute of Macromolecular Chemistry AS CR, Prague, Czech Republic) for preparation of P 119 nanoparticles. The work has been supported by GACR (14-18344S in panel P301) and Charles University in Prague (UNCE 204025/2012).

## 6.REFERENCES

[1]Stiborová M., Bieler C.A., Wiessler M., et al.: Biochemical Pharmacology, 62 (2001), 1675-1684.

[2]Stiborová M., Rupertová M., Schmeiser H.H., et al.: Biomedical Papers, 150 (2006), 13-23.

[3]Stiborová M., Rupertová M., Frei E.: Biochimica et Biophysica Acta, 1814 (2011), 175-185.

[4]Kizek R., Adam V., Hrabeta J., et al.: Pharmacology & Therapeutics, 133 (2012), 26-39.

[5]Garbett N.C., Graves D.E.: Current Medicinal Chemistry. Anti-Cancer Agents, 4 (2004), 149-172.

[6]Stiborová M., Frei E.: Current Medicinal Chemistry, 21 (2014), 575-591.

[7]Hruby M., Konák C, Ulbrich K.: Journal of Control Release, 103 (2005) 137-148.

# THE SITE DIRECTED MUTAGENESIS OF KEY AMINOACIDS IN THE HEME DISTAL SIDE OF AN OXYGEN SENSOR, YDDV, PROBABLY CONVERTS ITS CHARACTER FROM A $O_2$ SENSING PROTEIN TO A HEME OXYGENASE ENZYME

Martin STRÁŇAVA[1], Markéta MARTÍNKOVÁ[1*], Marie STIBOROVÁ[1], Petr MAN[1,2], Kenichi KITANISHI[1], Lucie MUCHOVÁ[3], Libor VÍTEK[3], Václav MARTÍNEK[1], Toru SHIMIZU[1]

[1] *Department of Biochemistry, Faculty of Science, Charles University in Prague, Hlavova (Albertov) 2030/8, Prague 2, 128 43 Czech Republic*

2 *Institute of Microbiology, Academy of Sciences of the Czech Republic, v.v.i., Videnska 1083, Prague 4, Czech Republic*

3 *Institute of Medical Biochemistry and Laboratory Diagnostics, 1st Faculty of Medicine, Charles University in Prague, Czech Republic*

**marketa.martinkova@natur.cuni.cz*

**Abstract**

The globin-coupled oxygen sensor, YddV, is a heme-based oxygen sensor diguanylate cyclase. Oxygen binding to the heme Fe(II) complex in the N-terminal sensor domain of this enzyme substantially enhances its diguanylate cyclase activity which is conducted in the C-terminal functional domain. Leu65 is located on the heme distal side and is important for keeping the stability of the heme Fe(II)-$O_2$ complex by preventing the entry of the water molecule to the heme Fe(II) complex. Since Leu65 mutations are assumed to introduce the water molecule into the heme distal side of the isolated heme-bound domain of YddV (YddV-heme), it is suggested that the water molecule would significantly contribute to facilitating heme oxygenase reactions for the Leu65 mutants. This study suggests that mutations at the heme distal side could convert the characteristic properties of the heme-based oxygen sensor into heme oxygenase-acting fashion, as revealed by mass spectrometry and UV-vis spectroscopy.

## 1. INTRODUCTION

The heme-based gas sensor proteins (see [1] for a review) are composed of the N-terminal heme-bound sensor domain and the C-terminal functional domain. Globin-coupled oxygen sensors (GCS), such as YddV, AfGcHK and HemAT with the heme-bound globin fold, have specific characteristics. These are different from other oxygen sensors with the heme-bound

PAS fold (Ec DOS and FixL) and from those with the heme-bound GAF fold (DevS and DevT) [1]. The molecular mechanism of YddV action and its function is still not fully understood. Especially, the question regarding catalytic regulation by the $O_2$ binding to the heme Fe(II) complex remains to be answered. Moreover, the stability of the heme Fe(II)-$O_2$ complex that is important to elicit the oxygen sensor function is worthy to be studied.

## 2. MATERIAL AND METHODS

All YddV-heme proteins (WT, L65F, L65G, L65M, L65N, L65Q, L65T, Y43A, Y43F and Y43W) were prepared by **recombinant overexpression in *E. coli* cells** as described previously [2, 3]. **Optical absorption** spectral data were obtained using a HP 8453 UV-VIS spectrophotometer (Agilent Technologies, CA, USA) at 20 $^{o}$C under aerobic conditions as previously described [2, 3]. UV-vis spectra of YddV-heme proteins (from 5 to 8 μM) were recorded in 50 mM Tris-HCl buffer (pH 8.0) in order to examine the heme Fe(III), Fe(II) (sodium dithionite reduced) and Fe(II)-CO (CO bubbled) species. A solution of 20 μM YddV-heme protein was used for **mass spectrometric analysis** of the heme status. Half a microliter was spotted on a MALDI plate and overlaid with 0.5 μl of a saturated solution of α-cyano-4-hydroxycinnamic acid in methanol and water. Mass spectra were acquired on a MALDI-FT-ICR mass spectrometer equipped with 9.4 T superconducting magnet (Apex-Qe Ultra, Bruker Daltonics, Germany). Data were collected in positive ion mode over the mass range 350-1500 m/z at 1M data points, resulting in a maximum resolution of 200,000 at 400 m/z. The instrument was externally calibrated using singly-charged arginine clusters, resulting in sub-ppm accuracy. The spectra were processed and theoretical isotopic envelopes of heme and verdoheme were modeled in DataAnalysis 4.0 (Bruker Daltonics).

## 3. RESULTS AND DISCUSSION

We aimed to shed more light on the key amino acids necessary for the $O_2$ binding to the heme Fe(II) complex of YddV-heme and describe the exact role of Leu65 in the process. In order to study the YddV-heme properties dictated by the Leu65 mutations, we overexpressed and purified the following mutants of YddV-heme, L65F, L65G, L65M, L65N, L65Q and L65T. Overexpression and purification of L65G and L65N were extremely difficult because the green-colored protein solution was obtained instead of the red-colored solution of a typical heme protein (Figure 1A). The mass spectral analysis of L65G and L65N unequivocally proved that the major species responsible for the green color of their solutions is verdoheme (Figure 1B). Other modified heme complexes such as meso-hydroxyhemin, biliverdin, and

bilirubin were also found, but their signals were very weak. Note that verdoheme is the first stable product of the consecutive heme oxygenase reactions.

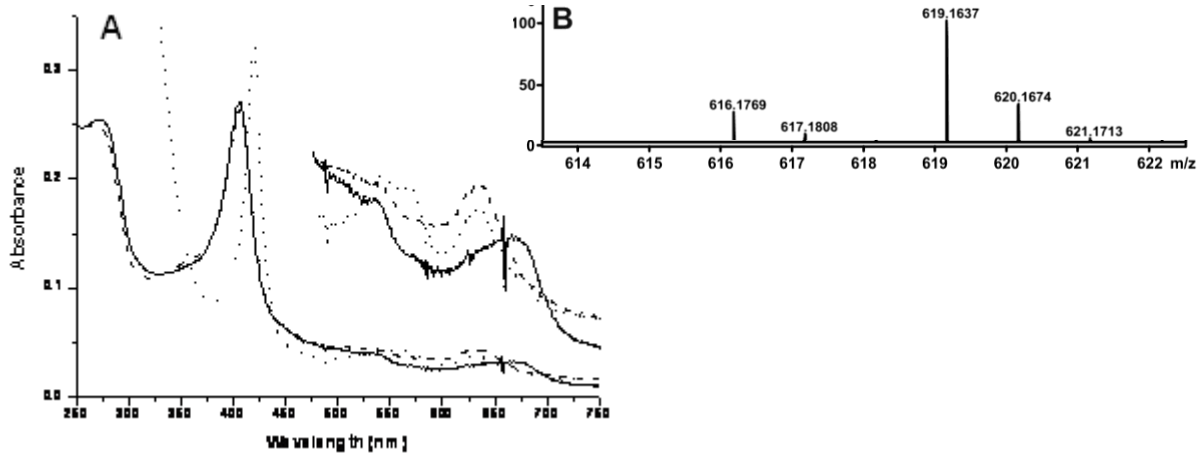


**Figure 1.: (A)** The absorption spectrum of the green solution (solid line) of L65N of YddV-heme (5.0 μM) and the CO added solution (broken line). CO addition substantially changed the spectrum of the purified L65N, suggesting that the modified heme Fe(II) complex exists in the solution without being reduced by sodium dithionite. Sodium dithionite addition also changed the spectrum of the final solution (dotted line), suggesting that the modified heme Fe(III) complex is also mixed in the solution. **(B)** Detailed view of the mass range covering heme and verdoheme region. Isotopic envelopes are shown a mixture of heme/verdoheme from mutant L65N of YddV-heme.

## 4. CONCLUSION

We confirmed a key role of well conserved Leu65 in a heme-bound sensor domain of a globin-coupled oxygen sensor, YddV. While in WT of the YddV protein, $O_2$ interaction with the heme-Fe(II) complex is important for the oxygen sensing process, mutation at Leu65 probably significantly changed the character of the YddV enzyme to simulate the heme oxygenase reaction. The tendency to simulate the heme oxygenase activity varies among the tested Leu65 mutants. The L65G and L65N were identified as the proteins showing the most efficient simulation of the heme oxygenase activity.

## 5. ACKNOWLEDGEMENT

This work was partially supported by the Grant-in-Aid from Charles University in Prague (UNCE 204025/2012), by the Grant Agency of the Czech Republic (grant P301/10/0356) and by the Grant Agency of the Charles University (grant 756214).

## 6. REFERENCES

[1]Martinkova M., Kitanishi K., Shimizu T.: J. Biol. Chem. 288 (2013) 27702-27711.

[2]Kitanishi K., Kobayashi K., Kawamura Y., et. al.: Biochemistry 49 (2010) 10381-10393.

[3]Nakajima K., Kitanishi K., Kobayashi K.,et. al: J. Inorg. Biochem. 108 (2012) 163-170.

# INHIBITORS OF CYCLIN-DEPENDENT KINASES AS NEW GENERATION OF ANTICANCER DRUGS

Miroslav STRNAD,[1*] Vladimír KRYŠTOF,[1] Radek JORDA,[1] Eva ŘEZNÍČKOVÁ,[1] Tomáš GUCKÝ,[1] Marek ZATLOUKAL,[1] Libor HAVLÍČEK[2]

[1]*Laboratory of Growth Regulators, Institute of Experimental Botany ASCR & Palacký University, Šlechtitelů 11CZ-783 71 Olomouc, Czech Republic*

[2] *Isotope Laboratory, Institute of Experimental Botany ASCR, Vídeňská 1042, CZ-142 20 Prague, Czech Republic,*

**miroslav.strnad@upol.cz*

Purine-based compounds have already been used in numerous applications, *inter alia* as agonists and antagonists of adenosine receptors, ligands of corticotropin-releasing hormone receptors, and inhibitors of numerous proteins, including heat shock proteins (HSPs), protein and lipid kinases, sulphotransferases and phosphodiesterases. Thus, systematic screening for purine derivatives with desired activities is likely to be highly rewarding. Originally, we focused on the primary action mechanisms of the plant hormones cytokinins ($N^6$-substituted adenine derivatives) in mammalian cell division cycles, and showed that natural cytokinins are rather non-specific inhibitors of various protein kinases.[1] Surprisingly, at that time, among aromatic cytokinin derivatives we discovered a compound, 2-(2-hydroxyethylamino)-6-benzylamino-9-methylpurine, named "olomoucine", which inhibits several cyclin-dependent kinases (CDKs) at micromolar concentrations.[1] In subsequent studies the purine heterocycle was one of the first systematically investigated scaffolds of kinase inhibitors (partly due to its amenability to various substitutions), leading to discovery of roscovitine, olomoucine II, purvalanol A,and LGR1406, which display an enhanced inhibitory activity toward CDK1, a higher selectivity toward some CDKs, an increased antimitotic activity at the G1/S and G2/M points of the cell cycle, and stronger and more selective antitumour effects..[2,3] Roscovitine is a pan-selective CDK inhibitor with multiple effects on cell proliferation, p53 expression and p53-dependent transcription and/or induction of apoptosis in cancer cells. Consequently, roscovitine was among the first CDK inhibitors to enter clinical trials. It was licensed to Cyclacel Pharmaceuticals and is currently being evaluated in phase 2b clinical trials with Oral Sapacitabine and Oral Seliciclib (see www. ClinicalTrials.gov).

Unfortunately, chemotherapeutic agents currently used for treating cancer probably influence few of the abovementioned hallmarks besides their key therapeutic targets, although

in many cases the effects on other cancer-related aberrations have never been tested (so they could have additional unknown negative or positive effects). Thus, "hallmark" biological activities should ideally be tested for each new lead substance to define as many of its pertinent biological activities as possible. For example, very little is known about the effects of known CDK inhibitors on other cancer hallmarks. However, we recently showed that the CDK inhibitor roscovitine blocks angiogenesis *in vitro* and *in vivo*.[5] Furthermore, in detailed investigation of its action mode our Munich colleagues identified a new function of CDK5 in endothelial cell migration and angiogenesis. Our further joint work suggests a new possible application of CDK inhibitors, particularlyCDK5 inhibitors, as antiangiogenic agents, indicating that structure-activity analyses of purine analogues could greatly facilitate the identification of potent new antiangiogenic compounds.[4,5] Some newly discovered hallmark activities will be described in this talks as well.

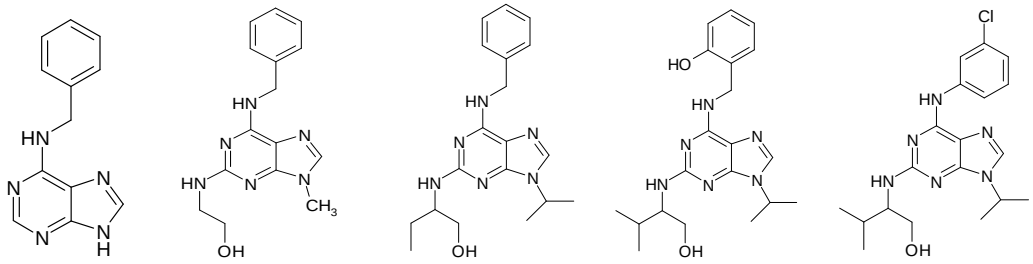


Fig. 1. Chemical structures of 6-benzylaminopurine (BAP), olomoucine, roscovitine, olomoucine II and purvalanol (from left to right).

**ACKNOWLEDGEMENTS**

We gratefully acknowledge grant no. LO1204 from Czech Ministry of Education for financial support to this work.

**REFERENCES**

[1] Vesely J, Havlicek L, Strnad M et al, Eur. J. Biochem. 1994, 224, 771-786.

[2] Meijer, L. et al, Eur. J. Biochem. 1997, 243, 527-536.

[3] Havlicek L, Hanus J, Vesely J et al, J. Med. Chem. 1997, 40, 408-412.

[4] Liebl J, et al, J Biol Chem. 2010 Nov 12;285(46):35932-43.

[5] Weitensteiner SB, Liebl J, Krystof V, et al, PLoS One. 2013;8(1):e54607

# EFFECT OF DEEP FREEZING TO QUALITY OF HEK293 TRANSFECTED WITH $CA_V$ 3.1 MEMBRANE CHANNEL

Ondřej SVOBODA[1,2*], Larisa BAIAZITOVA[1], Ivo PROVAZNÍK[1,4], Jaromír HUBÁLEK [2,3]

[1] *Department of Biomedical Engineering, Faculty of Electrical Engineering and Communication, Brno University of Technology, Technicka 3082/12, 616 00 Brno, Czech Republic*

*2 Central European Institute of Technology, Brno University of Technology, Technicka 3058/10, 616 00 Brno, Czech Republic*

*3 Department of Microelectronics, Faculty of Electrical Engineering and Communication, Brno University of Technology, Technicka 3082/12, 616 00 Brno, Czech Republic*

*4 International Clinical Research Center - Center of Biomedical Engineeering, St. Anne's University Hospital Brno, Brno, Czech Republic*

**ondrej.svoboda@ceitec.vutbr.cz*

**Abstract**

Storing of living cells in liquid nitrogen ($LN_2$) has been a standard for a long time. Disadvantages are well known – $LN_2$ evaporates. There is another possibility to store living cells using a freezer with temperatures of -80 °C. In this work, we focus on the study of HEK293 cells stored in the low temperature freezer and evaluation of cell quality. Our experiments involved 190 individual cells, 87 of them frozen for ten days. Then, cells were thawed and their ability to establish a gigaseal in patch-clamp measurement was tested. Ten-day freezing did not influenced quality of cells comparing to those stored in $LN_2$ but there were small differences comparing to control group of cells.

## 1. INTRODUCTION

Freezing cells in liquid nitrogen ($LN_2$) with DMSO is well known and commonly used procedure for long time cell storing. Liquid nitrogen boils at −196 °C and is used as a cryogenic fluid in life-sciences. It causes rapid freezing on contact with living tissue. However, small laboratories with limited number of experiments suffer from difficulties to access and manage $LN_2$. Another possibility is based on an idea to freeze cells in a special low temperature freezer with stable temperature about −80 °C. The main question is if i) higher temperature of deep freezers and/or ii) slower freezing, can negatively influence quality of the stored cells.

## 2. MATERIAL AND METHODS

HEK293 cells were used in our experiment. These cells were isolated in 1970s by Graham and van der Eb [1]. Since 1970s, the use of HEK293 cell lines really expand especially due to their easy cultivation, rapid growth [2], no calcium and sodium channel expression [3] and easy transfection [2]. HEK293 used in this experiment were transfected by $Ca_V$ 3.1 membrane current channel. This channel belongs to T-type (LVA) voltage gated calcium channel group. $Ca_V$ 3.1 channel is characterized by presence of $\alpha_1$ subunit with combination of other auxiliary β, $\alpha_2$-δ and γ subunits [4], fast activation [3] and relative fast recovery from inactivation. $Ca_V$ 3.1 can be commonly found in cardiac tissue and neurons [4], [5], [6].

Cell quality was evaluated by standard patch clamp technique. This electrophysiology technique was developed by Hamill et all [7] in 1980s. It allows the user to study membrane potentials and channel currents. Patch clamp technique is well described in e.g. [7]. One of the patch clamp key step is establish a gigaseal which can be made by extra suction on hollow glass pipette filled with solution which is similar to the intracellular fluid. The pipette is in well contact with measured cell before gigaseal. Cells were placed in bath solution during measurement. The solution is similar to the extracellular solution [8].

Cells were cultivated in EMEM with 10% FBS and 1% P/S, L-Glutamine and G-418. All patch clamp measurements used the same bath and pipette solutions to avoid artificial variability. No membrane channel blockers were used. Patch clamp pipettes were prepared from borosilicate glass with output resistance between 2.1 and 2.8 MΩ. Experimental setup consisted of Axopatch 200B, Digidata 1440 and PC with Clampex software.

As the main indicator for cells quality, ability of the cell to establish gigaseal was chosen. Such indicator is strictly dichotomic but it is necessary for a lab using patch-clamp technique. Non-frozen cells, cells frozen in $LN_2$ and cells frozen in freezer were measured separately. For each type of cells, gigaseal-to-total number of cells ratio was calculated.

## 3. RESULTS AND DISCUSSION

Gigaseal-to-total number of cells ratio was calculated for control group and both experimental groups of cells. The results are presented in Table 1. The control group shows that about 20.4% of non-frozen HEK293 cells can be successfully gigasealed. Both experimental groups express roughly doubled quality. Cells frozen in a low temperature freezer can be gigasealed in 29.0% comparing to 30.6% of cells frozen in $LN_2$. Table 1 shows some difference between the control group and frozen cell groups. It is most probably effect of improper measurement conditions, ie. measurement solutions quality and longtime cells. The difference in gigaseal/number of cells cell ratio between frozen cells by both techniques is subtle. Freezing

cells in $LN_2$ and a low temperature freezer for ten days does not change cell quality. The results are limited by limited storage time and the used type of. However, the results are satisfactory for the main purpose of the experimental work. Future work of the team will be focused on the experiments with cells frozen for periods longer than ten days. Further, $Ca_V$ 3.1 current responses will be measured as another potential quality indicator.

**Table 1**: Cell statistics from individual experiments

| | No. of cells | No. of gigaseals | Gigaseal/Cell ratio |
|---|---|---|---|
| **Non-frozen cells (control group)** | 103 | 21 | **0.204** |
| **Cells frozen in a freezer** | 38 | 11 | **0.290** |
| **Cells frozen in $LN_2$** | 49 | 15 | **0.306** |

## 4. CONCLUSION

In this paper, comparison of two techniques of low temperature cell freezing is presented. Subtle differences between freezing in a low temperature freezer and liquid nitrogen was found. However, difference between non-frozen and frozen cells caused by improper measurement conditions appeared.

## 5. ACKNOWLEDGEMENT

The article was supported by grant project GACR P102/11/1068, European Regional Development Fund - Project FNUSA-ICRC (No. CZ.1.05/1.1.00/02.0123) and by projet FEKT-S-14-2300 A new types of electronic circuits and sensors for specific applications.

## 6. REFERENCES

[1]Graham FL, van der Eb AJ. A new technique for the assay of infectivity of human adenovirus 5 DNA. *Virology.* 1973, 52, 2.

[2]Thomas P, Smart TG. HEK293 cell line: a vehicle for the expression of recombinant proteins. *Journal of Pharmacological and Toxicological Methods.* 2005, Vol. 3, 51.

[3]Kamaržínová M, Lacinová Ľ. Measurement of Cellular Excitability by Whole Cell Patch Clamp. *Physiological Research.* 2010, S1-S7.

[4]Catterall WA. Structure and regulation of voltage-gated Ca2+ channels. *Annual Review of Cell and Developmental Biology.* 2000, 16.

[5]Catterall WA. Voltage-Gated Calcium Channels. *Cold Spring Harbor Perspectives in Biology.* 2010.

[6]Kostyuk P G. Calcium channels in the cell membrane. *Neuroscience and Behavioral Physiology.* 1986, Vol. 5, 16, pp. 401-410.

[7]Hamill OP, Marty A, Neher E, Sakmann B, Sigworth FJ. Improved patch-clamp techniques for high-resolution current recording from cells and cell-free membrane patches. *Pflugers Archive.* 1981, Vol. 2, 391.

[8]Okada Y. *Patch Clamp Techniques : From Beginning to Advanced Protocols.* 2012. 978-4-431-53992-6.

# FLUORESCENCE STUDY OF MIXED MICELLES FORMATION

Jana Szewieczková[1*], Filip Mravec[1], Miloslav Pekař[1]

1 *Centre for Materials Research, Faculty of Chemistry, Brno University of Technology, Purkynova 118, 612 00 Brno, Czech Republic*

**xcszewieczkovaj@fch.vutbr.cz*

**Abstract**

An aggregation process of sugar-based surfactant and phospholipid was studied. All experiments were realized by using fluorescence spectroscopy method with pyrene as a fluorescence probe.

At the beginning, aggregation behaviour of DPPC (1,2-dipalmitoyl-*sn*-glycero-3-phosphatidylcholine) was studied in two different ways. Then, sugar-based surfactant (dodecyl-β-D-maltoside) aggregation was studied in the presence and absence of DPPC.

## 1. INTRODUCTION

Dodecyl maltoside (in excess) can well solubilize DPPC. In the case of equimolar mixture was achieved complete DPPC bilayer solubilization into mixed micelles, too 0.

The dependence of mixed micelle stoichiometry on the concentration of aqueous sugar-based surfactant is consistent with the assumptions of ideal mixing of the two amphiphiles in the mixed micelles 0.

Pyrene is highly sensitive fluorescence probe suitable for studying polarity of local environment. Intensity of first emission band is sensitive for local polarity and intensity of third emission band 0 is used as a reference and then we can use their ratio as emission polarity index (EmPI). This parameter is often used for CMC determination 0 and can be used for characterization of mixed surfactant systems 0.

Dependences of pyrene EmPI as a function on the total surfactant concentration show around CMC sigmoidal decrease and after fitting by sigmoidal curve to CMC obtaining. The same is valid for ExPI (ExPI – excitation polarity index) obtained from pyrene excitation spectra as a ratio of intensity at 335 and 338 nm.

Nile red is another fluorescence probe. In the presence of aqueous suspension of phosphatidylcholine vesicles It fluorescence intensely, while its fluorescence is quenched in water 0.

## 2. MATERIAL AND METHODS

**Materials**. Dodecyl-β-D-maltoside was purchased from Fluka (resp. Sigma), 1,2-dipalmitoyl-*sn*-glycero-3-phosphatidylcholine DPPC, Fluka, GmbH), nile red, pyrene and chloroform were purchased from Fluka, GmbH. All experiments were performed in water adjusted by MiliPore system.

## 3. RESULTS AND DISCUSSION

CAC (critical concentration of aggregation) of DPPC was determined by two different methods – in saturated pyrene solution and with nile red as a fluorescence probe.

In the Figure 1 are shown dependences of pyrene ExPI and total integral of nile red emission spectra in the range of 525–750 nm on the DPPC concentration. In the case of pyrene ExPI and EmPI (EmPI not shown) CACs were obtained as a point of inflexion after fitting by Boltzmann curve, and concentration at the first break of the Boltzmann curve (CBA – concentration of the beginning of an aggregation) was calculated. In the dependence of total integral of nile red emission spectra are evident two breaks, which well correspond to the first break of Boltzmann curve and its point of inflection.

In aqueous solution probably occurs transformation from micelle-like structures to another aggregates (liposomes, vesicles), begins at CBA and at CAC are these new aggregates (new type of aggregates) formed. All measured concentrations are listed in Table 1. As can be seen, data obtained from measurements of pyrene EmPI and nile red total integral are in good agreement to each other. On the other hand, CBA and CAC obtained from measurements of pyrene ExPI are slightly lower.

For further measurements of mixed micelles formation, DPPC concentration of 5 mg $dm^{-3}$ (close to CBA) was chosen.

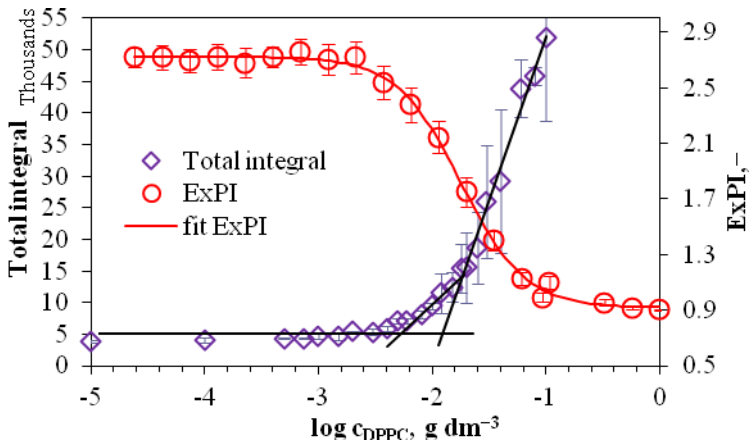


**Figure 1.:** Dependences of pyrene ExPI and Total Integral emission spectra of nile red on the DPPC concentration

**Table 1**: CBA and CAC of DPPC.

| Fluorescence probe | Dependence | CBA [g dm$^{-3}$] | CAC [g dm$^{-3}$] |
|---|---|---|---|
| Pyrene | EmPI | 0.004 | 0.014 |
| Pyrene | ExPI | 0.003 | 0.011 |
| Nile red | Total integral | 0.005 | 0.015 |
| Average | | 0.004 ± 0.001 | 0.013 ± 0.002 |

CMC of dodecyl-β-D-maltoside (hereinafter the C12Mal) was determined, and then, behaviour of mixed system with DPPC (0.005 g dm$^{-3}$) was measured. Dependences of pyrene EmPI (ExPI not shown) for both systems are shown in Figure 2.

For pure C12Mal smooth dependences of pyrene ExPI and EmPI on C12Mal concentration were obtained and values of CMC were received. These values are shown in Table 2. In the presence of DPPC decrease of EmPI (and ExPI too) was observed at C12Mal concentration about 0.01 mM followed by its increase in the range of C12Mal concentration 0.04–0.1 mM. This variation of EmPI can indicate formation of premicelar aggregates and their disintegration just before CMC and micelle formation.

These dependences were by two Boltzmann curves fitted, when the first point of inflection was named CAC (formation of first aggregates with hydrophobic core), and the second CMC. Values are again shown in Table 2. It is apparent, that CMC is decreasing with addition of DPPC to C12Mal. In the case of mixture of C12Mal and DPPC, CAC is localized approximately at ten times lower concentration that CMC is.

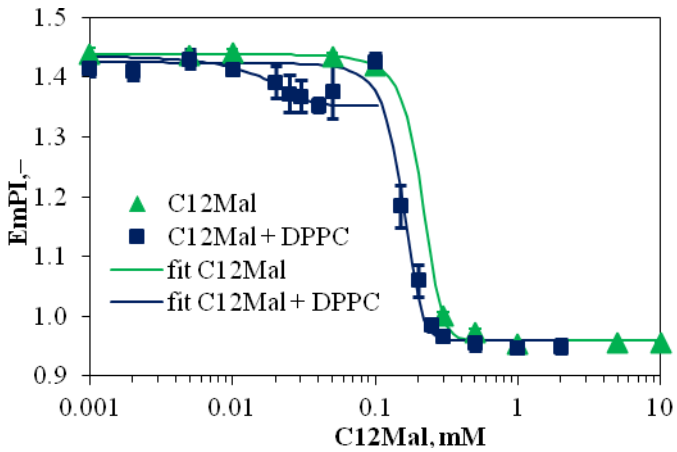


**Figure 2.:** Dependences of pyrene EmPI on the C12Mal concentration of C12Mal and its mixture with DPPC

**Table 2**: Parameters of Boltzmann curves for C12Mal and its mixture.

| | CMC [mM] | | | | CAC [mM] | | |
|---|---|---|---|---|---|---|---|
| **System** | **EmPI** | **ExPI** | **Average** | **Literature** | **EmPI** | **ExPI** | **Average** |
| C12Mal | 0.21 | 0.19 | 0.20 ± 0.01 | 0.17 00 | - | - | - |
| C12Mal+DPPC | 0.16 | 0.14 | 0.15 ± 0.01 | - | 0.0167 | 0.015 | 0.16 ± 0.001 |

## 4. CONCLUSION

In this paper we explained, that interaction of DPPC with non-ionic surfactant (sugar-based surfactant) is possible.

After addition of DPPC (at concentration 5 mg $dm^{-3}$) to sugar-based surfactant (C12Mal) was its CMC reduced, premicelar aggregates were probably formed and CACs of systems were founded.

## 5. ACKNOWLEDGEMENT

This work has been supported by Ministry of Education, Youth and Sports, Project LO1211.

## 6. REFERENCES

[1]Carion-Taravelal B, Chopineau J, et all.: Langmuir, 14 (1998), 14, 3767-3777
[2]Eidelman O, Blumenthal R, et all.: Biochemistry, 27 (1988), 2839–2846
[3]Lakowicz, JR: Principles of Fluorescence Spectroscopy. 3rd edition. Baltimore: Springer, 2006. 954
[4]Aguiar J, Carpena P, et all.: Journal of Colloid and Interface Science, 258 (2003), 116–122
[5]Hierrezuelo JM, Aguiar J, et all.: Langmuir, 20 (2004), 10419–10426
[6]Greenspan P, Fowler, SD: Journal of lipid research, 26 (1985), 781–789
[7]Hong W-X, Baker KA, et all.: Langmuir, 26 (2010), 11, 8690–8696
[8]Tsamaloukas AD, Beck A, et all.: Langmuir, 25 (2009), 8, 4393–4401

# INTERACTION OF HEAVY METALS WITH GRAPHENE AND IRON BASED PARTICLES

Dana FIALOVA[1,2], David HYNEK[1,2], Pavel KOPEL[1,2], Vojtech ADAM[1,2], Rene KIZEK[1,2*]

[1] *Department of Chemistry and Biochemistry, Faculty of Agronomy, Mendel University in Brno, Zemedelska 1, 613 00 Brno, Czech Republic*

[2] *Central European Institute of Technology, Brno University of Technology, Technicka 3058/10, 616 00 Brno, Czech Republic*

**kizek@sci.muni.cz*

**Abstract**

This study is aimed at determining the effectiveness of reduced graphene oxide and paramagnetic particles ($Fe_2O_3$) to adsorption of cadmium(II), lead(II), and copper(II) on its surface. Different interaction time from 1 minute to 24 hours was tested. The main attention was paid to the detection of these metals using differential pulse voltammetry.

## 1. INTRODUCTION

Metal ions are still a threat polluting environment and having great bioaccumulation potential [1, 2]. For isolation of heavy metals, it is possible to use different materials with high sorption properties that are able to adsorb metal ions onto their surface or into their structure. Different modifications of carbon, such as graphene, nanotubes, or fullerenes are important members of this group [3]. Instead of various carbon modifications, paramagnetic particles (PMPs) with comparable properties can be also used [4].

## 2. MATERIAL AND METHODS

### Chemicals

$FeCl_3 \cdot 6H_2O$, $FeCl_2.6 \cdot H_2O$, and other chemicals were purchased from Sigma Aldrich (Sigma-Aldrich, USA) unless noted otherwise. Stock solutions were prepared with ACS water.

### Preparation of graphene and $Fe_2O_3$ MPs

The reduced graphene oxide and paramagnetic particles ($Fe_2O_3$) were prepared according to the [5-8].

### Electrochemical determination of metal ions

Determination of cadmium, lead, and copper by differential pulse voltammetry at HMDE was performed using a 797 VA Stand (Metrohm). Acetate buffer (0.2 M $CH_3COONa$ +

$CH_3COOH$, pH 5) was used as a supporting electrolyte. The parameters of the measurement were as it follows: purging time 120 s, initial potential -1.3 V, end potential 0.2 V, deposition potential -1.15 V, accumulation time 240 s, pulse amplitude 25 mV, pulse time 0.04 s, voltage step 5.035 mV, voltage step time 0.3 s, sweep rate 0.0168 V/s, volume of injected sample: 15 µl, volume of measurement cell 2 ml (15 µl of sample; 1985 µl acetate buffer). Characteristic peak for cadmium was measured at potential of -0.62 V, for lead at potential of -0.40 V, and for copper at potential of -0.03 V.

## 3. RESULTS AND DISCUSSION

For determination of the concentration capacity, 10 mg of adsorbent was applied. 1 ml of solution of cadmium, lead, and copper in various concentrations was added to the adsorbent. Concentration of metals was as it follows: 1, 50, 100, 200, and 500 µM. Time of interaction was 1 hour.

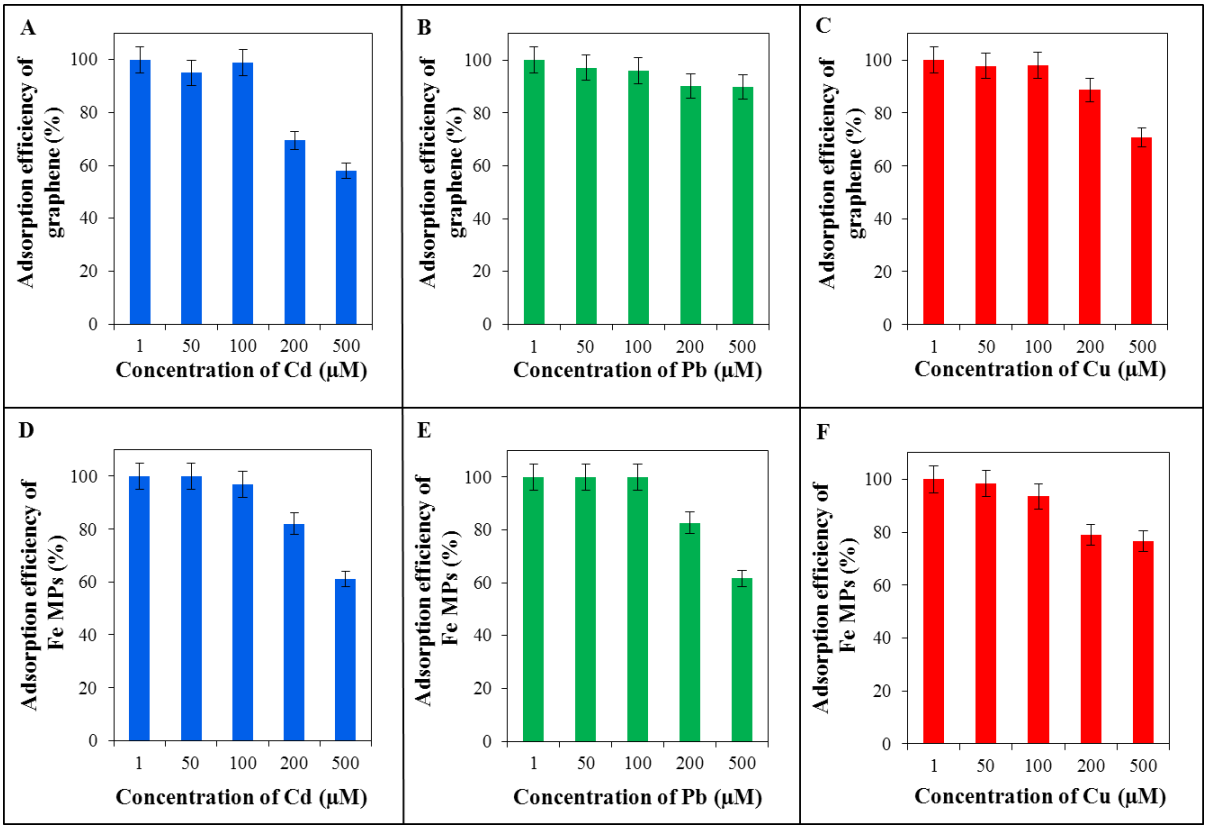


**Figure 1.:** Determination of the concentration of adsorbent capacity of graphene (reduced graphene oxide): concentration capacity (**A**) for cadmium, (**B**) for lead, and (**C**) for copper and of $Fe_2O_3$ MPs: concentration capacity (**D**) for cadmium, (**E**) for lead, and (**F**) for copper. Efficiency of adsorption for each metal is plotted on the y-axis %. Applied concentrations of metals ($Cd^{2+}$, $Pb^{2+}$, $Cu^{2+}$) were 1 µM, 50 µM, 100 µM, 200 µM, and 500 µM.

The concentration capacity of selected adsorbents was determined using differential pulse voltammetry. Based on the measured and evaluated data, the value of concentration, which is the limit for both adsorbents (reduced grapheme oxide in Figs. 1A, B and C, $Fe_2O_3$ particles in Figs. 1D, E and F) was determined. The limit value of concentration is 100 μM. The efficiency of adsorption was calculated according to the formula: Absorption efficiency = 100 % - ($C_D$ / $C_V$) * 100 (%). ($C_D$ is the detected concentration of metal in the filtrate. $C_V$ is the bound concentration of metal). With application of increasing concentration of metal ions the efficacy of adsorption decreased. The reason for the reduced efficiency of adsorption with the increasing concentration of the metal is the formation of a monolayer on the surface of adsorbent. The studied absorption effect is mainly caused by chemisorption [9, 10].

This fact is shown in Fig. 1. The graphs in Fig. 1 show the specificity of metals for each adsorbent. Reduced grapheme oxide preferably binds lead ions on its surface. Ferrous magnetic particles bind all three metals to their surface with the same specificity.

## 4. CONCLUSION

Monitoring of adsorption properties of reduced graphene oxide and $Fe_2O_3$ particles related to cadmium, lead and copper ions was investigated in this paper. From presented results seems that 100 μM concentration of metal ions was limiting in the adsorption process of reduced graphene oxide and $Fe_2O_3$ particles.

## 5. ACKNOWLEDGEMENT

Financial support from CEITEC CZ.1.05/1.1.00/02.0068 is greatly acknowledged.

## 6. REFERENCES

[1] Adam V, Zehnalek J, Petrlova J, *et al.*, Sensors, 5 (2005), 70-84.

[2] Fisher I J, Pain D J, Thomas V G, Biol. Conserv., 131 (2006), 421-432.

[3] Sitko R, Zawisza B, Malicka E, TRAC-Trends Anal. Chem., 51 (2013), 33-43.

[4] Hsing I M, Xu Y, Zhao W T, Electroanalysis, 19 (2007), 755-768.

[5] Hummers W S, Offeman R E, J. Am. Chem. Soc., 80 (1958), 1339-1339.

[6] Chua K C, Pumera M, Chem. Soc. Rev., in press, 10.1039/C3CS60303B (2014).

[7] Magro M, Sinigaglia G, Nodari L, *et al.*, Acta Biomater., 8 (2012), 2068-2076.

[8] Stankovich S, Dikin D A, Piner R D, *et al.*, Carbon, 45 (2007), 1558-1565.

[9] Song J, Kong H, Jang J, J. Colloid Interface Sci., 359 (2011), 505-511.

[10] Mahdavi S, Jalali M, Afkhami A, J. Nanopart. Res., 14 (2012), 1-18.

# FIA-ED: OPTIMIZATION OF METHOD FOR ELECTROCHEMICAL STUDY OF DOXORUBICIN

Roman GURAN[1], Marketa KOMINKOVA[1], Miguel Angel MERLOS RODRIGO[1], Pavel KOPEL[1,2], Iva BLAZKOVA[1], Dagmar CHUDOBOVA[1], Lukas NEJDL[1], Zbynek HEGER[1], Branislav RUTTKAY-NEDECKY[2], Ondrej ZITKA[1,2], Vojtech ADAM[1,2], Rene KIZEK[1,2*]

[1] *Department of Chemistry and Biochemistry, Faculty of Agronomy, Mendel University in Brno, Zemedelska 1, 613 00 Brno, Czech Republic*

[2] *Central European Institute of Technology, Brno University of Technology, Technicka 3058/10, 616 00 Brno, Czech Republic*

**kizek@sci.muni.cz*

**Abstract**

In the cancer treatment the drug doxorubicin, among others, is widely used. This drug has over its good cytostatic properties also cardiotoxic properties. For its negative properties there are still developed a new application possibilities that lead to reductions in dosage of this substance. Due to continuous development in this area it is necessary to establish low concentrations of doxorubicin in various matrices. In this work, we focused on improving the electrochemical detection of doxorubicin in combination with flow injection analysis. The most suitable condition for the electrochemical detection of doxorubicin an alkaline pH was determined.

## 1. INTRODUCTION

Doxorubicin is a drug that is used to treat a variety of cancers, alone or in combination with other cytostatic agents. Currently a liposomal doxorubicin is mainly used, as liposomal packaging reduces significantly the cardiotoxicity of doxorubicin itself. Cardiotoxicity of doxorubicin is a limiting factor in the use of this cytostatic drug [1]. To test a negative impact of doxorubicin on organisms it is necessary to prove how to determine the concentration of this substance in the samples of tissues, cells and body fluids. These concentrations can be very low and still can affect the organism. Therefore, it is necessary to develop new methods for detection of doxorubicin and reduce the cost of analysis. As one of the possible options appears a flow injection analysis (FIA-ED).

## 2. MATERIAL AND METHODS

### Electrochemical determination

Flow injection analysis system consisted of a chromatographic pump Model 584 ESA (ESA Inc., Chelmsford, MA) (working range 0.001-9.999 ml.min$^{-1}$) and of an electrochemical detector Coulochem (ESA, USA), to which the amperometric cell (model 5040, ESA, USA) was connected. The cell contained a working electrode made from glassy carbon.

## 3. RESULTS AND DISCUSSION

To determine doxorubicin in body fluids, cells or tissues, we optimized buffer environment that will be suitable for the detection of this substance by flow injection analysis (FIA-ED).

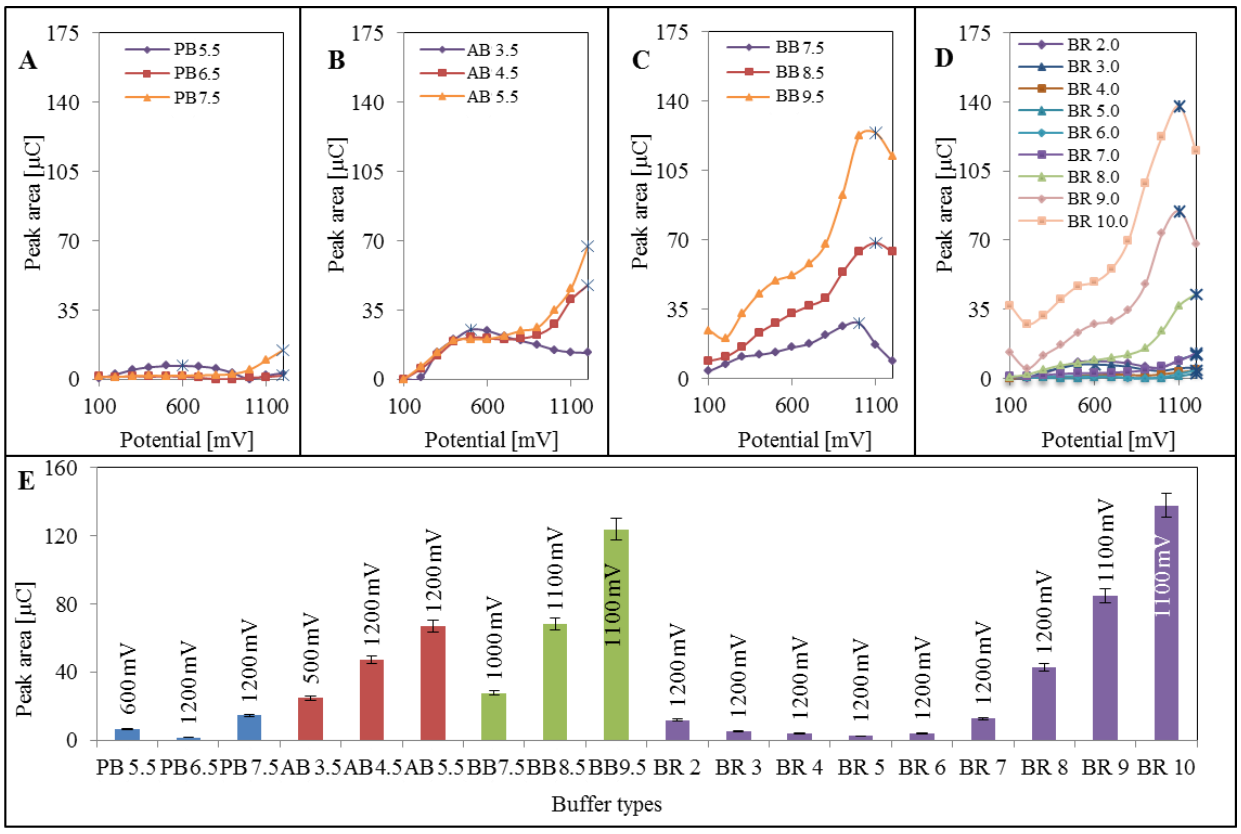


**Figure 1.:** Analysis of doxorubicin (50 mg.ml$^{-1}$) in different buffers by FIA-ED. The buffer, which was used for dilution of doxorubicin aliquot, was used also as the mobile phase. The potential range was 100 -to 1200 mV with 100 mV step. Blue marks in graphs represent maximal measured values. (**A**) Phosphate buffer (PB) with pH 5.5, 6.5 and 7.5. (**B**) Acetate buffer (AB) with pH 3.5, 4.5 and 5.5. (**C**) Borate buffer (BB) with pH 7.5, 8.5 and 9.5. (**D**) Britton-Robinson buffer (BR) with pH 2, 3, 4, 5, 6, 7, 8, 9 and 10. (**E**) The highest detector responses considering different buffers and applied potential.

Each buffer was used in its natural buffering range: Britton-Robinson buffer (pH 2, 3, 4, 5, 6, 7, 8, 9, 10), acetate buffer (pH 3.5, 4.5, 5.5), phosphate buffer (pH 5.5, 6.5, 7.5) and borate buffer (pH 7.5, 8.5, 9.5). In each buffer with each pH the hydrodynamic voltammograms (HDVs) were measured with a 100 mV step within the range from 100 to 1200 mV for phosphate buffer, acetate buffer, borate buffer and Britton-Robinson buffer (Figs. 1A, B, C, and D).

The largest peak area was achieved using the highest pH, which a Britton-Robinson buffer at pH 10. With decreasing pH the peak area of doxorubicin measured by FIA-ED was also decreasing. This effect of pH was surprising because with other types of electrochemical detection the low pH is preferably used [2-5] . For similar types of detection in HPLC the lower pH is used as well. Often a phosphate buffer with addition of triethylamine is used at pH lower than 5 [5,6]. These conditions are mainly used for separation but the signal of detector is distinctly lower than with use of our optimized conditions of Britton-Robinson buffer at pH 10 (Fig. 1E).

## 4. CONCLUSION

Optimization of the buffer environment suitable for electrochemical detection using flow injection analysis (FIA-ED) was carried out in this work. Best detection was achieved using a Britton-Robinson buffer of pH 10. Decrease of pH lead to the reduction of the signal intensity. These results suggest the possibility of improving the detection limits, when methods such as HPLC-ED are used, where buffers with substantially lower pH are commonly used.

## 5. ACKNOWLEDGEMENT

The work has been supported by CEITEC CZ.1.05/1.1.00/02.0068.

## 6. REFERENCES

1. Y. Z. Wang, Y. F. Ding, Z. M. Liu, X. R. Liu, L. Chen and W. L. Yan, *Pharmaceutical Research*, 30 (2013) 2902.
2. D. Hynek, L. Krejcova, O. Zitka, V. Adam, L. Trnkova, J. Sochor, M. Stiborova, T. Eckschlager, J. Hubalek and R. Kizek, *International Journal of Electrochemical Science*, 7 (2012) 13.
3. Y. J. Guo, Y. H. Chen, Q. Zhao, S. M. Shuang and C. Dong, *Electroanalysis*, 23 (2011) 2400.
4. D. Nieciecka and P. Krysinski, *Langmuir*, 27 (2011) 1100.
5. Z. Jemelkova, J. Zima and J. Barek, *Collection of Czechoslovak Chemical Communications*, 74 (2009) 1503.
6. G. Nicholls, B. J. Clark and J. E. Brown, *Journal of Pharmaceutical and Biomedical Analysis*, 10 (1992) 949.

# FLOW INJECTION ANALYSIS WITH ELECTROCHEMICAL DETECTION FOR RAPID IDENTIFICATION OF PLATINUM-BASED CYTOSTATICS AND PLATINUM CHLORIDES IN WATER

Marketa KOMINKOVA[1], Zbynek HEGER[1], Ondrej ZITKA[1], Rene KIZEK[1,2*]

[1] *Department of Chemistry and Biochemistry, Faculty of Agronomy, Mendel University in Brno, Zemedelska 1, 613 00 Brno, Czech Republic*

[2] *Central European Institute of Technology, Brno University of Technology, Technicka 3058/10, 616 00 Brno, Czech Republic*

**kizek@sci.muni.cz*

**Abstract**

During the cancer treatment high concentration of platinum cytostatics from the urine of patients ends up in wastewater. This leads to an increase in concentration of the platinum ions (PGEs) in wastewater. In order to facilitate the detection of various types of platinum, we have developed a new, rapid screening flow injection analysis method with electrochemical detection (FIA-ED). The developed method is based on monitoring changes in the electrochemical behavior of analytes in Britton-Robinson buffers of pH 2 and 5. Changes are observed in a comparison of the response of amperometric detector using a glassy carbon electrode at an applied potential of 1000, 1100 and 1200 mV.

## 1. INTRODUCTION

Due to the negative effects on organisms it is necessary to properly identify the presence of PGEs and especially cytostatics in the water environment which serves as the distribution route [1]. The most widely used platinum-based cytostatic, cisplatin, is applied in concentrations of 75–100 mg/m$^{-2}$ of body surface area, oxaliplatin in concentrations of 150 mg/m$^{-2}$ and carboplatin in concentrations of 400 mg/m$^{-2}$. Some 75% of the applied amounts may be excreted through urine into wastewaters [2]. These values indicate the potential seriousness of wastewater contamination with platinum-based cytostatics and highlight the importance of determination of their content.

## 2. MATERIAL AND METHODS

### Electrochemical determination

The instrument for flow injection analysis with electrochemical detection (FIA-ED) consisted of a solvent delivery pump (Model 582 ESA Inc., Chelmsford, MA, USA) and an

electrochemical detector. The electrochemical detector includes a flow-volume flow-through analytical cell (Model 5040, ESA), which consists of a glassy carbon electrode as a working electrode, a hydrogen-palladium electrode as a reference electrode and an auxiliary electrode, and a Coulochem III unit as a control potentiostat module.

## 3. RESULTS AND DISCUSSION

Analyte detection is dependent on the environment, pH and on the applied potential. For oxaliplatin, cisplatin, carboplatin, $PtCl_2$ and $PtCl_4$ detection, Britton-Robinson buffers of pH 2; 3; 3.5; 4; 5 and 6 were evaluated. Applied potential was chosen by earlier analyzes of 1000, 1100 and 1200 mV. To express the rates of change of electrochemical signal of platinum, peak heights after deduction of blank were rated.

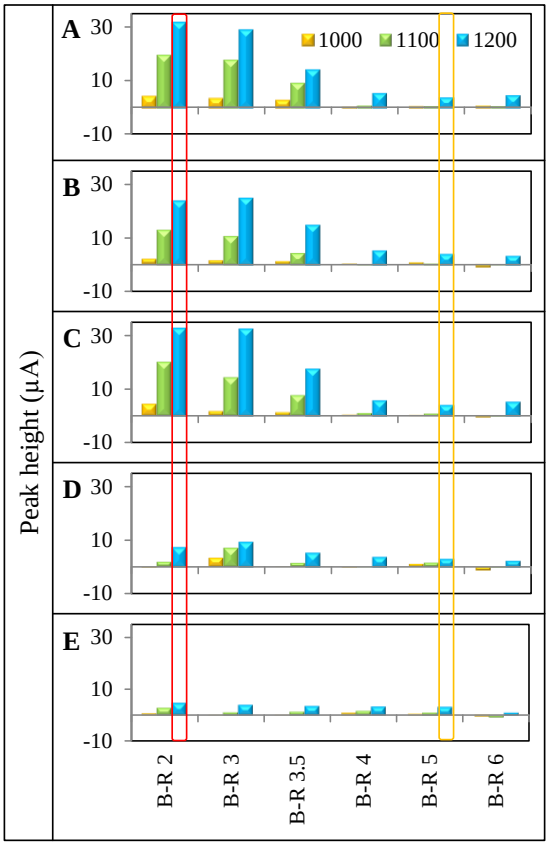


**Figure 1.:** Expression of potentials (range 1000–1200 mV) in buffers Britton-Robinson buffer (B-R) with pH 2–6 for each of PGEs obtained from HDVs. Ideal potentials for (A) oxaliplatin; (B) cisplatin; (C) carboplatin; (D) $PtCl_2$; (E) $PtCl_4$ are shown. Optimal potential and pH buffer for determination of platinum-based cytostatics from platinum chlorides is highlighted with red color. Potential and pH buffer, characterizing concentration of platinum in sample is highlighted with orange.

As seen in Fig. 1, the most significant differences are in the detection in Britton-Robinson buffer of pH 2 and an applied potential of 1200 mV (Fig. 1, highlighted by a red borders), contrast, when using a buffer pH 5 and the applied potential of 1200 mV (Fig. 1, highlighted by an orange border), minimal differences were reported in the detection of all tested PGEs variants. If the peak height of platinum measured in Britton-Robinson of pH 2 shows an approximately 1.5–2.5 × higher value that in the same buffer with pH 5, the result points to platinum chlorides. In the case that the peak height of platinum analyzed in the Britton-Robinson buffer of pH 2 is 5–9 × higher than in the same buffer of pH 5, platinum drugs are present in the water sample. Our method is based only on changing two buffers forming the mobile phases of the FIA-ED system. This approach is rapid, cheap and it can be miniaturized and thus used for biosensor applications.

## 4. CONCLUSION

Based on the obtained results, we suggest a rapid and inexpensive method with the potential to be miniaturized. The FIA-ED method, based on the comparison of the responses of an amperometric detector using a glassy carbon working electrode, can be used to distinguish the presence of platinum-based cytostatics from platinum chlorides.

## 5. ACKNOWLEDGEMENT

The work has been supported by CEITEC CZ.1.05/1.1.00/02.0068.

## 6. REFERENCES

[1] Supalkova V, Beklova M, Baloun J, *et al.*, Bioelectrochemistry, 72 (2008), 59-65.

[2] Lenz K, Hann S, Koellensperger G, *et al.*, Sci. Total Environ., 345 (2005), 141-152.

# ELECTROPHORETIC BEHAVIOR OF DOXORUBICIN

Romana KONECNA[1], Hoai Viet NGUYEN[1], Maja STANISAVLJEVIC[1], Iva BLAZKOVA[1], Sona KRIZKOVA[2], Marketa VACULOVICOVA[2], Marie STIBOROVA[3], Tomas ECKSCHLAGER[4], Ondrej ZITKA[1,2], Vojtech ADAM[1,2], Rene KIZEK[1,2]

[1]*Department of Chemistry and Biochemistry, Faculty of Agronomy, Mendel University in Brno, Zemedelska 1, CZ-613 00 Brno, Czech Republic, European Union*

[2]*Central European Institute of Technology, Brno University of Technology, Technicka 3058/10, CZ-616 00 Brno, Czech Republic, European Union*

[3]*Department of Biochemistry, Faculty of Science, Charles University, Albertov 2030, CZ-128 40 Prague 2, Czech Republic, European Union*

[4]*Department of Paediatric Haematology and Oncology, 2nd Faculty of Medicine, Charles University, and University Hospital Motol, V Uvalu 84, CZ-150 06 Prague 5, Czech Republic, European Union*

**kizek@sci.muni.cz*

**Abstract**

Doxorubicin (DOX) belongs to the group of anthracycline antibiotics with very effective anticancer properties. In this work, the DOX behavior in capillary electrophoresis was investigated. Electrophoretic mobilities in of the background electrolyte (pH range from 3 to 11) were determined in the range from 16.3 to -13.3 × $10^{-9}$ $m^{-2}$. $V^{-1}$. $s^{-1}$.

## 1. INTRODUCTION

Generally, anthracyclines belong to the most effective anticancer drugs, and DOX is highly efficient and widely used. This compound was firstly isolated from *Streptomyces peucetius* in 1960s [1]. The administration of the drug over the cumulative dose 550 mg/$m^2$ of body surface area leads to severe side effects including high risk of cardiomyopathy [2, 3]. Nevertheless, cardiac failures can be identified at smaller doses too. This cardiotoxicity is the main force driving the progress towards less toxic formulations, enabling also targeted delivery of the drug [4-10]. Due to the optical properties of DOX as well as its biological activity, this molecule is still a target of numerous investigations [11-13].

## 2. MATERIAL AND METHODS

### Capillary electrophoresis with laser induced fluorescenc detection (CE-LIF)

DOX was analyzed by CE-LIF (PACE MDQ, Beckman Coulter, USA). A fused silica capillary with internal diameter of 75 µm and with the total length 64.5 cm (54 cm to detector window) was used. The separation voltage of 20 kV and hydrodynamic injection by 3 psi for 10 s was employed.

## 3. RESULTS AND DISCUSSION

The behavior of the analyte in various environments is one of the key aspects that have to be considered prior to analysis by capillary electrophoresis. Analysis by separation methods such as capillary electrophoresis with laser-induced fluorescence detection may provide valuable information on the presence of various components, contaminations or even analyte species in the studied solution. Due to the complex structure of DOX and due to the presence of several functional groups, DOX may occur as a cation, anion, zwitterion and/or neutral molecule depending on the environment.

To determine the ionic form of DOX and its pI, phosphate buffer with pH 3, 4, 6, 8, 10, or 11 was used as a separation electrolyte and coumarine 334 was employed as an EOF marker. The obtained electropherograms are shown in Fig. 1. pH as low as 3 caused very slow EOF and therefore only DOX peak was obtained, however, the increasing pH above this value, peaks of both DOX and coumarine 334 were detected. DOX migrated as a cation (before the EOF marker) in the pH up to 10. When the pH was increased to 11, the peak of DOX occurred after the EOF marker, which confirmed the anionic form of DOX. As expected, based on previous fluorimetric experiments, the peak height of DOX decreased with the increasing pH. From the migration times, the electrophoretic mobilities were calculated. It clearly follows from the results obtained that the electrophoretic mobilities change over the range from $16.3\times10^{-9}$ to $-13.2\times10^{-9}$ $m^2.V^{-1}.s^{-1}$.

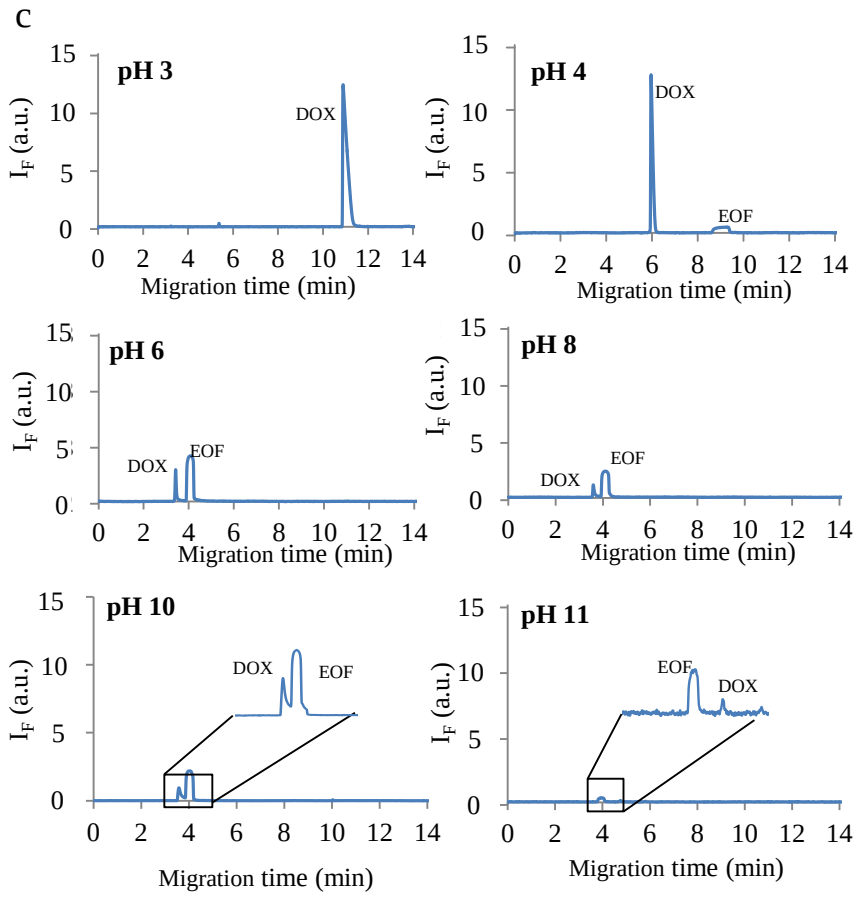


**Figure 1.:** CE-LIF of DOX with pH matching to BGE pH, DOX concentration 0.5 µg/mL, CE conditions: capillary 75 µm, 64.5/54 cm; voltage +20 kV; injection 3 psi, 10 s; BGE 10 mM sodium phosphate pH 3, 4, 6, 8, 10 or 11. (c) Left - DOX peak heights obtained when BGE pH matched sample zone pH (BGE 10 mM phosphate buffer pH 4, 6 and 8), right - electrophoretic mobilities of DOX under conditions matching the pH of BGE and DOX zone.

## 4. CONCLUSION

The fluorescence properties of DOX are strongly dependent on the environment and the increasing pH as well as the presence of water causes the fluorescence quenching. Using CE, the electrophoretic mobility of DOX as well as the pI was calculated.

## 5. ACKNOWLEDGEMENT

The financial support from GA CR CYTORES P301/10/0356 is highly acknowledged.

## 6. REFERENCES

[1] Weiss R B, Semin. Oncol., 19 (1992), 670-686.

[2] Zagotto G, Gatto B, Moro S, *et al.*, Journal of Chromatography B, 764 (2001), 161-171.

[3] Singal P K, Iliskovic N, New England Journal of Medicine, 339 (1998), 900-905.

[4] Zhen Z P, Tang W, Guo C L, *et al.*, ACS Nano, 7 (2013), 6988-6996.

[5] Meng L J, Zhang X K, Lu Q H, *et al.*, Biomaterials, 33 (2012), 1689-1698.

[6] Tacar O, Sriamornsak P, Dass C R, Journal of Pharmacy and Pharmacology, 65 (2013), 157-170.

[7] Wang Y G, Wei X L, Zhang C L, *et al.*, Therapeutic Delivery, 1 (2010), 273-287.

[8] Blazkova I, Nguyen H V, Dostalova S, *et al.*, Int. J. Mol. Sci., 14 (2013), 13391-13402.

[9] Drbohlavova J, Chomoucka J, Adam V, *et al.*, Curr. Drug Metab., 14 (2013), 547-564.

[10] Tmejova K, Hynek D, Kopel P, *et al.*, Int. J. Electrochem. Sci., 8 (2013), 12658-12671.

[11] Baran T M, Foster T H, Lasers Surg. Med., 45 (2013), 542-550.

[12] Li D A, Zhang Y T, Yu M, *et al.*, Biomaterials, 34 (2013), 7913-7922.

[13] Schenone A V, Culzoni M J, Campiglia A D, *et al.*, Anal. Bioanal. Chem., 405 (2013), 8515-8523.

# UTILIZATION OF ELECTROCHEMISTRY FOR DETECTION OF BACTERIA ON A 3D PRINTED FLOW CHIP

Lukas NEJDL[1], Jiri KUDR[1], Kristyna CIHALOVA[1], Dagmar CHUDOBOVA[1], Michal ZUREK[1], Ludek ZALUD[2], Lukas KOPECNY[2], Frantisek BURIAN[2], Branislav RUTTKAY–NEDECKY[1,2], Sona KRIZKOVA[1,2], Marie KONECNA[1,2], David HYNEK[1,2], Pavel KOPEL[1,2], Jan PRASEK[2], Vojtech ADAM[1,2], Rene KIZEK[1,2*]

[1] *Department of Chemistry and Biochemistry, Faculty of Agronomy, Mendel University in Brno, Zemedelska 1, 613 00 Brno, Czech Republic*

2 *Central European Institute of Technology, Brno University of Technology, Technicka 3058/10, 616 00 Brno, Czech Republic*

**kizek@sci.muni.cz*

**Abstract**

The electrochemical method of differential pulse voltammetry was used for detection of electrochemically active 1-naphthol as the result of enzymatic cleaving of electrochemically inactive 1-naphthyl phosphate. 3D printed flow chip performed detection of Staphylococcus aureus based on alkaline phosphatase activity. Bacteria from the solution were captured by application of modified magnetic particles in the chip. The detection limit of electrochemical determination of 1-naphthol was 20 nM.

## 1. INTRODUCTION

Alkaline phosphatase (ALP) is produced during the growth and sporulation of various bacterial strains (*Staphylococcus aureus* [1], *Bacillus cereus* and *Bacillus amyloliquefacians* [2-4], *Escherichia coli* [5], thermophilic bacteria [6] like *Thermotoga neapolitana*, *Thermus caldophilus*, *Thermus thermophiles*, *Bacillus stearothermophilus*, *Pyrococcus abyssi* and *Deinococcus radiodurans* [7-9]). For detection of an enzyme activity, electrochemical detectors (ECD) can provide competitive advantages with respect to other detection systems such as portability, low cost, and low power requirements [10-12].

## 2. MATERIAL AND METHODS

### Fabrication of 3D microfluidic chip

The microfluidic chip was 3D processed in Blender 2.65 (Blender foundation, Amsterdam, Netherlands) and further edited in NetFabb (Netfabb, Parsberg, Germany). Acrylonitrile butadiene styrene was used as a material (DO-IT, Straznice, Czech Republic), and every printed chip was fitted with five input tubes with a diameter of 0.5 mm, one output tube with diameter 0.5 mm, two electromagnet and thermostatic system.

**Screen printed electrode (SPE) design and fabrication**

Electrode system was designed and fabricated as a disposable planar three-electrode sensor in LabSensNano laboratories (Brno University of Technology, Czech Republic). The properties of design and optimization can be found in the following papers.

**Microfluidic analysis with differential pulse voltammetric detection**

The flow cell for SPE was designed in the shape of a cuboid with sides of 1 cm (width) × 1.5 cm (height) × 3 cm (length). The reaction zone was dimensioned for 20 µl of analyte with 0.7 mm wide inlet and outlet channel. The sample was injected using a peristaltic pump (Amersham Biosciences, Uppsala, Sweden). After optimization of the automated flow system additionally a peristaltic pump Minipuls®3 (Gilson, Middleton, USA) and a stirred water bath WB-4MS (Biosan, Riga, Latvia) were used. Changes of reduction signals were measured with a potentiostat PGSTAT 101 (Metrohm, Herisau, Switzerland) and the results were evaluated by the Software NOVA 1.8 (Metrohm, Herisau, Switzerland). Settings of the potentiostat were as it follows: initial potential -0.2 V, end potential +0.5 V, step potential 0.005 V, modulation amplitude 0.1 V, modulation time 0.004 s, interval time 0.1 s, deposition time 60 s and equilibration time 5 s. For ALP detection 50 mM carbonate buffer (32 mM $Na_2CO_3$ and 68 mM $NaHCO_3$) pH 9.9 with 1 mM 1-naphthyl phosphate was used [13, 14].

## 3. RESULTS AND DISCUSSION

For electrochemical determination of 1-naphthol by DPV the optimal conditions (measurement temperature, flow rate or accumulation time) were measured. The calibration curve of 1-naphthol with regression coefficient $R^2$=0.999 was measured (Fig. 1) and the limit of detection and quantification was calculated (Table 1).

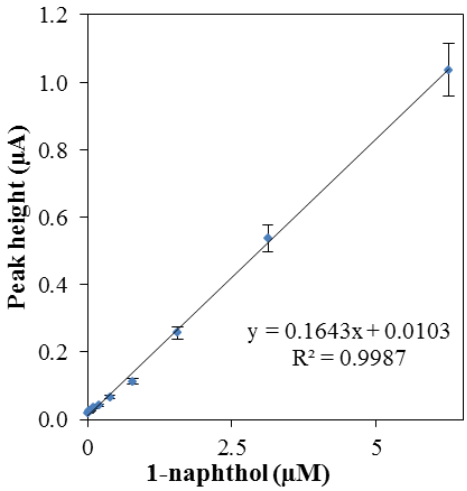


**Figure 1.:** Calibration curve of 1-naphthol obtained by DPV under the optimized conditions (measurement temperature 35 °C, flow rate 500 µl.min$^{-1}$, accumulation time 60 s)

**Table 1.** Analytical parameters of electrochemical determination of 1-naphthol.

| Substance | Regression equation | Linear dynamic range (μM) | $R^{2*}$ | LOD** (nM) | LOQ*** (nM) | RSD**** (%) |
|---|---|---|---|---|---|---|
| 1-naphthol | y = 0.1643x + 0.0103 | 0.079 - 6.25 | 0.999 | 20 | 79 | 6.5 |

* …regression coefficients

** …limits of detection of detector (S/N = 3)

*** …limits of quantification of detector ( S/N = 10)

**** …relative standard deviations

## 4. CONCLUSION

A flow chip was used for electrochemical detection of bacteria by electrochemically active 1-naphthol. The chip could be the part of robotic system and it can serve for remote control of bacteria presence [15].

## 5. ACKNOWLEDGEMENT

Financial support from the project CEITEC CZ.1.05/1.1.00/02.0068 is highly acknowledged. The authors wish to express their thanks also to Jan Zitka, Lukas Zima, Martina Stankova, Lukas Melichar and Radek Chmela for perfect technical assistance.

## 6. REFERENCES

[1]Krizkova S, Jilkova E, Krejcova L, et al., Electrophoresis, 34 (2013), 224-234.

[2]Panosian T D, Nannemann D P, Watkins G R, et al., Journal of Biological Chemistry, 286 (2011), 8043-8054.

[3]Iverson T M, Panosian T D, Birmingham W R, et al., Biochemistry, 51 (2012), 1964-1975.

[4]Ramesh A, Sharma S K, Joshi O P, et al., Indian Journal of Microbiology, 51 (2011), 94-99.

[5]Koksharov M, Lv C Q, Zhai X H, et al., Protein Expression and Purification, 90 (2013), 186-194.

[6]Takano Y, Edazawa Y, Kobayashi K, et al., Earth and Planetary Science Letters, 229 (2005), 193-203.

[7]Nitzan Y, Ashkenazi H, Photochemistry and Photobiology, 69 (1999), 505-510.

[8]Brim H, McFarlan S C, Fredrickson J K, et al., Nature Biotechnology, 18 (2000), 85-90.

[9]Sghaier H, Bouchami O, Desler C, et al., Annals of Microbiology, 62 (2012), 493-500.

[10]Wang J, Electroanalysis, 17 (2005), 1133-1140.

[11]Vandaveer W R, Pasas-Farmer S A, Fischer D J, et al., Electrophoresis, 25 (2004), 3528-3549.

[12]Nugen S R, Asiello P J, Baeumner A J, Microsystem Technologies-Micro-and Nanosystems-Information Storage and Processing Systems, 15 (2009), 477-483.

[13]Zitka O, Krizkova S, Krejcova L, et al., Electrophoresis, 32 (2011), 3207-3220.

[14]Nejdl L, Merlos Rodrigo M A, Kudr J, et al., Electrophoresis, 35 (2014), 393-404.

[15]Nejdl L, Kudr J, Cihalova K, et al., Electrophoresis, (2014).

# LIPOSOMAL TRANSPORTER WITH GFP MARK FOR TARGETED BINDING USING A NUCLEIC ACID ANCHOR SYSTEM

Lukas NEJDL[1], Iva BLAZKOVA[1], Jiri KUDR[1], Branislav RUTKAY-NEDECKY[2], Pavel KOPEL[2], Ondrej ZITKA[1,2], Vojtech ADAM[1,2] , Rene KIZEK[2*]

[1] *Department of Chemistry and Biochemistry, Faculty of Agronomy, Mendel University in Brno, Zemedelska 1, 613 00 Brno, Czech Republic*

2 *Central European Institute of Technology, Brno University of Technology, Technicka 3058/10, 616 00 Brno, Czech Republic*

**kizek@sci.muni.cz*

**Abstract**

In our work, we focused on the possibility of modification of liposomes with gold nanoparticles (AuNPs). In addition, AuNPs-modified liposomes were labelled by green fluorescent protein (GFP). Modified liposomes were isolated using magnetic microparticles (oligo(DT)$_{25}$)-nucleic acid anchor system (ODN- 5´TCTGCATTCCAGAAAAA). Isolation efficiency of lipoGFP-AuNPs was 20 %. Gel electrophoresis, MALDI-TOF, UV/VIS spectrophotometry and fluorescence imaging were used to characterize individual parts of the system lipoGFP-AuNPs.

## 1. INTRODUCTION

Liposomes are artificially-prepared microscopic particles formed by an (phospho)lipid bilayer that encloses an aqueous compartment. Their size varies in the range from 0.1 – 1 μm. Due to the inner aqueous compartment, they are able to carry various types of compounds (drugs, proteins, nucleic acids, and metal ions) [1-4]. Hydrophobic molecules can be loaded into bilayer and hydrophilic to the cavity, where are protected against degradation processes [5, 6]. In addition, changes in the lipid composition, surface charge, and the method of preparation significantly affect their properties [7]. Due to this fact, liposomes have found an application in the medicine and pharmacy, for the delivery of new biotechnology products, for example antisense oligonucleotides, cloned genes, and recombinant proteins. It has been established that numerous anti-cancer agents are non-toxic in the liposomal form in comparison with conventional free drugs [8-10].

## 2. MATERIAL AND METHODS

### Chemicals

Cholesterol, 1,2-dioleoyl-sn-glycero-3-phospho-rac-(1-glycerol) sodium salt, chloroform, $Zn(NO_3)_2.6H_2O$, sodium citrate, $HAuCl_4 \cdot 3H_2O$ and water were purchased from Sigma-Aldrich (St. Louis, MO, USA) in ACS purity, unless noted otherwise. Hydrogenated phosphatidylcholine from soybean was a gift from Lipoid GMBH (Ludwigshafen, Germany). Magnetic particles (MPs) oligo$(DT)_{25}$ were purchased from Invitrogen (Oslo, Norway). To pipette volumes down to microlitres, pipettes used were purchased from Eppendorf Research (Hamburg, Germany) with the highest certified deviation (±12 %). The deionised water was prepared using reverse osmosis equipment Aqual 25 (Aqual, Brno, Czech Republic).

### Fluorescence measurement

Fluorescence spectra were acquired by a multifunctional microplate reader Tecan Infinite 200 PRO (TECAN, Switzerland). Wavelength 400 nm was used as an excitation wavelength and the fluorescence scan was measured within the range from 440 to 800 nm per 5-nm steps. The detector gain was set to 100. To each well was placed 50 µl of sample. All measurements were performed at 30 °C controlled by the Tecan Infinite 200 PRO (TECAN, Switzerland).

## 3. RESULTS AND DISCUSSION

The whole system consisted of GFP encapsulated in liposome (LipoGFP) whose surface was modified by gold nanoparticles (Fig. 1 a). Due to high affinity of gold to thiol groups (-SH), oligonucleotide (ODN-SH) that was linked complementary with the second part of ODN, which contained adenine moieties (AAAAA), see Fig. 1 b. The liposomal transporter (LipoGFP-AuNPs) was anchored to magnetic microparticles (MBs)oligo$(DT)_{25}$ via adenine moieties, see Fig. 1 c. The functionality of individual connections (AuNPs-ODN-SH-ODN-AAAA-(MBs)oligo$(DT)_{25}$) was tested electrochemically (differential pulse voltammetry).

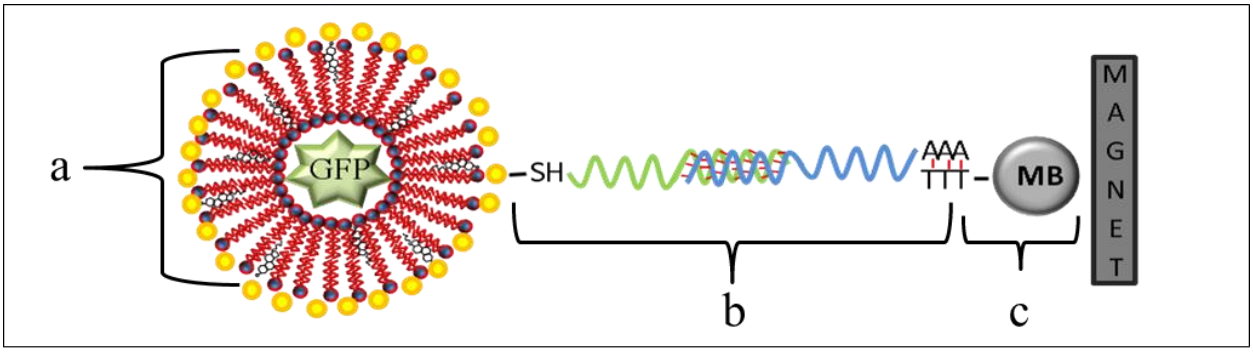


**Figure 1:** Schematic representation of nanoconstruct consisting of (a) a liposome with encapsulated GFP and nano gold (AuNP) attached to the liposome surface (b) the anchoring system comprising two oligonukleotides and (c) magnetic particle.

## 4. CONCLUSION

Amplified GFP was isolated and further characterized by gel electrophoresis, MALDI-TOF, and fluorescence imaging. Subsequently, GFP was enclosed in nanogold-modified liposomes that were isolated using magnetic microparticles and nucleic acid anchor system. Effectiveness of the whole isolation process was 20%. The functionality of the whole procedure was verified using fluorimetry.

## 5. ACKNOWLEDGEMENT

Financial support from the project CYTORES GA CR P301/10/0356 is highly acknowledged

## 6.REFERENCES

[1] Schafer J, Hobel S, Bakowsky U, et al., Biomaterials, 31 (2010), 6892-6900.

[2] Chen X, Wang X, Wang Y, et al., Journal of Controlled Release, 145 (2010), 17-25.

[3] Villares G J, Zigler M, Wang H, et al., Cancer Research, 68 (2008), 9078-9086.

[4] Martins S, Sarmento B, Ferreira D C, et al., International Journal of Nanomedicine, 2 (2007), 595-607.

[5] Milla P, Dosio F, Cattel L, Current Drug Metabolism, 13 (2012), 105-119.

[6] Bochot A, Fattal E, Journal of Controlled Release, 161 (2012), 628-634.

[7] Akbarzadeh A, Rezaei-Sadabady R, Davaran S, et al., Nanoscale Research Letters, 8 (2013).

[8] Ding Z-Y, Zhou L, Liu Y-M, et al., Thoracic Cancer, 4 (2013), 14-19.

[9] Xu X, Wang L, Xu H-Q, et al., Asian Pacific Journal of Cancer Prevention, 14 (2013), 2591-2594.

[10] Zhao C, Feng Q, Dou Z, et al., PloS one, 8 (2013), e73860-e73860.

# INTERACTION STUDY OF ARSENIC(III) IONS WITH METALLOTHIONEIN GENE (MT2A) FRAGMENT ASSESSED BY SPECTROMETRY AND ELECTROCHEMISTRY

Lukas NEJDL[1], Sylvie SKALICKOVA[1], Jiri KUDR[1], Branislav RUTTKAY-NEDECKY [1,2], Simona DOSTALOVA[2], Monika KREMPLOVA[1], Marie KONECNA[1], Vojtech ADAM[1,2] and Rene KIZEK[1,2*]

[1] *Department of Chemistry and Biochemistry, Faculty of Agronomy, Mendel University in Brno, Zemedelska 1, 613 00 Brno, Czech Republic*

2 *Central European Institute of Technology, Brno University of Technology, Technicka 3058/10, 616 00 Brno, Czech Republic*

**kizek@sci.muni.cz*

**Abstract**

Interactions between As(III) and metallothionein gene Mt2A were monitored using UV/vis spectrophotometry, atomic absorption spectrometry, electrochemical measurements and agarose gel electrophoresis. By application of the mentioned methods it was observed the As(III) forms the stable structure with DNA in the concentration range of As(III) 0.4 – 6.25 μg/ml. The higher concentration of As(III) caused the DNA degradation.

## 1. INTRODUCTION

Arsenic is classified as a worldwide pollutant and human carcinogen. Oxidative stress due to arsenic exposure is proposed as one potential mode of carcinogenic action [1]. There are currently over 100 active clinical trials involving inorganic arsenic or organoarsenic compounds registered with the Food and Drug Administration for the treatment of cancers [2]. Arsenic trioxide is presently the most active single agent in the treatment of acute promyelocytic leukemia (APL) [3, 4].

## 2. MATERIAL AND METHODS

### Chemicals

Standards of As(III) – Arsenic chloride ($AsCl_3$) was purchased from Sigma-Aldrich (St. Louis, MO, USA) in ACS purity. Standards were dissolved in ACS water

*DNA fragment amplification and isolation*

Human genomic DNA was isolated from blood via MagNA Pure Compact (Roche, Germany) using Nucleic Acid Isolation Kit I and protocol DNA_Blood_100_400.

**Electrochemical Measurements of As - DNA**

Determination of DNA was performed with 797 VA Stand instrument connected to 889 IC Sample Center (Metrohm, Switzerland). The analyser (797 VA Computrace, Metrohm, Switzerland) employs a conventional three-electrode configuration with a hanging mercury drop electrode (HMDE) with a drop area of 0.4 $mm^2$ was the working electrode. An Ag/AgCl/3M KCl electrode was the reference and glassy carbon electrode was auxiliary.

## 3. RESULTS AND DISCUSSION

The As-DNA interaction was proved using square wave voltammetry (SWV). First reports about electrochemical reduction and oxidation signal of nucleic acids were published at the end of 1950s and in the beginning of 1960s [5]. It was pointed out that these signals are due to residues of bases in DNA. Adenine and cytosine in DNA yielded reduction signals (CA peak) [6]. As-DNA was demonstrated due to the significant change of CA peak with increasing concentrations of As(III) from control DNA, Fig. 1. Using this method, it was proven that the studied concentration of As(III) plaied an important role (RSD 6%) in the DNA damage.

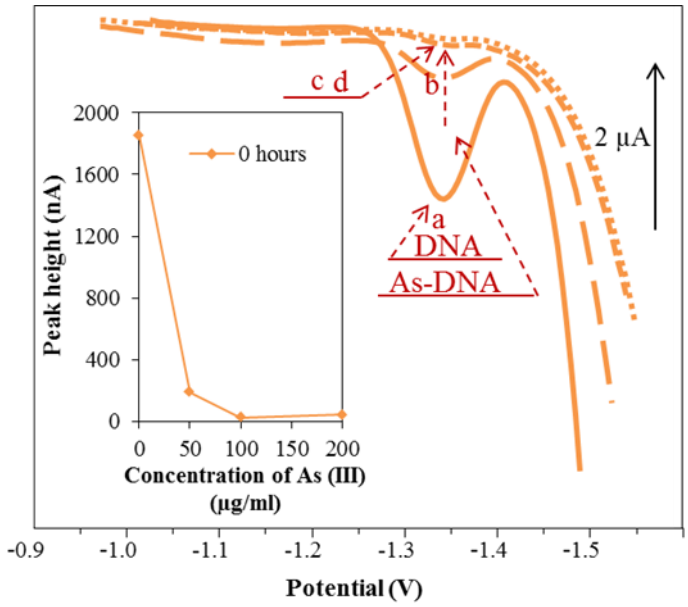


**Figure 1.:** Voltamograms (a) of 5 µg/ml DNA and 5 µg/ml DNA with As (III) in concentrations (b) 50, (c) 100 and (d) 200 µg/ml.

## 4. CONCLUSION

In this study, it was proven that the As(III) caused damage of the secondary structure of DNA. These properties of As(III) play an important role in the apoptosis induction by APL.

**5. ACKNOWLEDGEMENT**

Financial support from the project NANOLABSYS CZ.1.07/2.3.00/20.0148 is highly acknowledged

**6. REFERENCES**

[1] Ding W, Hudson LG, Liu KJ (2005) Mol. Cell. Biochem. 279.

[2] Swindell EP, Hankins PL, Chen HM, Miodragovic DU, O'Halloran TV (2013) Inorg. Chem. 52.

[3] Yang H, Lin S, Cui JR (2014) Gene 535.

[4] Yujiri T, Tanaka M, Taguchi A, Tanaka Y, Nakamura Y, Tanizawa Y (2014) Ann. Hematol. 93.

[5] Palecek E (2002) Talanta 56:809-819.

[6] Krejcova L, Huska D, Hynek D, Kopel P, Adam V, Hubalek J, Trnkova L, Kizek R (2013) Int. J. Electrochem. Sci. 8:689-702.

# AUTOMATIC ELECTROCHEMICAL DETERMINATION OF HEAVY METALS AND APPLICATION TO A REMOTE-CONTROLLED ROBOTIC PLATFORM ORPHEUS-HOPE

Hoai Viet NGUYEN[1,2], Lukas ZIMA[1], Lukas NEJDL[1], David HYNEK[1,2], Rene KIZEK[1,2*]

[1] *Department of Chemistry and Biochemistry, Faculty of Agronomy, Mendel University in Brno, Zemedelska 1, 613 00 Brno, Czech Republic*

2 *Central European Institute of Technology, Brno University of Technology, Technicka 3058/10, 616 00 Brno, Czech Republic*

**kizek@sci.muni.cz*

**Abstract**

Heavy metals are natural components of Earth's crust. They can be found in many places such as soil, water, and air. High concentration of heavy metals can affect negatively human health and environment. The main aim of this study is to determine heavy metals ions such as zinc, cadmium, lead, and copper by automatic electrochemical analysis. We chose a carbon tip as a working electrode. Furthermore, this system was applied into a remote-controlled robotic platform ORPHEUS-HOPE.

## 1. INTRODUCTION

Heavy metals pollution is a major health problem, representing a danger for worldwide citizens. "Heavy metal" term describes metallic species that typically include the transition metals, some metalloids, lanthanides, and actinides. Although many metals are essential for cell metabolism and function, excess amounts can be toxic. Some metals can bio-accumulate in the food chain and are regarded as serious environmental pollutants, because of their toxicity to higher species [1]. In order to prevent the accumulation of these toxic chemical species, it is needed for a portable, low cost monitoring of heavy metals concentrations. Electrochemical detection is the very sensitive analytical methods available for determination of heavy metals ions [2]. In this study, automatic electrochemical detection was employed for determination of zinc, cadmium, lead, and copper. Moreover, this system was applied into the remote-controlled robotic platform ORPHEUS-HOPE. ORPHEUS-HOPE is a rugged robotic system which easily equipped with additional devices, such as radiation and biological sensors. Robot can work well during night or in bad visibility conditions, since it has sensitive full user control. In addition, Robot performs well in mud and snow, but it is also fully

capable of indoor operation. Even the control of the robot is ready for narrow spaces operation [3].

## 2. MATERIAL AND METHODS

Automatic electrochemical detection was performed by an electrochemical robotic using three electrodes. The commercial carbon tip was used as a working electrode. Ag/AgCl/3M KCl was reference electrode (Metrohm, Swizerland) and counter electrode was injection needle (Metrohm). Electrochemical signal was recorded with a potentiostat PGSTAT 101 (Metrohm, Herisau, Switzerland) and software NOVA 1.8 (Metrohm, Herisau, Switzerland) was employed for data evaluation. The electrochemical robotic has two parts. The first part connected with a new holder which is printed by PROFI 3D MARKER printing system. Three electrodes were put on this holder. This holder can easily move up and down through the vertical axis. The second part of the system connected with plate containing sample. This part can move left and right through the horizontal axis. ElChemRo software was employed for automatic moving of the system. The differential pulse voltammetry parameters were as it follows: initial potential -1.6 V, end potential 0.2 V, step potential 0.005, modulation amplitude 0.1 V, modulation time 0.004 s, interval time 0.1 s. All experiments were carried out at room temperature. Acetate buffer (0.2 M $CH_3COOH$ and 0.2 M $CH_3COONa$) was used as the supporting electrolyte.

## 3. RESULTS AND DISCUSSION

### a. Determination of each heavy metal by automatic electrochemical detection

The commercial carbon tip electrode was used as working electrode for detection of cadmium, lead, and copper ions. By applying a conditioning time of 60 s at -0.9 V into $Hg(NO_3)_2$ solution, thin-film mercury was created. This carbon tip electrode modified with mercury film was employed for detection of zinc ion. Firstly, effect of accumulation time was tested and then 120 s of accumulation time was chosen for finding calibration curve as well as limit of detection of these heavy metals, which is shown in Fig. 1. Copper and zinc produced lowest limit of detection (200 nA).

### b. Determination of mixture of heavy metals by automatic electrochemical detection

Mixture of 4 heavy metals was monitored using carbon tip electrode modified by mercury film. Firstly, 10 µg/ml of each heavy metal was used for the mixture. There is a difference between signals of each heavy metal in the mixture in comparison with single heavy metal.

Therefore, different concentrations (10, 5, 2.5, and 1.25 µg/ml) of each heavy metals in the mixture were tested.

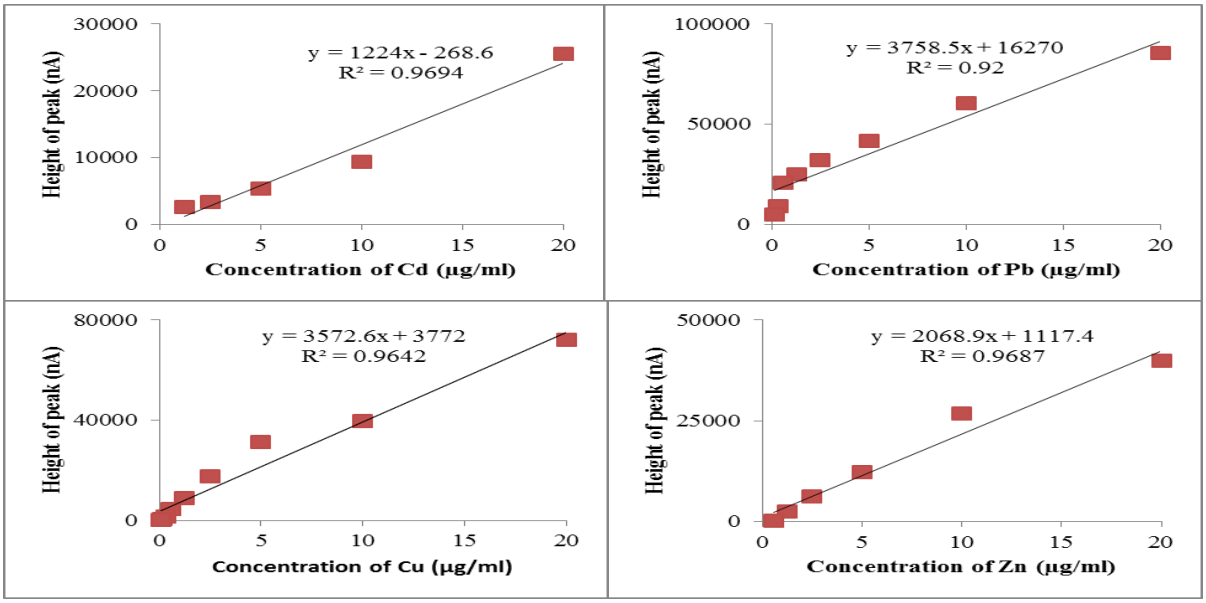


**Figure. 1.:** Calibration curve of cadmium, lead, copper, and zinc ions. The parameters were as it follows: accumulation time of 120 s, initial potential -1.6 V, end potential 0.2 V, step potential 0.005, modulation amplitude 0.1 V, modulation time 0.004 s, interval time 0.1 s.

## 4. CONCLUSION

Electrochemcial monitoring of heavy metals by the commercial carbon tip electrode was presented in this study. Based on the result, it can be concluded that copper and zinc produced lower limit of detection in comparison with lead and cadmium.

## 5. ACKNOWLEDGEMENT

The work has been supported by CEITEC CZ. 1.05/1.1.00/02.0068.

## 6. REFERENCES

[1] Musameh M M, Hickey M, Kyratzis I L, Research on Chemical Intermediates, 37 (2011), 675-689.

[2] Krystofova O, Trnkova L, Adam V, *et al.*, Sensors, 10 (2010), 5308-5328.

[3] Nejdl L, Kudr J, Cihalova K, *et al.*, Electrophoresis, (2014), 1-13.

# MICRORNA ELECTROCHEMICAL DETECTION IN CONNECTION WITH SPECIFIC MAGNETIC SEPARATION

Kristyna SMERKOVA[1], Kristyna HUDCOVA[2], Veronika VLAHOVA[1], Marketa VACULOVICOVA[1,3], Vladimir PEKARIK[4], Michal MASARIK[2], Vojtech ADAM[1,3], Rene KIZEK[1,3*]

[1]*Department of Chemistry and Biochemistry, Faculty of Agronomy, Mendel University in Brno, Zemedelska 1, CZ-613 00 Brno, Czech Republic, European Union*

[2]*Department of Pathological Physiology, Faculty of Medicine, Masaryk University, Kamenice 5, CZ-625 00 Brno, Czech Republic, European Union*

[3]*Central European Institute of Technology, Brno University of Technology, Technicka 3058/10, CZ-616 00 Brno, Czech Republic, European Union*

[4]*Department of Cellular and Molecular Neurobiology, Central European Technology Institute, Masaryk University, Kamenice 735/3, CZ-625 00 Brno, Czech Republic, European Union*

**kizek@sci.muni.cz*

**Abstract**

The microRNAs (miRNAs) belong to small non-protein-coding RNAs. These miRNAs have different expressions at different diseases and they can serve as diagnostic and prognostic markers. That's why the sensitive, simple, fast and cost-effective detection method is required.

## 1. INTRODUCTION

Small RNA molecules are effective regulators of gene expression, and the expression signature of one subgroup of small RNA, the miRNAs, has been linked to disease development and progression. The abnormal expression of specific miRNAs is associated with many diseases including cancer and/or diabetes [1, 2]. Effect of miRNAs is based on binding to the untranslated region (3'UTR) of target mRNA and causing degradation (or inhibition) of target mRNA and their effects are involved in many cellular processes such as proliferation, differentiation, apoptosis, metastases, angiogenesis, and immune response [3, 4]. Therefore, detection of miRNAs in biological samples will greatly improve the understanding of their functions and broaden effective tools for cellular process control and disease prevention. However there are several limitations of miRNAs detection such as their short length and tissue-specific occurrence. Basic methods used to detection are northern

blotting, real time RT-PCR, ISH (*in situ* hybridization) and micro-RNA arrays [5-12]. But these methods demand labeling amplification and/or enzymatic reaction. In this work the electrochemical detection based on specific magnetic separation was used because there is no need of labeling or amplification.

## 2. MATERIAL AND METHODS

The miR-124 (5´-UAA GGC ACG CGG UGA AUG CC-3´) and complementary biotinylated oligonucleotide (ODN) anti-miR-124 (5´-Btn-GG CAT TCA CCG CGT GCC TTA-3´ were used for optimization of magnetic separation. For the binding specificity confirmation ODNs at the following sequences were used: ODN 10 (ATGGCAGACA), ODN 21 (GCGATTGATGGTGATACGGTT), ODN 55 (GGGGACAAGTTTGTACAAAAAAG CAGGCTGTGGCTAATACGAAAAAAACAACATT) and miR-150 (UAAGGCACG CGGUGAAUGCCA). The ODNs were synthesized by Sigma-Aldrich (USA).

### Electrochemical analysis

Electrochemical measurements were performed with AUTOLAB PGS30 Analyzer (EcoChemie, Netherlands) connected to VA-Stand 663 (Metrohm, Switzerland) using a standard cell with three electrodes. A hanging mercury drop electrode (HMDE) with a drop area of 0.4 $mm^2$ was employees the working electrode. An Ag/AgCl/3M KCl electrode served as the reference electrode. Pt electrode was used as the auxiliary electrode.

Adsorptive transfer technique was used for the electrochemical determination of RNA. The adsorptive transfer technique is based on the sample accumulation (120 s) onto the working electrode surface and consequently on the electrode washing and square wave voltammetric (SWV) measurement. All experiments were carried out at room temperature (21°C). SWV measurements were carried out in the presence of acetate buffer pH 5.0. SWV parameters: start potential 0 V, end potential -1.8 V, potential step 5 mV, frequency 280 Hz, and amplitude 25.05 mV. For smoothing and baseline correction the software GPES 4.9 supplied by EcoChemie was employed.

## 3. RESULTS AND DISCUSSION

For optimal MPs utilization the binding capacity of MPs surface was determined. To the MPs the anti-miR-124 was added and after immobilization step and MPs separation the amount of unbound antisense ODN in retantate was measured. In the Fig. 1A the dependence of anti-miR-124 amount remained in the retentate on applied concentration to MPs is shown. In

addition of 3µM probe the unbound probe amount was only 3.3%. So for following experiments was 3µM anti-miR-124 added to 500 µg of MPs.

The next optimization step was the elution temperature determination (Fig. 1B). During the elution dsRNA denaturation occurs and the miR-124 is released into the elution solution. The goal was to find such a temperature at which would be released maximum miR-124 amount and simultaneously that does not cause the damage of streptavidin-biotin binding. For following experiments was elution temperature of 70°C was used, the peak height was 349 nA and the SWV signal of blank was insignificant. The optimized method selectivity was proofed using oligonucleotides of different lengths and miR-150 with non-complementary sequences (Fig. 1C). The oligonucleotides lengths were 10 nt (ODN 10), 21 nt (ODN 21) and 55 nt (ODN 55). The signals of non-complementary sequences were at the same level as control solutions. To determine the sensitivity of the optimized separation method a calibration curve for the whole isolation process was performed (Fig. 1D).

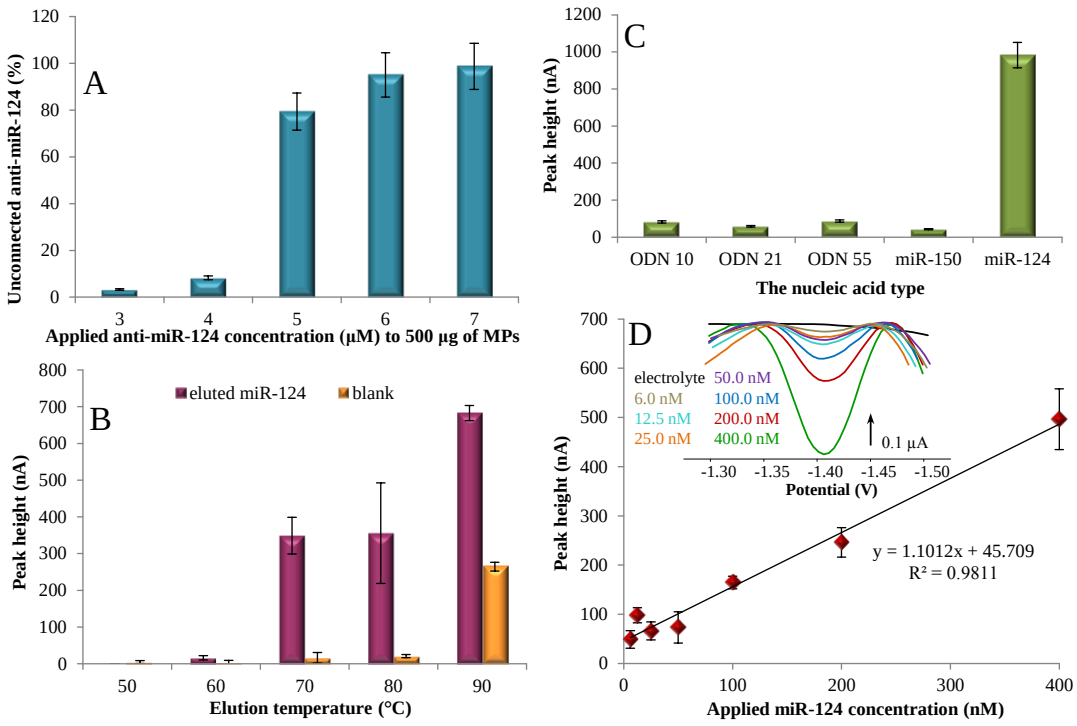


**Figure 1.:** (A) MPs binding capacity (anti-miR-124) optimization. The dependence of biotinylated anti-miR-124 which was not bound to MPs on applied anti-miR-124 concentration.. (B) The peak height dependence of eluted miR-124 amount/the eluate without miR-124 on elution temperature. (C) The binding specificity verification. The peak height dependence of the eluted target oligonucleotides on target nucleotide sequence. The non-complenmentary ODNs were ODN 10, ODN 21, ODN 55, miR-150 and the complementary was miR-124. (D) Dependence of the peak height on applied miR-124 concentration using the optimized MPs-based isolation. Inset: the isolated miR-124 voltammograms.

## 4. CONCLUSION

The miRNA specific separation based on magnetic microparticles was optimized. The developed electrochemical detection in connection with specific magnetic separation is label-free, simple and low-cost method for miRNA analysis.

## 5. ACKNOWLEDGEMENT

The work has been supported by NanoBioTECell GA CR P102/11/1068.

## 6. REFERENCES

[1] Karolina, D. S., Armugam, A., Tavintharan, S., Wong, M. T. K., *et al.*, *PLoS One* 2011, *6*.

[2] Ruan, Q. G., Wang, T., Kameswaran, V., Wei, Q., *et al.*, *Proc. Natl. Acad. Sci. U. S. A.* 2011, *108*, 12030-12035.

[3] Mirnezami, A. H. F., Pickard, K., Zhang, L., Primrose, J. N., Packham, G., *Ejso* 2009, *35*, 339-347.

[4] Ruan, K., Fang, X., Ouyang, G., *Cancer Letters* 2009, *285*, 116-126.

[5] Bernardo, B. C., Charchar, F. J., Lin, R. C. Y., McMullen, J. R., *Heart Lung and Circulation* 2012, *21*, 131-142.

[6] Li, W., Ruan, K. C., *Analytical and Bioanalytical Chemistry* 2009, *394*, 1117-1124.

[7] Obernosterer, G., Martinez, J., Alenius, M., *Nature Protocols* 2007, *2*, 1508-1514.

[8] Pena, J. T. G., Sohn-Lee, C., Rouhanifard, S. H., Ludwig, J., *et al.*, *Nature Methods* 2009, *6*, 139-141.

[9] Schmittgen, T. D., Lee, E. J., Jiang, J. M., Sarkar, A., *et al.*, *Methods* 2008, *44*, 31-38.

[10] Streit, S., Michalski, C. W., Erkan, M., Kleeff, J., Friess, H., *Nature Protocols* 2009, *4*, 37-43.

[11] Valoczi, A., Hornyik, C., Varga, N., Burgyan, J., *et al.*, *Nucleic Acids Research* 2004, *32*.

[12] Wang, X. W., *Rna-a Publication of the Rna Society* 2009, *15*, 716-723.

# INTERACTION OF METALLOTHIONEIN WITH CDTE QUANTUM DOTS STUDIED BY ELECTROCHEMISTRY

Katerina TMEJOVA[1,2], David HYNEK[1,2], Pavel KOPEL[1,2], Vojtech ADAM[1,2], Rene KIZEK[1,2*]

[1] *Department of Chemistry and Biochemistry, Faculty of Agronomy, Mendel University in Brno, Zemedelska 1, 613 00 Brno, Czech Republic*

[2] *Central European Institute of Technology, Brno University of Technology, Technicka 3058/10, 616 00 Brno, Czech Republic*

**kizek@sci.muni.cz*

**Abstract**

This study is focused on investigation of interaction of metallothionein with CdTe quantum dots. Application of electrochemical technique for such interaction monitoring was tested. Concretely using of differential pulse voltammetry Brdicka reaction was applied. Two new voltammetric peaks X and Y were detected with the prolonged time of interaction up to 6 hours.

## 1. INTRODUCTION

Metallothionein (MT) as a low-molecular protein with mass of 6–7 kDa has the tertiary structure based on the presence of two domains. These domains readily form cysteine clusters to bind metal ions [1]. The main functions of MT consist in the transport of metal ions, accumulation of Zn, and detoxification of metals [1]. Due to high affinity of MT to heavy metals, its interaction with quantum dots (QDs) is also possible [2]. An increased expression of MT after exposure of model organisms to Cd-based QDs was found in studies dealing with toxicity of QDs [3, 4]. Further, the biosynthesis of QDs in rats and earthworms exposed to $CdCl_2$ was found [5, 6].

## 2. MATERIAL AND METHODS

### Chemicals

All chemicals for preparation QDs were purchased from Sigma-Aldrich (USA) in ACS purity. CdTe QDs were done according to Skalickova et al. [7]. QDs were stored at 4 °C. MT was isolated from rabbit liver according to Skalickova et al. [7].

### Electrochemical determination of metal ions

Electrochemical determination was carried out by differential pulse voltammetry (DPV) in the Brdicka electrolyte [8] by using a standard cell with three electrodes and cooled sample holder and measurement cell to 4 °C (Julabo F25, JulaboDE). A hanging mercury drop

electrode (HMDE) with a drop area of 0.4 $mm^2$ was the working electrode. An Ag/AgCl/3M KCl electrode was the reference and platinum electrode was auxiliary. Sample consisting of 10 µl 0.8 µM MT and 10 µl 500 µM QDs was pipetted into an electrochemical cell (2 ml) and then the electrolyte (1 980 µl) was added. The MT-QD interaction was studied for 0, 240, 480, 960 s, and 30, 60, 90 min, and 2, 3, 4, 5, 6 hours at 4°C. After that, monitoring of the interaction was performed using the electrochemical detection (DPV). More details about electrochemical Brdicka experiments is shown in the paper Petrlova et al. [9].

## 3. RESULTS AND DISCUSSION

The interaction of QDs with MT was also monitored electrochemically in the Brdicka electrolyte. The mixture of 500 µM QDs and 0.6 µM MT was left to interact for the interaction time from 0 s to 6 h with MT. Five peaks were detected (X, Y, RS2Co, Cat1, Cat2) in the obtained voltammograms. However, we were interested in peak X (potential -0.90±0.05 V) and peak Y (potential -1.00±0.05 V) that appeared during the interaction.

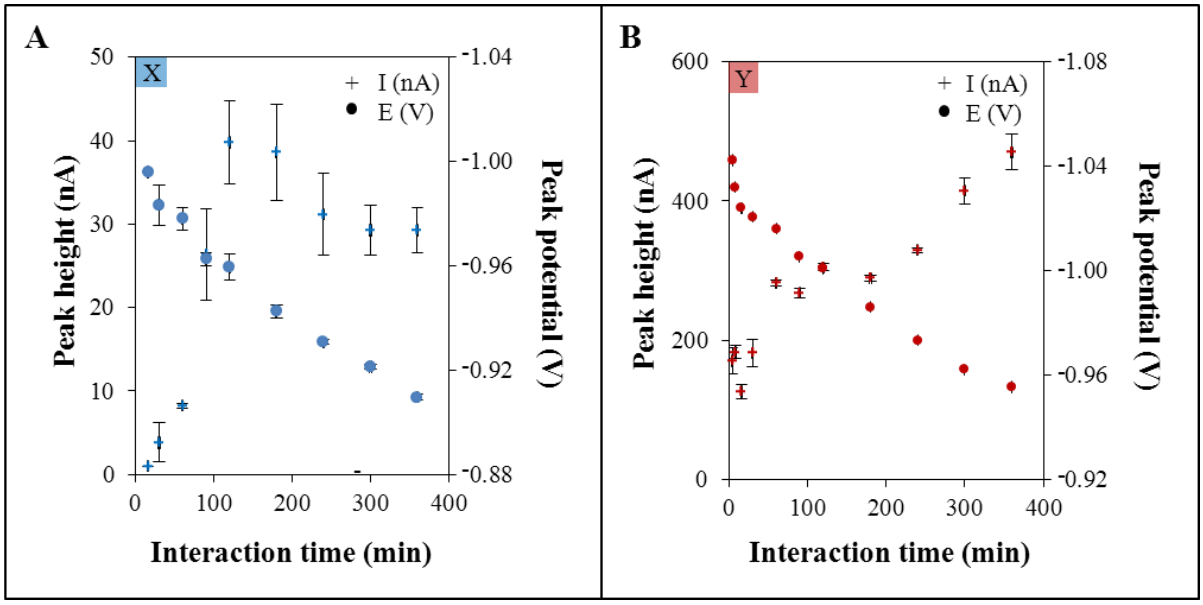


**Figure 1.:** Interaction of CdTe with MT in time interval from 0 s to 6 h. Dependence of peak height and peak potential on interaction time for peak X (**A**) and peak Y (**B**). Error bars were calculated by standard deviation, n = 3.

Increase of the peak X was very rapid (forty times in 120 min) and next slightly decreased. The potential was shifted significantly to positive values (from -0.99 to -0.91 V) and this shift mainly linear. Analogical situation was observed in the case of the peak Y, but changes in its peak height were not so distinct (1.7x). With increasing interaction time height of peak Y increased quite linearly opposite to the change of height of peak X. Changes in potentials of

both peaks were linearly. On the other hand, Cat2 peak (data are not presented) decreased. The Cat2 peak corresponds to the presence of –SH moieties, and MT interacts with QDs via these sulfhydryl moieties within its structure. During the interaction between MT and QDs, free -SH groups in MT are probably saturated by QDs and this effect causes observed increase of height of the X and Y peaks as a proof of metal reduction in the complex MT-QD [9].

## 4. CONCLUSION

Complexes formed during interaction of QDs with MT were studied in our work by Brdicka catalytic reaction, which providing new peaks X and Y associated with MT-QD complexes. These new peaks could bring new information about interaction of QDs with metalloproteins because application of QDs in organism will be connected with question of various QDs interactions.

## 5. ACKNOWLEDGEMENT

Financial support from CEITEC CZ.1.05/1.1.00/02.0068 is greatly acknowledged.

## 6. REFERENCES

[1] Babula P, Masarik M, Adam V, *et al.*, Metallomics, 4 (2012), 739-750.

[2] Sharma S, Rais A, Sandhu R, *et al.*, Int. J. Nanomed., 8 (2013), 1477-1488.

[3] Gagne F, Fortier M, Yu L, *et al.*, J. Environ. Monitor., 12 (2010), 1556-1565.

[4] Lin C H, Yang M H, Chang L W, *et al.*, Nanotoxicology, 5 (2011), 650-663.

[5] Sturzenbaum S R, Hockner M, Panneerselvam A, *et al.*, Nature Nanotechnol., 8 (2013), 57-60.

[6] Trabelsi H, Azzouz I, Sakly M, *et al.*, Int. J. Nanomed., 8 (2013), 1121-1128.

[7] Skalickova S, Zitka O, Nejdl L, *et al.*, Chromatographia, 76 (2013), 345-353.

[8] Heyrovsky M, Norrish R G W, Nature, 200 (1963), 880-881.

[9] Petrlova J, Potesil D, Mikelova R, *et al.*, Electrochim. Acta, 51 (2006), 5112-5119.

# PHYSICAL CHEMISTRY OF INORGANIC-ORGANIC NANOSTRUCTURES

Lubomir SPANHEL[1, 2*]

1 *CEITEC-Masaryk University, Faculty of Chemistry, Kamenice 5, 625 00 Brno, Czech Republic*

2 *Institute of Chemical Sciences Rennes ICSR, CNRS-UMR 6226, Université de Rennes 1, France*

**lubomir.spanhel@ceitec.muni.cz, lspanhel@seznam.cz, spanhel@univ-rennes1.fr*

**Abstract**

Concentrated semiconductor and metal nanocolloids represent an ideal basis for fundamental photophysical chemistry research as well as for applied nanobiomaterials sciences. This talk addresses the usefulness of various spectroscopic, electrochemical and calorimetric methods in nanoparticle research. The following four examples will be given:

1) Structure/optical spectral profile relationships, nucleation chaos and fractal law based electromagnetic resonance/cluster size correlation diagrams
2) Mechanistic aspects of MX nanocolloid growth (M = Zn, Cd; X = O, S, Se, Te)
3) Multifunctionalisation of nanoparticle surfaces with foreigner atoms
4) Glass formation and confined salt melting in nanoparticulate ZnO fractals

## REFERENCES

[1] L. Spanhel and M. Anderson, **J. Am. Chem. Soc**. *1990*, **112**, 2278 "Synthesis of Porous Quantum Size CdS Membranes: Photoluminescence Phase Shift and Demodulation Measurements"; **J. Am. Chem. Soc**. *1991*, **113**, 2826 "Semiconductor Clusters in the Sol-Gel-Process: Quantized Aggregation, Gelation and Crystal Growth in Concentrated ZnO Colloids"

[2] V. Ptatschek, T. Schmidt, M. Lerch, G. Müller, L. Spanhel, A. Emmerling, J. Fricke, A.H. Foitzik and E. Langer, **Ber. Bunsenges. Phys. Chem**. 1998, **102**, 85. "Quantized Aggregation Phenomena in II-VI Semiconductor Colloids"

[3] C. Lorenz, A. Emmerling, J. Fricke, T. Schmidt, M. Hilgendorff, L. Spanhel, **J. Non.-Cryst. Solids** 1998, **238**, 1-5. "Aerogels containing strongly luminescing ZnO nanocrystals"

[4] M. Kohls; M. Bonnani, L. Spanhel **Appl. Phys. Lett**. 2002, **81**, 3858. Green $Er^{III}$ luminescence in fractal ZnO Nanolattices"

[5] M Kohls, G. Müller, L. Spanhel, C. Le Luyer, J.C. Plenet, J. Mugnier, M. Giersig, Su, G. McMahon, **Review in "Low-Dimensional Systems: Theory, Preparation, and Some Applications**, Kluwer Publishers, Eds. L.M. Liz-Marzan, M. Giersig, 2003, p. 107-120. "Nanocrystalline $Er^{III}/Si^{IV}$@ZnO Multilayers:

A Detailed Optical and Structural Study"

[6] L. Spanhel, **Review** in **J. Sol-Gel Sci. & Technol.** 2006, **39**, 7-24.
"Colloidal ZnO Nanostructures and Functional Coatings: A Survey

[7] S. Toscani, O. Hernandez, C. Aparicio, L. Spanhel, **J. Sol-Gel Sci.& Technol.** 2014, 69, 457-463.
"Glass formation and confined melting in nanoparticulate ZnO Aggregates".

# ELIMINATION SQUARE WAVE VOLTAMMETRY

Libuse TRNKOVA[1,2*], Iveta PILAROVA[1], Rudolf NAVRATIL[1], Libor GURECKY[1], Vimal SHARMA[1]

[1] *Department of Chemistry, Faculty of Science, Masaryk University, Kamenice 5, CZ-625 00 Brno, Czech Republic*

[2] *Central European Institute of Technology, Brno University of Technology, Technická 3058/10, CZ-616 00 Brno, Czech Republic*

**libuse@chemi.muni.cz*

**Abstract**

In this contribution it is shown that the elimination voltammetric procedure (EVP) gives a new dimension for the data evaluation not only in linear sweep (LSV) or cyclic (CV) voltammetry but also in square wave voltammetry (SWV).

## 1. INTRODUCTION

Square wave voltammetry (SWV), originated from an idea of Barker and Gardner [1-2], is in fact a variant of pulse voltammetry [3]. In this technique the change of the potential of the working electrode combines a large amplitude square wave and staircase modulation with the tuneable step (Fig.1A). The current is measured at the end of each potential half-cycle change, right before the next, so that the contribution of the charging current to the current signal is minimized. The current measured on the backward half-cycle ($I_b$) is subtracted from the current measured on the forward half-cycle ($I_f$) and this difference is displayed as a function of the applied potential (Fig.1B). The SWV maxima reflect the concentration dependency of electroactive species with the detection limits in the nanomolar range.

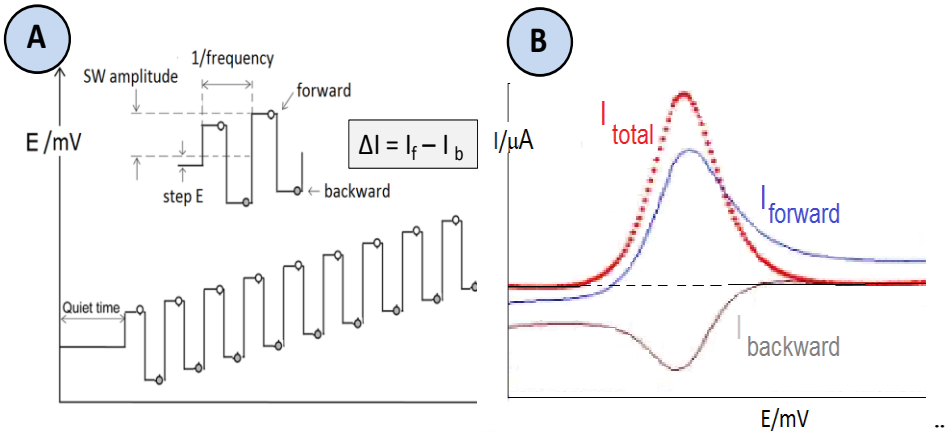


**Fig.1** Potential wave form for SWV (1A) and measured SWV currents (1B).

Various transformations of voltammetric data (semi derivative, semi integral, derivative and integral) can help to extract the specific information (number of transferred electrons, mechanism etc.) and can reveal details concerning the adsorption phenomena in the studied electrochemical system. Optionally, the recently developed transformation based on the elimination voltammetric procedure (EVP) can be used to remove chosen current components from the total voltammetric current ($I_{tot}$). Consequently, the measured current on scan rate ($v$) dependencies follow a power law relationship ($I \sim v^x$) with the power law coefficient $x$ that should have a value of 0, 1 and 1/2 for the kinetic ($I_k$), charging ($I_c$) and diffusion ($I_d$) current component, respectively. Using the power low and the reference scan rate every total current can be expressed as:

$$I_{v/vref} = \left(\frac{v}{v_{ref}}\right)^0 I_k + \left(\frac{v}{v_{ref}}\right)^1 I_c + \left(\frac{v}{v_{ref}}\right)^{1/2} I_d \qquad (1)$$

The EVP function $f(I)$ eliminating required current components is calculated from different total currents measured at different scan rates. This approach is frequently used in LSV or CV (linear sweep or cyclic voltammetric) measurements.

## 2. MATERIAL AND METHODS

All electrochemical experiments were performed using the electrochemical analyzer μAUTOLAB TYPE III (Metrohm, Switzerland) connected with VA Stand 663 and controlled by GPES Manager software. The sample of adenine (Sigma-Aldrich) was dosed into the electrochemical cell, consisting of three electrodes: a hanging mercury drop electrode (HMDE) with an effective area of 0.3 $mm^2$ or a pencil graphite electrode (PeGE) with an effective area of 15.9 $mm^2$ as the working electrodes, and Ag/AgCl/3M KCl and Pt wire as the reference and auxiliary electrodes, respectively. The experimental conditions for SWV: $c_{Ade} = 2 \cdot 10^{-4}$ M, frequency: 400, 200 and 100 $s^{-1}$, accumulation time $t_a$ = 0 – 300 s, phosphate–acetate buffer (pH 5.8); the potential range for Ade reduction on a mercury electrode was from 0 to -1.7 V and for Ade oxidation on PeGE was from -0.15 to 1.6 V. The SWV curves obtained were smoothed by using the Savitzky–Golay filter, level 2, and the elimination voltammetric procedure EVP according to (3).

## 3. RESULTS AND DISCUSSION

The scan rate ($v$) is not adjustable parameter within the frame of SWV method but it can be calculated by knowing the modulation frequency $f$ and the voltage step $E_{step}$ according to:

$$v = E_{step} f \quad (2)$$

With the same step and different frequency we can obtain the desired scan rate values. For the integer 2, when the value $\left(\frac{v}{v_{ref}}\right) = 2 \text{ or } 1/2$ the most common EVP function eliminating $I_k+I_c$ and conserving $I_d$ is expressed in the case of LSV:

$$f(I) = -11.657 I_{vref/2} + 17.485 I_{vref} - 5.8284 I_{2vref} \quad (3)$$

and in case of SWV:

$$f(I) = -11.657 I_{2\,fref} + 17.485 I_{fref} - 5.8284 I_{1/2\,fref} \quad (4)$$

The verification of the aforementioned relationships was performed using known electroactive substances on the mercury and the carbon electrodes.

## 4. CONCLUSION

The integration of the elimination voltammetric procedure (EVP) into the square wave voltammetry (SWV) measurements has shown to be governed by the scan rate – frequency dependence.

## 5. ACKNOWLEDGMENTS

The work has been supported by projects: (a) MUNI/A/0972/2013 and (b) KONTAKT II (LH 13050) of the Ministry of Education, Youth and Sports of the Czech Republic, (c) CEITEC – Central European Institute of Technology Project CZ.1.05/1.1.00/02.0068.

## 6. REFERENCES

[1] G. C. Barker, A. W. Gardner, Z. Anal.Chem, 173 (1960) 79.

[2] L. Ramaley, M.S. Krause, Jr., Anal.Chem., **41** (1969) 1362.

[3] A. J. Bard, L. R. Faulkner, Electrochemical Methods. Fundamentals and Applications, John Willey&Sons, INC., (2nd edition) 2000. p. 293.

[4] L. Trnkova (a) and F. Jelen, S. Hason, L. Trnkova (b) in: V. Adam and R. Kizek (Eds.); Utilizing of Bio-electrochemical and Mathematical Methods in Biological Rese-arch, Signpost, Kerala, India 2007, (a) Chapter 4, p. 51 and (b) Chapter 8, p. 153.

[5] L. Trnkova, F. Jelen, M. Ozsoz in: M. Ozsoz (Ed.), Electrochemical DNA Biosensors, Pan Stanford Publishing, Singapore, 2012, Ch. 11, p. 355.

# DEVICE FOR DEHYDRATION MONITORING USING POTASSIUM CONCENTRATION IN URINE MEASUREMENT

Jaromír ŽÁK[1], Petra MAJZLÍKOVÁ[1], Jaromír HUBÁLEK[1*]

[1] *Department of Microelectronics, Faculty of Electrical Engineering and Communication, Brno University of Technology, Technicka 3058/10, 616 00 Brno, Czech Republic*

**hubalek@feec.vutbr.cz*

**Abstract**

Real-time dehydration monitoring is one of the key methods for organism state determination especially for elderly people and sportsmen. Dehydration is a complex value and its precise automated determination is not a simple task. A lot of measurement methods can be used for its determination. One of the measurement method and its implementation into automated electronic acquisition system is described in this article.

## 1. INTRODUCTION

One of the possibilities for dehydration measurement is its determination from potassium concentration in urine [1]. This concentration is reciprocally proportional to total amount of water in the human body. Standard values vary between 100 mg/l and 2000 mg/l in the most cases [2]. The concentration can be measured by standard ion-selective sensor [3] and processed in any type of medical measurement device or data logger [4] and recalculated into organism hydration value. This value will be probably inexact due to ordinary potassium concentration which depends e.g. on gender, age or condition of the tested person. Long term measurement has to be performed for basic potassium concentration value determination for each measured person separately.

More accurate results with faster measurement response can be achieved by combination of multiple measurement methods not only by potassium concentration in urine measurement. The results can be acquired and evaluated automatically and sent to the physician in case of emergency state. The second big advantage of the automated measurement system is located in the possibility of non-obtrusive real-time measurement in the real conditions.

## 2. EXPERIMENTS

Potassium concentration has been measured by standard potassium ion-selective electrode obtained from Elektrochemické detektory s.r.o. (Trutnov, Czech Republic) [3] with simple voltage output setting. The voltage is converted into data value in the form of digital number by standalone wireless battery powered electronic circuit after each measurement (see figure 1). Measured data are collected into PC database where they can be viewed or analyzed later. Additional values like personal information and other measurement results can be measured automatically or inserted manually by user or physician.

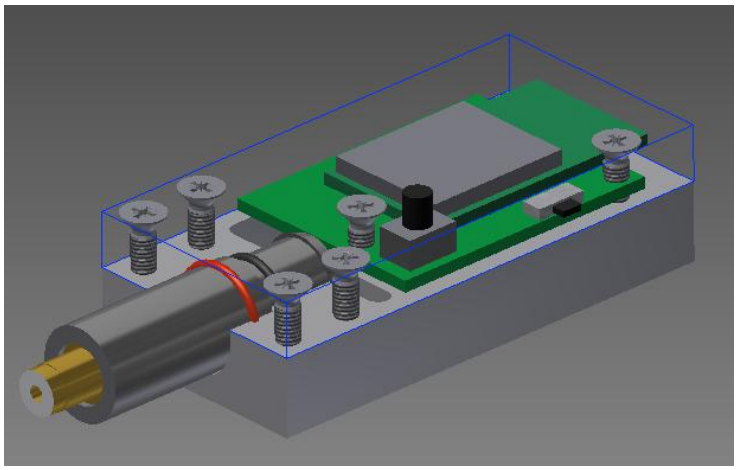

**Figure 1.:** Design of the developed wireless device for automated potassium in urine concentration measurement

After the measurement platform built-up, calibration of the system was performed. Interference of the other urine substances had been expected but this expectation was disconfirmed by calibration measurement. No interferences were observed in the typical potassium concentration range [2]. The interferences were registered only for potassium concentrations below 10 mg/l (see figure 2a). KCl solutions (concentrations between 1 mg/l and 10 g/l) in Milli-Q water (Millipore, USA) with addition of synthetic urine (concentrations from 0 % to 2 % - typical values) has been used for basic calibration measurement. Ion-selective electrode had been conditioned before use in a 0.5 mmol/l KCl (PENTA, Czech Republic) aqueous solution for 1 h.

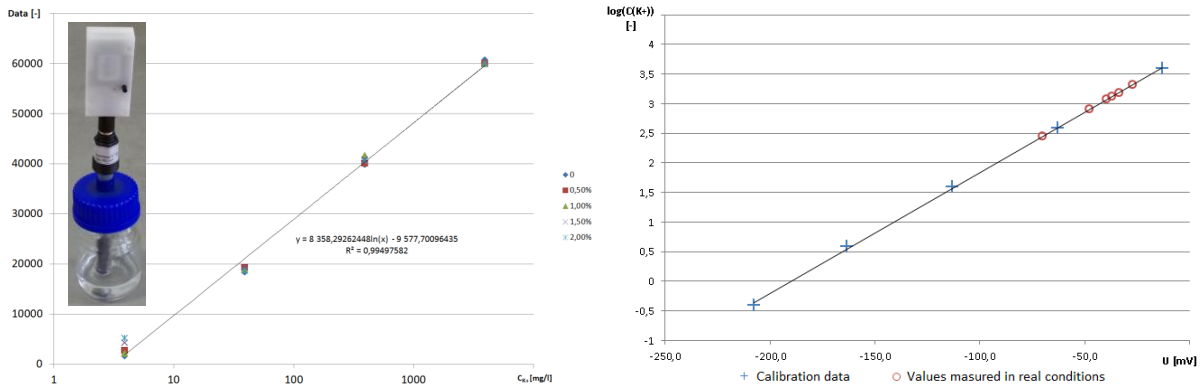


**Figure 2.:** A) Calibration of the sensor system with dependency on urine addition concentration and B) measured values in human urea

Calibrated measurement system was tested in laboratory and later in real conditions. Other methods measurement results, water intake/outtake value and subjective feeling of the tested persons corresponded with dehydration state determined by automated potassium in urine measurement (see figure 2b).

## 3. CONCLUSION

The automated measurement of potassium concentration in urine by newly created system for real-time data acquisition was realized for dehydration detection. The whole system was created, calibrated and tested in the laboratory and real conditions. This system can be useful for many medical and sport branches in the future.

## 4. ACKNOWLEDGEMENT

This work has been supported by the project MAS No. 120228 (7H10021) supported by ENIAC JU and the project SIX No. CZ.1.05/2.1.00/03.0072.

## 5. REFERENCES

[1]LE. Armstrong, et al., Int J Sport Nutr, vol. 8, pp. 345–355, 1998

[2]Putnam, D. F., NASA contractor report, 1971 Elektrochemické detektory s.r.o., [online] <http://www.elektrochemicke-detektory.cz/iontove-selektivni-elektrody/>, 2014

[3]Solovei, D., et al., Procedia Engineering, 2012. 47: p. 200-203

# SEMICONDUCTIVE $SnO_2$/MWCNTs GAS SENSOR

Imrich GABLECH[1,2*], Jan PRASEK[1,2], Petra MAJZLIKOVA[1,2], Jaromir HUBALEK[1,2]

[1] *Brno University of Technology, Faculty of Electrical Engineering and Communications, Department of Microelectronics, Technicka 3058/10, 616 00 Brno, Czech Republic*

[2] *Central European Institute of Technology, Brno University of Technology, Technicka 3058/10, 616 00 Brno, Czech Republic*

**imrich.gablech@ceitec.vutbr.cz*

**Abstract**

The metal oxide semiconductive tin dioxide based gas sensor for detection of explosive gasses was designed and fabricated. There were prepared and compared two different types of active layer materials – unmodified tin dioxide nanopowder and tin dioxide nanopowder modified with multiwalled carbon nanotubes (MWCNTs). We were able to detect 50 ppm of isobutane with satisfactory sensitivity using the MWCNTs modified active layers.

## 1. INTRODUCTION

Nowadays, monitoring of dangerous explosive gasses as they are butane or methane is needed. Therefore the reliable and sufficiently sensitive sensors for fast detection of very low concentrations are developed. Metal-oxide semiconductive gas sensors represent one possibility for such requirements [1-3].

## 2. SENSOR FABRICATION

### Heater fabrication and packaging

Semiconductive gas sensors usually work at higher temperatures up to 450 °C [1-3]. The appropriate heater element and package is therefore needed. One possibility for such solution is the usage of LTCC and thick-film technology in combination with TO-8 microelectronic package. The fabricated LTCC frame in combination with TO-8 package is shown in the Figure 1.

**Figure 1.:** The fabricated LTCC frame and its placement in TO-8 package

The heating meander made of ESL 5545-G paste is placed from the bottom side of the LTCC frame in which the silicon or alumina substrate with maximal dimensions 8 × 8 mm containing electrodes and sensitive layer could be inserted. This substrate is then mechanically fixed to LTCC frame using Ferro 11-036 thick-film paste. The conductive interconnection from electrodes to the LTCC frame is made using wirebonding. The LTCC frame is fixed to TO-8 package using conductive thick-film AgPd based paste (see Figure 1).

**Active layer electrode substrate design and fabrication**

The active electrode substrate was designed to be made from 525 µm thick silicon / 475 nm thick silicon dioxide wafer with dimensions of 8 × 8 mm. On the silicone substrate, the interdigital structure in the area of 6 × 6 mm was designed. The fingers width was designed to be 100 µm with a gap of 50 µm between them (see. fig. 2).

**Figure 2.:** Interdigital structure design, its detail and fabricated gold active layer electrode substrate

The interdigital structure is made of evaporated 100 nm thick titanium layer with high temperature resistance as the adhesive layer. The 250 nm thick gold layer was evaporated over it to form the wire-bondable and high electrically conductive electrodes.

**Sensitive layers preparation and deposition**

There were fabricated three types of active layers: one unmodified ($SnO_2$ – 100 wt%) and two modified with multiwalled carbon nanotubes ($SnO_2$/MWCNTs – 1.5 wt% and $SnO_2$/MWCNTs – 3.0 wt%). The layers were spray-coated on previously prepared active layer substrate from 1 ml suspension of nanopowder dispersed in dimethylformamide.

Then the active layer substrates were annealed at 450 °C in vacuum for 48 hours to make basic stabilization. Final stabilization was made in gas chamber at 350 °C. The stabilization was finished after four hours under 500 sccm/min gas flow of synthetic air or 2500 ppm of isobutane in synthetic air mixture changing.

**3. RESULTS AND DISCUSSION**

All sensors were characterized at 350 °C for the detection of isobutane in the range of concentration from 50 ppm to 4000 ppm in synthetic air. The resistance was stabilized within

120 seconds after each isobutane concentration change. From the measured data, the plot of calibration curves was created (see Figure 3). From the results shown in figure 3 is clear that the higher sensitivity of MWCNTs modified active layers was achieved.

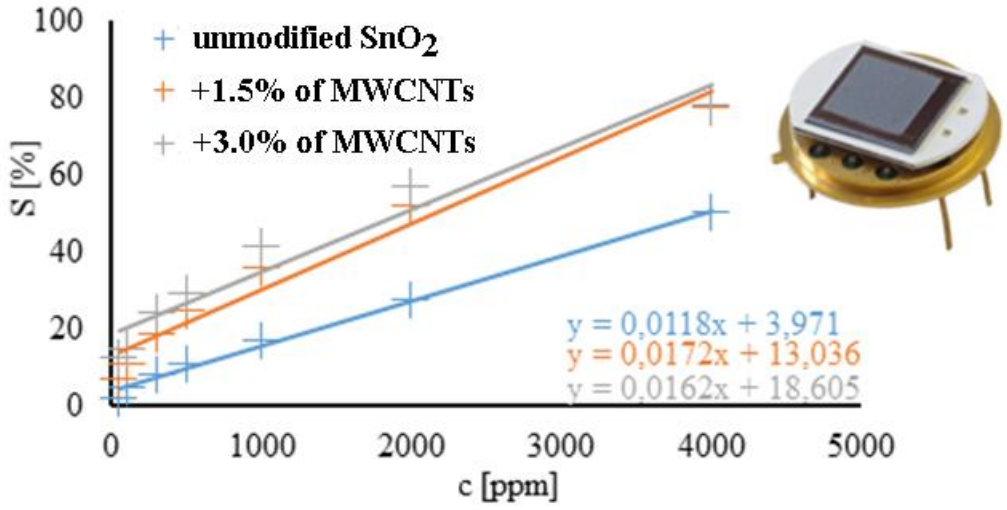


**Figure 3.:** Calibration curves of all types of prepared active layers and the photo of fabricated sensor

## 4. CONCLUSION

The semiconductive tin dioxide based or tin dioxide with MWCNTs mixture based gas sensor for detection of isobutane was designed and fabricated. From the obtained results is clear that the higher sensitivity was achieved using MWCNTs modified sensitive layers which allowed detection of concentrations of isobutane from the levels of 50 ppm to 100 ppm in synthetic air. The unmodified sensor showed the satisfying sensitivity of 8% from the 300 ppm of isobutane. All three types of sensors could serve as the sensor of in time detection of explosive level of isobutane, because the explosive level of isobutane in air is in range from 14000 to 83000 ppm. The selectivity of fabricated sensors to isobutane was not confirmed.

## 5. ACKNOWLEDGEMENT

The financial support from the projects SIX CZ.1.05/2.1.00/03.0072 and GAP205/10/1374 is highly acknowledged.

## 6. REFERENCES

[1]Rembeza S I, Shamatova Y V, Svistova T V, et al.: Semiconductors, 46 (2012), 1190-1193

[2]Bakin A S, Bestaev M V, Dimitrov D T, et al.: Thin Solid Films, 269 (1997), 168-171

[3]Quaranta F, Rella R, Siciliano P, et al.: Sensors and Actuators B: Chemical 58 (1999) 350-355

# HIGH RESOLUTION TECHNICS FOR FABRICATION OF SPECIAL NANOELECTRODES

Marian MÁRIK[*1,2], Vojtěch SVATOŠ[1,2], Jaromír HUBÁLEK[1,2]

1 *Central European Institute of Technology, Brno University of Technology, Technicka 3058/10, 616 00 Brno, Czech Republic, *marian.marik@ceitec.vutbr.cz*

2 *LabSensNano, Department of Microelectronics, Faculty of Electrical Engineering and Communication, Brno University of Technology, Technicka 3058/10, 616 00 Brno, Czech Republic*

**Abstract**

In-vivo impedance measurements of cells are the objective of current scientific research in area of biological sciences. A problem that needs to be solved is how to measure extracellular potential without causing trauma or damage in living cells. One possible solution is based on nanoelectrodes that are fabricated due to current high technology level. The main goal of this work is to design and create nanoelectrode with pair of gold or platinum nanowires using standard thin-film techniques (micro- and nanotechniques) and high resolution ion- and electron beam methods.

## 1. INTRODUCTION

Design and preparation of novel nanoelectrode pair was realized. Nowadays the measurement of electrical potential in living cells is a very trendy analysis in the sphere of biotechnology. The cells communicate with each other with the help of electric signals. Additionally based on certain changes of the electrical potential it is possible to observe the reactions of living cells in their life cycles or reactions due to various external influences. The novel nanoelectrode pair has been fabricated for a short and also a long term extracellular potential measurement in water based medium. [1, 2]

## 2. MATERIAL AND METHODS

The novel two nanoelectrode system was designed and simulated in software CoventorWare. Sensitivity of living cells to temperature changes is high. In nanoelectrodes the joule heating can increases the temperature of the sample or device as accompanying effect of large current densities should be considered. To decrease the undesirable thermal shock the electrodes were designed to be thermal stable against the current flow. The thermal simulation for nanowires

was provided by software CoventorWare. Amount of Joule heating was confirmed by calculations. [3, 4]

Designed two-electrode electrochemical system operates on the basis of impedance sensors. Low dimensions of electrodes require a combination of micro and nanotechnology techniques for fabrication. For the base of chip a silicon wafer coated with thermal silicon oxide with a thickness 500 nm was used. Fabrication of base electrodes was realized by PVD and lithograpy techniques. Gold was used as the base material for the electrode.

The preparation of vertical nanoelectrodes was provided by high resolution techniques. The submicron electrodes and the mark for electron beam lithography (EBL) were etched into gold and NiCr layer with FIB. The vertical electrodes were fabricated by electrochemical deposition of gold into the photoresist mask. The mask was prepared by e-beam lithography.

## 3. RESULTS AND DISCUSSION

The vertical nanoelectrode system for a long term measurement was realized by electrochemical deposition of gold and for short term measurement was realized by EBID platinum. Fabricated gold electrodes shape is similar to a cone. It was caused by EBL process when the nanoholes were little bit affected by proximity effect of electron beam. It could be expected that this alteration of nanoelectrode shape would have no effect on a function of electrodes.

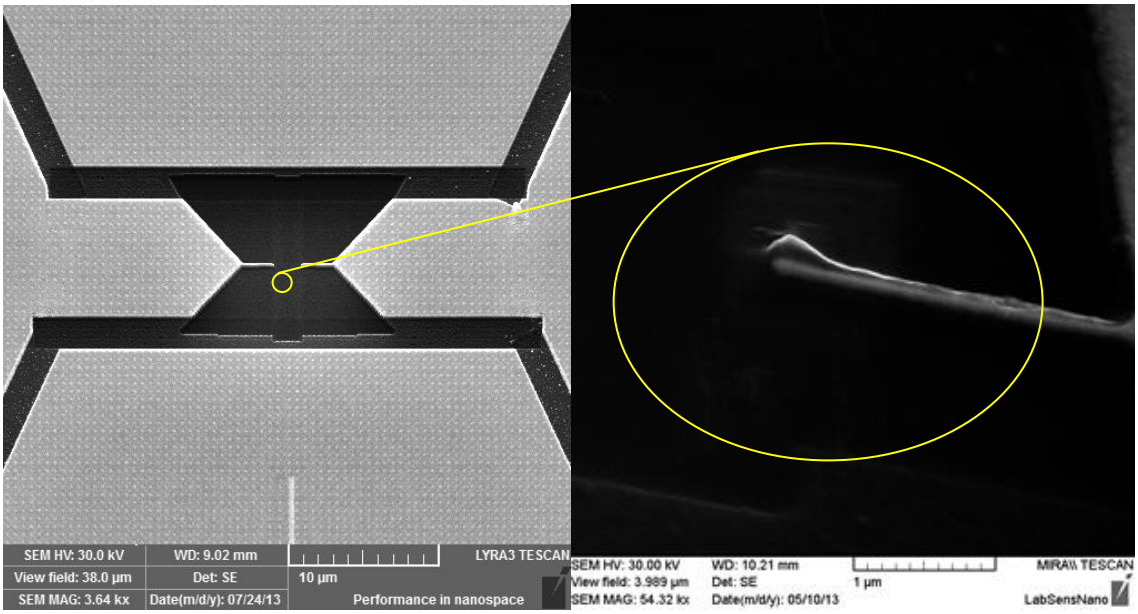


**Figure 1.:** Details of submicron electrodes and the place, where vertical nanoelectrodes are deposited (left) and vertical nanoelectrode on the edge of the horizontal submicron electrode (right).

## 4. CONCLUSION

Novel vertical nanoelectrode system for extracellular potential measurement of cells was designed and fabricated. In the first part of this work electrode system was designed and the thermal influence on nanowires was simulated. The second part of this work was the fabrication of the electrode system. Electrode system for a long term measurement was realized from gold and for short term measurement was realized from platinum. The sensor testing will begin in near future on living cells.

## 5. ACKNOWLEDGEMENT

This work has been performed in laboratories supported by the SIX project CZ.1.05/2.1.00/03.0072 and supported by Grant Agency of the Czech Republic under the contract GACR P102/11/1068 NaNoBioTECell.

## 6. REFERENCES

[1]FRADEN, J. (2004). Handbook of modern sensors: physics, designs, and applications, New York, Springer Verlag, ISBN 0-387-00750-4.

[2]CUI, Z. (2008). Nanofabrication: Principles, Capabilities and Limits, Didcot, UK, Springer, ISBN 978-0-387-75576-2.

[3]ZOSKI, C. G. (2007). Handbook of electrochemistry, Elsevier, Oxford, ISBN 9780444519580.

[4]FANGOHR, H., CHERNYSHENKO, D. S., FRANCHIN, M., FISCHBACHER, T., MEIER, G. (2011)Joule heating in nanowires, Physical Review B..

[5]RAI-CHOUDHURY, P., (1997). Handbook of Microlithography, Micromachining, and Microfabrication: Microlithography, SPIE Press, ISBN 0819423-78-5.

# ZVYŠTE KVALITU SVÝCH VÝSLEDKŮ PŘESNÝM DÁVKOVÁNÍM

PIPETOR
Microlab 300

DÁVKOVAČ
eVOL


- sériové dávkování
- pipetování
- ředění a míchání
- příprava kalibračních roztoků

DILUTOR
Microlab 600

CHROMSERVIS®
www.chromservis.eu

KOMERČNÍ PREZENTACE

eppendorf


# Spektrakulární

**Eppendorf BioSpectrometer® fluorescence** je jedinečná kombinace spektrofotometru s fluorimetrem v jednom šikovném, univerzálním, kompaktním přístroji. Ideální pro kvantifikace biomolekul měřením absorbance nebo fluorescence.

Unikátní rozsah měřených koncentrací od 2,5 pg/µl DNA až do 150 ng/µl a nebo až do 1500 ng/µl při použití mikrokyvety **Eppendorf µCuvette™ G1.0 pro objemy od 1,5 µl do 10 µl.**

Eppendorf BioSpectrometer® fluorescence kombinuje možnosti měření v UV/VIS oblasti a měření fluorescence ve fixních vlnových délkách pro **stanovení velmi nízkých koncentrací** nukleových kyselin a proteinů (pg/µl) pomocí fluorescenčních barviček.

> Rozsah UV/VIS od 200 do 830 nm, krok 1 nm.
> Měření absorbance při jedné vlnové délce nebo v jednom vzorku více vlnových délek, proměří spektra, umí metody s faktory, standardy či sériemi standardů, spočítá koncentrace a čistoty.
> Fluorescenční modul umožňuje excitaci při 470 nm a měření emisních vlnových délek při 520 a 560 nm.
> Předprogramované základní metody u absorbance (kvantifikace dsDNA, ssDNA, RNA, BCA, Lowry, OD600…)
> Předprogramované základní metody u fluorescence (pro běžně používané fluorescenční barvičky).
> Umožňuje vytvořit a uložit vlastní metody měření.
> Malý (29,5 x 40 x 15 cm), lehký přístroj.
> Možnost propojit přímo do PC bez nutnosti použít další SW nebo přenos dat do USB paměti. Export dat do Excelu.
> Kompatibilní se standardními kyvetami i mikrokyvetami.


Otevřená mikrokyveta Eppendorf µCuvette™ G1.0

www.eppendorf.com/photometry
www.eppendorf.cz


# pragolab

laboratorní přístroje a zařízení

hmotnostní spektrometrie • separační techniky
elementární analýza • atomová spektroskopie
elektrochemie • uv-vis spektrometrie
reologie • analýza povrchů • spotřební materiál
laboratorní vybavení • servis

www • pragolab • eu
pragolab@pragolab • cz
Nad Krocínkou 55, 190 00 Praha
Jamborova 25, 615 00 Brno

**Sborník příspěvků**

**XIV. Pracovní setkání fyzikálních chemiků a elektrochemiků**

Editor: Libuše Trnková

Technická úprava Romana Ševčíková

Vydala Masarykova univerzita, Brno

Vydání první, 2014

ISBN 978-80-210-6842-1

muni
PRESS